universe

IMPACT FACTOR 2.5

CITESCORE 4.3

Review

Three-Dimensional Quantum Black Holes: A Primer

Emanuele Panella, Juan F. Pedraza and Andrew Svesko

Topic Collection

Open Questions in Black Hole Physics

Edited by

Dr. Gonzalo J. Olmo and Dr. Diego Rubiera-Garcia

MDPI

https://doi.org/10.3390/universe10090358

universe

MDPI

Review

Three-Dimensional Quantum Black Holes: A Primer

Emanuele Panella [1,†], Juan F. Pedraza [2,†] and Andrew Svesko [3,*,†]

[1] Department of Physics and Astronomy, University College London, Gower Street, London WC1E 6BT, UK; emanuele.panella.21@ucl.ac.uk
[2] Instituto de Física Teórica UAM/CSIC, Calle Nicolás Cabrera 13-15, 28049 Madrid, Spain; j.pedraza@csic.es
[3] Department of Mathematics, King's College London, Strand, London WC2R 2LS, UK
* Correspondence: andrew.svesko@kcl.ac.uk
† These authors contributed equally to this work.

Abstract: We review constructions of three-dimensional 'quantum' black holes. Such spacetimes arise via holographic braneworlds and are exact solutions to an induced higher-derivative theory of gravity consistently coupled to a large-c quantum field theory with an ultraviolet cutoff, accounting for all orders of semi-classical backreaction. Notably, such quantum-corrected black holes are much larger than the Planck length. We describe the geometry and horizon thermodynamics of a host of asymptotically (anti-) de Sitter and flat quantum black holes. A summary of higher-dimensional extensions is given. We survey multiple applications of quantum black holes and braneworld holography.

Keywords: black holes; semi-classical gravity; AdS/CFT; gravitational holography; braneworlds

1. Overview

Semi-classical gravity remains a useful proxy to study quantum effects in gravity from the perspective of a macroscopic observer. In this context, quantum fields live in a classical dynamical spacetime where the combined system is characterized by the semi-classical Einstein equations [1,2]

$$G_{ab}(g) + \Lambda g_{ab} = 8\pi G_N \langle T^{\rm QFT}_{ab} \rangle. \tag{1}$$

On the left-hand side is the usual Einstein tensor for a classical spacetime g_{ab} with cosmological constant Λ, while on the right-hand side $\langle T^{\rm QFT}_{ab} \rangle$ is the expectation value of the (renormalized) stress–energy tensor of the quantum field theory in some quantum state $|\Psi\rangle$. Semi-classical gravity should be viewed as an approximation and only valid in a certain regime. Indeed, the semi-classical approximation fails near the Planck scale, as at this level, quantum gravity effects become important, such that (1) can no longer be trusted. Further, the semi-classical fields in Equation (1) are not expected to be valid for generic quantum states $|\Psi\rangle$, e.g., macroscopic superpositions [3]. They are, however, known to be valid when $|\Psi\rangle$ is approximately classical, i.e., a coherent state.

Even in its regime of validity, solutions to semi-classical gravity, particularly black holes, are difficult to study consistently. Largely, this is because solving (1) amounts to solving the problem of a backreaction—how quantum matter influences the classical geometry and vice versa—which is a notoriously difficult and open problem, as it requires simultaneously solving a coupled system of geometry and quantum correlators. Often, in three spacetime dimensions and higher[1], the problem is examined perturbatively, offering limited insight, especially when backreaction effects become large. These difficulties only compound when there are a large number of quantum fields, or when the field theory is strongly coupled, as is the case for quantum chromodynamics and the standard model of particle physics.

A context in which the physics of a large-N number of strongly interacting quantum fields may be probed is the Anti-de Sitter/conformal field theory (AdS/CFT) correspondence [6]. Born out of studies in string theory, AdS/CFT is a non-perturbative candidate

Citation: Panella, E.; Pedraza, J.F.; Svesko, A. Three-Dimensional Quantum Black Holes: A Primer. *Universe* **2024**, *10*, 358. https://doi.org/10.3390/universe10090358

Academic Editors: Gonzalo J. Olmo and Diego Rubiera-Garcia

Received: 5 July 2024
Revised: 20 August 2024
Accepted: 22 August 2024
Published: 6 September 2024

model of quantum gravity, where gravitational physics in a bulk $d+1$-dimensional asymptotically AdS spacetime has a dual description in terms of a CFT living on the d-dimensional conformal boundary of AdS. This duality is therefore a concrete realization of gravitational holography [7,8]. More specifically, in a large-N expansion, the planar diagram limit of the CFT, the bulk is well approximated by classical gravity (we will state this dictionary more precisely below). A powerful feature of the AdS/CFT correspondence is strong–weak coupling duality: coupling constants between the bulk and boundary theories are inversely related, $G_N \sim N^{-1}$. Thus, computations of strongly coupled field theories may instead be performed via a classical gravity calculation. While the boundary geometry on which the CFT lives may be curved (and even contain black holes [9]), it is fixed. Consequently, standard AdS/CFT holography alone is insufficient for addressing the semi-classical backreaction problem[2].

Enter braneworld holography [11]. Historically introduced as a possible solution to the hierarchy problem [12,13], braneworld models treat the four-dimensional universe we experience as a membrane sitting in a spacetime with large extra-dimensions. When combined with holography, braneworlds function as a useful toolkit to address difficult problems in semi-classical gravity. In this framework, AdS/CFT duality is adapted to incorporate situations where a portion of the bulk, including its boundary, is removed by a d-dimensional Randall–Sundrum [13,14] or Karch–Randall [15,16] braneworld. Crucially, the geometry of the end-of-the-world (ETW) brane is dynamical, having an induced theory of gravity. More precisely, the brane serves as an infrared cutoff in the bulk, translating to a ultraviolet (UV) cutoff for the holographic CFT. As in holographic renormalization [17–21], a tower of higher-derivative corrections to the d-dimensional Einstein–Hilbert action are induced by the holographic cutoff CFT_d. From the brane perspective, the induced theory may thus be interpreted as a semi-classical theory of gravity [22], where the higher-derivative corrections incorporate backreaction effects due to the CFT living on the brane, which is governed by

$$G_{ij} + \Lambda_d g_{ij} + (\text{higher-curvature}) = 8\pi G_d \langle T_{ij}^{\text{CFT}} \rangle_{\text{planar}}. \tag{2}$$

Here, Λ_d and G_d are induced cosmological and Newton constants on the brane, and the right-hand side indicates the holographic CFT is in its planar limit[3].

At first glance, it would appear the braneworld has only complicated the situation with its higher-derivative corrections: solving the induced field Equation (2) requires solving the problem of backreaction in a complex higher-derivative theory of gravity. The computational advantage of braneworld holography, however, is that the semi-classical induced brane theory has an equivalent bulk description in terms of classical AdS_{d+1} gravity coupled to a brane obeying Israel junction conditions. Thus, exact spacetimes solving the classical bulk field equations with brane boundary conditions automatically correspond to exact solutions to the semi-classical brane equations of motion (2). Holographic braneworlds thus provide a means to exactly study the problem of backreaction without having to explicitly solve semi-classical field equations. In particular, classical AdS_{d+1} black holes which localize on the ETW brane are conjectured to precisely map to black holes in d-dimensions, including all orders of quantum backreaction [22], i.e., 'quantum' black holes.

The primary purpose of this article is to review the state of the art regarding such holographic quantum black holes. Emphasis is given to a particular class of analytic black holes which localize on an AdS_4 braneworld, which were first uncovered by Emparan, Horowitz and Myers [23,24], corresponding to three-dimensional quantum black holes [22,25–27]. These braneworld black holes lead to an important observation: a backreaction can lead to the existence of black holes where there were none before. That is, famously, there are no black hole solutions in vacuum to classical Einstein gravity in three dimensions with positive or vanishing cosmological constant. Rather, the geometry of a point mass in Mink_3 or dS_3 is described as a conical defect without a black hole horizon [28,29]; Schwarzschild-dS_3, for example, is a conical defect with a single cosmological horizon but no black hole horizon. Quantum corrections due to backreaction alter the three-dimensional geometry in

such a way that a black hole horizon is induced, leading to a type of (quantum) censorship of conical singularities. Meanwhile, classical black holes do exist in three-dimensional Einstein gravity with a negative cosmological constant [30,31], which is a consequence of the tendency for gravitational collapse afforded by the negatively curved geometry. Nonetheless, in such contexts, a backreaction yields behavior strikingly different from their classical counterparts.

A secondary goal of this review is to advertise a host of applications of holographic quantum black holes. These include the exact study of semi-classical horizon thermodynamics, holographic entanglement entropy and complexity, and the prospect of probing black hole singularities. Combined, quantum black holes serve as a theoretical laboratory to exactly test ideas in semi-classical/quantum gravity, deserving of further exploration.

Road Map and High-Level Summary

Backreaction without holography. Section 2 sets the stage by exploring quantum corrections to three-dimensional geometries at the perturbative level. This demonstrates that one need not appeal to AdS/CFT or holographic braneworlds to see how a quantum backreaction alters classical three-dimensional geometry. For example, a conformally coupled scalar field in Schwarzschild-(A)dS$_3$ produces a Casimir effect with negative energy density such that, upon solving the semi-classical Einstein Equation (1), the linear-order change to the tt-component of the metric in static patch coordinates goes like [32,33]

$$\delta g_{tt} = \frac{2L_{\rm P}F(M)}{r}, \tag{3}$$

where $L_{\rm P} = \hbar G_3$ is the Planck length in three dimensions[4] and $F(M)$ is a positive function of the mass of the point particle generating the conical defect. The $1/r$-correction—which is solely a quantum effect—modifies the original blackening factor and its root structure, implying a black horizon may arise due to a backreaction. However, since the correction is on the order of the Planck length, this conclusion is tenuous, since quantum gravity effects are expected to play a role at this scale. If there is a large-c amount of such quantum fields, it is conceivable that their combined quantum effect is to produce a correction proportional to $cL_{\rm P} \gg L_{\rm P}$, for which quantum gravity effects can be neglected. Unfortunately, it is thus far unknown how to solve the backreaction problem with such a large number of fields via non-holographic methods. Thus, while the perturbative analysis is suggestive, it advocates for the holographic braneworld approach described above.

Holographic braneworlds and quantum black holes. In Section 3, we present a general portrait of braneworld holography and quantum black holes. Historically, this framework is a natural extension of holographic renormalization, and it is a prescription where bulk infrared (IR) divergences are eliminated by introducing an IR cutoff hypersurface near the AdS boundary, adding local counterterms, and employing a minimal subtraction scheme. In standard braneworld holography, the IR cutoff surface is replaced by an end-of-the-world brane $\mathcal{B}$ of tension τ. The would-be divergent counterterms now combine with the brane action as seen from the bulk, leading to an induced theory of higher-derivative gravity on the brane (34)

$$I_{\rm Bgrav} = \frac{1}{16\pi G_d}\int_{\mathcal{B}} d^d x\sqrt{-h}\left[R - 2\Lambda_d + \frac{L_{d+1}^2}{(d-4)(d-2)}\left(R_{ij}^2 - \frac{dR^2}{4(d-1)}\right) + \cdots\right], \tag{4}$$

coupled to a CFT with an ultraviolet cutoff. Here, G_d and Λ_d are induced scales dependent on the bulk Newton and cosmological constant and brane tension, and the ellipsis denotes an infinite tower of higher-derivative terms, which is proportional to increasing positive powers of the bulk AdS length scale L_{d+1}. A metric variation of this action results in the semi-classical equations of motion (2), the solutions of which are conjectured to constitute quantum-corrected geometries due to the backreaction of a large-c holographic CFT with a UV cutoff.

Benchmarking quantum black holes. Section 4 is devoted to constructing three-dimensional quantum black holes using holographic braneworlds, including static and rotating black holes in AdS_3 (Section 4.2), dS_3 (Section 4.3), and Minkowski$_3$ (Section 4.4). In all cases, the bulk geometry is taken to be the AdS_4 C-metric, with either a Karch–Randall (asymptotically AdS_3) or Randall–Sundrum (asymptotically flat or dS_3) end-of-the-world brane embedded inside. The neutral, static geometries induced on the brane include corrections of the type (3), supporting the intuition gained from the perturbative analysis. For example, the static quantum BTZ black hole is (64)

$$ds^2_{\rm qBTZ} = -\left(\frac{\bar{r}^2}{\ell_3^2} - 8\mathcal{G}_3 M - \frac{\ell F(M)}{\bar{r}}\right)d\bar{t}^2 + \left(\frac{\bar{r}^2}{\ell_3^2} - 8\mathcal{G}_3 M - \frac{\ell F(M)}{\bar{r}}\right)^{-1} d\bar{r}^2 + \bar{r}^2 d\bar{\phi}^2, \quad (5)$$

where M is the black hole mass, and $\mathcal{G}_3$ is a renormalized Newton's constant due to an all-order resummation of the higher-derivative terms appearing in the induced action (4). One notable difference between the black hole (5) and the perturbative geometry (3) is that $\ell \sim cL_{\rm P} \gg L_{\rm P}$, where c is the central charge of the cutoff CFT_3 on the brane. Thus, the correction appears on a scale where quantum gravitational effects can be consistently ignored; the geometry (5) is a quantum-corrected black hole much larger than the Planck length. Further, the geometry (5) is an exact solution to the semi-classical brane theory.

Quantum black hole thermodynamics. Section 5 focuses on the horizon thermodynamics of quantum black holes. As with the geometry, the thermodynamics of the braneworld black hole is induced from the thermodynamics of the bulk AdS_4 black hole. For example, the bulk and brane horizon temperatures coincide. Meanwhile, the bulk entropy, given by the Bekenstein–Hawking area relation, is reinterpreted as generalized entropy

$$S^{(4)}_{\rm BH} \Longleftrightarrow S^{(3)}_{\rm gen}, \quad (6)$$

the sum of gravitational and matter entanglement entropies. Consequently, from the brane perspective, the first law of thermodynamics of quantum black holes is

$$dM = TdS^{(3)}_{\rm gen} + ..., \quad (7)$$

where the ellipsis refers to possible additional variations such as rotation or charge. Thus, by accounting for a semi-classical backreaction, classical gravitational entropy is replaced by its semi-classical generalization. Since the bulk thermodynamic variables are exactly known, the first law holds to all orders of backreaction. This is highly non-trivial from the brane perspective. Indeed, the induced semi-classical theory includes an infinite tower of higher-derivative terms and the matter entropy of the cutoff CFT_3. To determine the entropy and mass non-perturbatively in a backreaction would require a resummation of the infinite tower of terms and knowledge of how to compute the von Neumann entropy of the CFT_3, which is a supremely challenging task. Via holography, this resummation is performed by the bulk.

Holographic braneworlds, moreover, provide a natural higher-dimensional origin of *extended* black hole thermodynamics (Section 5.6), where the cosmological constant is treated as a dynamical pressure. This is because the cosmological constant on the brane is partly induced by the brane tension. Tuning the brane tension alone amounts to varying the induced brane cosmological constant, such that mechanical work performed by the brane is interpreted as extended thermodynamics of the black hole on the brane. Intriguingly, all AdS_3 quantum black holes obey a semi-classical generalization of the reverse isoperimetric inequality, indicating quantum black holes have a maximal entropy state at fixed volume.

Quantum black holes can also have a wildly different thermal phase structure than their classical counterparts (Section 5.8). Specifically, in the case of the static quantum BTZ black hole, a large enough backreaction triggers *reentrant* phase transitions, e.g., a transition from thermal AdS to the quantum black hole back to thermal AdS. The first

of these transitions can be understood as a quantum analog of the familiar first-order Hawking–Page transition of AdS black holes, while the second transition back to thermal AdS is entirely a consequence of non-perturbative backreaction effects.

Puzzles in higher-dimensions. Section 6 briefly reviews the history and status of higher-dimensional braneworld black holes and their semi-classical interpretation. Indeed, while we focus on three-dimensional quantum black holes, the conjecture [22,34] that classical bulk black holes correspond to quantum-corrected black holes on the brane, in principle, holds in arbitrary spacetime dimensions. After assessing arguments that imply four and higher-dimensional quantum black holes must be evaporating, we describe static four-dimensional braneworld black holes and their peculiar features when viewed as quantum black holes. We conclude with a short summary regarding the holographic duals of evaporating black holes.

Applications. In Section 7, we present a non-exhaustive list of applications and possible avenues for future research using the quantum black hole constructions described in this review. Historically, braneworlds, motivated by string theory, were conceived as possible resolutions to problems in high-energy phenomenology, e.g., the hierarchy problem of the standard model of particle physics [12,13]. Although there are yet to be any experimental signatures of extra dimensions or braneworlds, the view taken here is that braneworld holography provides an invaluable framework to test ideas in (non-perturbative) semi-classical gravity and beyond. For example, prescriptions in holographic information theory, i.e., entanglement entropy and complexity, can be tested in the context of quantum black holes. Moreover, classical ideas such as cosmic censorship can be revisited using quantum black holes as a guide.

Appendices. While unnecessary to follow the core narrative of this review, we include a number of appendices to be self-contained and pedagogical. The conventions used in the majority of this review are presented in Appendix A. In Appendix B, we provide further details about holographic regularization, including a detailed derivation of the local counterterms that give rise to the induced gravity theory on the brane. Appendix C summarizes the relevant history and physics of braneworlds. Geometric elements of the C-metric utilized in the main text are given in Appendix D. Appendix E presents a derivation of the thermodynamics of the static, neutral quantum BTZ black hole using a (bulk) canonical partition function.

2. Black Holes and Backreaction in 3D: A Perturbative Analysis

2.1. Three-Dimensional Black Holes and Conical Defects

In vacuum general relativity, black holes tend to disappear when lowering the spacetime dimension from four to three. This can be understood at the level of dimensional analysis. If the only dimensionful parameter is three-dimensional Newton's constant G_3, then introducing a massive object of mass M does not introduce an additional length scale needed to characterize a black hole horizon solely in terms of its mass; indeed, $G_3 M$ is dimensionless[5]. In fact, a massive point particle in flat $(2+1)$-dimensional general relativity is a conical defect with angular deficit $\delta = 2\pi(1 - \sqrt{1 - 8G_3 M})$ and a conical singularity at the origin [28]. Moreover, while a cosmological constant Λ will introduce another length scale, this alone is not sufficient to have a black hole horizon. Gravitational attraction is also required.

To elaborate, there are black holes in asymptotically AdS_3. Namely, the Bañados–Teitelboim–Zanelli (BTZ) black hole [30,31]

$$ds^2 = -N(r)dt^2 + N^{-1}(r)dr^2 + r^2(d\phi + N_\phi dt)^2, \tag{8}$$

with lapse and shift metric functions

$$N(r) \equiv -8G_3 M + \frac{r^2}{L_3^2} + \frac{(4G_3 J)^2}{r^2}, \quad N_\phi \equiv -\frac{4G_3 J}{r^2}, \tag{9}$$

for mass M and spin J. The roots of the lapse,

$$r_{\pm}^2 = \frac{L_3^2}{2}\left[8G_3M \pm \sqrt{(8G_3M)^2 - \left(\frac{8G_3J}{L_3}\right)^2}\right], \tag{10}$$

characterize the outer (r_+) and inner/Cauchy (r_-) horizons, with $r_+ \geq r_- \geq 0$, assuming $ML_3 \geq J > 0$ to avoid naked singularities. The reason we can interpret the BTZ metric as a 'black hole' is because the negatively curved geometry of AdS_3 provides an innate geometric tendency for gravitational collapse (see, e.g., [35])[6]. Alternatively, there are no black holes in dS_3; the positively curved dS_3 background leads to an inability for collapse[7]. Consequently, a point mass in dS_3, is described by a conical defect [29] with a single cosmological horizon.

To see this latter point, consider the Kerr–dS_3 metric. The line element formally takes the same form as (8) except now with lapse and shift functions

$$N(r) \equiv 1 - 8G_3M - \frac{r^2}{R_3^2} + \frac{(4G_3J)^2}{r^2}, \quad N_\phi \equiv +\frac{4G_3J}{r^2}, \tag{11}$$

where R_3 denotes the dS_3 length scale and the '+' sign in N_ϕ denotes convention. Next, we introduce dimensionless parameters $\gamma \equiv r_+/R_3$ and $\alpha \equiv -4G_3J/\gamma R_3 = ir_-/R_3$, where $r_\pm$ are

$$r_{\pm}^2 = \frac{R_3^2}{2}\left[(1 - 8G_3M) \pm \sqrt{(1 - 8G_3M)^2 - \left(\frac{8G_3J}{R_3}\right)^2}\right], \tag{12}$$

with only a single positive root, r_+, identified as the cosmological horizon. Then, the coordinate transformation [27,29,39]

$$\tilde{t} = \gamma t + \alpha R_3 \phi, \quad \tilde{\phi} = \gamma\phi - \alpha t/R_3, \quad \tilde{r}/R_3 = \sqrt{\frac{(r/R_3)^2 + \alpha^2}{\gamma^2 + \alpha^2}} \tag{13}$$

brings the Kerr–dS_3 geometry into an empty dS_3 form, i.e.,

$$ds^2 = -\left(1 - \frac{\tilde{r}^2}{R_3^2}\right)d\tilde{t}^2 + \left(1 - \frac{\tilde{r}^2}{R_3^2}\right)^{-1} d\tilde{r}^2 + \tilde{r}^2 d\tilde{\phi}^2. \tag{14}$$

Here, however, the coordinates $(\tilde{t}, \tilde{\phi})$ do not have the same periodicity as standard dS_3, where $(t, r, \phi) \sim (t, r, \phi + 2\pi)$. Rather,

$$(\tilde{t}, \tilde{\phi}) \sim (\tilde{t} + 2\pi R_3\alpha, \tilde{\phi} + 2\pi\gamma). \tag{15}$$

Thence, Kerr–dS_3 is a conical defect geometry with angular deficit $\delta = 2\pi(1 - \gamma)$.

It is worth pointing out that the AdS_3 geometry (8) is not always a black hole. For $8G_3M < 0$, the geometry is a conical defect, taking the form of empty AdS_3 (the line element (14) with Wick rotation $R_3 = -iL_3$), with the same periodicity (15), where now $\alpha \equiv r_+/L_3$ and $\gamma \equiv 4G_3iJ/L_3$[8]. In particular, when $J = 0$, the states with $-1 < 8G_3M < 0$ correspond to conical defects with angular deficit $\delta = 2\pi(1 - \sqrt{-8G_3M})$, while for $8G_3M < -1$, the geometry has a conical excess; at $8G_3M = -1$, the BTZ geometry is exactly empty AdS_3. Furthermore, when $8G_3M < 0$ (for arbitrary J), the metric components are well defined everywhere; i.e., there is no horizon and the conical singularity at $r = 0$ is 'naked'.

2.2. Backreaction and Quantum Dressing

Another way to introduce a dimensionful parameter is to allow for quantum effects. Namely, for $\hbar \neq 0$, there exists the three-dimensional Planck length $L_P = \hbar G_3$ (though

there is no notion of Planck mass in three dimensions). The question then is whether such quantum effects can modify the classical three-dimensional geometry so as to induce a (black hole) horizon when there was none before.

Evidence of this comes from perturbatively solving the semi-classical Einstein Equation (1) for a conformally coupled scalar field Φ [26,27,40–45], which is characterized by the action

$$I = \frac{1}{16\pi G_3}\int d^3x\sqrt{-g}[R-2\Lambda] - \frac{1}{2}\int d^3x\sqrt{-g}\left[(\nabla\Phi)^2+\frac{1}{8}R\Phi^2\right]. \tag{16}$$

In such a set-up, the first step is to determine the renormalized stress tensor $\langle T_{ab}\rangle$. This is accomplished by first constructing the Green function associated with the equation of motion for the scalar field Φ in (A)dS$_3$, $(\Box - \frac{1}{8}R)\Phi = 0$. Generically, the Green function is

$$G(x,x') = \frac{1}{4\pi}\frac{1}{|x-x'|} + \frac{\lambda}{4\pi}\frac{1}{|x+x'|}, \tag{17}$$

where $\lambda = 0, 1, -1$ corresponds to the scalar field obeying transparent, Neumann, or Dirichlet boundary conditions, respectively. For non-rotating backgrounds[9] and assuming transparent boundary conditions, the renormalized stress tensor has the form

$$\langle T^a_b\rangle = \frac{\hbar F(M)}{8\pi r^3}\mathrm{diag}(1,1,-2), \tag{18}$$

where $F(M)$ is a positive function of the mass. The explicit expression for $F(M)$ is different depending on whether the background is conical (A)dS$_3$ or the BTZ geometry (see, e.g., [26,27,44,45] for details), while the radial dependence and diagonal tensorial structure will change when considering non-transparent boundary conditions [42]. In any case, the Green function of the quantum scalar field in the BTZ background is in the Hartle–Hawking state, satisfying the Kubo–Martin–Schwinger (KMS) condition at the black hole temperature [42].

Having the stress tensor (18) source the right-hand side of the semi-classical Einstein's Equation (1), one finds for the static geometry the $\mathcal{O}(L_P)$ correction to the three-dimensional metric (8) is

$$N(r) = \frac{r^2}{L_3^2} - 8G_3M - \delta g_{tt}\,, \qquad \delta g_{tt} = \frac{2L_{\rm P}F(M)}{r}\,, \tag{19}$$

for the AdS$_3$ geometries, and

$$N(r) = 1 - 8G_3M - \frac{r^2}{R_3^2} - \delta g_{tt}\,, \qquad \delta g_{tt} = \frac{2L_{\rm P}F(M)}{r}\,, \tag{20}$$

for conical dS$_3$. Notably, $\delta g_{tt} > 0$, indicating gravitational attraction [32,33][10]. This attractive effect suggests that a horizon induced due to a semi-classical backreaction might appear to dress the naked AdS$_3$ conical singularity or, in the case of conical dS$_3$, lead to a black hole horizon in addition to its classical cosmological horizon.

The 'horizon' radius, however, is proportional to the Planck length at the scale when quantum gravitational effects are expected to become important. Consequently, the above perturbative semi-classical analysis cannot be trusted, and we are not able to conclude the backreacted geometry results in a genuine horizon. This is not to say a semi-classical backreaction will always result in Planckian-sized horizons. Indeed, both gravitational and quantum effects are at play: a large $c \gg 1$ number of conformally coupled scalars results in a combined quantum effect $\propto c\hbar$ which may gravitate to yield large semi-classical black holes, i.e., those with horizon radius $\sim Gc\hbar = cL_{\rm P} \gg L_{\rm P}$, for which quantum gravity effects may be safely neglected. To verify this, the backreaction problem of a large number of fields must be non-linearly accounted for, and, thus far, perturbative methods have been

unable to accomplish this consistently. Braneworld holography provides a framework for which the backreaction problem due to a large-c holographic conformal field theory can be exactly solved.

3. Braneworld Holography and Quantum Black Holes

The perturbative analysis above suggests that a semi-classical backreaction due to quantum fields can lead to the appearance of a black hole horizon when there was none before. Due to the limitations of the perturbative approach, however, the observation is cursory at best. Since the perturbative correction to the classical geometry is on the order of the Planck scale, we cannot definitively argue that a black horizon appears. Only if there are a large-c number of quantum fields present would this conclusion be plausible. The only known framework where a solution with these requirements can be consistently achieved is braneworld holography, where one innately works in a large-c limit. Below, we summarize the relevant aspects of holographic braneworlds.

3.1. AdS/CFT Dictionary and Holographic Renormalization

The AdS/CFT correspondence [6], in its strongest form, describes a duality between a theory of gravity and conformal field theory at the level of their partition functions, as summarized by Gubser, Klebanov, Polyakov and Witten (GKPW) [46,47]

$$\left\langle e^{-\int_{\partial\mathcal{M}}\mathcal{O}\phi_{(0)}}\right\rangle_{\text{CFT}} = Z_{\text{grav}}[\phi_{(0)}]|_{\mathcal{M}}. \tag{21}$$

On the right-hand side, we have the gravitational partition function of a bulk field Φ over an asymptotically $d+1$-dimensional AdS spacetime $\mathcal{M}$, with conformal boundary $\partial\mathcal{M}$, and $\phi_{(0)}$ is the fixed boundary value of the bulk field Φ. On the left-hand side is the generating functional for the dual d-dimensional CFT living on $\partial\mathcal{M}$, where $\mathcal{O}$ is the field theory operator dual to the bulk field. Taking variations with respect to $\phi_{(0)}$ and then setting $\phi_{(0)}=0$, one can obtain correlation functions of $\mathcal{O}$, which are sourced by $\phi_{(0)}$. This equivalence of partition functions (21) is often dubbed the standard AdS/CFT dictionary, and, at least formally, it defines a model of non-perturbative quantum gravity.

One of the essential features of the AdS/CFT correspondence is that it can probe strongly coupled field theories on a non-dynamical background using weakly coupled, classical (super)gravity. This is because, typically, the holographic field theories are non-Abelian gauge theories with a gauge group of rank N and 't Hooft coupling λ, where, at large-N and $\lambda \gg 1$ (the planar-diagram limit), the dynamics are effectively classical, with $\mathcal{O}(1/N)$ corrections in the dual field theory corresponding to bulk gravity quantum corrections $\mathcal{O}(G)$[11]. More generally, the dual field theory degrees of freedom are encoded in the central charge c, which, for known holographic theories scale with N, i.e., $c \sim N^{\alpha}$ for positive, real α. Thus, the large-c limit coincides with the classical limit[12] in the bulk, and the right-hand side of the dictionary (21) may be approximately given by a sum over classical saddles $\{\Phi_i\}$

$$\lim_{c\to\infty}\left\langle e^{-\int_{\partial\mathcal{M}}\mathcal{O}\phi_{(0)}}\right\rangle_{\text{CFT}} = \sum_i e^{-I_{\text{grav}}^{\text{on-shell}}[\Phi_i]}, \tag{22}$$

where each field configuration Φ_i is a solution to the bulk classical gravity equations of motion subject to the prescribed boundary conditions[13]. A particular case of interest is to turn off all sources $\phi_{(0)}$ except those with the boundary value of the bulk metric. In such an event, at large c, it is consistent to turn off all bulk fields except the metric, such that the bulk is described by a pure theory of gravity, which is often taken to be the Einstein–Hilbert action.

Holographic Renormalization

The standard dictionary (21), however, requires special care in regard to divergences. Indeed, even at tree level (22), the gravity partition function exhibits long-distance infrared (IR) divergences, which correspond to ultraviolet (UV) divergences in the CFT correlation functions. These divergences may be removed via holographic renormalization, which is a prescription that adds appropriate local counterterms [17–21] in a minimal subtraction scheme. Since they will become relevant momentarily, let us outline the holographic renormalization procedure, leaving further computational details for Appendix B.

Consider a bulk asymptotically AdS_{d+1} spacetime $\mathcal{M}$ of curvature scale L_{d+1} and cosmological constant $\Lambda_{d+1} = -d(d-1)/2L_{d+1}^2$, which is governed by classical Einstein gravity

$$I_{\text{bulk}} = \frac{1}{16\pi G_{d+1}} \int_{\mathcal{M}} d^{d+1}x\sqrt{-\hat{g}}\left(\hat{R} - 2\Lambda_{d+1}\right) + \frac{1}{8\pi G_{d+1}} \int_{\partial\mathcal{M}} d^d x\sqrt{-h}K. \tag{23}$$

Here, G_{d+1} is the $d+1$-dimensional Newton's constant, $\hat{g}_{ab}$ is the metric endowed on $\mathcal{M}$, and K in the Gibbons–Hawking York (GHY) boundary term is the trace of the extrinsic curvature of the boundary submanifold $\partial\mathcal{M}$ endowed with induced metric h_{ij}. Working in the large-c, planar-diagram limit, the bulk gravity theory has a dual holographic description in terms of a CFT_d living on the asymptotic conformal boundary $\partial\mathcal{M}$.

Asymptotically, the bulk AdS spacetime can be cast in a Fefferman–Graham gauge [48,49] such that near the boundary

$$ds^2 = \hat{g}_{ab}dx^a dx^b = L_{d+1}^2\left(\frac{d\rho^2}{4\rho^2} + \frac{1}{\rho}g_{ij}(x,\rho)dx^i dx^j\right), \tag{24}$$

where the d-dimensional metric has the expansion $g_{ij}(x,\rho) = g_{ij}^{(0)}(x) + \rho g_{ij}^{(2)}(x) + \ldots + \rho^{d/2}g_{ij}^{(d)}(x)$. The conformal boundary is located at $\rho = 0$. By perturbatively solving the bulk Einstein's equations, the higher-order metric coefficients $g_{ij}^{(k>0)}(x)$ may be cast covariantly in terms of the metric $g_{ij}^{(0)}$ and derivatives thereof.

On shell, the bulk action (23) has IR divergences at $\rho = 0$. To isolate and regulate these divergences, we introduce an IR cutoff $\rho = \epsilon$, for $\epsilon \ll 1$, near the asymptotic boundary, and integrate over bulk coordinate ρ between $\epsilon < \rho < \rho_c$, where $\rho_c > \epsilon$ is some constant[14]. See Figure 1 for an illustration. This procedure produces a regulated bulk action,

$$I_{\text{bulk}}^{\text{reg}} = \frac{1}{16\pi G_{d+1}}\left[\int_{\rho>\epsilon} d^{d+1}x\sqrt{-\hat{g}}\left(\hat{R} - 2\Lambda_{d+1}\right) + 2\int_{\rho=\epsilon} d^d x\sqrt{-h}K\right]. \tag{25}$$

Using the perturbative expansion for $g_{ij}(x,\rho)$, the regulated action (25) may be divided into a contribution I_{div} which diverges in the limit $\epsilon \to 0$ and a finite contribution I_{fin}

$$I_{\text{bulk}}^{\text{reg}} = I_{\text{div}} + I_{\text{fin}}. \tag{26}$$

Schematically, the IR divergent contribution is (see Appendix B for details)

$$I_{\text{div}} = \frac{L_{d+1}}{16\pi G_{d+1}} \int d^d x\sqrt{g_{(0)}}\left[\epsilon^{-d/2}a_{(0)} + \epsilon^{-d/2+1}a_{(2)} + \ldots + \epsilon^{-1}a_{(d-2)} - \log\epsilon a_{(d)}\right], \tag{27}$$

with coefficients $a_{(0)}, a_{(2)}, \ldots$ that are covariant combinations of $g_{ij}^{(0)}$ and its derivatives. In terms of the boundary metric h_{ij}, it may be cast as

$$I_{\text{div}} = \frac{L_{d+1}}{16\pi G_{d+1}} \int_{\partial\mathcal{M}} d^d x\sqrt{-h}\left[\frac{2(d-1)}{L_{d+1}^2} + \frac{R}{(d-2)} + \frac{L_{d+1}^2}{(d-2)^2(d-4)}\left(R_{ij}^2 - \frac{dR^2}{4(d-1)}\right) + \ldots\right] \tag{28}$$

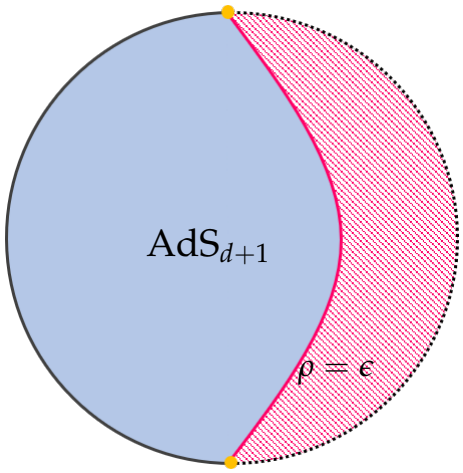

Figure 1. Holographic regularization. A constant timeslice of empty AdS$_{d+1}$. An IR cutoff surface is introduced at $\rho = \epsilon$ (thick, red line). The regulated action follows from integrating out the bulk radial coordinate from $\epsilon < \rho < \rho_c$. As $\epsilon \to 0$, the cutoff surface recedes to the AdS boundary.

where the ellipsis indicates higher-curvature and higher-derivative contributions (see, e.g., [17,21,51,52]). The finite contribution $I_{\text{fin}} \sim \mathcal{O}(\epsilon^0) + \mathcal{O}(\epsilon)...$ survives the $\epsilon \to 0$ limit, though it will also typically include higher-curvature terms. Its interpretation will be given momentarily.

At this stage, the renormalized action is obtained by minimal subtraction,

$$I^{\text{ren}}_{\text{bulk}} = \lim_{\epsilon \to 0} (I^{\text{reg}}_{\text{bulk}} + I_{\text{ct}}), \tag{29}$$

where a local counterterm action has been introduced, $I_{\text{ct}} = -I_{\text{div}}$, to precisely cancel the IR divergences. Then, via the standard AdS/CFT dictionary, variations with respect to the metric h_{ij} of the renormalized action yields the quantum expectation value of the stress tensor of the holographic CFT,

$$\langle T^{\text{CFT}}_{ij} \rangle = \lim_{\epsilon \to 0} \left(-\frac{2}{\sqrt{\hat{g}(x,\rho)}} \frac{\delta I^{\text{ren}}_{\text{bulk}}}{\delta \hat{g}^{ij}(x,\epsilon)} \right) \equiv -\frac{2}{\sqrt{h}} \frac{\delta W_{\text{CFT}}[h]}{\delta h^{ij}}, \tag{30}$$

such that the renormalized bulk action is identified with the quantum effective action of the CFT, $W_{\text{CFT}}[h]$. Thus, at leading order, the finite action I_{fin} characterizes the CFT.

3.2. Braneworld Holography

In braneworld holography [11], the bulk IR cutoff surface $\partial\mathcal{M}$ is instead replaced by a d-dimensional end-of-the-world (ETW) Randall–Sundrum [13,14] or Karch–Randall [15,16] brane $\mathcal{B}$ at a small fixed distance away from the boundary (for a lightning review of braneworlds, see Appendix C). Hence, the physical space is cut off at the ETW brane and there are no longer IR divergences to be removed. For simplicity, assume the brane is purely tensional, having an action

$$I_\tau = -\tau \int_{\mathcal{B}} d^d x \sqrt{-h}, \tag{31}$$

where τ is the brane tension. Since a portion of the bulk has been removed, to complete the space, a second copy of AdS$_{d+1}$ with a brane is sewn to the first cutoff geometry along the cutoff surface (see Figure 2). This surgical procedure leads to a discontinuity in the extrinsic curvature K_{ij} across the junction. The Israel junction conditons [53] relate this discontinuity to the brane stress tensor S_{ij} via

$$\Delta K_{ij} - h_{ij} \Delta K = 8\pi G_{d+1} S_{ij} = -8\pi G_{d+1} \tau h_{ij}, \tag{32}$$

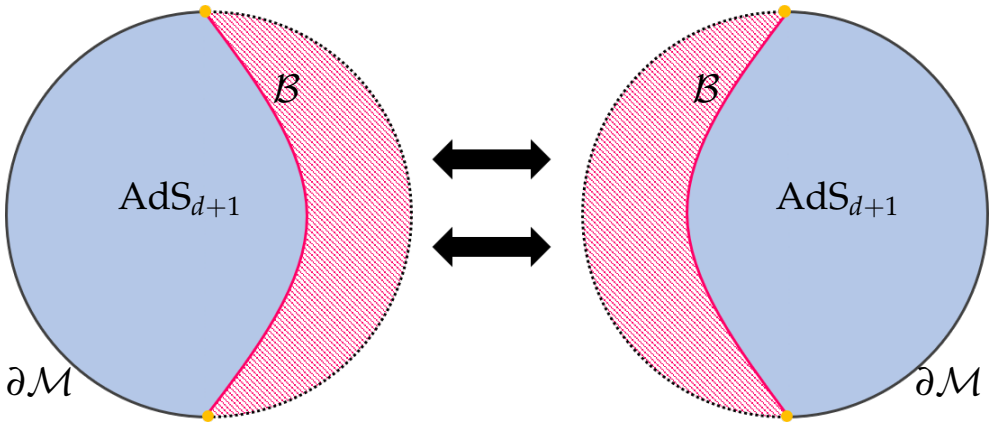

Figure 2. Braneworld surgery. Replace the IR cutoff surface with an end-of-the-world (Karch–Randall) brane $\mathcal{B}$ (thick, red line), excising the shaded region from the bulk spacetime. To complete the space, two copies of the spacetime are glued along $\mathcal{B}$, making the brane double-sided. A BCFT_d lives on the AdS_{d+1} boundary $\partial\mathcal{M}$ and is coupled to a defect CFT_{d-1} where $\mathcal{B}$ intersects the AdS boundary (yellow dot). The induced brane theory is characterized by a specific higher-derivative gravity coupled to a CFT_d with a UV cutoff.

where $\Delta K_{ij} = K^+_{ij} - K^-_{ij}$ denotes the difference between the extrinsic curvature across either '+' and '−' sides of the brane (here, we take $K^+_{ij} = -K^-_{ij}$ such that $\Delta K_{ij} = 2K_{ij}$), and the last equality follows from taking the metric h_{ij} variation of the brane action (31), i.e., $S_{ij} \equiv -\frac{2}{\sqrt{-h}}\frac{\delta I_\tau}{\delta h^{ij}}$. Thus, the location of the brane in the completed space is determined by the junction conditions (32), which in the present case amounts to tuning the brane tension τ.

Moreover, unlike the metric on the AdS boundary, the brane metric is dynamical, and it is governed by a holographically induced higher-curvature theory of gravity coupled to matter. Precisely, the induced brane theory is found by adding to the bulk theory (23) the brane action (31). Integrating out the bulk up to the ETW brane $\mathcal{B}$, as in holographic regularization, leads to an effective induced theory with action I

$$I \equiv I_{\mathrm{Bgrav}}[\mathcal{B}] + I_{\mathrm{CFT}}[\mathcal{B}], \tag{33}$$

where the brane gravity theory is (cf. [52,54])

$$\begin{aligned} I_{\mathrm{Bgrav}} &= 2I_{\mathrm{div}} + I_\tau \\ &= \frac{1}{16\pi G_d}\int_{\mathcal{B}} d^d x\sqrt{-h}\left[R - 2\Lambda_d + \frac{L^2_{d+1}}{(d-4)(d-2)}\left(R^2_{ij} - \frac{dR^2}{4(d-1)}\right) + \cdots\right], \end{aligned} \tag{34}$$

where the factor of two accounts for integrating out the bulk on both sides of the brane, and the ellipsis corresponds to higher curvature densities, entering with higher powers of L^2_{d+1}. So far, the higher-derivative contributions have been computed up to quintic order in curvature for arbitrary d and sextic order for $d = 3$ [52]. In principle, these results could be extended to arbitrary order, even though the calculations might be practically prohibitive. Here, G_d represents the effective brane Newton's constant induced from the bulk

$$G_d = \frac{d-2}{2L_{d+1}} G_{d+1}, \tag{35}$$

and $\Lambda_d = -(d-1)(d-2)/2L^2_d$ is an effective brane cosmological constant with an induced curvature scale L_d

$$\frac{1}{L^2_d} = \frac{2}{L^2_{d+1}}\left(1 - \frac{4\pi G_{d+1} L_{d+1}}{d-1}\tau\right). \tag{36}$$

As written, it has been assumed the brane has a negative cosmological constant such that the bulk theory is coupled to a Karch–Randall brane [15]. When coupled to a Randall–Sundrum brane, the brane cosmological constant can be tuned to be positive or zero, as will be considered later.

Due to the presence of higher-derivative terms in the induced action (34), the brane theory of gravity is in general 'massive' since a massive graviton bound state will localize on the brane [15]. This brane graviton mass, however, will become negligible for a brane very near the boundary. Furthermore, general higher-derivative theories of gravity are often sick since they are typically accompanied by ghosts. In the present case, however, provided the series of higher-derivative terms is not truncated, the brane theory is not expected to inherit these usual pathologies, since the starting bulk theory and the procedure of integrating out bulk degrees of freedom are not pathological.

The action $I_{\rm CFT}[\mathcal{B}]$, meanwhile, describes the CFT theory, now living on the brane, and corresponds to the finite contribution to the regulated bulk action upon integrating out the bulk. To see this, note that upon integrating out the bulk degrees of freedom on both sides of the brane, we have

$$I \equiv 2I^{\rm reg}_{\rm bulk} + I_\tau. \tag{37}$$

Then, add and subtract the $2I_{\rm div}$, giving

$$I \equiv (2I_{\rm div} + I_\tau) + (2I^{\rm reg}_{\rm bulk} - 2I_{\rm div}), \tag{38}$$

where the first term in parentheses is recognized as $I_{\rm Bgrav}$ (34). The second term is simply $2I_{\rm fin} \equiv I_{\rm CFT}$, which, to leading order in the cutoff ϵ, is identified with the quantum effective action of the CFT, $I_{\rm CFT} = W_{\rm CFT} + \mathcal{O}(\epsilon)$. In most cases of interest, we work in the limit that ϵ is small, i.e., when the brane is close to the (now fictitious) AdS$_{d+1}$ boundary, such that the matter on the brane has an approximate description as a large-c holographic CFT. Roughly speaking, a portion of the conformal AdS$_{d+1}$ boundary has been pushed into the bulk, such that the dual CFT$_d$ is now residing on the brane—however, this comes at a cost. Since the brane represents an IR cutoff surface, the CFT has a UV cutoff [55,56]. The cutoff, from the perspective of the boundary $g^{(0)}_{ij}$ metric, is denoted by ϵ, while from the induced brane metric $h_{ij} = (L^2_{d+1}/\epsilon)g^{(0)}_{ij}$, the UV cutoff of the CFT is $\delta_{\rm UV} = L_{d+1}$.

3.3. Double Holography

A Karch–Randall braneworld[15] has three equivalent descriptions: (i) *bulk*, (ii) *intermediate*, and (iii) *boundary*.

- **Bulk:** The bulk perspective is that of classical dynamical gravity in AdS$_{d+1}$ coupled to an asymptotically AdS$_d$ ETW brane of tension τ. The simplest set-up assumes Einstein gravity plus a purely tensional brane; however, it is in principle possible to include higher-curvature corrections or fields to the bulk or brane actions. Israel junction conditions determine the location of the brane in the bulk, such that for a purely tensional brane, tuning the tension constitutes changing the position of the brane.
- **Intermediate:** The intermediate brane viewpoint describes induced dynamical gravity coupled to a UV cutoff CFT$_d$ UV, which further communicates with a boundary CFT$_d$ (BCFT$_d$) via transparent boundary conditions. Bulk graviton fluctuations localize on the brane [13,14]. A subset of these graviton modes are light states with mass controlled by the tension; hence, the induced brane theory is an example of a massive theory of gravity. The remaining bulk graviton modes appear as a tower of Kaluza–Klein modes with masses set by the effective AdS$_d$ brane length scale $1/L_d$.
- **Boundary:** Holographically, the bulk system has a dual description in terms of a CFT$_d$ with a boundary (where the brane intersects the AdS$_{d+1}$ boundary), i.e., a boundary CFT$_d$. This set-up constitutes AdS/BCFT [57,58]. This perspective emerges when the brane gravity itself has a dual description in terms of a $(d-1)$-dimensional conformal defect. Upon replacing the brane gravity by a conformal defect (by integrating out

the bulk and brane), the boundary perspective is characterized by the CFT_d on a fixed background, which is coupled to the defect. The boundary perspective is thus a UV/microscopic description of the bulk/brane gravity viewpoints.

Specific models exhibiting this type of 'double holography'—holographic spacetimes dual to a BCFT that have three equivalent descriptions—have top–down string theoretic realizations [59]. We, however, will work with bottom–up constructions, for which their doubly holographic nature will play an important role in studying aspects of holographic entanglement and complexity, as we summarize in Section 7[16].

3.4. Holographic Quantum Black Holes: A Conjecture

Two equivalent ways to interpret the theory (33) are as follows. From the bulk perspective, I characterizes a theory of a $(d+1)$-dimensional system with dynamics ruled by Einstein gravity coupled to an end-of-the-world brane obeying appropriate boundary conditions. Meanwhile, from the (intermediate) brane perspective, I represents a specific higher-curvature gravity in d dimensions coupled to a large-c cutoff CFT that backreacts on the brane metric h_{ij}. The tower of higher-order derivative terms to the Einstein–Hilbert contribution represents quantum corrections induced by the backreaction of the CFT_d. We refer to this higher-derivative tower as 'corrections' because in most cases of interest, one treats the brane action as an effective theory, assuming $L_d \gg L_{d+1}$ and guaranteeing the higher-derivative terms are suppressed by at least $\mathcal{O}(L_{d+1}^2/L_d^2)$[17]. Consistency between these two viewpoints implies solutions to the classical bulk equations satisfying proper brane boundary conditions exactly correspond to solutions to the semi-classical field equations on the brane. Therefore, the classical $(d+1)$-dimensional geometry encodes the entire series of quantum corrections to the d-dimensional brane geometry, accounting for all orders in the backreaction. Thus, holographic braneworlds provide a distinct computational advantage: rather than directly solving a complicated semi-classical theory of gravity, one may instead solve simpler classical gravitational field equations one dimension higher.

This philosophy, combined with the observation [62] that the $\sim 1/r^3$ corrections to the four-dimensional Newtonian potential due to massive Kaluza–Klein modes in the Randall–Sundrum model precisely coincide with corrections induced by one-loop quantum effects of the graviton propagator [63], suggests braneworld black holes from the brane perspective are quantum-corrected geometries. These insights in part motivated Emparan, Fabbri and Kaloper [22] to make the following conjecture:

Conjecture: Classical black holes which localize on a brane in AdS_{d+1} exactly map to d-dimensional quantum-corrected black holes including all orders of backreaction.

Such quantum-corrected black holes are dubbed 'quantum' black holes, though, they technically are solutions to the semi-classical theory induced on the brane. An illustration is given in Figure 3.

Explicit tests of this proposal include the exact localized AdS_4 braneworld black holes discovered by Emparan, Horowitz, and Myers [23,24] with their projection onto the brane being reinterpreted as three-dimensional quantum black holes[18]. As we will see below, at least for the neutral, static geometries, the exact quantum black holes receive the same modifications to their geometry as suggested by the (non-holographic) perturbative analysis summarized in Section 2. The rotating and charged holographic quantum black holes, meanwhile, do not match the non-holographic perturbatively corrected counterparts (cf. [27,40,45]). In particular, a perturbative backreaction to the rotating BTZ black hole or Kerr–dS_3 solution due to a conformally coupled scalar field leads to a wildly more complicated radial dependence than that of a holographic CFT and a quantum stress tensor with a qualitatively different singularity structure, having an impact on the status of strong cosmic censorship. The remainder of this review will focus on these three-dimensional quantum black holes.

Before moving on to analyze the three-dimensional black holes, it is worth briefly commenting on the status of the proposal [22] in higher and lower dimensions. For brane

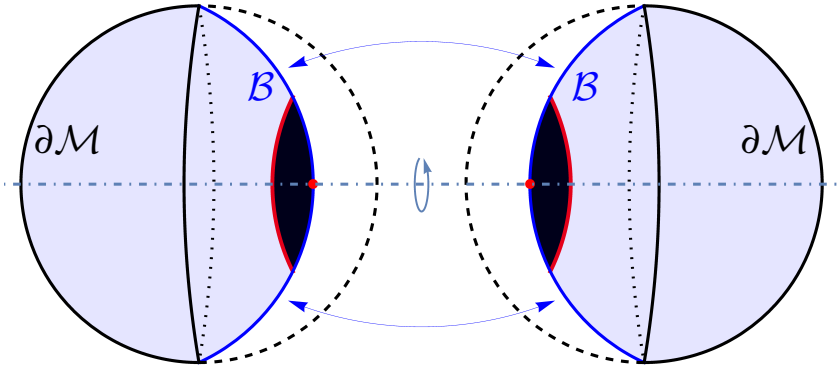

Figure 3. Braneworld black hole. The bulk white region is excised down to the brane $\mathcal{B}$ (blue line) and glued to a copy of itself. A bulk black hole with an event horizon (red line) is intersected by (depicted here, Karch–Randall) brane, inducing a horizon on the brane.

dimensions $d \geq 4$, the most physically relevant case being $d = 4$, there are still no known exact stationary solutions (see [64] for a review of analytic and numerical braneworld black holes)[19]. In fact, there is a no-go theorem [66] which alleges the exterior geometry on the brane in $d \geq 4$ cannot be static. The lack of exact solutions makes identifying the specific state of the CFT_d more difficult. In [22,34], for $d \geq 4$, it was qualitatively argued the obstruction to having static quantum black holes can be understood as a consequence of backreaction due to Hawking effects, such that any black hole that localizes on the brane must evaporate. However, static braneworld black holes in higher dimensions have been found numerically, e.g., [67–72], and the qualitative argument was shown to have flaws [69]. We review the status of the conjecture for higher-dimensional quantum black holes in Section 6.

In $d = 2$ dimensions, the induced theory on the brane is characterized by a matter quantum effective action, which to leading order in expansion in the UV cutoff is characterized by the Polyakov action [4] coupled to a topological term and a cosmological constant. The precise form of the brane action likewise follows from a modification of holographic renormalization [19,50,73], where the counterterm action exactly truncates (see also [74,75]). Such a theory does not admit black hole solutions by itself. Thus, in order to find two-dimensional braneworld black holes, the theory must be modified by including a Dvali–Gabadadze–Porrati (DGP) term [76] to the tensional brane action (31). For example, one may replace the brane action (31) with a non-minimally coupled dilaton theory, e.g., Jackiw–Teitelboim (JT) gravity [77,78], as seen in [54][20]. Such dilaton models of gravity admit exactly solvable black hole solutions including a semi-classical backreaction, e.g., [84–87].

Lastly, let us make some general remarks about static black holes localized on the brane. First, a brane with non-vanishing tension is an accelerated trajectory with respect to the bulk, i.e., the brane does not undergo geodesic motion. Thus, a black hole which localizes on the brane is in an accelerating frame, and it is the same for any observer glued to the brane. Next, a static black hole stuck to the brane will neither eat the brane nor slide off it. The reason is as follows [88]. To be static, the brane intersects the black hole orthogonally; otherwise, the black hole would grow by eating the brane[21]. Consequently, the brane bends to remain orthogonal to the black hole if the latter is being pulled off the brane (by, say, another black hole in the bulk). Thus, a static black hole localized on the brane experiences a restoring force due to the tension of the brane and does not slide off. Evaporating black holes, on the other hand, eventually slide off the brane.

4. Quantum Black Hole Taxonomy

Having laid the groundwork of braneworld holography in general dimensions, here we focus on the $d = 3$ case, i.e., a holographic AdS_4 bulk with a three-dimensional ETW brane. In this set-up, it is possible to write down a host of analytic braneworld black hole

solutions to the bulk field equations plus Israel junction conditions. From the brane perspective, these black holes may be interpreted as 'quantum' black holes—those which exactly solve the induced semi-classical brane gravity including all orders of backreaction due to a large-c holographic CFT_3 with a UV cutoff. Below, we classify known quantum black holes in three-dimensional (A)dS and Minkowski backgrounds. These include the quantum BTZ family of black holes (static, rotating, and charged) and their de Sitter/Minkowski analogs. Each of these braneworld black holes arise from specific parametrizations of the AdS_4 C-metric coupled to a Randall–Sundrum or Karch–Randall brane.

4.1. Bulk Geometry: AdS C-Metric

In this review, the bulk AdS_4 gravity is taken to be Einstein–Maxwell theory. The most general metric solving the Einstein–Maxwell$-\Lambda$ gravity is the Plebański–Demiański type-D metric [89]. We are interested in a specific sub-class of solutions, namely the AdS_4 C-metric, which can be interpreted as a single or pair of accelerating black holes in an AdS_4 background, depending on the parameters of the solution. Here, we summarize the essentials for the braneworld construction (see Appendix D for a longer review). In particular, the neutral, non-rotating C-metric in Boyer–Lindquist-like coordinates has a line element (primarily following the conventions of [25])

$$ds^2 = \frac{\ell^2}{(\ell + xr)^2}\left[-H(r)dt^2 + \frac{dr^2}{H(r)} + r^2\left(\frac{dx^2}{G(x)} + G(x)d\phi^2\right)\right], \tag{39}$$

with metric functions

$$H(r) = \frac{r^2}{\ell_3^2} + \kappa - \frac{\mu\ell}{r}, \qquad G(x) = 1 - \kappa x^2 - \mu x^3. \tag{40}$$

We treat t and r as time and radial coordinates, respectively. However, the range for r is not the usual one for Boyer–Lindquist coordinates, with the AdS_4 conformal boundary shifted from its familiar location, $r = \infty$. Rather, the position of the boundary depends on the coordinate x: for some values of x, the conformal boundary is closer than infinity, while for other values of x, the boundary is 'further' than infinity. That is, the radial coordinate has range $r \in (-\infty, r_{\text{bdry}}) \cup (0, \infty)$, with $xr_{\text{bdry}} = -\ell$ being the location of the asymptotic AdS_4 boundary, where the conformal factor diverges (this unfamiliar range for the radial coordinate can be seen more readily using the (t, x, y, ϕ) coordinates in Appendix D). Further, (x, ϕ) are angular variables, with $x \in [-1, 1]$ analogous to $\cos\theta$, and ϕ is a general azimuthal coordinate whose periodicity will be discussed below.

Here, μ, κ, ℓ and ℓ_3 are real parameters characterizing the solution whose physical meaning will become more apparent momentarily. For now, $\kappa = \pm 1, 0$ describes different possible slicings of the brane geometry, e.g., $\kappa = -1$ will recover the classical BTZ geometry on the brane; however, here, we leave κ unspecified, thereby describing a family of braneworld black holes. The non-negative parameter μ is related to the mass of the bulk black hole. When interpreted as an accelerating black hole, the parameter $\ell \geq 0$ equals the inverse acceleration, $A = \ell^{-1}$, and is related to the bulk AdS_4 length scale L_4 via

$$L_4 = \left(\frac{1}{\ell^2} + \frac{1}{\ell_3^2}\right)^{-1/2}, \tag{41}$$

Lastly, the positive parameter ℓ_3 will be related to the AdS_3 brane curvature scale, however, with $0 \leq \ell < \infty$, such that $\ell_3 > L_4$.

To gain further intuition for the global aspects of the metric (39), first set $\mu = 0$ and perform the coordinate transformation [25]

$$\cosh(\sigma) = \frac{\ell_3}{L_4}\frac{1}{|1+\frac{rx}{\ell}|}\sqrt{1+\frac{r^2x^2}{\ell_3^2}}, \qquad \hat{r} = r\sqrt{\frac{1-\kappa x^2}{1+\frac{r^2x^2}{\ell_3^2}}}. \tag{42}$$

This brings the C-metric line element (39) to the form

$$ds^2 = L_4^2 d\sigma^2 + \frac{L_4^2}{\ell_3^2}\cosh^2(\sigma)\left[-\left(\kappa+\frac{\hat{r}^2}{\ell_3^2}\right)dt^2 + \left(\kappa+\frac{\hat{r}^2}{\ell_3^2}\right)^{-1}d\hat{r}^2 + \hat{r}^2 d\phi^2\right], \tag{43}$$

which is recognized to be empty AdS_4, which is foliated by AdS_3 slices with radius $L_4\cosh(\sigma)$ at constant σ. Written this way, the role of κ becomes apparent: for constant σ, $\kappa = +1, -1$ and 0, respectively, correspond to global AdS_3, BTZ and Poincaré AdS_3.

To obtain a better sense for the parameter ℓ and why the geometry (39) describes a black hole, perform the parameter and coordinate rescalings $\mu = 2m/\ell$ and $r = \ell_3\rho/\ell$. Keeping m, L_4, and ρ finite, the limit $\ell \to \infty$ results in

$$ds^2 = -f(\rho)dt^2 + f^{-1}(\rho)d\rho^2 + \rho^2\left(\frac{dx^2}{(1-\kappa x^2)} + (1-\kappa x^2)d\phi^2\right), \quad f(\rho) = \kappa + \frac{\rho^2}{L_4^2} - \frac{2m}{\rho}, \tag{44}$$

the metric for static, neutral AdS_4 black holes (further clarified upon transforming $x = \cos\theta$). Since $\ell^{-1} = A$, the limiting geometry (44) shows the acceleration distorts spherical surfaces parametrized by (x, ϕ).

4.1.1. Horizons and Bulk Regularity

The limiting geometry (44) also shows black holes appear for $\mu \neq 0$. More generally, whether the C-metric (39) has a black hole depends on the root structure of the metric functions (40). In particular, the roots of $H(r)$ correspond to Killing horizons generated by the time translation Killing vector ∂_t, where we desire positive roots if we are to describe physical black hole horizons. Since the system is accelerating, it will also have non-compact Rindler-like acceleration horizons. To rid ourselves of the acceleration horizon, it is sufficient to work in the case where $\ell > L_4$. With this restriction, $H(r)$ has a single positive root r_+ representing a black hole horizon[22], and the C-metric describes a single 'slowly accelerating' black hole suspended away from the center of AdS_4 by a cosmic string attached at the horizon [90]. As with other spherical surfaces, the acceleration distorts the horizon into a conical shape.

Real roots of $G(x)$, meanwhile, correspond to symmetry axes of the Killing vector $\xi^a = \partial^a_\phi$, i.e., $\xi^2 \sim G(x)$, vanishing at a zero of $G(x)$. These roots characterize the geometry of the horizon in the bulk. To ensure a finite black hole horizon in the bulk, one must be in the parameter space where there exists at least one positive root of $G(x)$, the smallest of which will be denoted x_1, and then work in the restricted range $0 \leq x \leq x_1$. The general strategy is the following [23,24]. Treat the root x_1 as a primary parameter while μ is derived from x_1 via $G(x_1) = 0$, i.e.,

$$\mu = \frac{1-\kappa x_1^2}{x_1^3}. \tag{45}$$

The desired parameter range follows from taking $x_1 > 0$ and

$$x_1 \in (0, 1] \quad \text{for} \quad \kappa = +1, \tag{46}$$

$$x_1 \in (0, \infty) \quad \text{for} \quad \kappa = -1, 0. \tag{47}$$

Observe μ monotonically decreases from $+\infty$ to zero, where $\mu = 0$ coincides with the upper limit of x_1, e.g., when $\kappa = +1$, $\mu \to 0$ as $x_1 \to 1$.

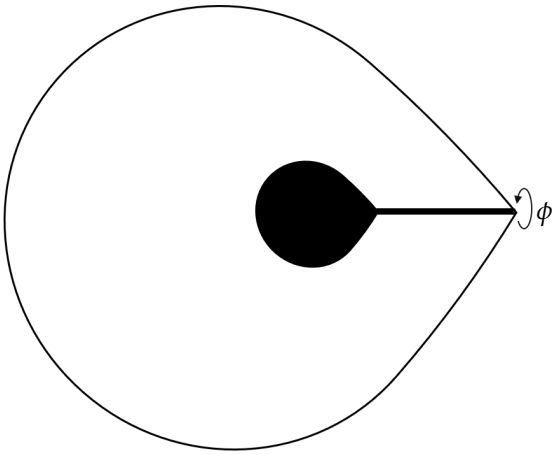

Figure 4. Accelerating black hole. A constant t and ϕ slice of the AdS_4 C-metric in the 'slow acceleration' limit. Conical singularities in the C-metric distort the black hole horizon, giving it a conical shape at one pole where a cosmic string is attached. The string pulls the black hole toward the conformal boundary, suspending it away from the center.

Further, for the range of μ and κ we are interested in, $G(x)$ has three distinct zeros, each of which leads to a distinct conical singularity. The conical singularity at $x = x_1$, for example, is removed via the identification

$$\phi \sim \phi + \Delta\phi, \qquad \Delta\phi = \frac{4\pi}{|G'(x_1)|} = \frac{4\pi x_1}{3 - \kappa x_1^2}. \tag{48}$$

We see for the range of x_1, the function $G'(x_1) = -\frac{3-\kappa x_1^2}{x_1} < 0$, and that $\Delta\phi$ is independent of ℓ and ℓ_3. Moreover, $\Delta\phi$ grows monotonically from 0 to 2π. Fixing the period of ϕ in this way, the spacetime will have conical singularities at the remaining roots of $G(x)$. The effect of these conical singularities is a distortion to the black hole horizon, which may be viewed as a cosmic string with a tension proportional to the angular deficit pulling the black hole away from the center of AdS_4 toward the boundary, generating the black hole acceleration (see Figure 4). Below, we will see how the spacetime surgery used to construct a $\mathbb{Z}_2$ braneworld will eliminate these conical singularities from the surgically complete bulk geometry.

4.1.2. Karch–Randall Braneworld Construction

The most advantageous geometric feature of the C-metric (39), for any μ and κ, is that the $x = 0$ timelike hypersurface is *umbilic*. That is, the extrinsic curvature K_{ij} of the hypersurface is proportional to the induced metric h_{ij} on $x = 0$. In particular, the outward unit normal to timelike surfaces of constant x is $n^i = -\left(\frac{x}{\ell} + \frac{1}{r}\right)\sqrt{G(x)}\partial_x^i$, such that[23] (see Appendix D.4)

$$K_{ij} = \frac{1}{\ell} h_{ij}, \tag{49}$$

at $x = 0$. Umbilic surfaces automatically satisfy the Israel junction conditions (32). In this case, upon substituting (49), a brane at $x = 0$ has tension

$$\tau = \frac{1}{2\pi G_4 \ell}. \tag{50}$$

Thus, the tension is proportional to the acceleration of the bulk black hole. The tensionless limit corresponds to $\ell \to \infty$, where $\ell_3 \to L_4$ by virtue of (41).

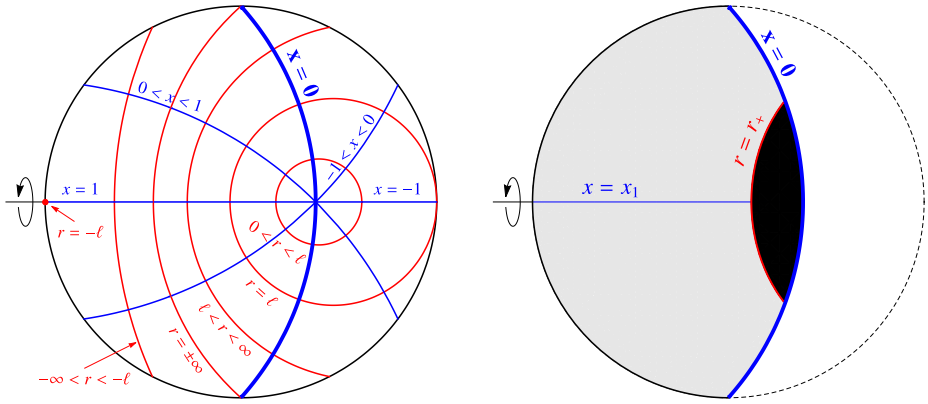

($\mu = 0$) ($\mu \neq 0$)

Figure 5. Karch–Randall braneworld. **Left**: A constant t and ϕ slice of the AdS_4 C-metric with $\mu = 0$ and $\kappa = +1$ (Poincaré disc). Lines of constant x are denoted in blue, while lines of constant r are denoted in red. The ϕ-axis of rotation is at $x = \pm 1$. **Right**: Schematic of a Karch–Randall ETW brane at $x = 0$ with a static black hole ($\mu \neq 0$). Only the (gray) shaded region, $0 \leq x \leq x_1$, is kept where $x = x_1$ is the ϕ-axis of rotation. To complete the space, a second copy of the shaded region is glued along $x = 0$, resulting in a $\mathbb{Z}_2$-symmetric double-sided braneworld.

To see how tuning the tension amounts to changing the position of the brane, recall the empty AdS_4 metric (43). The $x = 0$ brane amounts to surfaces of fixed $\sigma = \sigma_b$ obeying

$$\cosh(\sigma_b) = \frac{\ell_3}{L_4} = \sqrt{1 + \frac{\ell_3^2}{\ell^2}}, \tag{51}$$

and the brane geometry is AdS_3 with curvature radius ℓ_3, i.e., a Karch–Randall brane. In the tensionless limit, $\ell \to \infty$, then $\sigma_b = 0$, cutting the bulk in half through the equator. Alternatively, as the tension becomes larger, $\ell \to 0$, it follows $\sigma_b \to \infty$, i.e., the brane is pushed to the asymptotic boundary of AdS_4. The solution is valid for all $0 \leq \ell < \infty$; however, we will be primarily interested in the case where the brane is near the AdS_4 boundary (before it has been removed via the ETW brane). See Figure 5 for an illustration (and refer to Appendix D.5 for details projecting to the Poincaré disk).

More generally, the induced metric at $x = 0$ simply follows from setting $x = 0$ in the bulk C-metric (39), resulting in

$$ds^2|_{x=0} = -\left(\frac{r^2}{\ell_3^2} + \kappa - \frac{\mu\ell}{r}\right)dt^2 + \left(\frac{r^2}{\ell_3^2} + \kappa - \frac{\mu\ell}{r}\right)^{-1} dr^2 + r^2 d\phi^2, \tag{52}$$

For $\kappa = -1$, the boundary geometry ($\ell \to 0$) has a black hole with horizon radius $r_+ = \ell_3$. For $\ell \neq 0$, it is clear the geometry (52) is capable of describing a static black hole, which will ultimately be understood as the quantum BTZ black hole as we detail below.

Recall the bulk geometry will retain conical singularities at the remaining roots of $G(x)$ (not $x = x_1$). As it happens, there are no conical singularities in the restricted range $0 \leq x \leq x_1$; for $\mu > 0$, the remaining conical singularities live in the range $x < 0$. Then, treating the $x = 0$ hypersurface as a cutoff brane, excising the $x < 0$ region leads to a spacetime free of conical singularities. To complete the space, a second copy of the $0 \leq x \leq x_1$ region is glued along $x = 0$, resulting in a $\mathbb{Z}_2$-symmetric double-sided Karch–Randall braneworld. Further, with the conical singularities removed, the final bulk solution no longer has a cosmic string. Nonetheless, the static black hole attached to the brane is in an accelerated frame.

4.1.3. Karch–Randall Braneworld Holography

Applying the formalism of Section 3, the induced brane action is (setting $d = 3$ in (33))

$$I = \frac{1}{16\pi G_3}\int_{\mathcal{B}} d^3x\sqrt{-h}\left[R - 2\Lambda_3 + L_4^2\left(\frac{3}{8}R^2 - R_{ij}^2\right) + ...\right] + I_{\text{CFT}}, \tag{53}$$

with induced Newton's constant

$$G_3 = \frac{G_4}{2L_4} \tag{54}$$

and effective (AdS_3) brane cosmological constant and curvature scale,

$$\Lambda_3 = -\frac{1}{L_3^2}, \qquad \frac{1}{L_3^2} = \frac{2}{L_4^2}\left(1 - \frac{L_4}{\ell}\right), \tag{55}$$

where we used tension (50). Note that while L_3 appears in the action, the solutions on the brane are characterized by ℓ_3.

In fact, we will primarily be interested in the case when $L_3 \approx \ell_3$. This is because we are interested in the case when the three-dimensional graviton becomes effectively massless, i.e., when the brane is near the boundary. Hence, using the bulk length scale (41), it follows

$$\frac{1}{L_3^2} = \frac{1}{\ell_3^2}\left[1 + \frac{\ell^2}{4\ell_3^2} + \mathcal{O}\left(\frac{\ell^4}{\ell_3^4} + ...\right)\right], \tag{56}$$

with $\ell \sim L_4 \ll \ell_3$. In this limit, the induced theory is

$$I = \frac{1}{16\pi G_3}\int_{\mathcal{B}} d^3x\sqrt{-h}\left[R + \frac{2}{\ell_3^2} + \ell^2\left(\frac{3}{8}R^2 - R_{ij}^2\right) + ...\right] + I_{\text{CFT}}, \tag{57}$$

such that the higher-curvature expansion can be viewed as an expansion in an effective cutoff scale ℓ. Notice higher-curvature corrections enter at quadratic order.

The parameter ℓ also features into the coupling to the gravity theory of the cutoff CFT_3 on the brane. To see this, first note the central charge c_3 of the CFT_3 is normalized such that

$$c_3 = \frac{L_4^2}{G_4} = \frac{\ell}{2G_3\sqrt{1+\nu^2}}, \tag{58}$$

where we introduced the parameter $\nu \equiv \ell/\ell_3$. Expanding for small (ℓ/ℓ_3) gives

$$2c_3G_3 = L_4 \approx \ell\left(1 - \frac{\ell^2}{2\ell_3^2} + \frac{3}{8}\frac{\ell^4}{\ell_3^4} + ...\right), \tag{59}$$

and $c_3 \sim \frac{\ell}{G_3}$, which enters at a linear order in ℓ. Thus, the matter contributions enter at order $\mathcal{O}(\ell)$, while higher-curvature corrections appear at $\mathcal{O}(\ell^2)$. Proceeding, the typical value of I_{CFT} is $|I_{\text{CFT}}| \sim c_3$, while the typical value of the gravitational part of the action (53) is $|I_{\mathcal{B}_{\text{grav}}}| \sim \frac{L_3}{G_3}$. Combined, this leads to an effective dimensionless coupling g_{eff} quantifying the size of the effects the CFT_3 has on the brane geometry [91]

$$g_{\text{eff}} \sim \frac{|I_{\text{CFT}}|}{|I_{\mathcal{B}_{\text{grav}}}|} \sim \frac{G_3c_3}{L_3}. \tag{60}$$

Thus, for small $\ell < \ell_3$, we see $g_{\text{eff}} \approx \nu \ll 1$, backreaction effects are 'small', and the induced theory is effectively characterized by the action (57). Further, from (59), we see for a fixed c_3, gravity becomes weak ($G_3 \to 0$) as $\ell \to 0$. Alternatively, when $\nu \geq 1$, backreaction effects are said to be large.

It is worth comparing the cutoff length scale to the three-dimensional Planck length $L_{\rm P} = \hbar G_3$ (where here, we have temporarily restored factors of $\hbar$). From (59), it follows

$$\ell \sim c_3 \hbar G_3 = c_3 L_{\rm P} \gg L_{\rm P}, \tag{61}$$

since the holographic cutoff CFT_3 obeys $c_3 \gg 1$[24]. Recalling the induced brane metric (52), notice the blackening factor includes a $\mathcal{O}(r^{-1})$ term which goes like $\mu\ell$. We can anticipate this term as a semi-classical correction which sets the size of the braneworld black hole to be much larger than the Planck length.

4.2. Quantum BTZ Black Holes

Let us now delve into the geometry of quantum black holes. We begin with the simpler neutral, static quantum BTZ solution to establish its essential features, which we later enrich by adding rotation and charge.

4.2.1. Static Quantum BTZ

Recall the induced geometry at $x = 0$ (52). Naively, we might refer to this as the quantum black hole; however, the angular coordinate ϕ has period $\Delta\phi$ (48). We thus rescale coordinates (t, r, ϕ) to put the naive metric (52) in canonically normalized coordinates $(\bar{t}, \bar{r}, \bar{\phi})$. Specifically,

$$t = \eta \bar{t}\,, \qquad r = \frac{\bar{r}}{\eta}\,, \qquad \phi = \eta\bar{\phi}\,, \tag{62}$$

with

$$\eta \equiv \frac{\Delta\phi}{2\pi} = \frac{2x_1}{3 - \kappa x_1^2}\,. \tag{63}$$

The line element for the brane metric is now

$$ds^2_{\rm qBTZ} = -\left(\frac{\bar{r}^2}{\ell_3^2} - 8\mathcal{G}_3 M - \frac{\ell F(M)}{\bar{r}}\right)d\bar{t}^2 + \left(\frac{\bar{r}^2}{\ell_3^2} - 8\mathcal{G}_3 M - \frac{\ell F(M)}{\bar{r}}\right)^{-1} d\bar{r}^2 + \bar{r}^2 d\bar{\phi}^2\,. \tag{64}$$

Here, we have suggestively identified the three-dimensional mass

$$M \equiv -\frac{\kappa}{8G_3}\frac{\ell}{L_4}\eta^2 = -\frac{1}{2\mathcal{G}_3}\frac{\kappa x_1^2}{(3-\kappa x_1^2)^2}\,, \qquad \mathcal{G}_3 \equiv G_3\frac{L_4}{\ell} = \frac{G_3}{\sqrt{1-\nu^2}}\,, \tag{65}$$

and

$$F(M) \equiv \mu\eta^3 = 8\frac{(1-\kappa x_1^2)}{(3-\kappa x_1^2)^3}. \tag{66}$$

The mass identification (65) is primarily motivated by the fact that for in Einstein–AdS gravity, the mass corresponds to the subleading constant term in the g_{tt} metric in appropriate coordinates. However, the induced theory on the brane is a higher-derivative theory, and thus the definition of mass is expected to be modified due to higher-derivative corrections, starting at $\mathcal{O}(\ell^2)$. When treated as corrections to Einstein gravity, the mass M may still be identified as the constant term in g_{tt}; however, now the classical Newton's constant G_3 is 'renormalized' by the higher-derivative terms [92]

$$\mathcal{G}_3 = \left(1 - \frac{\ell^2}{2L_3^2} + \mathcal{O}\left(\frac{\ell}{L_3}\right)^4\right)G_3 = \left(1 - \frac{\nu^2}{2}\right)\frac{G_4}{2L_4} + \mathcal{O}\left(\frac{\ell}{L_3}\right)^4. \tag{67}$$

Alternatively, here, it is assumed that the renormalized Newton's constant be identified as $\mathcal{G}_3 \equiv G_3\frac{L_4}{\ell}$ at all orders in ℓ, although this differs from (67) at order $\mathcal{O}(\ell/L_3)^4$[25]. As such, $\mathcal{G}_3$ in mass (67) is interpreted as an all-order resummation of the higher-derivative corrections to the mass [25], whilst G_3 is the 'bare' Newton constant, since it is the physical constant $G_3 M$ which is being corrected. Further evidence for the identification of the mass

will be given when we explore the horizon thermodynamics of the three-dimensional black hole. Lastly, the form function $F(M)$ (66) is purely a function of mass M because it depends on M only through x_1 and is otherwise independent of $\nu = \ell/\ell_3$.

The metric (64) is highly reminiscent of the perturbative geometry (19) incorporating the semi-classical backreaction effects of a conformally coupled scalar[26]. We emphasize, however, that the $1/r$ correction in g_{tt} (19) is perturbative, while it is *exact* in (64). In particular, the geometry (64) is an exact solution to the gravitational field equations of the semi-classical induced action (57)

$$\begin{aligned} 8\pi G_3\langle T_{ij}\rangle = R_{ij} - \frac{1}{2}h_{ij}\left(R + \frac{2}{L_3^2}\right) \\ + \ell^2\left[4R_i^{\ k}R_{jk} - \frac{9}{4}RR_{ij} - \Box R_{ij} + \frac{1}{4}\nabla_i\nabla_j R + \frac{1}{2}h_{ij}\left(\frac{13}{8}R^2 - 4R_{kl}^2 + \frac{1}{2}\Box R\right)\right], \end{aligned} \tag{68}$$

where $\Box \equiv \nabla^2$. Decomposing the holographic stress tensor in an expansion in ℓ^2, i.e., $\langle T^i_{\ j}\rangle = \langle T^i_{\ j}\rangle_0 + \ell^2\langle T^i_{\ j}\rangle_2 + ...$, it follows

$$8\pi G_3\langle T^i_{\ j}\rangle_0 = R^i_{\ j} - \frac{1}{2}\delta^i_{\ j}\left(R + \frac{2}{\ell_3^2}\right), \tag{69}$$

$$8\pi G_3\langle T^i_{\ j}\rangle_2 = 4R^{ik}R_{jk} - \Box R^i_{\ j} - \frac{9}{4}RR^i_{\ j} + \frac{1}{4}\nabla^i\nabla_j R + \frac{1}{2}\delta^i_{\ j}\left(\frac{13}{8}R^2 - 3R_{kl}^2 + \frac{1}{2}\Box R - \frac{1}{2\ell_3^4}\right). \tag{70}$$

Substituting in the metric (64), we obtain for the renormalized stress-energy tensor

$$\langle T^i_{\ j}\rangle_0 = \frac{1}{16\pi G_3}\frac{\ell F(M)}{\bar{r}^3}\mathrm{diag}\{1,1,-2\} \tag{71}$$

to leading order and

$$\langle T^i_{\ j}\rangle_2 = \frac{1}{16\pi G_3}\frac{\ell F(M)}{\bar{r}^3}\left(\frac{1}{2\ell_3^2}\mathrm{diag}\{1,-11,10\} - \frac{24\mathcal{G}_3 M}{\bar{r}^2}\mathrm{diag}\{3,1,-4\} + \frac{\ell F(M)}{2\bar{r}^3}\right) \tag{72}$$

for the $\mathcal{O}(\ell^2)$ corrections. Notice $\langle T_{ij}\rangle_2$ has a non-zero trace, which is a consequence of breaking the conformal symmetry due to the cutoff ℓ. In principle, one could compute $\langle T_{ij}\rangle$ at all orders of backreaction—unlike the non-holographic perturbative analysis—however, it proves cumbersome to do so.

Since the backreaction is turned off as $\ell \to 0$, the metric (64) in this limit may be interpreted as 'classical'; indeed, the $1/r$ correction is eliminated, and the resulting geometry solves the three-dimensional vacuum Einstein equations. Hence, for $\ell \neq 0$, the geometry (64) is naturally understood as a quantum black hole in AdS_3, namely, the *quantum BTZ* (qBTZ) black hole. Notice further, in the limit of a small backreaction ($\nu < 1$), the $1/r$ term in (64) is proportional to $\ell \sim cG_3 \gg L_P$ (61), such that the horizon size of the quantum BTZ black hole is large compared to the Planck length. Further, it is worth emphasizing that the solution (64) consistently solves the semi-classical brane equations of motion for any $\ell > 0$, including large backreaction effects ($\nu > 1$).

Unlike the classical BTZ black hole, the quantum BTZ (64) has a curvature singularity at $\bar{r} = 0$, as evidenced by the Kretschmann invariant,

$$R^{ijkl}R_{ijkl} = \frac{12}{\ell_3^4} + \frac{6F(M)^2\ell^2}{\bar{r}^6}. \tag{73}$$

The curvature singularity descends from the curvature singularity of the bulk four-dimensional C-metric at $r = 0$, and it is hidden behind the (bulk) horizon $r = r_+$. Here, the singularity at $\bar{r} = 0$ sits behind the horizon at $\bar{r} = \bar{r}_+$, the largest positive root of the metric function $H(\bar{r})$, where the time-translation Killing vector $\bar{\zeta}^i = \eta \partial^i_{\bar{t}}$ goes null. Thus, at least for holographic quantum matter, the singularity structure of a classical black hole becomes dramatically altered due to a semi-classical backreaction. Note, moreover, relative to $\bar{\zeta}^i$, the surface gravity, defined via $\bar{\zeta}^i \nabla_i \bar{\zeta}_j = \kappa_+ \bar{\zeta}_j$, is

$$\kappa_+ = \frac{\eta}{2}|H'(r_+)| = \frac{1}{2}|H'(\bar{r}_+)| = \frac{1}{2\ell_3^2}\left|2\bar{r}_+ + \frac{\mu \ell \eta^3}{\bar{r}_+^2}\right|, \tag{74}$$

In the limit $\ell \to 0$, this corresponds to the surface gravity of the classical BTZ black hole.

Aside from the match of the perturbed geometry, the leading order contribution to $\langle T_{ij} \rangle$ (71) agrees with the renormalized stress tensor of the free conformal scalar (except $L_{\rm P} \to \ell$). This match between the holographic and free field results is because transparent boundary conditions have been imposed on the CFT or the free scalar. In the former, these boundary conditions are naturally selcted because bulk fluctuations, which are dual to CFT excitations, move freely throughout the bulk. For the free field computation, however, transparent boundary conditions were an explicit choice. In either case, notice the leading order contribution to the stress tensor is not of the standard thermal type, i.e., $\mathrm{diag}\{-2, 1, 1\}$. Nonetheless, the CFT is in a thermal state. Indeed, the Green's function from which $\langle T_{ij} \rangle$ is derived (in the perturbative treatment) is periodic in imaginary time with a period given by the (inverse) Tolman temperature [42]. Further, the Green function obeys analyticity properties shared by the Hartle–Hawking state, which is a state describing a black hole in thermal equilibrium with its own radiation.

A family of quantum black holes. From the mass identification (65), M takes values in the finite range [23,24],

$$-\frac{1}{8\mathcal{G}_3} \leq M \leq \frac{1}{24\mathcal{G}_3}, \tag{75}$$

where ℓ is held fixed. The upper bound follows from studying for the end behavior of $M(x_1)$, with $x_1 = \sqrt{3}$ (excluding $x_1 = -\sqrt{3}$ on account of the parameter range (46)) at $\kappa = -1$ being a maximum. The lower bound, meanwhile, occurs for $\kappa = +1$ and $x_1 = 1$ (where $\mu = 0$ according to (45)), and $M = 0$ for either $x_1 = 0$ or $\kappa = 0$. Thus, the qBTZ solution has negative and positive masses.

In fact, the solution may be categorized into physically distinct branches:

$$\begin{aligned} &\text{Branch 1:} \qquad -1 < -\kappa x_1^2 < 3\,, \\ &\text{Branch 2:} \qquad 3 < -\kappa x_1^2 < \infty\,. \end{aligned} \tag{76}$$

To understand how these branches arise, it is first natural to distinguish solutions with negative mass versus those with positive mass. All negative mass solutions occur for $\kappa = +1$ and for $x_1 \in (0, 1]$, while all positive mass solutions occur for $\kappa = -1$ and $x_1 \in (0, \infty)$. Note further $M = 0$ for either $x_1 = 0$ (for both $\kappa = \pm 1$) or $x_1 \to \infty$ (and $\kappa = +1$). This suggests the positive mass solutions subdivide along the range $x_1 \in (0, \sqrt{3})$ and $x_1 \in (\sqrt{3}, \infty)$, smoothly joining at $x_1 = \sqrt{3}$. Further, since it is the combination κx_1^2 that appears in all physical quantities of interest, the negative mass branch and the positive mass branch with $x_1 \in (0, \sqrt{3})$ smoothly connect at $x_1 = 0$. Succinctly, the qBTZ solution is characterized by the two branches (76); however, a finer subdivision of the two branches is [25]

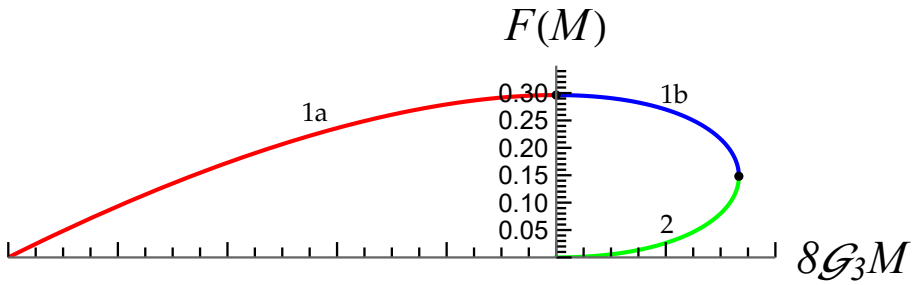

Figure 6. The qBTZ family of solutions. The qBTZ black hole consists of quantum-dressed conical singularities, branch 1a (red) and quantum-corrected BTZ black holes, branch 1b (blue) and branch 2 (green). Branches 1a and 1b join at $M = 0$ and $F = 8/27$ ($x_1 = 0$), while branches 1b and 2 coincide at $8G_3M = 1/3$ and $F = 4/27$ ($x_1 = \sqrt{3}$). Another branch describes (uncorrected) BTZ black holes with mass $M \geq 0$ induced from the bulk BTZ black string (the positive horizontal axis).

$$\begin{aligned} &\text{Branch 1a:} \quad \kappa = +1, \quad 0 < x_1 < 1\,, \\ &\text{Branch 1b:} \quad \kappa = -1, \quad 0 < x_1 < \sqrt{3}\,, \\ &\text{Branch 2:} \quad \kappa = -1, \quad \sqrt{3} < x_1 < \infty\,. \end{aligned} \tag{77}$$

Although each of the mass branches (77) smoothly connects, each branch has a different physical interpretation. This can be better understood by considering the types of solutions belonging to each branch in the limit of vanishing backreaction. Firstly, branch 1a contains the ground state $M = -\frac{1}{8G_3}$, where $F(M) = 0$ (substitute $x_1 = 1$ into (66)). Geometrically, the qBTZ line element (64) takes the form of global AdS_3. Notably, however, this ground state is valid for any $\ell \geq 0$, and thus for $\ell \neq 0$, it can be thought of as three-dimensional *quantum* anti-de Sitter spacetime, $qAdS_3$, accounting for a large-c cutoff CFT_3 living in AdS_3 with a vanishing renormalized stress tensor. Above this ground state, negative mass solutions (branch 1a) correspond to AdS_3 conical defects in the limit $\ell \to 0$, such that for $\ell \neq 0$, the negative mass family of solutions are understood to be quantum-corrected conical singularities, though are still referred to as quantum 'black holes'. Classically, the conical defects are horizonless, while when $\ell > 0$, the quantum Casimir stress tensor shrouds the conical singularity in a horizon.

Branches 1b and 2, having $M \geq 0$, both describe quantum corrections to the classical BTZ black hole geometry. The sources of the corrections of these two branches, however, differ. Since branch 1a and 1b connect at $x_1 = 0$ (where $M = 0$ and $F(0) = 8/27$) and 1a black holes form due to the backreaction of Casimir stress–energy, so too are the corrections resulting in the 1b black holes dominated by Casimir energy. Alternatively, the $M = 0$ state of the branch 2 black holes (where $x_1 \to \infty$) have zero $F(M)$ and hence stress–energy. This suggests the non-zero stress–energy of the $M > 0$ states among the branch 2 black holes is due to Hawking radiation in thermal equilibrium with the finite temperature black hole (where the dominant Casimir energy has been subtracted from the quantum state appearing in $\langle T_{ij} \rangle$ [25]).

Classically, the negative mass conical singularities and positive mass BTZ black holes are disconnected sets of solutions to Einstein–AdS_3 gravity—there is a 'mass gap' [31]. Evidently, a semi-classical backreaction smoothly connects these solutions, such that the quantum BTZ geometry represents a family of quantum black holes. We illustrate this family in Figure 6.

It is natural to wonder if there exist any other bulk solutions which give rise to a BTZ black hole on the brane with masses $M \geq 0$, including those that exceed the upper bound in the range (75). Indeed, recall the AdS_4 geometry (43) for which $\mu = 0$. When $\kappa = -1$, this four-dimensional geometry is dubbed the 'BTZ black string', since sections of constant σ contain a BTZ black hole. Despite $\mu = 0$, a BTZ black hole lives on the brane at $x = 0$ with

mass $M \geq 0$ in the canonically normalized coordinates $(\bar{t}, \bar{r}, \bar{\phi})$; however, the geometry is uncorrected from its classical counterpart, since the quantum stress tensor vanishes (on account of $F(M) = 0$ for all $M \geq 0$). Unlike the three branches (77), this braneworld black hole has no upper bound on M, and hence solutions with $M > 1/24\mathcal{G}_3$ are induced by a BTZ black string localized on the AdS_3 brane.

4.2.2. Rotating Quantum BTZ

Bulk and Brane Geometry

It is reasonably straightforward to find rotating quantum BTZ black holes. The starting point is the rotating AdS C-metric describing accelerating Kerr–AdS_4 black holes,

$$ds^2 = \frac{\ell^2}{(\ell + xr)^2}\Bigg[-\frac{H(r)}{\Sigma(x,r)}\Big(dt + ax^2 d\phi\Big)^2 + \frac{\Sigma(x,r)}{H(r)}dr^2 + r^2\left(\frac{\Sigma(x,r)}{G(x)}dx^2 + \frac{G(x)}{\Sigma(x,r)}\Big(d\phi - \frac{a}{r^2}dt\Big)^2\right)\Bigg], \tag{78}$$

where

$$H(r) = \frac{r^2}{\ell_3^2} + \kappa - \frac{\mu\ell}{r} + \frac{a^2}{r^2}, \quad G(x) = 1 - \kappa x^2 - \mu x^3 + \frac{a^2}{\ell_3^2}x^4, \quad \Sigma(x,r) = 1 + \frac{a^2x^2}{r^2}. \tag{79}$$

Here, a controls the rotation (the angular momentum per unit mass) and for $a = 0$, we recover the static C-metric (39). By evaluating the Kretschmann scalar invariant $R^{abcd}R_{abcd}$, there is a curvature singularity when $r^2\Sigma = r^2 + a^2x^2 = 0$, i.e., where $r = x = 0$. This is the familiar ring singularity of Kerr black holes.

Despite complicating the geometry by including rotation, the $x = 0$ hypersurface remains umbilic, such that $K_{ij} = \ell^{-1}h_{ij}$ (49) and a Karch–Randall brane at $x = 0$ has tension (50). The geometry at $x = 0$ is

$$ds^2|_{x=0} = -H(r)dr^2 + H^{-1}(r)dr^2 + r^2\Big(d\phi - \frac{a}{r^2}dt\Big)^2. \tag{80}$$

At first glance, this line element looks like a rotating black hole in Boyer–Lindquist-like coordinates. As in the static case, however, this geometry does not reflect the whole story. In particular, the 'naive metric' (80) unexpectedly no longer has a ring singularity but instead a curvature singularity at $r = 0$. Of course, we should not yet expect the geometry (80) to describe a black hole, since bulk regularity conditions to deal with the conical nature of the bulk solution have not yet been imposed. Unlike the static system, however, bulk regularity conditions for the rotating solution are more subtle because they affect more than just the periodicity of angular coordinate ϕ. Our treatment below follows the analysis in [27].

Firstly, notice that the Killing vector ∂_ϕ of the bulk C-metric (78) no longer has a vanishing norm at a zero x_i of $G(x)$. Rather, it is the Killing vector

$$\xi^b = \partial^b_\phi - ax_i^2\partial^b_t, \tag{81}$$

which obeys $\xi^2|_{x_i} = 0$. Thus, avoiding conical defects at $x = x_i$ requires one to identify points along the integral curves of (81) with an appropriate period. To determine the correct periodicity, consider the rotating C-metric (78) near a zero $x = x_i$ such that $G(x) \sim G'(x_i)(x - x_i)$. The removal of a conical singularity at, say $x = x_1$ (denoting the smallest

positive root of $G(x)$), has us simultaneously perform a coordinate transformation $\tilde{t} = t + ax_i^2\phi$ together with the periodicity condition for ϕ

$$\phi \sim \phi + \Delta\phi, \quad \Delta\phi = \frac{4\pi}{|G'(x_1)|} = \frac{4\pi x_1}{3 - \kappa x_1^2 - \tilde{a}^2}, \tag{82}$$

where to arrive to the second equality, we recast the parameter μ in terms of x_1 and define

$$\mu = \frac{1 - \kappa x_1^2 + \tilde{a}^2}{x_1^3}, \quad \tilde{a} \equiv \frac{a x_1^2}{\ell_3}. \tag{83}$$

In other words, identifying points along the orbits of (81) are made on surfaces of constant

$$\tilde{t} \equiv t + a x_1^2 \phi. \tag{84}$$

As in the static braneworld construction, the remaining zeros $x_i \neq x_1$ are effectively removed by gluing a second copy of the spacetime with the end-of-the-world brane at $x = 0$ such that the complete bulk spacetime has the restricted range $0 \leq x \leq x_1$.

Now, return to the naive metric (80) and consider the limit $r \to \infty$. The metric is asymptotic to 'rotating AdS_3', where the $dtd\phi$ metric component is a constant. The coordinates (t, r, ϕ), however, are not canonically normalized due to the periodicity in ϕ (82). Further, since points along orbits of (81) are identified, the ϕ-periodicity returns one to a different point in time t: indeed, from (84), we see that assuming $\tilde{t} \sim \tilde{t}$, then $t \sim t - 2\pi\eta a x_1^2$, for $\eta \equiv \Delta\phi/2\pi$. Unfortunately, this means we cannot merely rescale coordinates $(t, r, \phi) \to (\bar{t}, \bar{r}, \bar{\phi})$ as in the static case. Moreover, the periodicity alters the asymptotic form of the metric such that the $dtd\phi$ would instead grow as r^2, implying a diverging angular momentum[27].

The r^2-divergence can be ameliorated by changing coordinates (t, ϕ) to $(\tilde{t}, \tilde{\phi})$ where,

$$t = \tilde{t} - a x_1^2 \tilde{\phi}, \quad \phi = \tilde{\phi} - \frac{\tilde{a}}{\ell_3}\tilde{t}. \tag{85}$$

The coefficient $-\frac{\tilde{a}}{\ell_3}$ in ϕ is carefully chosen such that the r^2 divergence in the $\tilde{t} - \tilde{\phi}$ component of the naive brane metric is eliminated. Even still, the angular coordinate $\tilde{\phi}$ is not periodic in 2π. Luckily, this is now easily resolved by the simple rescaling, $\tilde{t} = \eta\bar{t}$ and $\tilde{\phi} = \eta\bar{\phi}$, such that the transformation [25]

$$t = \eta(\bar{t} - \tilde{a}\ell_3\bar{\phi}), \quad \phi = \eta\left(\bar{\phi} - \frac{\tilde{a}}{\ell_3}\bar{t}\right), \tag{86}$$

places the brane geometry (80) in a more canonical form. It proves useful to also have the inverted coordinate transformation (86),

$$\bar{t} = \frac{1}{\eta(1 - \tilde{a}^2)}(t + \tilde{a}\ell_3\phi)\,, \qquad \bar{\phi} = \frac{1}{\eta(1 - \tilde{a}^2)}\left(\phi + \frac{\tilde{a}}{\ell_3}t\right). \tag{87}$$

From here, the Killing vectors transform as

$$\partial_t = \frac{1}{\eta(1 - \tilde{a}^2)}\left(\partial_{\bar{t}} + \frac{\tilde{a}}{\ell_3}\partial_{\bar{\phi}}\right), \qquad \partial_\phi = \frac{1}{\eta(1 - \tilde{a}^2)}\left(\partial_{\bar{\phi}} + \tilde{a}\ell_3\partial_{\bar{t}}\right). \tag{88}$$

Notice in the coordinates $(\bar{t}, \bar{\phi})$, the Killing vector (81) is now $\xi^b = \eta^{-1}\partial_{\bar{\phi}}$.

With the coordinate change (86), the brane metric does not quite have the canonical asymptotic form of a rotating AdS black hole. To do so, one introduces a normalized radial coordinate $\bar{r}$ such that [25].

$$r^2 = \frac{\bar{r}^2 - r_s^2}{(1-\tilde{a}^2)\eta^2}\,, \qquad r_s \equiv \ell_3 \frac{\tilde{a}\eta}{x_1}\sqrt{2-\kappa x_1^2} = \ell_3 \frac{2\tilde{a}\sqrt{2-\kappa x_1^2}}{3-\kappa x_1^2-\tilde{a}^2}\,, \tag{89}$$

Altogether, having imposed bulk regularity conditions, the brane geometry (80) in the canonically normalized coordinates $(\bar{t}, \bar{r}, \bar{\phi})$ is

$$\begin{aligned} ds^2|_{x=0} = &-\left(\kappa\eta^2\left(1+\tilde{a}^2-\frac{4\tilde{a}^2}{\kappa x_1^2}\right)+\frac{\bar{r}^2}{\ell_3^2}-\frac{\mu\ell\eta^2}{r}\right)d\bar{t}^2 \\ &+\left(\kappa\eta^2\left(1+\tilde{a}^2-\frac{4\tilde{a}^2}{x_1^2}\right)+\frac{\bar{r}^2}{\ell_3^2}-\frac{\mu\ell(1-\tilde{a}^2)^2\eta^4 r}{\bar{r}^2}+\frac{\ell_3^2\tilde{a}^2\mu^2 x_1^2\eta^4}{\bar{r}^2}\right)^{-1} d\bar{r}^2 \\ &+\left(\bar{r}^2+\frac{\mu\ell\tilde{a}^2\ell_3^2\eta^2}{r}\right)d\bar{\phi}^2-\ell_3\tilde{a}\mu x_1\eta^2\left(1+\frac{\ell}{x_1 r}\right)(d\bar{\phi}d\bar{t}+d\bar{t}d\bar{\phi}), \end{aligned} \tag{90}$$

where we have kept both r and $\bar{r}$ when convenient (treating $r = r(\bar{r})$).

Quantum Black Hole

As in the static case, we reexpress the metric (90) as

$$\begin{aligned} ds^2 = &-\left(\frac{\bar{r}^2}{\ell_3^2}-8\mathcal{G}_3 M-\frac{\ell\mu\eta^2}{r}\right)d\bar{t}^2+\left(\frac{\bar{r}^2}{\ell_3^2}-8\mathcal{G}_3 M+\frac{(4\mathcal{G}_3 J)^2}{\bar{r}^2}-\ell\mu(1-\tilde{a}^2)^2\eta^4\frac{r}{\bar{r}^2}\right)^{-1}d\bar{r}^2 \\ &+\left(\bar{r}^2+\frac{\mu\ell\tilde{a}^2\ell_3^2\eta^2}{r}\right)d\bar{\phi}^2-8\mathcal{G}_3 J\left(1+\frac{\ell}{x_1 r}\right)d\bar{\phi}d\bar{t} \end{aligned} \tag{91}$$

where we have suggestively identified the mass and angular momentum J of the black hole,

$$8\mathcal{G}_3 M = -\kappa\eta^2\left(1+\tilde{a}^2-\frac{4\tilde{a}^2}{\kappa x_1^2}\right) = 4\frac{-\kappa x_1^2+\tilde{a}^2(4-\kappa x_1^2)}{(3-\kappa x_1^2-\tilde{a}^2)^2} \tag{92}$$

$$4\mathcal{G}_3 J = \ell_3\eta^2\tilde{a}\mu x_1 = \frac{4\ell_3\tilde{a}(1-\kappa x_1^2+\tilde{a}^2)}{(3-\kappa x_1^2-\tilde{a}^2)^2}. \tag{93}$$

The above identifications are made on geometric grounds: in the asymptotic limit $\bar{r}\to\infty$, the terms proportional to ℓ decay faster than than the constant $-8\mathcal{G}_3 M$ or the J in the $d\bar{t}d\bar{\phi}$ component. Further, $\mathcal{G}_3 \equiv L_4 G_3/\ell$ is again the renormalized Newton's constant, which now also plays the role of accounting for higher-derivative corrections to the angular momentum.

Horizon and singularity structure. In the static case, roots of the bulk metric function $H(r)$ correspond to the bulk Killing horizon of the time-translation Killing vector ∂_t. Including rotation in the bulk, the Killing vector

$$\zeta^b = \partial_t + \frac{a}{r_i^2}\partial_\phi, \tag{94}$$

for r_i finite has modulus $\zeta^2 = g_{ab}\zeta^a\zeta^b = -\frac{\ell^2}{(\ell+xr)^2}H(r_i)\Sigma(x,r_i)$ at $r = r_i$. Taking r_i to be real, $\zeta^2 = 0$ when $H(r_i) = 0$, where r_i are positive real roots of $H(r)$ (79) (restricting to a

coordinate range where there exists at least one real root). Let r_+ denote the largest positive, real root of $H(r)$, corresponding to the radius of the outer black hole. As with Kerr–AdS$_4$, there is a second positive real root r_-, satisfying $r_- < r_+$, which corresponds to the inner black hole horizon. Using $H(r_\pm) = 0$ and assuming $r_+ \neq r_-$, it is straightforward to express

$$\begin{aligned} \mu\ell &= \frac{(r_+ + r_-)}{\ell_3^2}\Big[(r_+^2 + r_-^2) + \ell_3^2\kappa\Big], \\ a^2 &= \frac{r_+ r_-}{\ell_3^2}\Big[r_+^2 + r_-^2 + r_+ r_- + \ell_3^2\kappa\Big]. \end{aligned} \tag{95}$$

The limit of vanishing angular momentum, $a \to 0$, coincides with $r_- \to 0$.

In canonically normalized coordinates $(\bar{t}, \bar{r}, \bar{\phi})$, the inner and outer horizons of the quantum black hole are generated by orbits of the canonically normalized generator (94), i.e.,

$$\bar{\zeta}^b_\pm \equiv \frac{\eta(1-\tilde{a}^2)}{1 + \frac{a^2 x_1^2}{r_\pm}}\zeta^b = \frac{\partial}{\partial \bar{t}} + \Omega_\pm \frac{\partial}{\partial \bar{\phi}}, \tag{96}$$

where we used the Killing vector transformation (88). Here, $\Omega_\pm$ is the angular velocity of the horizons $r_\pm$ relative to a *non-rotating* frame at spatial infinity

$$\Omega_\pm \equiv \frac{a}{r_\pm^2 + a^2 x_1^2}\left(1 + \frac{r_\pm^2 x_1^2}{\ell_3^2}\right). \tag{97}$$

For $x_1 = 1$, this coincides with the familiar angular velocity of Kerr–AdS$_4$ (e.g., [94,95]). Meanwhile, the angular velocity Ω' relative to a *rotating* frame at spatial infinity is

$$\Omega'_\pm \equiv \frac{a}{r_\pm^2 + a^2 x_1^2}\left(1 - \frac{a^2 x_1^4}{\ell_3^2}\right), \tag{98}$$

obeying $\Omega_\pm - \Omega'_\pm = a x_1^2/\ell_3^2$. Further, relative to $\bar{\zeta}^b$, the surface gravity of the inner and outer horizons is

$$\kappa_\pm = \frac{\eta(1-\tilde{a}^2)}{(r_\pm^2 + a^2 x_1^2)}\frac{r_\pm^2}{2}|H'(r_\pm)| = \frac{\eta(1-\tilde{a}^2)}{(r_\pm^2 + a^2 x_1^2)}\frac{1}{2\ell_3^2 r_\pm}|\ell_3^2 \mu\ell r_\pm + 2r_\pm^4 - 2a^2\ell_3^2|, \tag{99}$$

where we used the definition of the surface gravity $\kappa_\pm$ on a Killing horizon generated by $\bar{\zeta}$, $\bar{\zeta}^b \nabla_b \bar{\zeta}^c \equiv \kappa_\pm \bar{\zeta}^c$. In particular, using parameters (95)

$$\begin{aligned} \kappa_+ &= \frac{\eta(1-\tilde{a}^2)}{2\ell_3^2(r_+^2 + a^2 x_1^2)}(r_+ - r_-)|(r_+^2 + r_-^2 + \ell_3^2\kappa) + 2r_+(r_+ + r_-)|, \\ \kappa_- &= \frac{\eta(1-\tilde{a}^2)}{2\ell_3^2(r_-^2 + a^2 x_1^2)}(r_- - r_+)|(r_+^2 + r_-^2 + \ell_3^2\kappa) + 2r_-(r_+ + r_-)|. \end{aligned} \tag{100}$$

In the limit of vanishing rotation, κ_+ becomes the surface gravity of the static qBTZ, (74). Further, the surface gravities vanish in the extremal limit, i.e., where the inner and outer black hole horizons coincide, $r_+ = r_-$.

The horizons shroud a ring curvature singularity at $r = 0$, i.e., $\bar{r} = r_s$. Further, near the ring singularity, there exists the possibility of closed timelike curves. Indeed, consider the norm of the axial Killing vector $\partial_{\bar{\phi}}$ of (91) to be

$$\partial_{\bar{\phi}}^2 = h_{\bar{\phi}\bar{\phi}} = \bar{r}^2 + \frac{\mu\ell\tilde{a}^2\ell_3^2\eta^2}{r} = \bar{r}^2 + \frac{\mu\ell\tilde{a}^2\ell_3^2\eta^3}{\sqrt{\bar{r}^2 - r_s^2}}\sqrt{1-\tilde{a}^2}\,, \tag{101}$$

meaning that if one has a too small and negative enough radii r, the axial vector becomes timelike, and its orbits are closed curves around the rotation axis. To ensure $\partial_\phi^2 \geq 0$ requires an additional restriction of the solution parameters: (i) $1 - \tilde{a^2} \geq 0$, and (ii) $\eta > 0$, which implies $-\kappa x_1^2 > \tilde{a}^2 - 3$. Notice the second condition is always implied by (i) if $\kappa = -1$.

Quantum stress tensor. As an exact solution to the full semi-classical theory (57), the metric (91) is known as the rotating quantum BTZ black hole. In the limit of vanishing backreaction, $\ell \to 0$, the classical rotating BTZ black hole is recovered for $\kappa = -1$, while for $\kappa = +1$, the geometry is that of a rotating AdS_3 conical defect. For $\ell \neq 0$, the non-vanishing components of the renormalized quantum-stress tensor (69) are found to be [25]

$$\begin{aligned}
\langle T^{\bar{t}}_{\bar{t}} \rangle_0 &= \frac{1}{16\pi G_3} \frac{\ell\mu}{(1-\tilde{a}^2) r^3} \left(1 + 2\tilde{a}^2 + \frac{3\tilde{a}^2 \ell_3^2}{x_1^2 r^2} \right) , \\
\langle T^{\bar{r}}_{\bar{r}} \rangle_0 &= \frac{1}{16\pi G_3} \frac{\ell\mu}{r^3} , \\
\langle T^{\bar{\phi}}_{\bar{\phi}} \rangle_0 &= -\frac{1}{16\pi G_3} \frac{\ell\mu}{(1-\tilde{a}^2) r^3} \left(2 + \tilde{a}^2 + \frac{3\tilde{a}^2 \ell_3^2}{x_1^2 r^2} \right) , \\
\langle T^{\bar{t}}_{\bar{\phi}} \rangle_0 &= -\frac{1}{16\pi G_3} \frac{3\ell_3 \ell\mu\tilde{a}}{(1-\tilde{a}^2) r^3} \left(1 + \frac{\tilde{a}^2 \ell_3^2}{x_1^2 r^2} \right) , \\
\langle T^{\bar{\phi}}_{\bar{t}} \rangle_0 &= \frac{1}{16\pi G_3} \frac{3\ell\mu\tilde{a}}{\ell_3 (1-\tilde{a}^2) r^3} \left(1 + \frac{\ell_3^2}{x_1^2 r^2} \right) .
\end{aligned} \tag{102}$$

These are most efficiently computed by first computing the components of the stress tensor in the naive coordinates (80) and then performing the appropriate coordinate transformations imposing bulk regularity. The $\mathcal{O}(\ell^2)$ components $\langle T_{ij} \rangle_2$ (70) are cumbersome to express in canonically normalized coordinates; however, in naive coordinates, $\langle T_{ij} \rangle_2$ is not traceless, indicating the presence of a UV cutoff breaking the conformal symmetry of the CFT_3.

Notice the mass (92) and angular momentum (93) only depend on $\tilde{a}$ and κx_1^2 and not on ℓ. Meanwhile, ℓ only enters as an overall prefactor in the stress tensor components (102). Hence, the leading-order stress tensor only depends on backreaction effects via $\mathcal{G}_3$ and not $\mathcal{G}_3 M$ or $\mathcal{G}_3 J$. Further, unlike the static solution (71), the stress tensor for the rotating qBTZ black hole is not characterized by a single function $F(M)$. Consider, however, the large-$\bar{r}$ asymptotics of the components (102). For example, substituting normalized coordinate (89) into $\langle T^{\bar{t}}_{\bar{t}} \rangle_0$, yields

$$\lim_{\bar{r}\to\infty} \langle T^{\bar{t}}_{\bar{t}} \rangle_0 \to \frac{\eta^3 \mu \ell \sqrt{1-\tilde{a}^2}}{16\pi G_3 \bar{r}^3} (1 + 2\tilde{a}^2). \tag{103}$$

Peeling off $\ell / 16\pi G_3 \bar{r}^3$, identify the form function

$$F(M,J) \equiv \eta^3 \mu \sqrt{1-\tilde{a}^2} (1 + 2\tilde{a}^2) = \frac{8\sqrt{1-\tilde{a}^2}(1+2\tilde{a}^2)(1-\kappa x_1^2 + \tilde{a}^2)}{(3 - \kappa x_1^2 - \tilde{a}^2)^3}, \tag{104}$$

such that for large $\bar{r}$

$$\langle T^{\bar{t}}_{\bar{t}} \rangle_0 \to \frac{1}{16\pi G_3} \frac{\ell F(M,J)}{\bar{r}^3}. \tag{105}$$

Due to the $\sim \mu / r^3$ behavior in each of the remaining components, up to unimportant factors, the large-$\bar{r}$ structure of (102) essentially depends on $F(M,J)$ as defined in (104). We will use $F(M,J)$ to better understand the family of rotating quantum black holes momentarily.

It is worth comparing the structure of the holographic stress tensor (102) to the stress tensor of a conformally coupled scalar field found by solving the semi-classical Einstein

equations perturbatively (in particular, see [25,45]). The non-holographic stress tensor may be expressed as an infinite sum over images, e.g.,

$$8\pi G_3 \langle T^{\bar{t}}_{\bar{t}} \rangle = \sum_{n=1}^{\infty} \frac{1}{r_n^3} \left(A_n + \frac{\bar{A}_n}{r_n^2} \right), \tag{106}$$

with $r_n = \sqrt{D_n \bar{r}^2 + \bar{D}_n}$, where coefficients A_n, $\bar{A}_n$, D_n and $\bar{D}_n$ are all complicated functions of M and J. An analogous structure holds for the remaining components. Coefficients aside, each term of the infinite sum has a similar radial dependence as the holographic stress tensor. The radial dependence of the entire infinite sum (106), however, is far more complicated than the radial dependence of the holographic stress tensor (102). Notably, while the holographic stress tensor is manifestly non-singular away from the ring singularity $\bar{r} = r_s$, it is not clear whether the same is true for the perturbative stress tensor.

Black hole branches revisited. In the non-rotating case, there are three branches of quantum black holes, branches 1a, 1b, and 2 (77). There is an analogous set of branches for non-vanishing J, where, in particular, branches 1b and 2 meet at a maximum value of M for fixed J. This occurs when

$$x_1^2 + \tilde{a}^2 = 3, \quad M = \frac{1}{8\mathcal{G}_3} \left(\frac{12}{x_1^4} - 1 \right), \quad J = \frac{\ell_3}{\mathcal{G}_3} \frac{\sqrt{3 - x_1^2}}{x_1^4}. \tag{107}$$

At $x_1 = \sqrt{2}$, one attains an extremal bound, where $M = J/\ell_3 = 1/4\mathcal{G}_3$. There is another extremal bound among the branch 2 black holes, founding by minimizing the mass M for fixed J,

$$\tilde{a} = 1, \quad M = \frac{J}{\ell_3} = \frac{1}{\mathcal{G}_3(2 + x_1^2)}, \tag{108}$$

which coincides with the bound (107) at $x_1 = \sqrt{2}$. Classically, the rotating BTZ black hole obeys the extremality bound $M \geq J/\ell_3$. For the quantum black hole, however, for any value of J, this classical extremality bound is violated, $M \leq J/\ell_3$, when $-\kappa x_1^2 < 2\tilde{a}^2$, giving rise to 'super-extremal' black holes among the branch 1 solutions. Pictorially, the branches of quantum black holes have a similar representation as Figure 6 (see Figure 6 of [25]).

4.2.3. Charged Quantum BTZ

Bulk and Brane Geometry

It is relatively straightforward to generalize the neutral quantum BTZ solutions to a charged system. Now, the bulk is characterized by the charged AdS_4 C-metric. For simplicity, setting rotation to zero, the line element is of the same form as (39), except the metric functions (40) receive an additional term:

$$ds^2 = \frac{\ell^2}{(\ell + xr)^2} \left[-H(r) dt^2 + \frac{dr^2}{H(r)} + r^2 \left(\frac{dx^2}{G(x)} + G(x) d\phi^2 \right) \right], \tag{109}$$

$$H(r) = \frac{r^2}{\ell_3^2} + \kappa - \frac{\mu \ell}{r} + \frac{q^2 \ell^2}{r^2}, \quad G(x) = 1 - \kappa x^2 - \mu x^3 - q^2 x^4. \tag{110}$$

This is a solution to four-dimensional Einstein–Maxwell gravity with negative cosmological constant $-2\Lambda_4 = 6/L_4^2$,

$$I = \frac{1}{16\pi G_4} \int d^4x \sqrt{-\hat{g}} \left[\hat{R} + \frac{6}{L_4^2} - \frac{\ell_*^2}{4} F^2 \right], \quad \ell_*^2 = \frac{16\pi G_4}{g_*^2} \tag{111}$$

where ℓ_* is a coupling constant with dimensions of length, g_* is the dimensionless gauge coupling constant, and $F_{ab} = \partial_a A_b - \partial_b A_a$ is the Maxwell field tensor. The $U(1)$ gauge field A_a for the charged C-metric (109)

$$A = A_a dx^a = \frac{2\ell}{\ell_*}\left[e\left(\frac{1}{r_+} - \frac{1}{r}\right)dt + g(x - x_1)d\phi\right], \tag{112}$$

where e and g, respectively, denote the electric and magnetic charge parameters of the accelerating black hole such that $q^2 = e^2 + g^2$. A gauge has been chosen for the gauge potential (112) such that it remains regular at the largest root of $H(r) = 0$, denoted r_+, and $x = x_1$.

As for the neutral black hole, real roots of $G(x)$ correspond to symmetry axes of the Killing vector ∂^a_ϕ, and we work in the restricted regime $0 \leq x \leq x_1$. The conical singularity at $x = x_1$ is removed via the identification

$$\phi \sim \phi + \Delta\phi, \quad \Delta\phi = \frac{4\pi}{|G'(x_1)|} = \frac{4\pi}{|-3 + \kappa x_1^2 - q^2 x_1^4|}, \tag{113}$$

where we treat μ as a 'derived' parameter following $G(x_1) = 0$,

$$\mu = \frac{1 - \kappa x_1^2 - q^2 x_1^4}{x_1^3}, \tag{114}$$

while x_1 and q are primary parameters.

Lastly, as usual, the $x = 0$ hypersurface is totally umbilic, such that the Israel junction conditions fix the brane tension to be $\tau = (2\pi G_4 \ell)^{-1}$. The Maxwell field strength also has junction conditions to obey. In particular, let n^a denote the normal to the brane at $x = 0$ (pointing toward increasing values of x) and let e^a_i be a basis for tangent vectors to the brane. Then, projecting F_{ab} onto the brane such that $F_{ij} \equiv F_{ab} e^a_i e^b_j$ and $f_i \equiv F_{ab} e^a_i n^b$, one has the following junction conditions [96] for a purely tensional brane

$$\begin{aligned} \Delta F_{ij} &= F^+_{ij} - F^-_{ij} = 0, \\ \Delta f_i &= f^+_i - f^-_i = 4\pi j_i, \end{aligned} \tag{115}$$

where j_i is the electromagnetic surface current.

Induced Brane Theory

As in the neutral examples, the induced theory on the brane essentially follows from replacing the IR bulk cutoff in holographic renormalization with a brane. When the bulk theory of gravity is Einstein–Maxwell, the induced brane action (53) receives corrections due to the bulk Maxwell contribution, such that the induced brane action is now

$$I = \frac{1}{16\pi G_3}\int_{\mathcal{B}} d^3x\sqrt{-h}\left[R - 2\Lambda_3 + L_4^2\left(\frac{3}{8}R^2 - R_{ij}^2\right) + ...\right] + I_{\rm EM} + I_{\rm CFT}, \tag{116}$$

where the electromagnetic term $I_{\rm EM}$ is

$$I_{\rm EM} = 2\int d^3x\sqrt{-h}A_i j^i + I^{\rm ct}_{\rm EM}. \tag{117}$$

The first contribution is a boundary term with respect to the bulk Maxwell term necessary to keep the Dirichlet variational problem well posed. The second contribution describes

local counterterms associated with the four-dimensional bulk Maxwell action that are included in holographic renormalization[28] [97]

$$I_{\rm EM}^{\rm ct} = \frac{L_4\ell_*^2}{8\pi G_4}\int d^3x\sqrt{-h}\Big[-\frac{5}{16}F^2 + L_4^2\Big(\frac{1}{288}RF^2 - \frac{5}{8}R^i{}_jF_{ik}F^{jk} + \frac{3}{98}F^{ij}(\nabla_j\nabla^kF_{ki} - \nabla_i\nabla^kF_{kj}) + \frac{5}{24}\nabla_iF^{ij}\nabla_kF^k_j\Big) + \mathcal{O}(L_4^3)\Big]. \tag{118}$$

Then, treating $\ell < \ell_3$ such that $L_4 \sim \ell$, the effective theory on the brane (57) is now

$$I = \frac{1}{16\pi G_3}\int d^3x\sqrt{-h}\Big[R + \frac{2}{\ell_3^2} - \frac{\tilde{\ell}_*^2}{4}F^2 + 16\pi G_3A_ij^i + \ell^2\Big(\frac{3}{8}R^2 - R_{ij}^2\Big) + \frac{4}{5}\ell^2\tilde{\ell}_*^2\Big(\frac{1}{288}RF^2 - \frac{5}{8}R^i{}_jF_{ik}F^{jk} + \frac{3}{98}F^{ij}(\nabla_j\nabla^kF_{ki} - \nabla_i\nabla^kF_{kj}) + \frac{5}{24}\nabla_iF^{ij}\nabla_kF^k_j\Big) + \mathcal{O}(\ell^3)\Big] + I_{\rm CFT}. \tag{119}$$

where in addition to the induced scales (54) $G_3 = G_4/2L_4$, and L_3 (55), there is an effective three-dimensional gauge coupling

$$\tilde{\ell}_*^2 = \frac{16\pi G_3}{g_3^2}, \quad g_3^2 = \frac{2}{5}\frac{g_*^2}{L_4} \approx \frac{2}{5}\frac{g_*^2}{\ell}, \tag{120}$$

such that $\ell_*^2 = 4\tilde{\ell}_*^2/5$. It is clear that in the limit $\ell \to 0$, the coupling $g_3 \to \infty$ becomes non-dynamical. Indeed, we will see how this 'charge' contribution to the metric disappears.

The metric equations of motion of the induced theory to order $\mathcal{O}(\ell^2)$ are as in the neutral case, except now with an additional contribution coming from the F^2 contribution in the action. That is,

$$8\pi G_3\langle T_{ij}\rangle = G_{ij} - \frac{1}{L_3^2}h_{ij} - \frac{\tilde{\ell}_*^2}{2}\Big(F_i^kF_{jk} - \frac{1}{4}h_{ij}F^2\Big) + 16\pi G_3A_kj^kh_{ij} + ..., \tag{121}$$

where the ellipsis constitutes terms at higher order in ℓ; the $\mathcal{O}(\ell^2)$ contribution is precisely the same as in the neutral case (70), while $\mathcal{O}(\ell^3)$ contributions arise from the $\ell^2\tilde{\ell}_*^2$ term in the action (119). Further, varying with respect to the gauge field A_i, we find the analog of the semi-classical Maxwell equations,

$$\langle J^j\rangle = j^j + \frac{\tilde{\ell}_*^2}{16\pi G_3}\Big\{\nabla_iF^{ji} + \frac{16}{5}\ell^2\Big(-\frac{1}{72}R\nabla_iF^{ji} + \frac{11}{18}F^j{}_i\nabla^iR + \frac{209}{294}R^{ij}\nabla_kF_i{}^k + \frac{5}{4}R^{ik}\nabla_kF^j{}_i + \frac{5}{4}F^{ik}\nabla_kR^j{}_i + \frac{317}{588}\nabla_i\nabla^i\nabla_kF^{jk} + \frac{317}{588}\nabla^j\nabla^k\nabla_iF^{ik}\Big) + \mathcal{O}(\ell^3)\Big\}. \tag{122}$$

Quantum Black Hole

Upon imposing bulk regularity conditions (equivalent to those for the neutral, static geometry), the induced geometry on the brane at $x = 0$, in terms of canonically normalized coordinates $(t, r, \phi) = (\eta\bar{t}, \eta^{-1}\bar{r}, \eta\bar{\phi})$, is [98] (see also [99])

$$ds^2_{\rm cqBTZ} = -H(\bar{r})d\bar{t}^2 + H^{-1}(\bar{r})d\bar{r}^2 + \bar{r}^2d\bar{\phi}^2,$$
$$H(\bar{r}) = -8M\mathcal{G}_3 + \frac{\bar{r}^2}{\ell_3^2} - \frac{\ell F(M,q)}{\bar{r}} + \frac{\ell^2Z(M,q)}{\bar{r}^2}. \tag{123}$$

Here, the mass is identified to be

$$M \equiv -\frac{\kappa}{8\mathcal{G}_3}\eta^2 = -\frac{\kappa}{8\mathcal{G}_3}\frac{4x_1^2}{(3-\kappa x_1^2+q^2x_1^4)^2}, \tag{124}$$

and form functions

$$F(M,q) \equiv \mu\eta^3 = 8\frac{1-\kappa x_1^2-q^2x_1^4}{(3-\kappa x_1^2+q^2x_1^4)^3}, \tag{125}$$

$$Z(M,q) \equiv q^2\eta^4 = \frac{16q^2x_1^4}{(3-\kappa x_1^2-q^2x_1^4)^4}. \tag{126}$$

As an exact solution to the semi-classical theory (119), the geometry (123) is recognized as the 'charged' version of the quantum BTZ black hole. Notice, however, in the limit $\ell \to 0$ the q-dependent correction vanishes, indicating the charge of the braneworld black is a consequence of backreaction. Notably, the classical geometry ($\ell = 0$) is not that of the charged BTZ metric [100]; we will return to this point momentarily.

Substituting the metric (123) into the stress tensor at the leading order in ℓ is equivalent to the neutral static qBTZ stress tensor (71), while the effects of charge arise at $\mathcal{O}(\ell^2)$. Further, in coordinates $(\bar{t},\bar{r},\bar{\phi})$, the projected components of the electromagnetic tensor are

$$F_{\bar{r}\bar{t}} = \frac{2e\ell}{\ell_*\bar{r}^2}\eta^2, \quad f_{\bar{\phi}} = -\frac{2g\ell}{\ell_*\bar{r}}\eta^2. \tag{127}$$

Using the junction conditions (115), the induced current density is

$$j^{\bar{\phi}} = \frac{g\ell\eta^2}{\pi\ell_*\bar{r}^3}. \tag{128}$$

With these, the leading-order $\mathcal{O}(\ell)$ contribution to the semi-classical current density (122) has components

$$\begin{aligned}\langle J^{\bar{t}}\rangle &= -\frac{\ell\tilde{\ell}_*^2}{8\pi G_3\ell_*}\frac{e\eta^2}{\bar{r}^3} \propto \frac{e\ell\sqrt{c}}{g_*\bar{r}^3},\\ \langle J^{\bar{\phi}}\rangle &= \frac{\ell}{\ell_*}\frac{g\eta^2}{\pi\bar{r}^3} \propto \frac{gg_*\sqrt{c}}{\bar{r}^3}.\end{aligned} \tag{129}$$

Interestingly, the temporal component vanishes in the limit $\ell \to 0$, while the azimuthal component is independent of backreaction. This is consistent with the three-dimensional dyonic defect in conical AdS_3 or a BTZ black hole [98].

Unlike the rotating case, the limit of vanishing backreaction does not return a classically AdS_3 geometry charged under three-dimensional Maxwell theory. Indeed, in three dimensions, the (electric) gauge field A_t has a logarithmic dependence, $A_t \sim q\log(r)$, producing a logarithmic correction to the three-dimensional blackening factor of a classical charged BTZ [100]. This lack of logarithmic behavior arises from the fact the bulk four-dimensional gauge field does not localize on the brane in the same way as a gravity [98]. Still, the quantum black hole (123) is charged. As with mass or angular momentum, computing charge Q from the brane perspective would require a resummation of the infinite tower of higher-derivative terms appearing in the induced theory. Alternatively, the bulk theory performs this resummation, and the charge of the brane black hole is identified with the electric charge of the bulk black hole [98] (see also [101])

$$Q = \frac{2}{g_*^2}\int \star F, \tag{130}$$

where the factor of two in the first equality is due to the $\mathbb{Z}_2$ symmetry, $\star F$ refers to the Hodge dual of the bulk Maxwell tensor, and the integration is taken to be at the boundary. In particular, the electric charge is

$$Q_e = \frac{2e\ell}{g_*^2\ell_*}\int_0^{2\pi\eta} d\phi \int_0^{x_1} dx = \frac{8\pi\ell e\eta x_1}{g_*^2\ell_*}, \tag{131}$$

where $\star F = r^2 F_{rt} d\phi dx$. Similarly, the magnetic charge Q_g is

$$Q_g = \frac{2}{g_*^2}\int F = \frac{8\pi\ell g\eta x_1}{g_*^2\ell_*}, \tag{132}$$

and $Q^2 = Q_e^2 + Q_g^2$. Notice Q^2 does not explicitly appear in the blackening factor (123).

Associated with the electric and magnetic charges are their respective potentials μ_e and μ_g. Since, holographically, the bulk Einstein–Maxwell theory (111) has a dual interpretation in terms of a CFT_3 with a chemical potential, it is natural to refer to μ_e and μ_g as chemical potentials. In particular, the electric chemical potential equals the electric component of the bulk gauge field (112) at the boundary intersecting the brane at $x = 0$ (where $r_{\text{bdry}} \to -\infty$),

$$\lim_{r_{\text{bdry}}\to-\infty} A_{\bar{t}} \equiv \mu_e = \frac{2\ell e\eta}{r_+\ell_*}. \tag{133}$$

Similarly, under electromagnetic duality of the bulk solution, the magnetic chemical potential μ_g has the same form as (133), except with $e \leftrightarrow g$. Notice $\mu_g Q_e - \mu_e Q_g = 0$.

A Family of Charged Quantum Black Holes

Having included q, the parameter x_1 depends on q and belongs to a different range than the static (46) or rotating case. To determine this range, two conditions are imposed [98]: (i) the bulk has a horizon $r_0 > 0$, and (ii) x_1 is finite, having a maximum $x_1^{\max}$, such that constant (t, r) surfaces are compact. The finite maximum value of x_1 is linked to the fact that the bulk (and brane) geometry has an extremal limit. Demanding there are no naked singularities requires μ to be bounded below by $\mu_{\text{ext}}^{(\kappa)}$, i.e., the value of μ when the bulk black hole becomes extremal. The parameter $x_1 = x_1^{\max}$ when $\mu = \mu_{\text{ext}}^{(\kappa)}$.

Explicitly, for arbitrary κ, the extremal mass is [98]

$$\mu_{\text{ext}}^{(\kappa)} = \sqrt{\frac{2}{3}}\frac{\sqrt{\sqrt{\kappa^2+12\nu^2q^2}-\kappa}\left(2\kappa+\sqrt{\kappa^2+12\nu^2q^2}\right)}{3\nu}. \tag{134}$$

This can be derived as follows. First, the condition of extremality requires two positive real roots of $H(r)$ to be coincident; i.e., $r_+ = r_- = r_0$ implies $H(r) = (r-r_0)^2 f(r)$ for some differentiable function $f(r)$ such that $H(r_0) = H'(r_0) = 0$. A little algebra yields

$$\mu_{\text{ext}}^{(\kappa)}(r_0) = \frac{2r_0}{\ell}\left(\kappa + \frac{2r_0^2}{\ell_3^2}\right), \qquad q_{\text{ext}}^{(\kappa)}(r_0) = \frac{r_0}{\ell}\sqrt{\kappa + \frac{3r_0^2}{\ell_3^2}}. \tag{135}$$

Inverting $q_{\text{ext}}^{(\kappa)}(r_0)$ for r_0 gives

$$r_0^{(\kappa)} = \frac{\ell_3\sqrt{\sqrt{\kappa^2+12\nu^2q^2}-\kappa}}{\sqrt{6}}. \tag{136}$$

Substituting this into $\mu_{\text{ext}}^{(\kappa)}$ (135) yields (134). Evidently, extremality occurs when a backreaction is non-vanishing ($\nu \neq 0$) or charge is non-zero for $\kappa = +1$. Alternatively, for $\kappa = -1$, there exists an extremal radius, $r_0^{(-1)} = \ell_3/\sqrt{3}$, even when $q = 0$ and where $\mu_{\text{ext}}^{(-1)} < 0$.

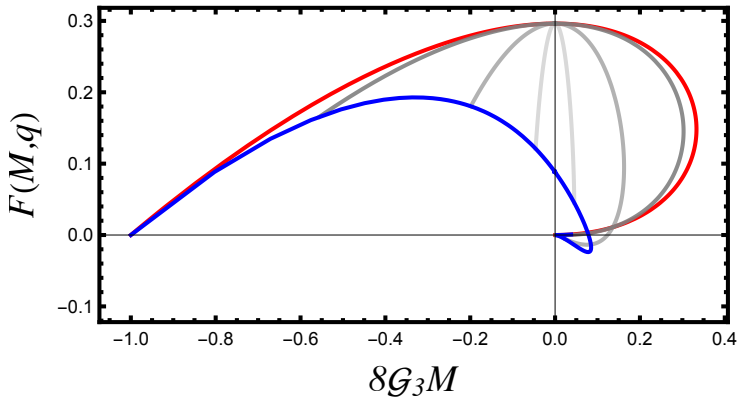

Figure 7. Branches of charged qBTZ. Metric function $F(M,q)$ as a function of mass M for fixed q and $\nu = 1/5$. The blue (bottom) and red (top) lines correspond to, respectively, extremal and neutral qBTZ solutions. The gray lines are non-extremal charged solutions with, from darkest to lightest, $q = 1/5, 1, 5$.

In fact, generally, $\mu_{\rm ext}^{(-1)}$ can become negative (whenever $q < \frac{1}{\sqrt{12\nu}}$), as does $F(M,q)$, for $\kappa = -1$; meanwhile, $\kappa = +1, 0$ gives $\mu_{\rm ext}^{(-1)} \geq 0$.

Furthermore, $x_1^{\rm max}$ is determined by substituting the extremal parameter (134) into (114) and solving for the resulting x_1 in terms of q and ν. An analytic expression for $x_1^{\rm max}$ is possible but cumbersome and not particularly illuminating. Some intuition can be gained, however, by looking at the limit when both q and ν are small. Three cases are worth highlighting:

- $\kappa = 1$: for $q = 0$, x_1 is bounded above by 1, as $\mu \to 0$. For $q \ll 1$, this upper bound is lowered to
$$x_1^{\rm max,1} = 1 - q + 2q^2. \tag{137}$$
- $\kappa = -1$: for $q = 0$, x_1 covers the whole real line, approaching $x_1 = 0$ from above as $\mu \to \infty$ and vice versa. Turning on $q \ll 1$, the maximum $x_1^{\rm max}$ is
$$x_1^{\rm max,0} = \frac{2}{3\sqrt{3}\nu q^2} + \frac{\sqrt{3}\nu}{2} - \frac{21\sqrt{3}\nu^3 q^2}{8} + \dots . \tag{138}$$
- $\kappa = 0$: in the neutral case, the parameter range is equivalent to the $\kappa = -1$ case; however, for $q \ll 1$, then
$$x_1^{\rm max,0} = \frac{h(\nu)}{\sqrt{q}}\,, \tag{139}$$
with $h(\nu) = 1 - \frac{\sqrt{\nu}}{3^{3/4}} + \frac{\nu}{2\sqrt{3}} + \mathcal{O}(\nu^{3/2}) + \dots$

A visual representation of the branches for the charged qBTZ black hole can be found in Figure 7. Notably, the branches have qualitatively similar features as the neutral qBTZ. This is because the finite mass range of the charged black holes is a subset of the mass range of the neutral qBTZ (75). The branch with $M < 0$ corresponds to the classically horizonless charged defects, now with a horizon induced by quantum backreaction. Note, however, unlike the neutral or rotating quantum BTZ solutions, here, $F(M,q)$ can go negative for any ν when charge parameter q is large enough.

The limit of vanishing backreaction, $\nu \to 0$, is more subtle than the neutral quantum BTZ solutions. As is usual, in this limit, the brane is sent closer to the asymptotic AdS_4 boundary, where both gravity and the gauge theory become frozen. The geometry becomes that of a charged defect in conical AdS_3 or $Mink_3$ ($\kappa = +1$) or a black hole ($\kappa = -1$). Since the latter is a black hole geometry, the backreaction ($\nu \neq 0$) produces a quantum-corrected charged black hole; i.e., the horizon is not induced solely due to a backreaction.

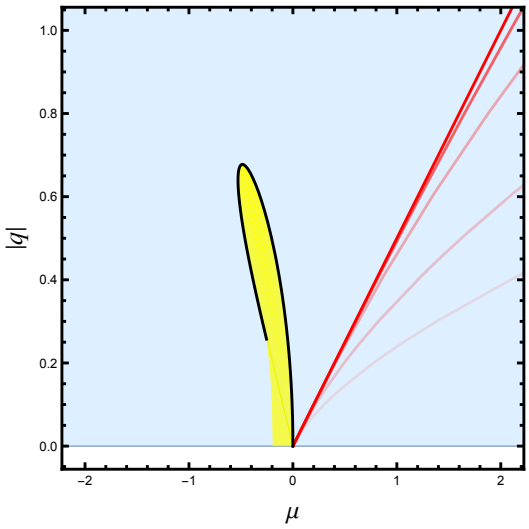

Figure 8. Parameter space for charged quantum BTZ. The blue square and yellow 'banana' regions correspond to solutions with a conical defect and excess, respectively, delimited by a thick black contour. The rightward directed (red) lines denote the extremal family of solutions at fixed ν (from darkest to lightest, $\nu = 0, 1/3, 1, 5, 20$). Here, $\kappa = 1$. For details, refer to [98].

Alternatively, for the conical charged defects, horizons can only arise via quantum effects. Unlike the neutral set-up, however, whether a horizon appears depends on a balance between μ and q—a backreaction does not always dress the conical defects with a horizon. Specifically, when the non-backreacted solution has $q \geq \mu/2$, then the backreaction will result in a spacetime possessing a naked (timelike) singularity [98]. Meanwhile, for $q < \mu/2$, a backreaction will produce a quantum black hole provided the backreaction is not too large. As ν increases for a fixed q, an extremal black hole forms, and an even stronger backreaction results in naked singularities. For an illustration, see Figure 8.

4.3. Quantum dS Black Holes

In Section 2, we saw, perturbatively, that a semi-classical backreaction modifies conical dS_3 geometries to induce a black hole horizon (in addition to its classical cosmological horizon). This observation is bolstered using braneworld holography. The construction and analysis are similar to the quantum BTZ black hole; however, there are some essential differences.

4.3.1. Bulk Set-Up

The starting point in the bulk is again the AdS_4 C-metric (39) with metric functions (40) except with fixed $\kappa = +1$ and $\ell_3^2 = -R_3^2$ (or Wick rotate $\ell_3 \to iR_3$). The AdS_4 length scale is then

$$\frac{1}{L_4^2} = \frac{1}{R_3^2} - \frac{1}{\ell^2}. \tag{140}$$

Unlike the qBTZ set-up, keeping $L_4^2 > 0$ requires $R_3^2 > \ell^2$, placing an upper bound on ℓ for fixed R_3. Further, rearranging (140) yields $\ell < L_4$—the opposite of the quantum BTZ construction. This condition is the first crucial difference between the quantum BTZ and dS set-ups, as maintaining $\ell < L_4$ implies the acceleration horizon is not effectively eliminated. To see this explicitly, consider the analog of the coordinate transformation (42) [26]

$$\sinh(\sigma) = \frac{R_3}{L_4} \frac{1}{|1 + \frac{rx}{\ell}|} \sqrt{1 - \frac{x^2 r^2}{R_3^2}}, \quad \hat{r} = r \sqrt{\frac{1 - x^2}{1 - \frac{x^2 r^2}{R_3^2}}}, \tag{141}$$

such that the line element of the C-metric (39) (with $\mu = 0$) becomes

$$ds^2 = L_4^2 d\sigma^2 + \frac{L_4^2}{R_3^2}\sinh^2(\sigma)\left[-\left(1-\frac{\hat{r}^2}{R_3^2}\right)dt^2 + \left(1-\frac{\hat{r}^2}{R_3^2}\right)^{-1} d\hat{r}^2 + \hat{r}^2 d\phi^2\right]. \tag{142}$$

Clearly, constant-σ slices give dS_3 in static patch coordinates with radius $R_3 = L_4\sinh(\sigma)$ and a cosmological horizon at $\hat{r} = R_3$.

The cosmological horizon at $\hat{r} = R_3$ (for constant σ) is in fact identified with the bulk acceleration horizon. This can be seen via the coordinate transformation

$$\frac{t}{R_3} = \frac{t_R}{L_4}, \quad \cosh(\sigma) = \frac{\rho}{L_4}\cosh(\vartheta), \quad \frac{\hat{r}^2}{R_3^2} = \frac{\rho^2\sinh^2(\vartheta)}{\rho^2\cosh^2(\vartheta) - L_4^2}, \tag{143}$$

which brings the line element (142) to AdS_4–Rindler form,

$$ds^2 = -\left(\frac{\rho^2}{L_4^2}-1\right)dt_R^2 + \left(\frac{\rho^2}{L_4^2}-1\right)^{-1} d\rho^2 + \rho^2(d\vartheta^2 + \sinh^2(\vartheta)d\phi^2). \tag{144}$$

Orbits of the Rindler-time translation Killing vector ∂_{t_R} correspond to uniformly accelerating trajectories. The cosmological horizon in (142) corresponds to the (non-compact) acceleration horizon $\rho = L_4$ with horizon temperature $T_R = (2\pi L_4)^{-1}$.

As in the qBTZ black hole, when $\mu \neq 0$, the root structure of the metric function $H(r)$ results in a black hole horizon. Meanwhile, real roots of $G(x)$ correspond to orbits of ∂_ϕ, and to ensure a finite black hole horizon, we again restrict to the range $0 \leq x \leq x_1$, where x_1 is the smallest root of $G(x)$. Specifically, since $\kappa = +1$, it follows $x_1 \in (0, 1]$ (46), where μ, via (45), is monotonically decreasing from $+\infty$ to zero, with $\mu = 0$ for $x_1 = 1$. Further, as before, the conical singularity at $x = x_1$ is removed via the identification (48) with $\kappa = +1$.

The next essential difference between the quantum AdS and dS black hole constructions is that an asymptotically dS_3 Randall–Sundrum brane is embedded AdS_4 at the umbilic $x = 0$ hypersurface. Israel junction conditions again fix the brane tension to be $\tau = (2\pi G_4\ell)^{-1}$. In terms of the empty dS_3 geometry (142), the brane sits at

$$\sinh(\sigma_b) = \frac{R_3}{L_4}, \tag{145}$$

excluding the region $\sigma > \sigma_b$. Notice, moreover, the area of the bulk horizon at $\hat{r} = R_3$ is finite,

$$2\pi L_4^2(\cosh(\sigma_b) - 1) = 2\pi R_3^2\frac{\ell}{\ell + R_3}. \tag{146}$$

That is, while the bulk acceleration horizon is generally non-compact (since it extends to the asymptotic boundary at $\sigma \to \infty$), its intersection with the brane is compact. Thus, the bulk acceleration horizon induces a (compact) cosmological horizon on the dS_3 brane. When $\mu \neq 0$, the bulk black hole horizon is projected onto the brane, resulting in an induced geometry

$$ds^2|_{x=0} = -\left(1-\frac{r^2}{R_3^2}-\frac{\mu\ell}{r}\right)dt^2 + \left(1-\frac{r^2}{R_3^2}-\frac{\mu\ell}{r}\right)^{-1} dr^2 + r^2 d\phi^2, \tag{147}$$

with a single black hole and cosmological horizon. See Figure 9 for an illustration.

Another caveat about the Randall–Sundrum brane construction is that the brane geometry will contain Big Bang and Big Crunch singularities in the asymptotic past and future. The reason follows because of the amount the brane radiates as it accelerates in the bulk. From the brane perspective, the time to reach the asymptotic past or future dS boundaries is infinite. Thus, the brane emits an infinite amount of radiation, thereby causing a piling

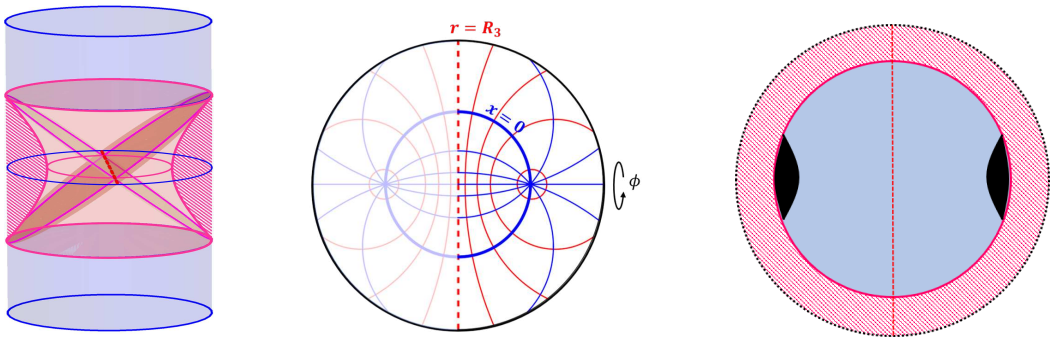

Figure 9. Randall–Sundrum braneworld. Left: Bulk AdS_4 with a dS_3 brane. The brane is represented as a (magenta) hyperboloid. The bulk region up to the brane ($x < 0$, dashed magenta region) is excluded. To complete the construction, glue a second copy along the two-sided brane. Cosmological horizons on the brane correspond to bulk acceleration horizons intersecting the brane (red dashed line). **Center**: AdS_4 C-metric with $\mu = 0$, in (r, x) coordinates in a slice at $t = 0$ and constant ϕ. Lines of constant x are blue arcs; lines of constant r are red arcs (full circles for $0 < r < \ell$). The thick blue circle $x = 0$ is where we place the dS_3 brane; its interior is $0 < x \leq 1$, with $x = 1$ the ϕ axis of rotation. The exterior region $x < 0$ is excluded in the braneworld construction. The vertical red dashed line is the horizon at $r = R_3$. Its intersection with the brane yields a dS_3 cosmological horizon. The coordinates only cover half of the disk with the other half being obtained through analytic continuation. **Right**: Constant t-time slice of a single AdS_4 cylinder with a de Sitter brane (thick red circle) containing black holes. The coordinates cover half of the disk, containing a single black hole and cosmological horizon, where the other half is obtained via analytic continuation.

of rays at future/past Cauchy horizons. The formation of the cosmological singularities is essentially the same phenomenon that enforces (strong) cosmic censorship at the inner Cauchy horizon in charged or rotating black holes. Alternatively, the Randall–Sundrum braneworld can be understood in terms of false vacuum decay [102–104] mediated by Coleman and de Luccia bubbles [105] of 'nothing'. This vacuum decay process inevitably leads to Big Bang/Big Crunch singularities.

4.3.2. Quantum Schwarzschild–de Sitter

The naive metric (147) is not cast in canonically normalized coordinates, as ϕ has periodicity $\phi \sim \phi + \Delta\phi$. Rescaling coordinates $(t, r, \phi) \to (\eta\bar{t}, \eta^{-1}\bar{r}, \eta\bar{\phi})$ with η given in (63) (for $\kappa = +1$), the geometry on the dS_3 brane is

$$ds^2_{\text{qSdS}} = -H(\bar{r})d\bar{t}^2 + H(\bar{r})^{-1}d\bar{r}^2 + \bar{r}^2 d\bar{\phi}^2, \quad H(\bar{r}) = \left(1 - 8\mathcal{G}_3 M - \frac{\bar{r}^2}{R_3^2} - \frac{\ell F(M)}{\bar{r}}\right) \tag{148}$$

where we identify

$$8\mathcal{G}_3 M \equiv 1 - \eta^2 = 1 - \frac{4x_1^2}{(3 - x_1^2)^2}, \qquad F(M) \equiv 8\frac{(1 - x_1^2)}{(3 - x_1^2)^3} \tag{149}$$

with renormalized Newton's constant $\mathcal{G}_3 \equiv G_3 \frac{L_4}{\ell}$. The mass identification is motivated by how the mass of de Sitter black holes in Einstein–dS gravity is typically given by the subleading constant term in the g_{tt} component of the metric.

Analogous to the quantum BTZ set-up, the dS metric (148) has the same form as the perturbative solution (20) to the semi-classical Einstein equations. Again, here, the $1/r$ correction is exact, and the metric is an exact solution to the whole tower of higher-derivative terms of the induced action. Substituting the metric into the gravitational equations of motion (see (69)—(70) with $\ell_3^2 = -R_3^2$) yields the same structure of the stress–energy tensor $\langle T^i_j \rangle_0$ (71) and $\langle T^i_j \rangle_2$ (72). In the limit of vanishing backreaction, the geometry

(148) takes the form of classical Schwarzschild–dS_3, which is a conical defect with a single cosmological horizon. For $\ell \neq 0$, the metric is interpreted as a static quantum black hole in dS_3, i.e., a three-dimensional *quantum Schwarzschild–de Sitter* black hole (qSdS) [26]. As in the qBTZ system, the qSdS black hole for $\ell > 0$ has a curvature singularity at $\bar{r} = 0$ that is hidden behind a black hole horizon induced by a semi-classical backreaction.

In contrast with the qBTZ system, the qSdS solution does not subdivide into several branches of quantum black holes. Indeed, since $\kappa = +1$, here, $0 < x_1 < 1$. In this range, given the mass identification (149), the qSdS always has $M \geq 0$, with $M = 1/8\mathcal{G}_3$ and $F = 8/27$ at $x_1 = 0$, and $M = F = 0$ at $x_1 = 1$. The $M = 0$ solution with $\ell \neq 0$ is dubbed *quantum* dS_3, accounting for a large-c cutoff CFT living in dS_3. Meanwhile, the $M = 1/8\mathcal{G}_3$ solution is the analog of the upper bound on the classical Schwarzschild–dS_3 conical defect.

The quantum SdS black hole, in fact, has a more stringent upper bound on mass than the conical defect mass. This is a consequence of the fact that the geometry (148) has both a black hole and cosmological horizon, and it is in complete analogy with classical higher-dimensional Schwarzschild–de Sitter black holes. It is well known that classical SdS black holes (in four or higher spacetime dimensions) have an upper bound on their mass in order to avoid the presence of a naked singularity. This largest mass black hole is known as the Nariai black hole [106] with mass $M_{\rm N}$. Geometrically, the Nariai black hole is one in which the (typically smaller) black hole horizon r_h coincides with the (typically larger) cosmological horizon r_c, i.e., $r_h = r_c \equiv r_{\rm N}$, which is the Nariai horizon radius. In the context of the AdS_4 C-metric, the four-dimensional geometry has a Nariai limit that induces a Nariai geometry on the brane at $x = 0$ [26]

$$ds^2_{\rm N} = -\left(1 - \frac{\rho^2}{\bar{r}^2_{\rm N}}\right) d\tau^2 + \left(1 - \frac{\rho^2}{\bar{r}^2_{\rm N}}\right)^{-1} d\rho^2 + \bar{r}^2_{\rm N} d\bar{\phi}^2. \tag{150}$$

Here, τ and ρ are time and radial coordinates, respectively, and $\bar{r}_{\rm N} = \eta r_{\rm N}$ with $r_{\rm N} = R_3/\sqrt{3}$. The (bulk) Nariai black hole places an upper bound on $(\mu\ell)$ in the C-metric; specifically, $(\mu\ell) \leq (\mu\ell)_{\rm N} = 2r_{\rm N}/3$. This bulk upper bound places an upper bound on the mass M of the qSdS black hole, which is denoted $M_{\rm N}$. The precise form of $M_{\rm N}$ is complicated; however, the Nariai mass was found to live in the finite range [26]

$$\frac{11}{27} < 8\mathcal{G}_3 M < 1, \tag{151}$$

where the upper limit corresponds to when $\ell/R_3 \to 0$, while the lower limit occurs for $\nu \approx 1$. Therefore, the Nariai mass bound $M \leq M_{\rm N}$ is generally more restrictive than the conical defect bound $M \leq 1/8\mathcal{G}_3$. Notably, the classical SdS_3 conical defect does not have a Nariai limit. Thus, a semi-classical backreaction induces an upper limit on the amount of mass allowed in dS_3 which does not saturate the maximum conical deficit angle.

Finally, the Nariai solution puts a bound on the quantum backreaction due to the CFT for which a quantum dS_3 black hole exists. In particular, for non-vanishing backreaction $(\ell \neq 0)$, the form function $F(M)$ has a maximum value. Correspondingly, the angular deficit $\Delta\phi$ has a maximum value. For too large angular deficits, a backreaction creates a black hole with a mass $M > M_{\rm N}$ such that it is too large to fit inside the dS_3 static patch. For such deficits, the quantum SdS solution no longer exists, and the resulting geometry is described by a naked conical defect spacetime, which is analogous to the braneworld geometry induced by the bulk BTZ black string.

4.3.3. Quantum Kerr–de Sitter

As in the static case, rotating quantum dS_3 black holes can be constructed in essentially the same way as the rotating qBTZ (91). Starting from the rotating C-metric (78) with

$\kappa = +1$ and replacing $a \to -a$, and imposing bulk regularity, the metric on the brane in canonically normalized coordinates is [27][29]

$$\begin{aligned} ds^2_{\text{qKdS}} = &-\left(1 - 8\mathcal{G}_3 M - \frac{\bar{r}^2}{R_3^2} - \frac{\mu\ell\eta^2}{r}\right) d\bar{t}^2 \\ &+ \left(1 - 8\mathcal{G}_3 M - \frac{\bar{r}^2}{R_3^2} + \frac{(4\mathcal{G}_3 J)^2}{\bar{r}^2} - \frac{\mu\ell(1+\tilde{a}^2)^2\eta^4 r}{\bar{r}^2}\right)^{-1} d\bar{r}^2 \\ &+ \left(\bar{r}^2 + \frac{\mu\ell\tilde{a}^2 R_3^2\eta^2}{r}\right) d\bar{\phi}^2 - 4\mathcal{G}_3 J\left(1 + \frac{\ell}{x_1 r}\right)(d\bar{\phi}d\bar{t} + d\bar{t}d\bar{\phi}). \end{aligned} \tag{152}$$

with mass and angular momentum identified as

$$8\mathcal{G}_3 M \equiv 1 - \eta^2\left(1 - \tilde{a}^2 + \frac{4\tilde{a}^2}{x_1^2}\right) = 1 - \frac{4[x_1^2 - \tilde{a}^2(x_1^2 - 4)]}{(3 - x_1^2 + \tilde{a}^2)^2}, \tag{153}$$

$$4\mathcal{G}_3 J \equiv -R_3\tilde{a}\mu x_1\eta^2 = \frac{4R_3\tilde{a}(x_1^2 + \tilde{a}^2 - 1)}{(3 - x_1^2 + \tilde{a}^2)^2}. \tag{154}$$

The metric (152) is dubbed the quantum Kerr–dS$_3$ black hole since when $\ell \to 0$, the geometry of the classical Kerr–ds$_3$ conical defect is recovered. There are a couple of limits worth noting: (i) when the parameter μ (83) vanishes, i.e., $x_1 = \sqrt{1 - \tilde{a}^2}$, both $M = J = 0$, resulting in the empty dS$_3$ geometry, and (ii) mass M also vanishes when $x_1 = \sqrt{9 - \tilde{a}^2}$; however, $J \neq 0$ and $\mu \neq 0$, resulting in a quantum rotating dS$_3$.

Substituting the geometry (152) into the gravity field equations results in a holographic stress tensor with components of essentially the same form as (102)—see [27] for explicit details. Now, the function $F(M, J)$ from evaluating the large-$\bar{r}$ behavior of $\langle T^{\bar{t}}_{\bar{t}}\rangle_0$ is

$$F(M, J) \equiv \mu\eta^3\sqrt{1 + \tilde{a}^2}(1 - 2\tilde{a}^2) = \frac{8\sqrt{1 + \tilde{a}^2}(1 - 2\tilde{a}^2)(1 - x_1^2 - \tilde{a}^2)}{(3 - x_1^2 + \tilde{a}^2)^3}. \tag{155}$$

Notice $F(M, J)$ will vanish either when $\mu = 0$, i.e., $x_1^2 = 1 - \tilde{a}^2$. The zero $\tilde{a}^2 = 1/2$, meanwhile, is unique only to the $\langle T^{\bar{t}}_{\bar{t}}\rangle_0$ component with the remaining components of the holographic stress tensor being non-zero for this value of $\tilde{a}$. This stands in contrast with the rotating qBTZ black hole, for which every component vanishes when $\tilde{a}^2 = 1$. Further, as in the qBTZ case, the radial dependence of the renormalized stress tensor due to a conformally coupled scalar field (found perturbatively in [27]) is significantly more complicated than the holographic stress tensor.

Horizon Structure

Horizons in the bulk correspond to positive real roots r_i of $H(r)$, where the Killing vector

$$\zeta^b = \partial_t - \frac{a}{r_i^2}\partial_\phi \tag{156}$$

becomes null. To classify the types of horizons, define the function $Q(r) \equiv r^2 H(r)$. Since $Q(r)$ is a quartic polynomial in r, it will generally have either four, two, or zero real roots. Consider the case when there are four real roots: three positive roots correspond to the cosmological horizon r_c, the outer black hole horizon r_+, and inner black hole horizon r_-,

obeying $r_- \leq r_+ \leq r_c$, while the fourth root, $r_n = -(r_c + r_+ + r_-) < 0$ and resides behind the singularity at $r = 0$. Using $H(r_c) = 0$, and $H(r_\pm) = 0$, we can express

$$\begin{aligned} R_3^2 &= r_c^2 + r_+^2 + r_c r_+ + r_-(r_c + r_+ + r_-), \\ \mu\ell &= \frac{(r_c + r_+)(r_c + r_-)(r_+ + r_-)}{r_c^2 + r_+^2 + r_c r_+ + r_-(r_c + r_+ + r_-)}, \\ a^2 &= \frac{r_c r_+ r_- (r_c + r_+ + r_-)}{r_c^2 + r_+^2 + r_c r_+ + r_-(r_c + r_+ + r_-)}. \end{aligned} \tag{157}$$

The limit $r_- \to 0$ coincides with $a = 0$, while $r_+ = r_- = 0$ corresponds to $\mu \to 0$, resulting in the Kerr–dS$_3$ geometry with a single cosmological horizon.

The positive roots r_i to $H(r)$ correspond to rotating horizons with rotation Ω_i,

$$\Omega_i \equiv \frac{a}{R_3^2} \frac{(x_1^2 r_i^2 - R_3^2)}{(r_i^2 + a^2 x_1^2)}, \tag{158}$$

generated by the (canonically normalized) Killing vector

$$\bar{\zeta}^b \equiv \frac{\eta(1+\tilde{a}^2)}{\left(1 + \frac{a^2 x_1^2}{r_i^2}\right)} \zeta^b = \partial_{\bar{t}}^b + \Omega_i \partial_{\bar{\phi}}^b. \tag{159}$$

Moreover, the surface gravity κ_i associated with each horizon r_i is given by

$$\kappa_i = \frac{\eta(1+\tilde{a}^2)}{(r_i^2 + a^2 x_1^2)} \frac{r_i^2}{2} |H'(r_i)| = \frac{\eta(1+\tilde{a}^2)}{(r_i^2 + a^2 x_1^2)} \frac{1}{2R_3^2 r_i} |R_3^2 \mu\ell r_i - 2r_i^4 - 2a^2 R_3^2|, \tag{160}$$

where we used the definition $\bar{\zeta}^b \nabla_b \bar{\zeta}^c = \kappa \bar{\zeta}^c$. Explicitly,

$$\begin{aligned} \kappa_c &= -\frac{\eta(1+\tilde{a}^2)}{2R_3^2(r_c^2 + a^2 x_1^2)} (r_c - r_+)(r_c - r_-)(r_+ + r_- + 2r_c), \\ \kappa_+ &= \frac{\eta(1+\tilde{a}^2)}{2R_3^2(r_+^2 + a^2 x_1^2)} (r_c - r_+)(r_+ - r_-)(r_c + r_- + 2r_+), \\ \kappa_- &= -\frac{\eta(1+\tilde{a}^2)}{2R_3^2(r_-^2 + a^2 x_1^2)} (r_c - r_-)(r_+ - r_-)(r_c + r_+ + 2r_-). \end{aligned} \tag{161}$$

Notice the cosmological horizon surface gravity κ_c vanishes when $r_c = r_+$ or $r_c = r_-$ and similarly for the other surface gravities. When $r_- \to 0$, i.e., κ_c and κ_+ simplify to the surface gravities of the cosmological horizon and black hole horizon of the qSdS black hole [26].

In the naive coordinates, a computation of the Kretschmann scalar reveals a curvature singularity at $r = 0$, corresponding to a ring singularity at $\bar{r} = r_s$ in canonically normalized coordinates. As in the rotating qBTZ black hole, closed timelike curves can appear near the ring singularity. These closed timelike curves can be eliminated via an appropriate periodic identification [107], such that constant $\bar{t}$ hypersurfaces are closed and span two black hole regions with opposite spin, cutting through intersections of $r = r_c$ and $r = r_+$.

Ergoregions. As with classical Kerr–dS spacetimes, the qKdS black hole has a stationary limit surface and two ergoregions associated with the outer black hole and cosmological horizons. Explicitly, the Killing vector ∂_t in the naive metric has norm $\mathcal{N}$

$$\mathcal{N} = -H(r) + \frac{a^2}{r^2}. \tag{162}$$

Thus, at the outer and cosmological horizons, the time-translation Killing vector ∂_t becomes spacelike. The locus of points where $\mathcal{N} = 0$ yields a stationary limit surface, satisfying

$r(R_3^2 - r^2) = R_3^2 \mu\ell$. Since there exist regions in between the outer and cosmological horizons where ∂_t is timelike, there are two ergoregions, where an observer is forced to move in the direction of rotation of the outer black hole horizon or cosmological horizon. In principle, the Penrose process of energy extraction in the qKdS solution operates in morally the same way as a classical four-dimensional Kerr–de Sitter black hole (see, e.g., [108]).

Extremal limits. As with the four-dimensional Kerr–de Sitter black hole, the quantum Kerr–dS$_3$ has a number of limiting geometries. Specifically, (i) extremal or 'cold' limit, where $r_+ = r_-$; (ii) rotating Nariai limit, where $r_c = r_+$, and (iii) the 'ultracold' limit where $r_c = r_+ = r_-$. In the near-horizon regime, the geometries appear as fibered products of a circle and two-dimensional anti-de Sitter, de Sitter, and Minkowski space, respectively. For details, see [27]. These limiting geometries, moreover, have the same qualitative features as (warped) dS$_3$ black hole solutions to topologically massive gravity, cf. [37,38,109]. There is also a 'lukewarm' limit, where the surface gravities $\kappa_c = \kappa_+$ at a value different from the surface gravity of the Nariai black hole.

Adding charge. Similar to the charged quantum BTZ black hole, quantum de Sitter black holes can be charged (see [110]). In this context, as with the classical charged dS black holes in $3+1$-dimensions and higher, the charged black hole has three horizons: outer and inner black hole horizons, and the cosmological horizon. As such, the solution has three limiting geometries: (i) the extremal limit, where $r_+ = r_-$; (ii) the charged Nariai limit, where $r_c = r_+$, and (iii) the ultracold limit, where $r_c = r_+ = r_-$. Moreover, the physical parameter space of the solution is characterized by a 'shark fin' diagram for non-zero backreaction parameter ν.

4.4. Quantum Black Holes in Flat Space

A point mass in three-dimensional Minkowski space, Mink$_3$, is described by a conical singularity with no horizon; the Schwarzschild solution in three dimensions is not a black hole. Again, quantum backreaction effects alter the geometry such that the black hole horizon appears to hide the conical singularity [32]. The only known way to consistently construct an exact quantum black hole in asymptotic Mink$_3$ space is via braneworld holography.

The bulk set-up is the same as for quantum dS$_3$ black holes: the AdS$_4$ C-metric with a two-sided Randall–Sundrum brane. In some respects, the asymptotically flat quantum black holes may be viewed as a special limit, $R_3 \to \infty$, of the dS$_3$ black holes. Although they were the first exact three-dimensional braneworld black hole solution to be discovered [23], quantum black holes in Mink$_3$ have received less attention than their (A)dS cousins [22]. For this reason, we present a fresh take on quantum Mink$_3$ black holes.

4.4.1. Bulk Set-Up

Consider the static C-metric (39) with metric functions (40), except $\kappa = +1$ and without the (A)dS factor, such that $H(r)$ has the form

$$H(r) = 1 - \frac{\mu\ell}{r}. \tag{163}$$

It is straightforward to verify the bulk geometry is an Einstein metric with a negative cosmological constant where the bulk length scale is

$$L_4 = \ell. \tag{164}$$

This is the first notable difference compared to the (A)dS examples and will have ramifications as we proceed. This means the acceleration horizon is present in the spacetime. However, it has a different effect than in the dS case where $\ell < L_4$.

For $\mu \neq 0$, the bulk geometry has a black hole horizon at $H(r_+) = 0$,

$$r_+ = \mu\ell, \tag{165}$$

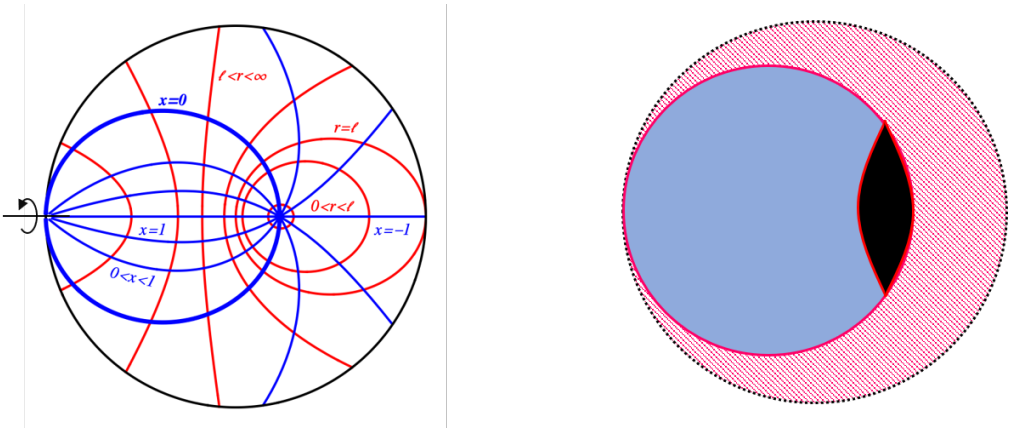

Figure 10. Randall–Sundrum braneworld. **Left**: A constant t and ϕ slice of the AdS_4 C-metric with $\mu = 0$ and $\kappa = +1$ (Poincaré disc). Lines of constant x are in blue, while lines of constant r are in red. The ϕ-axis of rotation is at $x = \pm 1$. The thick blue circle is $x = 0$. **Right**: Schematic of an asymptotically flat Randall–Sundrum ETW brane at $x = 0$ with a static black hole ($\mu \neq 0$). The shaded magenta region is excluded. The acceleration horizon for the dS_3 braneworld has been effectively pushed to the AdS_4 boundary.

hiding the curvature singularity at $r = 0$. There is a second horizon at $r \to \infty$ corresponding to the bulk AdS_4 horizon[30]. To see this, consider the bulk geometry with $\mu = 0$ (such that $H(r) = 1$ and $G(x) = 1 - x^2$). The coordinate transformation

$$w \equiv \ell + xr, \quad \hat{r} \equiv r\sqrt{1 - x^2}, \tag{166}$$

brings the bulk metric to empty AdS_4 in Poincaré form

$$ds^2 = \frac{\ell^2}{w^2}\left(-dt^2 + d\hat{r}^2 + \hat{r}^2 d\phi^2 + dw^2\right). \tag{167}$$

Evidently, $r = 0$ no longer represents a curvature singularity but instead a non-singular worldline $w = \ell$, $\hat{r} = 0$. Meanwhile, $xr = -\ell$ maps to the asymptotic boundary $w = 0$ and $r \to \infty$ to the AdS_4 horizon $w \to \infty$.

As is now standard, real roots of $G(x)$ correspond to orbits of ∂_ϕ. Let x_1 denote the smallest root of $G(x)$ and again restrict to the range $0 \leq x \leq x_1$. With $\kappa = +1$, $x_1 \in (0, 1]$ (46), where μ is defined in (45). The conical singularity at $x = x_1$ is removed via the identification (48) with $\kappa = +1$.

The $x = 0$ hypersurface is umbilic. In Poincaré coordinates with $\mu = 0$ (166), this surface is located at $w = \ell$. We place a two-sided ETW Randall–Sundrum brane at $x = 0$, retaining only the region $0 \leq x \leq x_1$ (Figure 10). To complete space, we glue another copy of the region $0 \leq x \leq x_1$ along the brane at $x = 0$. Israel junction conditions fix the brane tension to be $\tau = (2\pi G_4 \ell)^{-1}$. Notably, since $\ell = L_4$, the tension is said to be at its critical value. As we will see momentarily, this condition leads to a vanishing induced cosmological constant. The induced geometry at $x = 0$ is

$$ds^2_{x=0} = -\left(1 - \frac{\mu\ell}{r}\right)dt^2 + \left(1 - \frac{\mu\ell}{r}\right)^{-1} dr^2 + r^2 d\phi^2. \tag{168}$$

For $\ell \neq 0$, this geometry describes a black hole with horizon radius $r_+ = \mu\ell$. In terms of coordinate w, the black hole horizon is located at $w_+ = \ell + xr_+$. Therefore, the brane at $w = \ell$ cuts through the bulk black hole horizon such that the black hole extends only slightly off of the brane to a distance $w_{\max} = \ell + r_+ x_1 \leq \ell + r_+$ (since $x_1 \leq 1$).

The induced brane theory is (53); however, since $L_4 = \ell$, the induced brane cosmological constant (55) is zero, while the induced Newton's constant (54) is $G_3 = G_4/2\ell$. The

central charge of the cutoff CFT$_3$ is $c_3 = \frac{L_4^2}{G_4} = \frac{\ell}{2G_3}$. Higher-derivative terms enter at order $\mathcal{O}(\ell^2)$, and treating the cutoff as small, $\ell \leq 1$, the higher-derivative contributions serve as corrections to three-dimensional Einstein gravity.

4.4.2. Quantum Schwarzschild Black Hole

The angular coordinate ϕ in the naive metric (168) has a periodicity of $\phi \sim \phi + \Delta\phi$. Working with rescaled coordinates $(t, r, \phi) \to (\eta\bar{t}, \eta^{-1}\bar{r}, \eta\bar{\phi})$ for η (63) (with $\kappa = +1$), the geometry on the Mink$_3$ brane is[31]

$$ds^2_{\text{qSchw}} = -H(\bar{r})d\bar{t}^2 + H(\bar{r})^{-1}d\bar{r}^2 + \bar{r}^2 d\bar{\phi}^2, \quad H(\bar{r}) = 1 - 8G_3M - \frac{\ell F(M)}{\bar{r}} \tag{169}$$

where we identified the mass as in the de Sitter context (149)

$$M \equiv \frac{1}{8G_3}\frac{(x_1^2-1)(x_1^2-9)}{(3-x_1^2)^2}, \qquad F(M) \equiv 8\frac{(1-x_1^2)}{(3-x_1^2)^3}. \tag{170}$$

Since $L_4 = \ell$, the renormalized Newton's constant $\mathcal{G}_3 = G_3$.

The geometry (169) is an exact solution to the induced semi-classical equations of motion (68) (with $\ell_3 \to \infty$) with a quantum stress tensor as in (71) and (72) (with $\ell_3 \to \infty$). Thus, we interpret the solution as the three-dimensional *quantum Schwarzschild* black hole. A curvature singularity at $\bar{r} = 0$ is hidden behind a black hole event horizon at

$$\bar{r}_+ = \frac{\ell F(M)}{(1-8G_3M)}. \tag{171}$$

At the horizon, the time-translation Killing vector $\bar{\xi}^i = \eta\partial^i_{\bar{t}}$ goes null, having surface gravity

$$\kappa_+ = \frac{1}{2}|H'(\bar{r}_+)| = \frac{\ell F(M)}{\bar{r}_+^2} = \frac{(1-8G_3M)^2}{\ell F(M)}. \tag{172}$$

4.4.3. Quantum Kerr Black Hole

Rotating black holes in Mink$_3$ are constructed by embedding a Randall–Sundrum brane with critical tension inside the rotating C-metric (78), such that the metric functions are

$$\begin{aligned} &H(r) = 1 - \frac{\mu\ell}{r} + \frac{a^2}{r^2}, \quad G(x) = 1 - x^2 - \mu x^3, \\ &\Sigma(x,r) = 1 + \frac{a^2x^2}{r^3}. \end{aligned} \tag{173}$$

Formally, the bulk regularity analysis is the same; however, some of the expressions are simpler because in this limit $\tilde{a} = 0$, which is a consequence of the $G(x)$ function losing its quartic term compared to its (A)dS siblings. Thus, the metric on the brane in canonically normalized coordinates is

$$\begin{aligned} ds^2_{\text{qKerr}} = &-\left(1 - 8G_3M - \frac{\mu\ell\eta^2}{r}\right)d\bar{t}^2 + \left(1 - 8G_3M + \frac{(4G_3J)^2}{\bar{r}^2} - \frac{\mu\ell\eta^4 r}{\bar{r}^2}\right)^{-1}d\bar{r}^2 \\ &+ \left(\bar{r}^2 + \frac{\mu\ell a^2 x_1^4\eta^2}{r}\right)d\bar{\phi}^2 - 4G_3J\left(1 + \frac{\ell}{x_1 r}\right)(d\bar{\phi}d\bar{t} + d\bar{t}d\bar{\phi}), \end{aligned} \tag{174}$$

with canonical coordinates

$$\begin{aligned} \bar{t} &= \eta^{-1}(t - ax_1^2\phi), \qquad \bar{\phi} = \eta^{-1}\phi, \\ \bar{r}^2 &= \eta^2 r^2 + r_s^2, \qquad r_s \equiv -\frac{2ax_1^2\sqrt{2-x_1^2}}{(3-x_1^2)}, \end{aligned} \tag{175}$$

where $\eta = 2x_1/(3-x_1^2)$. Further, the angular momentum J is identified as

$$4G_3 J \equiv \frac{4ax_1^2(x_1^2-1)}{(3-x_1^2)^2}. \tag{176}$$

while the mass is identified as in the static case (170) and is thus independent of the rotation parameter a. A ring singularity appears at $\bar{r} = r_s$.

The metric (174) is dubbed the quantum Kerr$_3$ black hole. In the limit of vanishing backreaction, one recovers the classical conical Kerr geometry. At leading order in a small-ℓ expansion, the stress tensor of the holographic CFT$_3$ is

$$\begin{aligned} \langle T^{\bar{t}}_{\bar{t}} \rangle_0 &= \frac{\mu\ell}{16\pi G_3 r^3}\left(1 + \frac{3a^2x_1^2}{r^2}\right), \\ \langle T^{\bar{r}}_{\bar{r}} \rangle_0 &= \frac{\mu\ell}{16\pi G_3 r^3}, \\ \langle T^{\bar{\phi}}_{\bar{\phi}} \rangle_0 &= -\frac{\mu\ell}{16\pi G_3 r^3}\left(2 + \frac{3a^2x_1^2}{r^2}\right), \\ \langle T^{\bar{t}}_{\bar{\phi}} \rangle_0 &= \frac{3\mu\ell a x_1^2}{16\pi G_3 r^3}\left(1 + \frac{a^2x_1^2}{r^2}\right), \\ \langle T^{\bar{\phi}}_{\bar{t}} \rangle_0 &= -\frac{3\mu\ell a}{16\pi G_3 r^5}. \end{aligned} \tag{177}$$

Notice now that function $F(M,J)$ from evaluating the large-$\bar{r}$ behavior of $\langle T^{\bar{t}}_{\bar{t}} \rangle_0$ is exactly equal to $F(M) = \mu\eta^3$, as in the static case.

4.5. Horizon Structure

Bulk black hole horizons correspond to real roots r_i of $H(r)$, i.e.,

$$r_\pm = \frac{1}{2}(\mu\ell \pm \sqrt{(\mu\ell)^2 - 4a^2}). \tag{178}$$

These correspond to rotating horizons with rotation

$$\Omega_\pm = -\frac{a}{(r_\pm^2 + a^2x_1^2)}, \tag{179}$$

generated by Killing vector $\bar{\zeta}^j = \partial^j_{\bar{t}} + \Omega_\pm \partial^j_{\bar{\phi}}$. The surface gravities are

$$\kappa_\pm = \frac{\eta}{(r_\pm^2 + a^2x_1^2)}\frac{r_\pm^2}{2}|H'(r_\pm)| = \frac{\eta}{2(r_\pm^2 + a^2x_1^2)}\left|\mu\ell - \frac{2a^2}{r_\pm}\right|. \tag{180}$$

There is an extremal black hole when the inner and outer horizons coincide, $r_+ = r_- \equiv r_{\rm ex}$, i.e., when $\mu\ell = 2a$. In this limit, the surface gravities (180) vanish.

5. Quantum Black Hole Thermodynamics

Black hole thermodynamics [111–114] reveals an interplay between geometry, quantum mechanics, and thermodynamics. This is encapsulated by the Bekenstein–Hawking entropy–area relation,

$$S = \frac{k_B c^3}{\hbar G} \frac{A[H]}{4}, \tag{181}$$

for Boltzmann constant k_B, and we have temporarily restored factors of $\hbar$ and speed of light c. The area law states black holes carry a thermodynamic entropy proportional to the area of a codimension-2 cross-section of their event horizon H. Hence, black holes may be treated as genuine thermal systems with energy, entropy, and temperature, and other thermodynamic variables depending on the type of black hole. In the case of stationary black holes, the laws of black hole mechanics [115] may be reinterpreted as laws of thermodynamics. For example, the first law relates a variation in mass M to variations of the other thermodynamic variables

$$dM = TdS + ..., \tag{182}$$

with Hawking temperature T, and where the ellipsis implies variations of other possible thermodynamic variables, e.g., electric/magnetic charge, rotation, and so forth.

As we review below, just as the bulk geometry imprints itself on the brane, so too does its thermal description. Thus, classical thermodynamics of the bulk black hole geometry is interpreted as semi-classical thermodynamics of the quantum black hole system. This allows for an exact study of quantum black hole thermodynamics at any order in a backreaction.

5.1. Bulk Thermodynamics

When we think of mapping out the properties of a thermodynamic system, we typically think of one near equilibrium. Likewise, in black hole thermodynamics, often the first task is to check whether the system has a well-defined notion of thermal equilibrium. Such is the case, for example, of Kerr–Newman black holes in AdS, where thermal equilibrium is unambiguously defined [116]. Alternatively, the thermodynamics of black holes in de Sitter space is conceptually more subtle because a static patch observer encounters a system with two horizons at different temperatures (except in special limits, e.g., Nariai), such that the system is not generally in equilibrium. Similarly, due to the presence of an acceleration and black hole horizon, the thermodynamics of the C-metric is generally more subtle than non-accelerating black holes—even when the accelerating black holes are embedded in AdS. Furthermore, although the C-metric line element does not display time dependence, uniformly accelerating black holes will deliver non-vanishing radiation at asymptotic infinity [117]. Thus, it is not obvious how an accelerating black hole could possibly be in equilibrium.

The AdS_4 C-metric, does, however, have a distinct advantage over the flat or dS C-metrics. Working in a particular regime of parameters, the negative cosmological constant has the effect of essentially removing the acceleration horizon such that it can be consistently neglected. This regime is precisely the 'slowly accelerating' black hole [90] where the (inverse) acceleration and AdS_4 length scale satisfy

$$\textbf{Slowly accelerating:} \quad \ell > L_4. \tag{183}$$

In such situations, the AdS_4 C-metric is described by a single black hole suspended away from the origin by a cosmic string attached to the AdS boundary (recall Figure 4). Consequently, being able to ignore the acceleration allows for the temperature of the black hole system to be defined in a straightforward way. Even still, due to the presence of cosmic strings, the black hole is not isolated. This makes consistently carrying out the thermodynamic analysis of the slowly accelerating black hole non-trivial. Indeed, one must account for both the black hole and cosmic string, leading to a modified first law including variations of the tension of the cosmic string [118–121][32].

While the starting point is the same, the thermodynamics of the bulk black hole system used in the braneworld black hole constructions in Section 4 is ultimately different from the usual AdS_4 C-metric. Firstly, in the braneworld construction, there is no cosmic string; instead, there is a brane. For a purely tensional brane of constant tension, the brane does not play an obvious role in the bulk black hole thermodynamics (we will revisit this when we allow for variable tension). Second, the bulk geometry is regular in that the zeros to the metric function $G(x)$ are removed along with the conical defects they induce. These two facts make the thermodynamic analysis less subtle than the standard C-metric.

In general, however, the question of thermal equilibrium remains due to the presence of the bulk acceleration horizon. In fact, this question distinguishes the treatment of the Karch–Randall and Randall–Sundrum braneworld constructions. For the former, the bulk system started with a slowly accelerating black hole (183), such that the acceleration horizon does not imprint itself on the brane. Alternatively, for a dS_3 Randall–Sundrum brane, the bulk acceleration horizon cannot be ignored because one is not in the slow acceleration regime, thus complicating the thermal analysis. Instead, $\ell \leq L_4$. The edge case $\ell = L_4$ corresponds to the flat Randall–Sundrum brane. Recall in this scenario the acceleration horizon does not localize on the brane (as in the dS_3 Randall–Sundrum brane) such that the acceleration horizon may be ignored. We will return to these differences momentarily.

Moving forward, let us first consider the thermodynamics of the bulk system with an AdS_3 Karch–Randall braneworld. In the literature on the exact three-dimensional braneworld black holes, typically, one assumes the Bekenstein–Hawking entropy Formula (181) and Hawking temperature. The energy is then identified by demanding the first law hold, which is subsequently found to coincide with the mass M identified geometric construction. For example, consider the static, neutral black hole construction (39). It proves useful to introduce the real and non-negative parameter [24]

$$z \equiv \frac{\ell_3}{r_+ x_1}, \tag{184}$$

for black hole horizon radius r_+. Given the range of x_1, generally, $z \in [0, \infty)$. It is possible to express the parameters x_1, μ and r_+ solely in terms of z and $\nu \equiv \ell/\ell_3$. In particular, solving $H(r_+) = 0$ for x_1^2 yields

$$x_1^2 = -\frac{1}{\kappa} \frac{(1 - \nu z^3)}{z^2(1 + \nu z)}. \tag{185}$$

Rearranging z (184) and substituting for x_1^2 above gives

$$r_+^2 = -\ell_3^2 \kappa \frac{(1 + \nu z)}{(1 - \nu z^3)}. \tag{186}$$

Further, with (185), the parameter μ (45) obeys

$$\mu x_1 = -\kappa \frac{(1 + z^2)}{(1 - \nu z^3)}. \tag{187}$$

The Hawking temperature T of the bulk black hole horizon is proportional to the surface gravity relative to the canonical timelike Killing vector $\partial_{\bar{t}}$ (74). Using (185)–(187), the temperature can be recast in terms of z and ν,

$$T = \frac{\kappa_+}{2\pi} = \frac{1}{2\pi\ell_3} \frac{z(2 + 3\nu z + \nu z^3)}{1 + 3z^2 + 2\nu z^3}. \tag{188}$$

The Bekenstein–Hawking entropy, meanwhile, is (setting $c = \hbar = k_B = 1$)

$$\begin{aligned} S = \frac{\text{Area}(r_+)}{4G_4} &= \frac{2}{4G_4}\int_0^{2\pi\eta} d\phi \int_0^{x_1} dx r_+^2 \frac{\ell^2}{(\ell + x r_+)^2} \\ &= \frac{8\pi\ell_3^2}{4G_4}\frac{\nu z}{1+3z^2+2\nu z^3}, \end{aligned} \tag{189}$$

where the factor of two appearing in the second equality is because the brane is two-sided.

Keeping parameters ℓ_3 and ν fixed, we can identify the energy E via

$$\partial_z E = T \partial_z S, \tag{190}$$

such that the first law

$$dE = TdS \tag{191}$$

is obeyed. In particular, the energy E is explicitly found to be

$$E = \frac{\sqrt{1+\nu^2}}{2G_3}\frac{z^2(1-\nu z^3)(1+\nu z)}{(1+3z^2+2\nu z^3)^2} = M, \tag{192}$$

where in the second equality, we substituted (185)–(187) into the identified mass (65). This confirms M should indeed be identified as the mass of the bulk black hole.

Gravitational Path Integral Approach

The above method is sufficient for studying the thermodynamics, assuming the identification of the thermodynamic variables is correct. A more fundamental approach would be to evaluate the quantum gravitational canonical partition function in the semi-classical limit via the on-shell Euclidean action [123]. Such an approach was taken in [124] (see Appendix E for details).

Formally, the partition function $Z(\beta)$ is given by a Euclidean path integral whose fixed boundary data on field configurations corresponds to thermodynamic data defining the thermal ensemble. At leading order in a stationary phase approximation, this becomes

$$Z(\beta) \approx e^{-I_{\text{on-shell}}}, \tag{193}$$

where β is the (inverse) temperature of the system and $I_{\text{on-shell}}$ is the on-shell Euclidean action. In say, the Schwarzschild black hole, β is introduced as the periodicity of the Euclidean time circle to make the Euclidean solution regular at the horizon. In the case of the AdS_4 warped geometry, additional care is needed. Firstly, one Wick rotates the Lorentzian geometry (39) $t_E = it$ for Euclidean time t_E. To avoid a conical singularity at $r = r_+$, the Euclidean time direction is compactified into a circle, $t_E \sim t_E + \Delta t_E$, with period

$$\Delta t_E = \frac{4\pi}{|H'(r_+)|}. \tag{194}$$

Further, the bulk regularity conditions eliminating the conical singularity at x_1 must be respected. Combined, one works with Euclideanized canonically normalized time coordinate $\bar{t}_E$ with periodicity

$$\bar{t}_E \sim \bar{t}_E + \beta, \quad \beta = \frac{\Delta t_E}{\eta}. \tag{195}$$

Working at fixed β thus defines working in a canonical ensemble of fixed temperature $T = \beta^{-1}$. Indeed, the periodicity (195) is the inverse of the temperature (188).

With respect to the partition function (193), the thermodynamic energy E and entropy S are defined as

$$\begin{aligned} E &\equiv -\partial_\beta \log Z \approx \partial_\beta I_{\text{on-shell}}, \\ S &\equiv \beta E + \log Z \approx (\beta\partial_\beta - 1) I_{\text{on-shell}}. \end{aligned} \tag{196}$$

With some work, the on-shell action for the static, neutral black hole is

$$I_{\text{on-shell}} = -\frac{2\pi\ell^2 z}{G_4 \nu} \frac{[1 + 2\nu z + \nu z^3(2 + \nu z)]}{(2 + 3\nu z + \nu z^3)(1 + 3z^2 + 2\nu z^3)}, \tag{197}$$

from which one recovers the mass (192) and entropy (189). In summary, the thermodynamics of the bulk black hole directly follow from a Euclidean gravitational path integral.

Critical to this approach is being able to identify a system in thermal equilibrium. The black hole system in question has multiple non-degenerate horizons, as in the case with the dS_3 Randall–Sundrum brane. Thus, upon Wick rotating to Euclidean signature, the geometry will have multiple conical singularities: one associated with each horizon. In such cases, one removes a single conical singularity by fixing the periodicity of the Euclidean time coordinate for the associated horizon. Consequently, one is only able to treat a part of the entire system (neglecting the other horizons). Strictly speaking, however, in such situations, the complete system is not in thermal equilibrium, and it is not clear how to define a thermal partition function (without further modification).

5.2. Identifying Bulk and Brane Thermodynamics

The thermodynamics of the classical four-dimensional black hole is reinterpreted as the semi-classical thermodynamics of the three-dimensional quantum black hole. This is a by-product of the fact that the bulk black hole horizon localizes on the brane such that the temperature of the bulk black hole coincides with the temperature of the horizon induced on the brane. To wit, consider a $(d+1)$-dimensional static bulk geometry with line element

$$ds^2 = -A(r)dt^2 + A^{-1}(r)dr^2 + r^2 d\Omega_{d-1}^2, \tag{198}$$

where $r = r_h$ denotes the event horizon of the black hole, equal to the largest root of $A(r) = 0$, and is generated by the time-translation Killing vector ∂_t^a. Let $\Phi = \Phi(r, \phi^i)$ for $(d-1)$ Gaussian normal coordinates $\{\phi^i\}$ denote the hypersurface equation of the brane $\mathcal{B}$. The induced metric on $\mathcal{B}$ is [125]

$$\begin{aligned} ds_{\mathcal{B}}^2 &= -A(r)dt^2 + \left(A^{-1}(r) + r^2(\partial_r\Phi)^2\right)dr^2 + r^2\gamma_{ij}d\phi^i d\phi^j \\ &\equiv -f(r)dt^2 + g^{-1}(r)dr^2 + r^2\gamma_{ij}d\phi^i d\phi^j, \end{aligned} \tag{199}$$

having identified

$$f(r) \equiv A(r), \quad g(r) \equiv \frac{A(r)}{1 + A(r)r^2(\partial_r\Phi)^2}. \tag{200}$$

The bulk event horizon at $r = r_h$ corresponds to a horizon on $\mathcal{B}$, i.e., the bulk and brane blackening factors have the same root structure. Further, assuming $\partial_r\Phi$ is regular such that $A(r)(\partial_r\Phi)^2$ vanishes at $r = r_h$, the temperature of the bulk black hole coincides with the horizon induced on the brane:

$$T_{\text{bulk}}^h = \left.\frac{|A'(r)|}{4\pi}\right|_{r=r_h} = \left.\frac{\sqrt{f'(r)g'(r)}}{4\pi}\right|_{r=r_h} = T_{\mathcal{B}}^h. \tag{201}$$

Geometrically, the identification of the bulk and brane horizon temperatures is because the bulk time-translation Killing vector remains a time-translation Killing vector on the brane[33].

Below, we review the thermodynamics for each type of quantum black hole explored in Section 4, starting with the static neutral quantum BTZ family of black holes.

5.3. Quantum BTZ Black Holes

5.3.1. Static Quantum BTZ

The thermodynamic variables of the static bulk black hole worked out above are

$$\begin{aligned} M &= \frac{\sqrt{1+\nu^2}}{2G_3}\frac{z^2(1-\nu z^3)(1+\nu z)}{(1+3z^2+2\nu z^3)^2}, \\ T &= \frac{1}{2\pi\ell_3}\frac{z(2+3\nu z+\nu z^3)}{1+3z^2+2\nu z^3}, \\ S &= \frac{8\pi\ell_3^2}{4G_4}\frac{\nu z}{1+3z^2+2\nu z^3}. \end{aligned} \tag{202}$$

The claim is that these thermodynamic variables are to be interpreted as the thermodynamic quantities of the quantum black hole. Above, we already saw how the temperatures coincide. From the brane perspective, determining the mass is a highly non-trivial task due to the higher-derivative nature of the gravity action. Let us therefore first focus on the entropy S.

Entropy

From the bulk perspective, S is the classical four-dimensional Bekenstein–Hawking entropy, $S = S^{(4)}_{\rm BH}$ (189). Alternatively, from the brane point of view, S must be a sum of gravitational entropy and the von Neumann entropy of the holographic CFT$_3$. That is, S is identified as the *generalized* entropy [126]:

$$S^{(4)}_{\rm BH} \equiv S^{(3)}_{\rm gen} = \frac{4\pi\ell_3}{4G_3}\frac{z\sqrt{1+\nu^2}}{1+3z^2+2\nu z^3}, \tag{203}$$

where we replaced $G_4 = 2G_3L_4 = 2G_3\ell/\sqrt{1+\nu^2}$. Because we have the full bulk solution, $S^{(3)}_{\rm gen}$ is exact and valid for all ν. To parse the gravitational and matter contributions to the entropy, however, it is useful to expand (203) in a small ν expansion,

$$S^{(3)}_{\rm gen} = \frac{4\pi\ell_3 z}{4G_3(1+3z^2)} - \frac{8\pi\ell_3 z^4}{4G_3(1+3z^2)^2}\nu + \frac{2\pi\ell_3 z(1+6z^2+9z^4+8z^6)}{4G_3(1+3z^2)^3}\nu^2 + \mathcal{O}(\nu^3). \tag{204}$$

The first term can be understood as the three-dimensional Bekenstein–Hawking entropy of the classical BTZ black hole[34]

$$S_{\rm BTZ} = \frac{4\pi\ell_3 z}{4G_3(1+3z^2)} = \frac{\pi^2\ell_3^2}{G_3}T_{\rm BTZ} = \pi\ell_3\sqrt{\frac{2M_{\rm BTZ}}{G_3}}. \tag{205}$$

where $T_{\rm BTZ} \equiv \lim_{\nu\to 0} T$ and similarly for $M_{\rm BTZ}$. The second term in (204) is proportional to $\ell \sim c_3$. Since higher-derivative contributions to the entropy enter at order ν^2, the $\mathcal{O}(\nu)$ term can only correspond to the von Neumann entropy of the CFT$_3$ in the limit of weak backreaction. The $\mathcal{O}(\nu^2)$ and higher-order terms are in principle a combination of the matter and higher-derivative effects that are difficult to distinguish.

Since the brane theory is in general a higher-derivative theory, in principle, the entire gravitational entropy can be computed using the Iyer–Wald entropy functional [127,128],

$$S_{\rm IW} \equiv -2\pi\int_H d^{D-2}x\sqrt{q}\,\frac{\partial\mathcal{L}}{\partial R^{ijkl}}\epsilon_{ij}\epsilon_{kl}. \tag{206}$$

Here, q_{ij} is the induced metric of the codimension-2 cross-section H of the horizon with binormal ϵ_{ij}, and $\mathcal{L}$ is the scalar Lagrangian scalar characterizing the gravity theory, e.g.,

for the Einstein–Hilbert Lagrangian, $S_{\rm IW} = \frac{A[H]}{4G_D} = S_{\rm BH}$. In the case of the semi-classical induced theory on the brane (57), the Iyer–Wald entropy is [25][35]

$$S^{(3)}_{\rm IW} = \frac{1}{4G_3}\int dx\sqrt{q}\left[1+\ell^2\left(\frac{3}{4}R - g^{ij}_{\perp}R_{ij}\right)+\mathcal{O}(\ell^4/\ell_3^6)\right], \tag{207}$$

with $g^{\perp}_{ij} = g_{ij} - q_{ij}$ being the metric in the directions orthogonal to the horizon[36]. The leading contribution is the three-dimensional Bekenstein–Hawking entropy,

$$S^{(3)}_{\rm BH} = \frac{1}{4G_3}\int_H dx\sqrt{q} = \frac{1}{4G_3}\int_0^{2\pi} d\bar{\phi}\bar{r}_+ = \frac{2\pi\bar{r}_+}{4G_3}. \tag{208}$$

Substituting in parameters (185) and (186), notice

$$S^{(3)}_{\rm BH} = \frac{(1+\nu z)}{\sqrt{1+\nu^2}}S^{(3)}_{\rm gen} = S_{\rm BTZ} + \frac{\pi\ell_3 z^2(1+z^2)}{G_3(1+3z^2)^2}\nu + \mathcal{O}(\nu^2). \tag{209}$$

Due to its dependence on ν, $S^{(3)}_{\rm BH}$ contains semi-classical backreaction effects; only when $\nu = 0$ does (208) coincide with the classical entropy in (204). Notice the difference

$$S^{(3)}_{\rm BH} - S_{\rm BTZ} = \frac{\nu z(1+z^2)}{1+3z^2}S_{\rm BTZ}, \tag{210}$$

It is natural to interpret this difference as the leading contribution to the CFT entropy.

Evaluating the Iyer–Wald entropy (207) on the quantum BTZ background (64) yields

$$S^{(3)}_{\rm IW} = \left[1 - \frac{\nu^2}{2} - \frac{z(1+z^2)}{1+\nu z}\nu^3 + \mathcal{O}(\nu^4)\right]S^{(3)}_{\rm BH}. \tag{211}$$

Thus, the higher-derivative contributions to the gravitational entropy enter at order $\mathcal{O}(\nu^2)$.

With the Iyer–Wald and generalized entropies, the CFT$_3$ entropy can be determined. This is because the generalized entropy associated with a black hole horizon is, generally,

$$S_{\rm gen} = S_{\rm IW} + S^{\rm mat}_{\rm vN}, \tag{212}$$

where $S^{\rm mat}_{\rm vN} \equiv -{\rm tr}\rho\log\rho$ is the von Neumann entropy of state ρ of quantum fields living on the classical background confined to one side of the horizon. Typically, the matter entropy is UV divergent due to vacuum entanglement just across the horizon. The leading order divergence is of the form $A[H]/\epsilon^{D-2}$ for UV regulator ϵ, while there will also be subleading divergences in ϵ. The Bekenstein–Hawking contribution to $S_{\rm IW}$ (with renormalized Newton's constant) regularizes the area divergence of the matter entropy, while the subleading divergences are regulated via the higher-derivative contributions to $S_{\rm IW}$. Thence, the generalized entropy is UV finite and independent of the UV cutoff [130–132]. Therefore, the matter entanglement entropy can be formally computed by taking the difference of the generalized and gravitational entropies. Explicitly to leading order in ν[37]

$$S^{(3)}_{\rm CFT} \equiv S^{(3)}_{\rm gen} - S^{(3)}_{\rm IW} \approx -\frac{4\pi\ell_3 z^2\nu}{4G_3(1+3z^2)} = -\nu z S_{\rm BTZ}. \tag{213}$$

Note that the minus here does not imply the entanglement entropy is negative. Rather, here, $S^{(3)}_{\rm CFT}$ corresponds to the finite contribution to the entanglement entropy after the leading piece has been absorbed in a renormalization of G_3 (which differs from the renormalization of G_3 due to higher-derivatives effects on the mass).

Observe when $z \ll 1$, the matter entropy (213) takes the form

$$S^{(3)}_{\rm CFT}\big|_{z\ll 1} \approx -\frac{\pi \ell_3 \nu z^2}{G_3} = -2\pi c_3 (\pi \ell_3 T)^2, \tag{214}$$

where we used $T_{\rm BTZ}|_{z\ll 1} \approx z/\pi\ell_3$ and $\ell \approx 2c_3 G_3$. The proportionality to T^2 is consistent with the behavior of a $2+1$-dimensional conformal gas, implying the entropy is thermal. Meanwhile, for large-z but $\nu z \ll 1$,

$$S^{(3)}_{\rm CFT}\big|_{z\gg 1} \approx -\frac{\pi \ell_3 \nu}{3G_3} = -\frac{2\pi c_3}{3}, \tag{215}$$

a non-thermal entropy. Comparing the two limits of the matter entropy, we can infer $z \ll 1$ characterizes states where thermal effects dominate, while $z \gg 1$ describes states dominated by non-thermal effects. In fact, as we will see momentarily, the large and small-z limits, respectively, coincide with quantum states having large and small Casimir effects.

The First Law of Thermodynamics

Having identified the bulk horizon entropy with the generalized entropy on the brane (203), the bulk first law (191) from the brane perspective reads

$$dM = T dS^{(3)}_{\rm gen}. \tag{216}$$

This observation is consistent with two-dimensional quantum black holes (another context where the backreaction problem can be exactly solved) [133,134]. Thus, accounting for a semi-classical backreaction, the standard first law of horizon thermodynamics is modified by replacing 'classical' entropy with $S_{\rm gen}$. It is worth emphasizing this first law is exact and valid for all ν, i.e., for small or large backreaction.

From the brane perspective, since the theory includes an infinite tower of higher-derivative contributions, an unambiguous definition of the mass is lacking. Therefore, the first law (216) provides another route to determining the mass. That is, we demand that the quantum BTZ black hole satisfies the semi-classical first via which the right-hand side defines the mass M (202). Notice that in the large-z limit, the mass hits its minimum value

$$\lim_{z\to\infty} M = -\frac{1}{8\mathcal{G}_3}. \tag{217}$$

This mass can be thought of as the negative Casimir energy of the cutoff $\rm CFT_3$, thus explaining the non-thermality of the matter entropy (215). Alternatively, for small ν and z, the Casimir effects are suppressed, leading to a thermal matter entropy (214).

Recall that the qBTZ solution parametrizes a family of quantum black holes with three branches (76)[38]. As depicted in Figure 11, all quantum black holes have higher temperatures than classical BTZ with the same mass. Incidentally, the branch 1a quantum dressed conical singularities ($-1/(8\mathcal{G}_3) < M < 0$) have negative heat capacity, $\partial M/\partial T < 0$, except at $M = 0$, where the heat capacity diverges. In this range, where Casimir effects are dominant, the entropy S is most naturally understood to be entanglement entropy due to vacuum fluctuations across the horizon. Meanwhile, the largest black holes in branch 1b also have negative heat capacity, $M_{\rm c} < M < 1/24\mathcal{G}_3$, where $M_{\rm c} \neq 0$ is some critical value of the mass where the heat capacity diverges. Further, the branch 1b black holes have a larger entropy than branch 2, which is likely due to the fact that the branch 1b black holes are formed due to backreaction of the Casimir energy.

5.3.2. Rotating Quantum BTZ

Using the analysis of the static quantum BTZ as a guide, it is in principle straightforward to analyze the thermal properties of the rotating quantum BTZ black hole (91). The essential new feature here is that there is an outer and inner black hole horizon, r_+ and

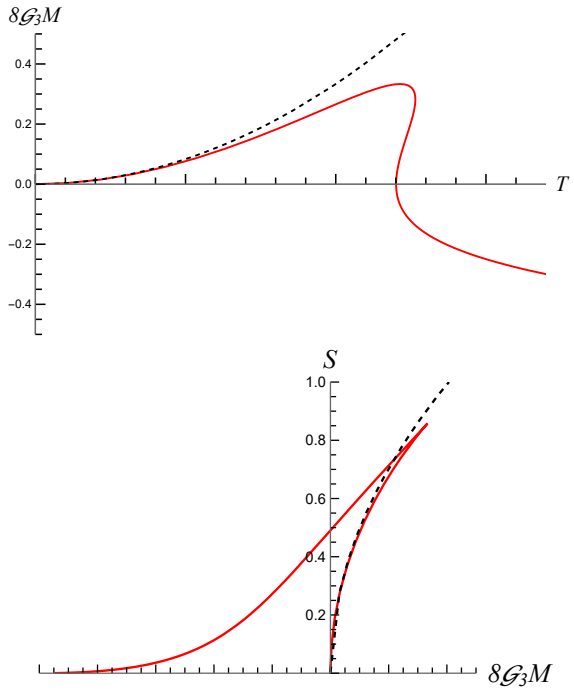

Figure 11. Quantum BTZ thermodynamics. **Top**: Mass (solid, red curve) versus temperature for $\nu = 1/3$. **Bottom**: Generalized entropy (solid, red curve) versus mass for $\nu = 1/3$. The black dashed lines correspond to the classical BTZ behavior.

r_-, with $r_- < r_+$. Thus, there is a parameter z (184) for each horizon. Below, we report only the thermodynamics for the outer horizon as the analysis of the inner horizon follows *mutatis mutandis*. In addition to $z = \ell_3/r_+x_1$, we also introduce the rotation parameter

$$\alpha \equiv \tilde{a}/\sqrt{-\kappa x_1}, \tag{218}$$

where, recall, $\tilde{a} \equiv a x_1^2/\ell_3$.

Following the logic leading to the parameters (185)–(187), now

$$\begin{aligned} x_1^2 &= -\frac{1}{\kappa}\frac{1-\nu z^3}{z^2[1+\nu z-\alpha^2(z-\nu)]}, \\ r_+^2 &= -\ell_3^2\kappa\frac{1+\nu z-\alpha^2 z(z-\nu)}{1-\nu z^3}, \\ \mu x_1 &= -\kappa\frac{(1+z^2)(1+\alpha^2(1-z^2))}{1-\nu z^3}. \end{aligned} \tag{219}$$

Substituting these into the expressions for mass (92), rotation (93), surface gravity (100), and angular velocity (97), the thermodynamic variables are [24,25]

$$\begin{aligned}
M &= \frac{\sqrt{1+\nu^2}}{2G_3}\frac{(1-\nu z^3)[z^2(1+\nu z)+\alpha^2(1+4\nu z^3(1+\alpha^2)-(1+4\alpha^2)z^4)]}{[1+3z^2+2\nu z^3-\alpha^2(1+4\nu z^3+3z^4)]^2},\\
T &= \frac{1}{2\pi\ell_3}\frac{[z^2(1+\nu z)-\alpha^2(1-2\nu z^3+z^4)][2+3\nu z(1+\alpha^2)-4\alpha^2 z^2+\nu z^3+\alpha^2\nu z^5]}{z(1+\nu z)[1+\alpha^2(1-z^2)][1+3z^2+2\nu z^3-\alpha^2(1-4\nu z^3+3z^4)]},\\
S &= \frac{\pi\ell_3\sqrt{1+\nu^2}}{G_3}\frac{z(1+\alpha^2(1-z^2))}{[1+3z^2+2\nu z^3-\alpha^2(1+4\nu z^3+3z^4)]},\\
J &= \frac{\ell_3\sqrt{1+\nu^2}}{G_3}\frac{\alpha z(1+z^2)[1+\alpha^2)(1-z^2)]\sqrt{(1-\nu z^3)[1+\nu z-\alpha^2 z(z-\nu)]}}{[1+3z^2+2\nu z^3-\alpha^2(1+4\nu z^3+3z^4)]^2},\\
\Omega &= \frac{\alpha(1+z^2)}{\ell_3}\frac{\sqrt{(1-\nu z^3)[1+\nu z-\alpha^2 z(z-\nu)]}}{z(1+\nu z)[1+\alpha^2(1-z^2)]}.
\end{aligned} \tag{220}$$

As with the static case, these variables serve as the thermal quantities of the bulk AdS_4 black hole and are identified to be the thermodynamic variables of the quantum black hole. In particular, the Bekenstein–Hawking entropy of the bulk black hole is

$$\begin{aligned}
S^{(4)}_{\rm BH} &= \frac{2}{4G_4}\int_0^{2\pi\eta}d\phi\int_0^{x_1}dx\frac{r_+^2\ell^2}{(\ell+r_+x)^2}\eta\left(1+\frac{a^2x_1^2}{r_+^2}\right)\\
&= \frac{\pi}{G_4}\eta\frac{\ell x_1(r_+^2+a^2x_1^2)}{\ell+r_+x_1},
\end{aligned} \tag{221}$$

and is identified to be the generalized entropy of the black hole on the brane $S^{(3)}_{\rm gen}$. Notice that in the limit of vanishing backreaction, the entropy reduces to the classical BTZ entropy

$$\lim_{\nu\to 0}S^{(3)}_{\rm gen} = \frac{\pi\ell_3}{\sqrt{2G_3}}\left(\sqrt{M+\frac{J}{\ell_3}}+\sqrt{M-\frac{J}{\ell_3}}\right). \tag{222}$$

The Wald entropy is formally no different than before, and the matter entropy (213) obeys the same relation at the leading order in ν.

It can be explicitly verified that the thermodynamic variables (220) satisfy (for fixed ν)

$$\begin{aligned}
\partial_z M - T\partial_z S - \Omega\partial_z J = 0,\\
\partial_\alpha M - T\partial_\alpha S - \Omega\partial_\alpha J = 0.
\end{aligned} \tag{223}$$

Consequently, from the brane perspective, the semi-classical first law is

$$dM = TdS^{(3)}_{\rm gen} + \Omega dJ. \tag{224}$$

Again, n.b., mass M and angular momentum J, from the point of view of the brane, include the infinite tower of higher-derivative contributions in the gravity action (encoded in $\mathcal{G}_3$), which was exactly resummed due to our knowledge of the bulk theory.

While the first law holds for any range of parameters, not all ranges are physically sensible. Thus, restrictions are made when exploring the thermodynamics of the rotating solution [25]. In particular, for non-extremal solutions, one takes

$$0 \le \alpha^2 \le \frac{1+\nu z}{z(z-\nu)}. \tag{225}$$

The lower bound is chosen to avoid naked closed timelike curves ($\kappa = +1$ negative mass quantum-dressed cones belonging to branch 1a have $\alpha^2 < 0$ (218)). The upper bound follows from demanding the outer black hole event horizon r_+ be real and positive. For

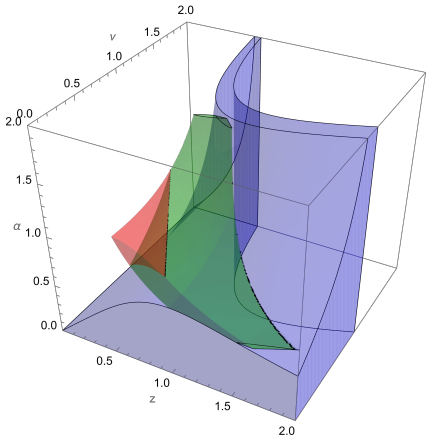

Figure 12. Parameter space for rotating quantum BTZ. The blue region covers solutions that obey the extremality bound of classical rotating BTZ black holes, $0 \leq \alpha \leq \alpha_{\text{ext}}$. Green and red regions correspond to superextremal black holes, $\alpha > \alpha_{\text{ext}}$. The red region contains black holes that violate the quantum reverse isoperimetric inequality (277) and are thermodynamically unstable.

$\kappa = -1$ and $\nu < z < \nu^{-1/3}$, the upper bound implies $1 + \alpha^2(1 - z^2) > 0$. Even with this bound, however, the temperature T of the black hole can go negative without further restricting the range of parameters. The classical BTZ extremal limit (108) occurs when

$$\alpha^2 = \alpha^2_{\text{ext}} = \frac{z^2(1 + \nu z)}{1 - 2\nu z^3 + z^4}, \tag{226}$$

where temperature $T = 0$.

As noted in Section 4.2.2, the rotating quantum black holes can exist beyond the classical extremality bound (226). This is because the temperature T and angular momentum J are in general non-monotonic with respect to α. There are thus two distinct types of rotating black holes: (i) those which respect the classical extremality bound, $0 \leq \alpha \leq \alpha_{\text{ext}}$, where T and J are monotonic in α, and (ii) the 'superextremal', i.e., $\alpha > \alpha_{\text{ext}}$, where T and J are non-monotonic. In Figure 12, we illustrate these distinct families, where the blue region corresponds to black holes respecting the extremality bound, while the green and red regions correspond to 'superextremal' solutions. The superextremal black hole solutions are possible due to the combined non-linear effects of the rotation and quantum backreaction, and they are consequently dubbed non-perturbative rotating black holes [135]. Among these solutions (those belonging to the red region) are black holes which are both thermodynamically unstable (having a negative heat capacity) and violate the so-called quantum reverse isoperimetric inequality (see Equation (277)).

5.3.3. Charged Quantum BTZ

As with the rotating case, the charged quantum BTZ black hole (123) has an outer and inner horizon. In addition to the parameter $z = \ell_3/r_+x_1$, it is useful to introduce

$$\gamma \equiv q x_1^2, \tag{227}$$

along with $\gamma_e \equiv e x_1^2$ and $\gamma_g \equiv g x_1^2$, obeying $\gamma^2 = \gamma_e^2 + \gamma_g^2$. Consequently, following the logic yielding parameters (185)–(187) gives [99][39]

$$\begin{aligned} x_1^2 &= -\frac{1}{\kappa}\frac{(1-\nu z^3+\gamma^2\nu z^3+\gamma^2\nu^2 z^4)}{z^2(1+\nu z)}, \\ r_+^2 &= -\frac{\kappa\ell_3^2(1+\nu z)}{(1-\nu z^3+\gamma^2\nu z^3+\gamma^2\nu^2 z^4)}, \\ \mu x_1 &= -\frac{\kappa(1+z^2-\gamma^2 z^2+\gamma^2\nu^2 z^4)}{(1-\nu z^3+\gamma^2\nu z^3+\gamma^2\nu^2 z^4)}. \end{aligned} \tag{228}$$

In terms of these parameters, the thermodynamic quantities are [98]

$$\begin{aligned} M &= \frac{\sqrt{1+\nu^2}}{2G_3}\frac{z^2(1+\nu z)[1-\nu z^3+\gamma^2\nu z^3(1+\nu z)]}{[1+3z^2+2\nu z^3+\gamma^2 z^2(1+\nu z)^2]^2}, \\ T &= \frac{z}{2\pi\ell_3}\frac{2+3\nu z-\nu z^3(\gamma^2(1+\nu z)^2-1)}{[1+3z^2+2\nu z^3+\gamma^2 z^2(1+\nu z)^2]}, \\ S &= \frac{\pi\ell_3\sqrt{1+\nu^2}}{G_3}\frac{z}{[1+3z^2+2\nu z^3+\gamma^2 z^2(1+\nu z)^2]}, \\ Q_e &= \sqrt{\frac{16\pi}{5g_3^2 G_3}}\frac{\gamma_e z^2(1+\nu z)\sqrt{1+\nu^2}}{[1+3z^2+2\nu z^3+\gamma^2 z^2(1+\nu z)^2]}, \\ \mu_e &= \sqrt{\frac{5g_3^2}{4\pi G_3}}\frac{\gamma_e\nu z^3(1+\nu z)}{[1+3z^2+2\nu z^3+\gamma^2 z^2(1+\nu z)^2]}. \end{aligned} \tag{229}$$

More specifically, parameters (228) are substituted into mass (124), electric charge (131) and potential (133) (the form of the magnetic charge Q_g and potential μ_g are of the same form but with $\gamma_e \to \gamma_g$). Further, the temperature follows from the surface gravity, $T = \frac{\kappa_+}{2\pi} = \frac{|H'(\bar{r}_+)|}{4\pi}$, while the entropy is

$$S = S_{\rm BH}^{(4)} = \frac{2}{4G_4}\int_0^{2\pi\eta} d\phi \int_0^{x_1} dx \frac{\ell^2 r_+^2}{(\ell + x r_+)^2} = \frac{4\pi\ell r_+^2 x_1 \eta}{G_4(\ell + r_+ x_1)}, \tag{230}$$

and is identified as the three-dimensional generalized entropy $S_{\rm gen}^{(3)}$. It can be easily verified that the thermodynamic quantities (229) satisfy

$$\begin{aligned} &\partial_z M - T\partial_z S - \mu_e \partial_z Q_e - \mu_g \partial_z Q_g = 0, \\ &\partial_\nu M - T\partial_\nu S - \mu_e \partial_\nu Q_e - \mu_g \partial_\nu Q_g = 0, \\ &\partial_{\gamma_i} M - T\partial_{\gamma_i} S - \mu_e \partial_{\gamma_i} Q_e - \mu_g \partial_{\gamma_i} Q_g = 0, \end{aligned} \tag{231}$$

where $\gamma_i = \gamma_e, \gamma_g$. Thus, from the brane perspective, the first law of thermodynamics is

$$dM = T dS_{\rm gen}^{(3)} + \mu_e dQ_e + \mu_g dQ_g. \tag{232}$$

Notice that in the limit $\nu \to 0$, the chemical potentials μ_e and μ_g vanish (as does the charge, which is readily apparent from (131)). This is indicative of the fact that the charge of the brane black hole is a quantum effect, and the charged quantum BTZ black hole does not reduce to the classical charged quantum BTZ black hole. Further, in the limit of vanishing backreaction $\nu \to 0$, the classical relation (205) between $S_{\rm BTZ}$, $T_{\rm BTZ}$ and $M_{\rm BTZ}$ continues to hold. In fact, the generalized entropy has a qualitatively similar behavior as the entropy of the neutral, static qBTZ (Figure 11). The only essential difference between entropies of the charged and neutral black holes is that, rather than reaching zero, the charged black hole entropy ends at a finite, non-zero value—the entropy of the extremal black hole [98]. Meanwhile, in stark contrast with the neutral qBTZ, with $q \neq 0$, as the mass

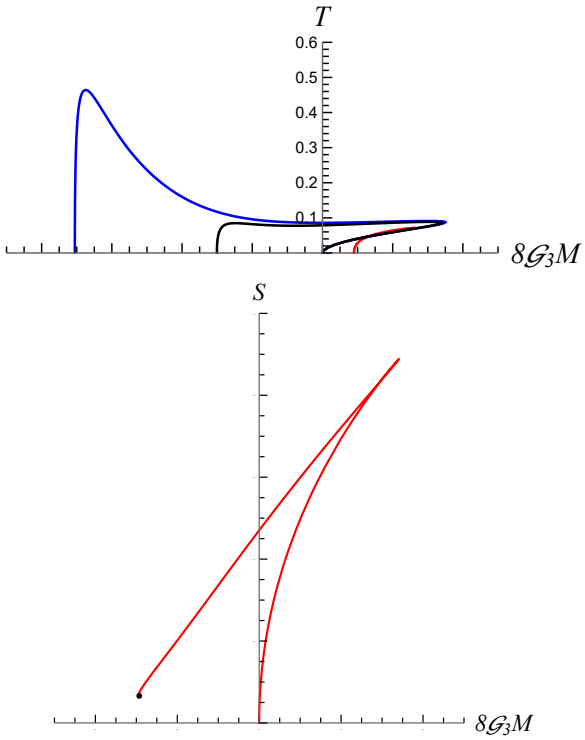

Figure 13. Charged quantum BTZ thermodynamics. **Top**: Temperature versus mass for $\nu = 1/3$ and $q = 0.1, 0.3, 1$ (left to right; blue, black, red). **Bottom**: Generalized entropy versus mass for $\nu = 1/3$ and $q = 0.3$. The entropy ends at a non-zero finite value (black dot).

decreases monotonically below zero, the temperature reaches a finite maximum value and then quickly tends to zero at the extremal limit (shown in Figure 13). For a more complete treatment of the thermodynamics of the extremal black hole, see [98].

5.4. Quantum dS Black Holes

Geometrically, the chief difference between the quantum BTZ and dS_3 black holes is that the latter are equipped with a cosmological horizon. As with classical de Sitter black holes, the black hole horizon is generally hotter than the cosmological horizon. According to a static patch observer, then, the system is characterized by two generally unequal temperatures and thus not in thermal equilibrium. This complicates and enriches the thermodynamic analysis of quantum de Sitter black holes.

5.4.1. Quantum Schwarzschild–de Sitter

Along with $\nu \equiv \ell/R_3$, it is useful to introduce the dimensionless parameter [26]

$$z \equiv \frac{R_3}{r_i x_1}, \tag{233}$$

where r_i refers to either the black hole or cosmological horizon, r_h and r_c, respectively. We can now express x_1, μ, and r_+ solely in terms of ν and z

$$\begin{aligned} x_1^2 &= \frac{1}{z^2}\frac{1+\nu z^3}{1+\nu z}, \\ r_+^2 &= R_3^2\frac{1+\nu z}{1+\nu z^3}, \\ \mu x_1 &= \frac{z^2-1}{1+\nu z^3}. \end{aligned} \tag{234}$$

These are the Wick rotated counterparts of the qBTZ solution parameters (185)–(187). Further, $G_4 = 2\ell_4 G_3 = 2G_3\ell/\sqrt{1-\nu^2}$. In terms of parameters (234), the mass (149) is

$$M = \frac{1}{8G_3}\sqrt{1-\nu^2}\frac{(z^2-1)(9z^2-1+8\nu z^3)}{(3z^2-1+2\nu z^3)^2}. \tag{235}$$

In the quantum de Sitter limit, where $z = 1$, it follows $M = 0$. Also note the mass M vanishes at large z, $\lim_{z\to\infty} M \approx \frac{1}{4G_3\nu z} + \mathcal{O}(1/z^2)$. For fixed $x_1 \neq 1$ and for $z = z_h$, it is natural to think of the large z_h limit as a *small* quantum Schwarzschild black hole, where $R_3 \gg r_h x_1$.

Temperature

On the brane, the black hole and cosmological horizons will appear to emit radiation at the Hawking and Gibbons–Hawking temperatures T_h, T_c, respectively. Explicitly,

$$T_h = -\frac{z_h}{2\pi R_3}\frac{2+3\nu z_h-\nu z_h^3}{3z_h^2-1+2\nu z_h^3}, \qquad T_c = \frac{z_c}{2\pi R_3}\frac{2+3\nu z_c-\nu z_c^3}{3z_c^2-1+2\nu z_c^3}. \tag{236}$$

In the limit $\nu \to 0$, the black hole temperature vanishes, since z_h diverges, while the cosmological horizon temperature reduces to

$$\lim_{\nu\to 0} T_c = \frac{1}{\pi R_3}\frac{z_c}{3z_c^2-1} \equiv T_{\mathrm{SdS}_3}. \tag{237}$$

Since in general $r_h < r_c$, and hence $z_c < z_h$, the black hole horizon has a higher temperature than the cosmological horizon, $T_h > T_c$. Thus, as usual for Schwarzschild–de Sitter spacetimes, the black hole and cosmological horizons are not in thermal equilibrium. Only in the Nariai limit do the temperatures of the two horizons coincide. There is more on this below.

Entropy and the First Law

The four-dimensional Bekenstein–Hawking entropy of the bulk black hole is

$$\begin{aligned} S^{(4)}_{\mathrm{BH}} &= \frac{\mathrm{Area}(r_+)}{4G_4} = \frac{2}{4G_4}\int_0^{2\pi\eta} d\phi \int_0^{x_1} dx r_+^2 \frac{\ell^2}{(\ell + x r_+)^2} \\ &= \frac{\pi R_3}{G_3}\frac{z\sqrt{1-\nu^2}}{3z^2-1+2\nu z^3}. \end{aligned} \tag{238}$$

As with the AdS_3 quantum black holes, from the brane perspective, the bulk entropy is interpreted as the three-dimensional generalized entropy $S^{(3)}_{\mathrm{gen}}$. In the limit $z = 1$, the generalized entropy of the quantum de Sitter solution is proportional to the Gibbons–Hawking entropy of the dS_3 cosmological horizon, i.e., the sum of gravitational entropy and entanglement entropy due to the CFT living outside of the cosmological horizon. Further, the generalized entropy is related to the three-dimensional Bekenstein–Hawking entropy $S^{(3)}_{\mathrm{BH}}$ of the horizon(s) on the brane via

$$S^{(3)}_{\mathrm{gen}} = \frac{\sqrt{1-\nu^2}}{1+\nu z} S^{(3)}_{\mathrm{BH}}, \tag{239}$$

where $S^{(3)}_{\mathrm{BH}} = \frac{2\pi r_+ \eta}{4G_3}$. In the limit of vanishing backreaction, the three-dimensional entropies coincide and are equal to the cosmological horizon entropy of classical Schwarzschild–dS_3 [136]

$$\lim_{\nu\to 0} S^{(3)}_{\mathrm{gen}} = \frac{\pi R_3}{G_3}\frac{z_c}{3z_c^2-1} = \frac{\pi^2 R_3^2}{G_3} T_{\mathrm{SdS}_3} = \frac{\pi R_3}{2G_3}\sqrt{1-8G_3M} = S_{\mathrm{SdS}_3}. \tag{240}$$

In a perturbative series expansion of small ν, the linear-order $\mathcal{O}(\nu)$ contribution to the generalized entropy (238) captures the CFT matter entropy, while quadratic and higher-order contributions include the effects of the higher-derivative corrections. Formally, the matter entropy is given by the difference of the generalized entropy and Iyer–Wald entropy, which, to leading order and for large-z, has the same non-thermal result as static quantum BTZ (215).

Putting together the mass (235), temperatures (236) and entropy (238), there is a separate first law for the black hole and cosmological horizons,

$$dM = T_h dS^{(3)}_{\text{gen},h}, \tag{241}$$

and

$$dM = -T_c dS^{(3)}_{\text{gen},c}. \tag{242}$$

In combination, notice

$$0 = T_h dS^{(3)}_{\text{gen},h} + T_c dS^{(3)}_{\text{gen},c}. \tag{243}$$

Thus, as the generalized entropy attributed to the black hole increases, the generalized entropy of the cosmological horizon decreases. This is a consequence of the minus sign appearing in the first law for the cosmological horizon (242), i.e., the entropy of the cosmological horizon decreases as the mass increases. Akin to classical de Sitter space, this suggests quantum dS_3 represents a maximum entropy state with a finite number of degrees of freedom. Hence, quantum de Sitter black holes behave as instantons constraining the states of the original de Sitter degrees of freedom (see, e.g., [137–139]).

Nariai Limit

As noted above, in general, a static patch observer sees the quantum SdS_3 black hole as one with two unequal temperatures. A special limit where the temperatures coincide is the (quantum) Nariai solution (150), i.e., the largest mass black hole able to fit inside the cosmological horizon, where $r_h = r_c = r_{\text{N}}$. Recall that in this limit, $(\mu\ell)$ attains a maximum

$$\mu_{\text{N}} = \frac{2}{3\sqrt{3}}\frac{1}{\nu}. \tag{244}$$

such that

$$z_{\text{N}} = \frac{R_3}{r_{\text{N}} x_1^{\text{N}}} = \frac{\sqrt{3}}{x_1^{\text{N}}}. \tag{245}$$

In this case, x_1^{N} is the particular value of x_1 in the Nariai limit found by solving $\mu_{\text{N}} = (1 - x_1^2)/x_1^3$ for x_1. For arbitrary ν, there will generally be one real solution for x_1 and one real solution, which for small ν takes the form

$$x_1^{\text{N}} = \sqrt{3}\left(\frac{\nu}{2}\right)^{1/3} - \frac{\sqrt{3}}{2}\nu + \mathcal{O}(\nu^{5/3}), \tag{246}$$

vanishing in the limit $\nu \to 0$ (as one would expect). In terms of x_1^{N}, the mass of the Nariai solution M_{N} is therefore defined by $M_{\text{N}} \equiv M|_{z=z_{\text{N}}}$. Similarly, the entropy of the Nariai solution is defined as $S^{(3)}_{\text{N}} \equiv S^{(3)}_{\text{gen}}|_{z=z_{\text{N}}}$. See Figure 14 for a plot of the horizon entropies as a function of mass M normalized with respect to the Nariai mass.

Regarding the temperature, the Nariai limit is subtle. Naively, setting $r_c = r_h$ leads to the horizon temperatures (236) vanishing. This is a consequence of working with surface gravities κ_h and κ_c defined with respect to the time-translation Killing vector $\xi = \partial_{\bar{t}}$:

$$\kappa_h = \frac{1}{2}H'(\bar{r}_h) = \frac{1}{2\bar{r}_h r_{\text{N}}^2}(\bar{r}_{\text{N}}^2 - \bar{r}_h^2), \quad \kappa_c = -\frac{1}{2}H'(\bar{r}_c) = -\frac{1}{2\bar{r}_c r_{\text{N}}^2}(\bar{r}_{\text{N}}^2 - \bar{r}_c^2), \tag{247}$$

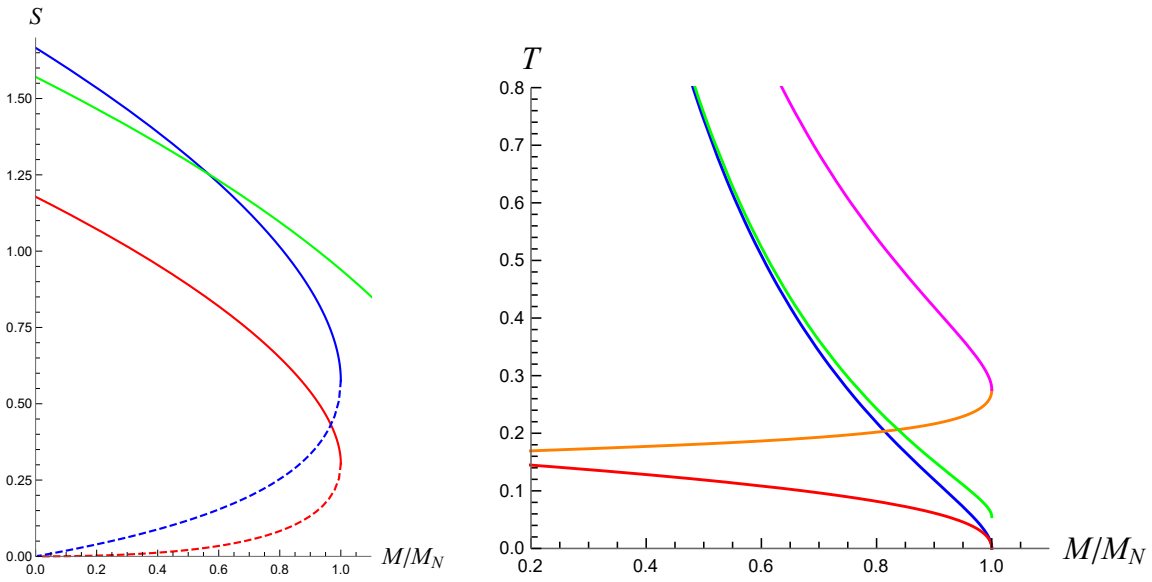

Figure 14. Quantum SdS_3 thermodynamics. Left: Plot of $S^{(3)}_{\rm gen}$ (red), $S^{(3)}_{\rm BH}$ (blue) and S_{SdS_3} (green) as a function of mass M and $\nu = 1/3$. Dashed curves refer to black hole entropies S_h, while the solid curves denote the entropies associated with the cosmological horizon S_c. **Right**: Temperature as a function of mass M for $\nu = 1/3$. Blue and red curves, respectively, correspond to temperatures T_h and T_c, while the magenta and orange curves denote $\bar{T}_h$ and $\bar{T}_c$, respectively. The green curve represents the temperature of the Schwarzschild limit ($R_3 \gg r_h$).

which clearly vanish when $\bar{r}_{h,c} \to \bar{r}_{\rm N} = \frac{R_3}{\sqrt{3}}\eta$. However, for Schwarzschild–de Sitter, there is a more natural choice of normalization of the time-translation Killing vector, owed to Bousso and Hawking [140], resulting in a non-vanishing Nariai temperature. Technically, the Bousso–Hawking normalization is chosen such that $\xi^2 = -1$ at the radius $\bar{r}_0$ where the blackening factor $H(\bar{r})$ obtains a maximum,

$$H'(\bar{r}_0) = 0 \quad \Longrightarrow \quad \bar{r}_0^3 = \frac{\bar{r}_i}{2}(3\bar{r}_{\rm N}^2 - \bar{r}_i^2). \tag{248}$$

for a positive real root $\bar{r}_i$ of $H(\bar{r})$. Physically, the radius $\bar{r}_0$ corresponds to the location where an observer can stay in place without accelerating, i.e., the position where the acceleration due to the gravitational attraction from the black hole balances out the cosmological acceleration. This is consistent with the asymptotically flat Schwarzschild black hole where $\bar{r}_0 \to \infty$ (since $R_3 \to \infty$), and it is empty de Sitter where $\bar{r}_0 \to 0$ (via $\bar{r}_i \to \eta R_3$).

In terms of radius $\bar{r}_0$, where

$$H(\bar{r}_0) = \frac{1}{r_{\rm N}^2}(\bar{r}_{\rm N}^2 - \bar{r}_0^2). \tag{249}$$

the analogous Bousso–Hawking temperature is

$$\bar{T} = \frac{T}{\sqrt{H(\bar{r}_0)}}. \tag{250}$$

In terms of the horizon radii $\bar{r}_{h,c}$,

$$\bar{T}_{h,c} = \mp \frac{1}{4\pi r_{\rm N}\bar{r}_{h,c}} \frac{\bar{r}_{\rm N}^2 - \bar{r}_h^2}{\sqrt{\bar{r}_{\rm N}^2 - \left(\frac{\bar{r}_{h,c}}{2}(3\bar{r}_{\rm N}^2 - \bar{r}_{h,c}^2)\right)^{2/3}}}, \tag{251}$$

where the minus sign corresponds to the black hole temperature, and the plus sign corresponds to the cosmological horizon temperature. Carefully taking the limit $\bar{r}_N \approx \bar{r}_{h,c}$, the temperature $\bar{T}_{h,c}$ of both horizons approaches the Nariai temperature $T_N = 1/(2\pi r_N)$ (see, e.g., Appendix B of [134]). The expression for $\bar{T}$ in terms of z and ν is cumbersome to leading order, for small ν is equal to the dS_3 Gibbons–Hawking temperature [26]. Figure 14 displays the temperatures T_c, T_h, and $\bar{T}$ as a function of mass M normalized by the Nariai mass. The behavior is essentially identical to classical four-dimensional Schwarzschild–de Sitter black holes (see, e.g., Figure 2 of [137]), reflecting the holographic character of the induced geometry.

5.4.2. Quantum Kerr–de Sitter

The new feature of the quantum Kerr–de Sitter black hole (152) compared to the quantum SdS is that now there is an outer and inner black hole horizon obeying $r_- < r_+ < r_c$. In addition to z (233), we introduce the rotation parameter

$$\alpha \equiv \frac{a x_1}{R_3} = \frac{\tilde{a}}{x_1}, \tag{252}$$

where $\{r_i\} = \{r_\pm, r_c\}$. We can express x_1, μ and r_i solely in terms z, ν, and α:

$$\begin{aligned} x_1^2 &= \frac{1+\nu z^3}{z^2[1+\nu z+\alpha^2 z(z+\nu)]}, \\ r_i^2 &= R_3^2 \frac{1+\nu z+\alpha^2 z(z+\nu)}{1+\nu z^3}, \\ \mu x_1 &= \frac{(z^2-1)(1+\alpha^2(1+z^2))}{1+\nu z^3}. \end{aligned} \tag{253}$$

Using the parameters (253), the thermodynamic variables are [27]

$$\begin{aligned} M &= \frac{1}{8G_3}\sqrt{1-\nu^2}\frac{(z^2-1)[1+\alpha^2(1+z^2)][9z^2-1+8\nu z^3+\alpha^2(9z^4-1+8\nu z^3)]}{(3z^2-1+2\nu z^3+\alpha^2(1+4\nu z^3+3z^4))^2}, \\ J &= \frac{\alpha R_3}{G_3}\sqrt{1-\nu^2}\frac{z(z^2-1)[1+\alpha^2(1+z^2)]\sqrt{(1+\nu z^3)(1+\nu z+\alpha^2 z(z+\nu))}}{(3z^2-1+2\nu z^3+\alpha^2(1+4\nu z^3+3z^4))^2}, \\ \Omega_i &= \frac{\alpha}{R_3}\frac{(z^2-1)\sqrt{(1+\nu z^3)(1+\nu z+\alpha^2 z(z+\nu))}}{z(1+\nu z)(1+\alpha^2(1+z^2))}, \\ T_i &= \frac{1}{2\pi R_3}\frac{(z^2(1+\nu z)+\alpha^2(1+2\nu z^3+z^4))|(2+3\nu z-\nu z^3+\alpha^2(4z^2+\nu z(z^4+3)))|}{z(1+\nu z)(1+\alpha^2(1+z^2))(3z^2-1+2\nu z^3+\alpha^2(1+3z^4+4\nu z^3))}, \\ S &= \frac{\pi R_3}{G_3}\frac{\sqrt{1-\nu^2}z(1+\alpha^2(1+z^2))}{(3z^2-1+2\nu z^3+\alpha^2(1+3z^4+4\nu z^3))}, \end{aligned} \tag{254}$$

which follow from substituting the parameters (253) into mass M (153), angular momentum J (154), rotation Ω_i (158), surface gravity (160), and the Bekenstein–Hawking area formula[40]. Collectively, the variables obey the first law

$$dM = T_i dS_i + \Omega_i dJ, \tag{255}$$

for all values of the parameters. On the brane, S has the usual interpretation as the generalized entropy $S^{(3)}_{\rm gen}$.

The quantum Kerr–dS_3 black hole has limits where two or more horizons become degenerate. These include the extremal ($r_+ = r_-$) black hole, where $T_{\rm ext} = 0$, the lukewarm black hole ($r_c = T_+$), and the Nariai geometry ($r_c = r_+$). As with quantum SdS_3, the Nariai black hole will have a vanishing temperature using the standard normalization of

the Killing vector. However, in its near horizon geometry, the temperature of the Nariai black hole and cosmological horizons are equal to the same non-zero temperature $T_{\rm N}$.

Lastly, two limiting cases include the quantum de Sitter, at $z = 1$ or $\mu = 0$, leading to

$$M = J = \Omega_i = 0, \tag{256}$$

$$S = \frac{2\pi R_3}{4G_3}\frac{\sqrt{1-\nu^2}}{1+\nu}, \quad T_c = \frac{1}{2\pi R_3}, \tag{257}$$

and the limit of vanishing backreaction, where

$$\begin{aligned}
M &= \frac{1}{8G_3}\frac{(z^2-1)(1+\alpha^2(1+z^2))(9z^2-1+\alpha^2(9z^4-1))}{(3z^2-1+\alpha^2(1+3z^4))^2},\\
J &= \frac{\alpha R_3}{G_3}\frac{z(z^2-1)(1+\alpha^2(1+z^2))\sqrt{1+\alpha^2 z^2}}{(3z^2-1+\alpha^2(1+3z^4))^2},\\
\Omega_c &= \frac{\alpha(z^2-1)\sqrt{1+\alpha^2 z^2}}{R_3 z(1+\alpha^2(1+z^2))},\\
T_c &= \frac{1}{2\pi R_3}\frac{2(1+2\alpha^2 z^2)(z^2+\alpha^2(1+z^4))}{z(3z^2-1+\alpha^2(1+3z^4))(1+\alpha^2(1+z^2))},\\
S_c &= \frac{\pi R_3}{G_3}\frac{z(1+\alpha^2(1+z^2))}{(3z^2-1+\alpha^2(1+3z^4))},
\end{aligned} \tag{258}$$

with $z = z_c$, since there are no black holes. It is straightforward to verify that the resulting thermodynamic variables (258) agree with classical Kerr–dS$_3$ [27].

5.5. Quantum Black Holes in Flat Space

As with the quantum de Sitter black holes, the thermodynamics of the asymptotically flat quantum black holes follow from the bulk AdS$_4$ black hole geometry with a Randall–Sundrum brane. Notably, however, in this case, the tension is tuned to its critical value (since $L_4 = \ell$) such that no cosmological horizon appears. Therefore, only the thermodynamics of the black hole horizons in the bulk are imprinted on the brane.

5.5.1. Quantum Schwarzschild Black Hole

In a sense, the thermodynamics of the quantum Schwarzschild black hole (169) is given by the $R_3 \to \infty$ limit of the thermodynamics of the quantum Schwarzschild–de Sitter. Some care must be taken, however, since in this limit, $z = R_3/r_+x_1$ diverges, while $\nu = \ell/R_3$ goes to zero. To be more illustrative, recall the mass (170). Rearranging $\mu x_1 = (1-x_1^2)/x_1^2$ such that $x_1^2 = 1/(1+\mu x_1)$ yields

$$M = \frac{\ell\hat{x}(8+9\hat{x})}{16G_4\left(1+\frac{3}{2}\hat{x}\right)^2}, \tag{259}$$

where

$$\hat{x} \equiv \mu x_1. \tag{260}$$

It is easy to verify $\mu^2 = \hat{x}^2(1+\hat{x})$. Meanwhile, from the surface gravity (172), the temperature of the bulk horizon is

$$T = \frac{1}{4\pi\ell\hat{x}}\frac{1}{\left(1+\frac{3}{2}\hat{x}\right)}. \tag{261}$$

Further, the four-dimensional Bekenstein–Hawking entropy is

$$\begin{aligned} S_{\rm BH}^{(4)} &= \frac{4\pi\eta}{4G_4}\int_0^{x_1} dx r_+^2 \frac{\ell^2}{(\ell + x r_+)^2} = \frac{4\pi}{4G_4}\frac{r_+^2 \ell x_1}{\ell + r_+ x_1} \\ &= \frac{4\pi\ell^2}{4G_4}\frac{\hat{x}^2}{(1+\frac{3}{2}\hat{x})}, \end{aligned} \tag{262}$$

where to reach the final line, we used $r_+ = \mu\ell$.

In summary, the thermodynamic variables of the bulk AdS_4 black hole are mass (259), temperature (261), and entropy (262), and they obey the first law[41]

$$dM = T dS_{\rm BH}^{(4)}. \tag{263}$$

From the brane perspective, these thermodynamic quantities are identified as the thermodynamic variables of the quantum Schwarzschild black hole, upon substituting $G_4 = 2\ell G_3$, and where $S_{\rm BH}^{(4)} = S_{\rm gen}^{(3)}$.

It is easy to verify the mass is a monotonically increasing function of $\hat{x}$ with a minimum $M = 0$ (at $\hat{x} = r_+ = 0$) and a maximum at $M = \frac{1}{8G_3}$, at $\hat{x} \to \infty$. Further, for small $\hat{x}$, the temperature goes like $T \sim 1/\hat{x}$ and $T \sim 1/\hat{x}^2$ for large $\hat{x}$, while the entropy behaves as

$$\begin{aligned} S_{\rm gen}^{(3)} &\approx \frac{\pi\ell\hat{x}^2}{2G_3} \qquad (\text{small } \hat{x}), \\ S_{\rm gen}^{(3)} &\approx \frac{\pi\ell\hat{x}}{3G_3} \qquad (\text{large } \hat{x}). \end{aligned} \tag{264}$$

It is useful to think about these limits in terms of the bulk parameter μ, where $\hat{x} \approx \mu$ for small $\hat{x}$ and $\hat{x} \approx \mu^{2/3}$ for large $\hat{x}$[42]. So, for small μ, the entropy $S_{\rm BH}^{(4)} \approx \frac{\pi(\mu\ell)^2}{G_4}$, having the behavior of a classical four-dimensional Schwarzschild black hole of mass $2MG_4 = \mu\ell$ and temperature $T = (4\pi\mu\ell)^{-1}$. Alternatively, for $\mu \gg 1$, the black hole extends a distance ℓ off of the brane, looking like a 'flattened pancake' [23].

Lastly, notice that in the limit of large ℓ, the temperature (261) vanishes while the entropy (262) diverges, whereas for small ℓ, the temperature diverges and the entropy decreases. The latter is consistent with the fact that for a vanishing backreaction, there is no black hole.

5.5.2. Quantum Kerr Black Hole

The (outer) horizon thermodynamics of the quantum Kerr black hole (174) are readily worked out to be

$$\begin{aligned} M &= \frac{(r_+^2 + a^2)x_1[8r_+\ell + 9x_1(r_+^2 + a^2)]}{8G_3[3x_1(r_+^2 + a^2) + 2r_+\ell]^2}, \\ T &= \frac{\ell}{2\pi r_+}\frac{(r_+^2 - a^2)(x_1(r_+^2 + a^2) + r_+\ell)}{(r_+^2 + a^2)x_1(r_+x_1 + \ell)[3(r_+^2 + a^2)x_1 + 2r_+\ell]}, \\ S_{\rm gen}^{(3)} &= \frac{\pi r_+(r_+^2 + a^2)x_1^2}{G_3[3x_1(r_+^2 + a^2) + 2r_+\ell]} \\ J &= \frac{a r_+(r_+^2 + a^2)x_1^2}{G_3[3x_1(r_+^2 + a^2) + 2r_+\ell]^2}\sqrt{\frac{\ell[x_1(r_+^2 + a^2) + r_+\ell]}{r_+}}, \\ \Omega &= \frac{a}{x_1(r_+^2 + a^2)(r_+x_1 + \ell)}\sqrt{\frac{\ell[x_1(r_+^2 + a^2) + r_+\ell]}{r_+}}. \end{aligned} \tag{265}$$

Alternatively, using $(r_+^2 + a^2) = r_+ \mu\ell$, $\hat{x} \equiv \mu x_1$, and introducing $\hat{a} \equiv a/(\mu\ell)$, the thermodynamic variables become

$$\begin{aligned}
M &= \frac{\hat{x}(8+9\hat{x})}{32G_3\left(1+\frac{3}{2}\hat{x}\right)^2}, \\
T &= \frac{(1+\hat{x})}{4\pi\ell\hat{x}\left(1+\frac{3}{2}\hat{x}\right)} \frac{(1-4\hat{a}^2+\sqrt{1-4\hat{a}^2})}{\left[1+\frac{\hat{x}}{2}(1+\sqrt{1-4\hat{a}^2})\right]\left[1-2\hat{a}^2+\sqrt{1-4\hat{a}^2}\right]}, \\
S^{(3)}_{\rm gen} &= \frac{\pi\ell}{4G_3}\frac{\hat{x}^2}{\left(1+\frac{3}{2}\hat{x}\right)}(1+\sqrt{1-4\hat{a}^2}), \\
J &= \frac{\hat{a}\ell\hat{x}^2}{4G_3\left(1+\frac{3}{2}\hat{x}\right)^2}\sqrt{1+\hat{x}}, \\
\Omega &= \frac{4\hat{a}\sqrt{1+\hat{x}}}{\hat{x}\ell[\hat{x}(1+\sqrt{1-4\hat{a}^2})+2][1+\sqrt{1-4\hat{a}^2}]},
\end{aligned} \tag{266}$$

and obey the first law

$$dM = TdS^{(3)}_{\rm gen} + \Omega dJ. \tag{267}$$

The quantum Schwarzschild black hole thermodynamics is recovered in the $\hat{a} \to 0$ limit. As before, $T \sim 1/\hat{x}$ for small $\hat{x}$ and $T \sim 1/\hat{x}^2$ for large $\hat{x}$, while $S^{(3)}_{\rm gen}$ has the same $\hat{x}$-dependence as in the non-rotating case (264).

5.6. Extended Black Hole Thermodynamics

While black holes have a thermodynamic description, they are peculiar in that the first law (182) lacks a pressure–volume work term. This is because for general black holes, there is no clear notion of pressure or volume. For black holes in spacetimes with a cosmological constant, the situation changes dramatically. A first glimpse of this comes from Euler's theorem of homogeneous functions, which implies black holes with a non-zero cosmological constant Λ_{d+1} obey [141]

$$(d-2)G_{d+1}M = (d-1)TS - 2P_{d+1}V + ..., \tag{268}$$

where T refers to temperature , S refers to Bekenstein–Hawking entropy, and the ellipsis refers to other possible thermodynamic variables, e.g., ΩdJ. The essential new feature is used to identify the cosmological constant as thermodynamic pressure

$$P_{d+1} \equiv -\frac{\Lambda_{d+1}}{8\pi G_{d+1}}. \tag{269}$$

Then, V is the conjugate variable to the pressure, which is dubbed the 'thermodynamic volume' [141–143] formally equal to[43]

$$V \equiv \left(\frac{\partial M}{\partial P}\right)_{S,...}. \tag{270}$$

For spacetimes with a vanishing cosmological constant, the relation (268) reduces to the Smarr formula; however, for $\Lambda_{d+1} \neq 0$, the $P - V$ term is required for consistency.

Going one step further, treating the cosmological constant as a dynamical variable leads to an extended framework of black hole thermodynamics, resulting in the first law of extended black hole thermodynamics

$$dM = TdS + VdP_{d+1} + ... \tag{271}$$

Glossing over the details, allowing for the cosmological constant to be a dynamical pressure means that the thermodynamics of anti-de Sitter black holes, in particular, acquire

a richer structure than their asymptotically flat counterparts, behaving as Van der Waals fluids [145,146], polymers [147] and allowing for the construction of black hole heat engines [148]. Thus, the extended thermodynamics of AdS black holes offer a rich gravitational perspective on everyday phenomena (for a review, see [149]).

Extended black hole thermodynamics is not without its criticisms. A common critique is treating the cosmological constant as a *variable* pressure. Indeed, while the $P - V$ term in the Smarr Formula (268) is required for consistency, its appearance does not imply the pressure should be made variable, at least from a gravitational perspective. Assuming AdS/CFT duality, it is more natural to allow for varying the cosmological constant since variations in Λ_{d+1} are dual to variations in the number of degrees of freedom of the dual theory [141,148,150–155].

Holographic braneworlds suggest a higher-dimensional origin for extended black hole thermodynamics [156]. In particular, a dynamical cosmological constant on the brane naturally follows from tuning the brane tension. In fact, keeping other bulk parameters L_{d+1} and G_{d+1} fixed, varying the tension alone corresponds to varying the induced brane cosmological constant on the brane Λ_d:

$$\delta\tau = \frac{\delta\Lambda_d}{8\pi G_d}. \tag{272}$$

Hence, classical black hole thermodynamics in the bulk including work completed by the brane induces extended thermodynamics of quantum black holes on the brane.

This observation can be made explicit in the context of the braneworld constructions considered here. Specifically, when treating the brane tension τ as a thermodynamic variable akin to the surface tension of liquids, the first law of the bulk black hole is

$$dM = TdS + A_\tau d\tau, \tag{273}$$

where $A_\tau \equiv \left(\frac{\partial M}{\partial \tau}\right)_S$ is the variable conjugate to τ. Consequently, tension variation $d\tau$ induces extended thermodynamics on the brane. Particularly, the bulk first law (273) maps to the extended first law on the brane

$$dM = TdS_{\text{gen}} + VdP_d + ..., \tag{274}$$

thus extending the quantum first law, where the pressure P_d is the pressure of the quantum black hole and V is its conjugate thermodynamic volume.

In summary, since the scales of the brane theory are induced, holographic braneworlds provide a gravitational motivation for treating the cosmological constant as a variable. For example, the pressure and volume of the static quantum BTZ black hole are [156]

$$\begin{aligned} P_3 &\equiv -\frac{\Lambda_3}{8\pi G_3} = \frac{\sqrt{1+\nu^2}}{4\pi\nu^2\ell_3^2 G_3}(\sqrt{1+\nu^2}-1), \\ V &\equiv \left(\frac{\partial M}{\partial P_3}\right)_{S_{\text{gen}},c_3} = -\frac{2\pi\ell_3^2 z^2[-2+\nu^2+3\nu^3 z^3+\nu^4 z^4+\nu z(\nu^2-4)]}{(1+3z^2+2\nu z^3)^2}. \end{aligned} \tag{275}$$

Together with the standard thermodynamic variables (202), it is straightforward to verify the extended first law (274) is obeyed. Extended thermodynamics for charged and rotating qBTZ black holes were computed in [135] (see also [99] for charged BTZ).

5.7. Quantum Reverse Isoperimetric Inequality

One of the more puzzling aspects of extended black hole thermodynamics is the thermodynamic volume V. In simple cases, e.g., $D \geq 4$ AdS-RN, volume V coincides with the geometric volume of the black hole, i.e., the amount of spacetime volume excluded by the black hole horizon. In general, however, the thermodynamic volume is not the geometric volume, cf. [142–144][44]. Nonetheless, the thermodynamic volume plays a crucial

role in understanding black hole thermodynamics. A sharp example of this is that there is strong evidence that AdS black holes obey the reverse isoperimetric inequality [143]

$$\mathcal{R} \equiv \left(\frac{(D-1)V}{\Omega_{D-2}}\right)^{\frac{1}{D-1}} \left(\frac{\Omega_{D-2}}{A_{\rm BH}}\right)^{\frac{1}{D-2}} \geq 1. \tag{276}$$

Here, Ω_{D-2} is the volume of a unit $(D-2)$ sphere, of D-dimensional AdS, and $A_{\rm BH}$ is the area of the black hole horizon. Notably, it is the thermodynamic volume for which this inequality holds, not the geometric volume. Refined generalizations of the inequality (276), inspired by the classical Penrose inequality [157,158], have been conjectured and tested for a plethora of examples [159].

Physically, the reverse isoperimetric inequality states an asymptotically AdS black hole with fixed thermodynamic volume has an entropy no larger than Schwarzschild–AdS of the same volume, i.e., Schwarzschild–AdS is a maximal entropy state at fixed (thermodynamic) volume. While there is no general proof of the inequality (276), there are very few known counterexamples[45] and all such 'superentropic' black holes have a negative heat capacity at constant volume, $C_{\rm V} < 0$, and are thus thermodynamically unstable [165]. Via $\mathrm{AdS}_3/\mathrm{CFT}_2$ duality, black hole superentropicity can be microscopically understood as an overcounting of the (naive) Cardy entropy of the CFT_2 [166].

When semi-classical quantum effects are accounted for, the classical inequality (276) is known to be violated [156]. A natural quantum generalization of (276) is proposed to be [135]

$$\mathcal{R}_{\rm Q} \equiv \left(\frac{(D-1)V_{\rm th}}{\Omega_{D-2}}\right)^{\frac{1}{D-1}} \left(\frac{\Omega_{D-2}}{4\mathcal{G}_D S_{\rm gen}}\right)^{\frac{1}{D-2}} \geq 1. \tag{277}$$

Here, the classical area has been replaced by the generalized entropy and $V_{\rm th}$ is the Casimir-subtracted thermodynamic volume,

$$V_{\rm th} = V - V_{\rm cas}, \tag{278}$$

where, in analogy with Casimir mass, $V_{\rm cas}$ is the thermodynamic volume assigned to empty AdS space. In the case of $D = 3$, the quantum reverse isoperimetric inequality (277) has been shown to hold for all AdS_3 quantum black holes at all orders of backreaction—except for a subspace of rotating black holes (those belonging to the red region in Figure 12), which are all found to be thermodynamically unstable, in accordance with Johnson's conjecture [165] regarding the classical inequality. This implies there exists a maximum entropy state among thermodynamically stable quantum black holes at fixed volume.

5.8. Phase Transitions of Quantum Black Holes

As with ordinary thermodynamic systems, black holes in AdS can undergo phase transitions. A paradigmatic example is the Hawking–Page (HP) phase transition [116]: below a certain temperature $T_{\rm HP}$, large AdS black holes in equilibrium with their radiation transition to thermal AdS. At the level of the quantum gravitational partition function, this transition signals an exchange between dominant contributions in the Euclidean path integral. The classical BTZ black hole also undergoes a HP phase transition [167,168]. To wit, the canonical free energy $F_{\rm BTZ} = -T \log Z$ of a static BTZ black hole is

$$F_{\rm BTZ} = M - TS = -\frac{\pi^2 \ell_3^2}{2G_3} T^2, \tag{279}$$

for temperature $T = r_+/2\pi\ell_3^2$. Comparing with the free energy of thermal AdS, $F_{\rm AdS} = M_{\rm AdS} = -1/8G_3$, a first-order phase transition occurs at a temperature

$$T_{\rm HP} = \frac{1}{2\pi\ell_3}. \tag{280}$$

When $T < T_{\rm HP}$, thermal AdS has a lower free energy than the black hole and is, therefore, the dominant contribution to the partition function; for $T > T_{\rm HP}$, the black hole has lower free energy and becomes the dominant contribution to the partition function.

Quantum AdS black holes also undergo thermal phase transitions [124,169]. In fact, large backreaction effects can trigger new transitions unseen by their classical counterparts. Consider, for example, static, neutral quantum BTZ. Working in the standard canonical ensemble, where c and P are held fixed[46], the free energy is

$$F_{\rm qBTZ} \equiv M - TS_{\rm gen} = -\frac{z^2\sqrt{1+\nu^2}}{2G_3}\frac{[1+2\nu z+\nu z^3(2+\nu z)]}{(1+3z^2+2\nu z^3)^2}. \tag{281}$$

As with the classical scenario, compare to 'quantum' thermal AdS_3 (qTAdS), i.e., pure AdS_3 including a backreaction due to the cutoff CFT_3, with free energy

$$F_{\rm TqAdS} = M_{\rm qTAdS} = -\frac{1}{8\mathcal{G}_3}. \tag{282}$$

In Figure 15, we present a side-by-side comparison of the canonical free energy of the classical BTZ black hole and quantum BTZ for large backreaction, $\nu > 1$. Focusing on the quantum BTZ black hole, as the temperature monotonically increases, there are *reentrant phase transitions* from thermal AdS to qBTZ and back to thermal AdS: (i) for temperatures up to a critical temperature (where $\Delta F \equiv F_{\rm qBTZ} - F_{\rm qTAdS} = 0$), thermal AdS has lower free energy, until at the critical temperature, there is a discontinuity in the slope of the free energy, i.e., a first-order phase transition and a quantum analog of the Hawking–Page phase transition. (ii) After this temperature, the qBTZ black hole has a lower free energy until there is a jump discontinuity in the free energy, a zeroth-order phase transition, beyond which TAdS always has a lower free energy. The reentrant phase transition is the combination of the first- and zeroth-order phase transitions as the temperature monotonically varies, and it is exhibited by an (inverse) swallow tail.

As displayed in Figure 15, reentrant phase transitions do not occur for the classical BTZ black hole. Reentrant phase transitions, however, are known to appear in (classical) higher-derivative theories of gravity in higher dimensions and Born–Infeld gravity [172–175]. In all such cases, the transitions are between different phases of the black hole, e.g., large to small and back to large black holes. For the quantum black hole, the reentrant phase is a reentrant Hawking–Page phase transition, moving between thermal AdS and the same black hole. Again, the zeroth-order phase transitions only occur for a large enough backreaction. In this regime, the brane has decreasing tension, and the gravitational theory on the brane becomes more massive and effectively four-dimensional. Meanwhile, for a small backreaction, thermal AdS dominates at all temperatures until the $\nu = 0$ limit where one recovers the phase behavior of classical BTZ.

Even though the phase structure admits a region where the black hole is thermodynamically favored, it may not contribute to the Euclidean path integral if it is thermally unstable. The heat capacity serves as a diagnostic to determine whether the black hole is stable against thermal fluctuations. For example, classically, the Hawking–Page transition is between thermal AdS and stable black holes (small AdS black holes are unstable). Likewise, in the case of quantum BTZ, a computation of the heat capacity [176] reveals reentrant phase transitions occur in the canonical ensemble between thermal AdS and a branch of thermally stable quantum black holes. More precisely, a study of the temperature of the qBTZ solution reveals three branches[47] of continuously connected black holes: (A) 'cold' black hole, (B) 'intermediate' black hole, and (C) 'hot' black hole. Black holes belonging to branches A and C have a negative heat capacity and are thus unstable, while branch B black holes have a positive heat capacity and are thermally stable. The reentrant phase transitions occur only between thermal AdS and these intermediate black holes.

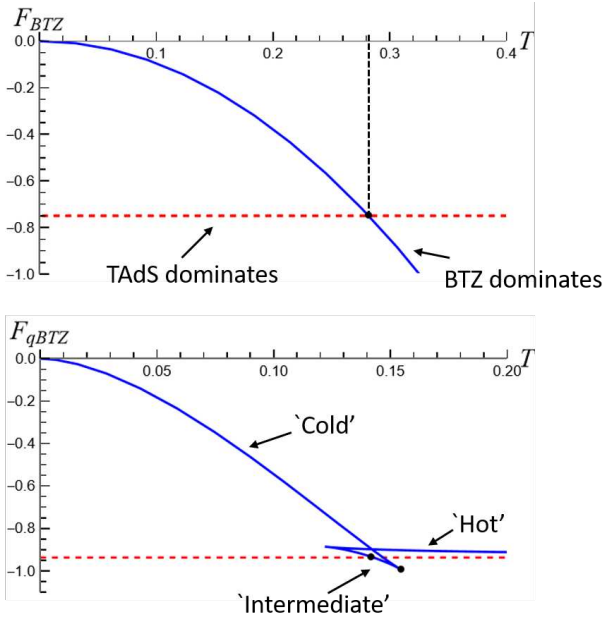

Figure 15. Phases of BTZ black holes. *Top:* Hawking–Page transition of classical BTZ. For temperatures $T < T_{\rm HP}$, thermal AdS has a lower free energy (red, dashed line) than the black hole (blue, solid curve). At $T = T_{\rm HP}$, there is a first-order phase transition, and for $T > T_{\rm HP}$, the black hole has a lower free energy, leading to an exchange in dominance in the quantum gravitational partition function. *Bottom:* Reentrant phase transition of quantum BTZ black hole with large backreaction. Below a critical temperature (the analog of the HP temperature), quantum TAdS has the lower free energy. At this critical temperature, there is a first-order transition between qTAdS and intermediate black holes. Between this HP-like temperature and a second critical temperature, the qBTZ has a lower free energy. At the second critical temperature, there is a zeroth-order transition back to TAdS.

6. Braneworld Black Holes in Higher Dimensions

The majority of this review focused on exact constructions of three-dimensional quantum black holes. From the perspective of the non-holographic perturbative treatment, working in three spacetime dimensions, $d + 1 \geq 4$ was solely to simplify the problem. Indeed, the expectation value of the renormalized quantum stress tensor $\langle T_{ij} \rangle$ is not known in general. Exceptions do exist[48]. For example, for even-dimensional homogeneous and isotropic FRW cosmologies, the trace anomaly for conformal quantum fields is known [178,179]. In the case of static, spherically symmetric backgrounds, however, the renormalized stress tensor is only known up to an arbitrary function of an appropriate radial coordinate [5].

One possible way to circumvent this issue is to instead work in a truncated s-wave sector of the matter theory and use the two-dimensional conformal anomaly to fix the form of the quantum-stress tensor and find quantum corrections to, say, the Schwarzschild black hole [180–183]. Another approach is to solve the (semi-classical) Tolman–Oppenheimer–Volkoff equations for a massless conformally coupled scalar field [184]. Working perturbatively in $\hbar$, one can construct analytic asymptotically flat, static, spherically symmetric solutions, while numerics yields non-perturbative corrections in $\hbar$[49]. Thus, the situation for solving the backreaction problem in $d + 1 \geq 4$ is more complicated and subject to quantum gravitational corrections. This again motivates the use of holographic techniques as employed in the three-dimensional case. However, as we now review, the status of finding higher-dimensional quantum black holes via braneworlds is more complicated.

6.1. Higher-Dimensional Quantum Black Holes?

Given the success of studying three-dimensional quantum black holes starting from the AdS_4 C-metric, it is natural to wonder if a similar analysis follows from a higher-dimensional C-metric. Notably, however, no exact solutions to Einstein's equations describing accelerating black holes in dimension $D = d + 1 > 4$ are known[50]. As reasoned in [192], this is because in $D \geq 5$, the string generating the acceleration has a singularity along its symmetry axis passing through the black hole, which is distinctly less mild than in $D = 4$. Put another way, in four dimensions, there exist more general accelerating black holes accelerated by Levi–Civita strings or rods. The C-metric is a special limit of such a geometry, which is singled out as a metric where the string has a milder singularity along its axis and better-behaved asymptotics than its brethren. In $D \geq 5$, it seems there is no such special limit for accelerating black holes. Alternately, one can perturbatively construct a C-metric in $D > 4$ by perturbing a higher-dimensional Schwarzschild black hole to give it uniform acceleration [193]. However, it was found that such a solution with constant string tension does not allow for localized braneworld black holes (they do not satisfy the Israel junction conditions). Moreover, allowing for non-uniform string tension results in infinitely many localized braneworld black hole solutions.

Historically, the first attempt at finding a four-dimensional braneworld black hole embedded in a five-dimensional bulk was carried out by Chamblin, Hawking and Reall [194]. Their starting point takes the original Randall–Sundrum model and replaces the Minkowski line element on the brane with a four-dimensional Ricci flat metric, e.g., the Schwarzschild black hole,

$$ds_5^2 = dy^2 + a^2(y) g_{ij}^{\text{Schw}} dx^i dx^j. \tag{283}$$

Here, y denotes the bulk extra direction, and $a^2(y)$ denotes the warp factor (for the RS-II scenario, $a^2(y) = e^{-2|y|/L_5}$ for bulk AdS_5 length scale L_5). The brane is located at $y = 0$, such that from the brane perspective, the geometry is exactly the static, four-dimensional Schwarzschild black hole. Note, however, the five-dimensional Chamblin, Hawking, Reall 'black string' (283) suffers from a classical *dynamical* instability [195] analogous to the Gregory–Laflamme instability of Kaluza–Klein black strings [196,197]. We will return to this instability momentarily. Further, the black string extends to the AdS_5 horizon at $y = \infty$ and where the black hole horizon becomes singular with diverging scalar curvature invariants.

The Chamblin, Hawking, Reall braneworld black hole thus cannot describe the end state of gravitational collapse. In fact, whilst searching for examples of Oppenheimer–Synder gravitational collapse of braneworld black holes, a no-go theorem was posed [66]: the exterior geometry of the dust cloud cannot be static. This theorem, and the dearth of evidence of exact static black holes localizing in the RS-II construction (circa 2002), in part motivated Tanaka [34] and Emparan, Fabbri, and Kaloper [22] to conjecture that higher-dimensional braneworld black holes must be time-dependent (see also [198]). Their reasoning utilized AdS/CFT holography and was argued to be consistent with the proposal that black holes that localize on the brane may be interpreted as quantum black holes.

6.2. Predictions from Holography

Let us review the arguments [22,34] predicting higher-dimensional braneworld black holes must be time-dependent. Take the bulk to be classical AdS_5 general relativity with a four-dimensional RS brane. According to braneworld holography, the induced theory on the brane describes a higher-derivative theory of gravity coupled to a large-N gauge theory in the 't Hooft planar limit with large 't Hooft coupling $\lambda = N g_{\text{YM}}^2$ (we refer to this matter theory as a large-c CFT_4 with an ultraviolet cutoff owed to the presence of the brane). In particular, the full AdS/CFT duality in this case is between type IIB string theory on $AdS_5 \times S^5$ and $\mathcal{N} = 4$ super Yang–Mills $SU(N)$ gauge theory with AdS length

$L_5 = L_{\rm P}^{(10)}(g_s N)^{1/4}$ (for string coupling g_s and ten-dimensional Planck length $L_{\rm P}^{(10)}$) and 't Hooft coupling $\lambda = g_s N$. The effective number of CFT degrees of freedom is[51]

$$c \sim N^2 = \left(\frac{L_5}{L_{\rm P}^{(5)}}\right)^3 = \left(\frac{L_5}{L_{\rm P}^{(4)}}\right)^2, \tag{284}$$

such that large $N = L_5/L_{\rm P}^{(4)}$ coincides with the four-dimensional Planck length going to zero. Further, notice the combination

$$N^2\hbar = \left(\frac{L_5}{L_{\rm P}^{(4)}}\right)^2 \frac{(L_{\rm P}^{(4)})^2}{G_4} = \frac{L_5^2}{G_4}, \tag{285}$$

remains fixed as $\hbar \to 0$ and keeping L_5, G_4 fixed.

Now, according to the conjecture [22], the braneworld black hole must be a solution to the semi-classical theory sourced by the CFT stress tensor $\langle T_{ij}\rangle$ in some quantum state. For a black hole background, in principle, the quantum state could be in any of the common choices of the vacuum state, i.e., the Hartle–Hawking, Boulware, or Unruh state. Recall that the Hartle–Hawking state describes a black hole in a thermal bath in equilibrium with its own radiation, producing a non-dynamical configuration. On the other hand, the Unruh vacuum describes a time-dependent evaporating black hole (there is a thermal flux of radiation at future null infinity). To infer whether a black hole in the Hartle–Hawking state is possible—without finding an explicit solution—one can instead estimate the evaporation time of a radiating black hole; if the time for evaporation is finite, then a static black hole solution is not possible. To this end, consider a weakly coupled CFT in four dimensions. In particular, the trace anomaly for $\mathcal{N} = 4$ $SU(N)$ super Yang–Mills theory to leading order in $\hbar$ is

$$\langle T^i_{\ i}\rangle = \frac{\hbar(N^2-1)}{32\pi^2}\left(R_{ij}^2 - \frac{1}{3}R^2\right) \approx \frac{\hbar N^2}{32\pi^2}\left(R_{ij}^2 - \frac{1}{3}R^2\right), \tag{286}$$

taking $N \gg 1$. Thus, the anomaly for such a CFT is simply the free field result enhanced by a $\mathcal{O}(N^2)$ factor. With this in mind, the power emitted by Hawking quanta modeled by the large-N CFT will be

$$\frac{dM}{dt} \sim \frac{N^2\hbar}{R_0^2}, \tag{287}$$

for initial horizon radius $R_0 = 2 \sim G_4 M$. Then, the time for evaporation $t_{\rm evap}$ heuristically is

$$t_{\rm evap}^{-1} \equiv \frac{1}{R_0}\frac{dR_0}{dt} = \frac{2G_4}{R_0}\frac{dM}{dt} \sim \frac{2}{R_0^3}\hbar G_4 N^2 = \frac{2L_5^2}{R_0^3}, \tag{288}$$

where we substituted in (285). Thus, the evaporation time is finite (even as $\hbar \to 0$). Moreover, such a black hole would evaporate rapidly due to the $\mathcal{O}(N^2)$ enhancement of the free theory result. Altogether, this suggests black holes cannot remain static on the brane: they shrink and evaporate in a finite time.

Assuming the bulk/brane correspondence holds, the semi-classical evaporation of the black hole localized on the brane should have a classical bulk signature. One possibility, originally put forth in [34] (see also [199]), is that the semi-classical evaporation is linked to a classical instability of the bulk five-dimensional solution. The intuition is as follows. Consider the five-dimensional black Chamblin, Hawking, Reall black string (283), and have a Randall–Sundrum brane intersect it. The radius of the black hole will exponentially shrink with the AdS_5 length L_5 as one moves away from the brane. Further, the black string suffers from a Gregory–Laflamme instability when the horizon radius becomes smaller than L_5. As a result of the instability, a portion of the horizon localized on the brane will pinch off and fall into a region of the bulk black hole away from the brane. Thus, while the horizon area of the bulk black hole does not shrink, the area of the horizon localized on the

brane shrinks. This five-dimensional deformation due to dynamical instability implies a type of classical evaporation of braneworld black holes.

Another view is that semi-classical radiation corresponds to gravitational radiation of the bulk black hole. Indeed, from the brane perspective, the Hawking quanta are modeled by the large-c CFT, corresponding to bulk Kaluza–Klein gravitons. Further, a black hole stuck to a brane is accelerating away from the center of AdS, thus producing gravitational waves. Thus, Hawking radiation from the brane perspective corresponds to bulk gravitational bremsstrahlung [22]. Qualitatively, moreover, the classical gravitational waves emitted into the bulk have a characteristic frequency ω which from the brane perspective is estimated to be $\omega \sim (G_4 M)^{-1}$, which is the four-dimensional Hawking temperature. This reasoning suggests why the classical bulk gravitational radiation appears as thermal radiation on the brane.

6.3. Counterexamples

The essential problem of the holographic argument leading to the finite evaporation time (288) is that the result assumes the large-N CFT is weakly coupled. Of course, for the holographic construction of the bulk/brane set-up to be valid, the cutoff CFT on the brane is strongly coupled, i.e., large 't Hooft coupling. Thus, as first recognized by Fitzpatrick, Randall, and Wiseman [69], it is not clear the radiation has access to all of its $\mathcal{O}(N^2)$ degrees of freedom. Importantly, being at strong coupling can lead to a reductionin the accessible degrees of freedom, from $\mathcal{O}(N^2)$ to $\mathcal{O}(1)$ via confinement (see also [200])[52]. Such a reduction thus makes it plausible that static braneworld black holes in higher dimensions do exist.

In fact, there are several examples of higher-dimensional static braneworld black holes, both analytically and numerically constructed [67–72,201–208]. The question is whether these static solutions are to be viewed as quantum black holes on the brane. To explore this point, reconsider the 5D/4D Randall–Sundrum construction with the five-dimensional Schwarzschild black string (283). Despite its dynamical instability, this is an example of a static braneworld black hole, where the black hole on the brane is simply the four-dimensional Schwarzschild geometry. Seemingly then, the cutoff CFT on the brane does not modify the geometry: from the looks of it, the brane geometry consists of a non-trivial zero mode and no excited Kaluza–Klein modes [69]. Nonetheless, Fitzpatrick, Randall, and Wiseman argued the dual quantum black hole description might be consistent with the existence of such static localized black hole solutions. It is simply that the quantum corrections to the geometry are suppressed[53].

To appreciate this last point, consider the set-up of [202], consisting of an asymptotically AdS_5 bulk spacetime, with two positive tension Karch–Randall branes with an AdS_5 Schwarzschild black string stretching between the two branes (see Figure 16). In particular, the bulk geometry has line element

$$ds_5^2 = \frac{L_5^2}{\cos^2(u)}\left[du^2 + \frac{1}{\ell_4^2} g_{ij} dx^i dx^j\right], \tag{289}$$

with bulk AdS_5 radius L_5, and induced four-dimensional radius $\ell_4 = L_5 \sec(u_0)$. The AdS_5 boundary is located at $u = \pm\pi/2$, while the two AdS_4 branes are at $u = \pm u_0$, each with the same positive tension $\tau = \frac{6\sin(u_0)}{8\pi G_5 L_5}$, and separated a finite distance apart. Further, take the four-dimensional metric g_{ij} to be the AdS_4–Schwarzschild black hole,

$$g_{ij} dx^i dx^j = -f(r) dt^2 + f^{-1}(r) dr^2 + r^2(d\theta^2 + \sin^2\theta d\phi^2), \quad f = 1 + \frac{r^2}{\ell_4^2} - \frac{2G_4 M}{r}. \tag{290}$$

Without branes, this system has an instability when $r_+/\ell_4 < 1$ (small black holes of horizon radius r_+), while it is stable for large black holes, $r_+/\ell_4 > 1$ [210]. The stability structure remains the same with branes included [202].

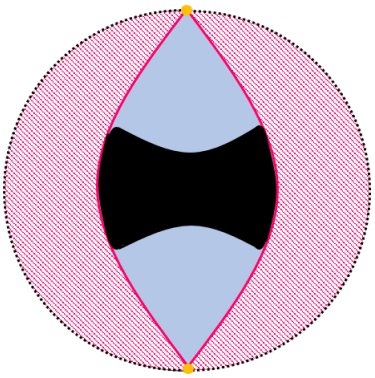

Figure 16. Black string with Karch–Randall branes. An AdS_5 black string stretches between two two end-of-the-world AdS_4 branes, such that all magenta regions (including the AdS_5 boundary) are removed. The black string can be replaced by a uniform black funnel, and the ETW branes may be replaced with Randall–Sundrum branes.

The classical bulk is stable for large mass black holes that localize on the branes (focus on only a single brane as a being living on one brane would not directly experience the other brane). From the brane perspective, the induced geometry is simply the AdS_4–Schwarzschild black hole. Seemingly, the geometry has no quantum corrections due to the backreacting holographic field theory living on the brane. This runs counter to what would be expected based on a weakly coupled analysis of the quantum-stress tensor[54]. Indeed, recall the trace anomaly of weakly coupled $\mathcal{N} = 4$ SU(N) super Yang–Mills theory (286). Substituting in the AdS_4–Schwarzschild geometry (290), the anomaly reads

$$\langle T^i_{\ i} \rangle = -\frac{3\hbar(N^2-1)}{8\pi^2\ell_4^4}. \tag{291}$$

Since $\langle T^i_{\ i} \rangle$ is non-vanishing, one expects the AdS_4–Schwarzschild black hole to become quantum-corrected due to backreaction. In view of the conjecture of holographic braneworld black holes, the question thus becomes in what sense can the AdS_4–Schwarzschild black hole on the brane be viewed as a 'quantum' black hole.

The resolution of this apparent tension with the conjecture is the following. The quantum stress tensor of the strongly coupled CFT (as required for a consistent holographic description of the bulk gravity) simply does not correct the geometry, at least at leading order. To see this, consider the boundary CFT stress tensor, which can be computed in full using holographic renormalization methods, leading to [202]

$$\langle T_{ij} \rangle = -\frac{3\hbar N^2}{32\pi^2\ell_4^4} g_{ij}. \tag{292}$$

Taking the trace returns the anomaly (291). The main takeaway is that the stress tensor is proportional to the metric. In such an instance, the CFT only renormalizes the effective brane cosmological constant and thus does not lead to any quantum-corrected geometry. Notice that in the limit, the brane cosmological constant vanishes, $\ell_4 \to \infty$, and so too does the quantum stress tensor, $\langle T_{ij} \rangle \to 0$. This is consistent with the Schwarzschild black string with a Randall–Sundrum brane construction in [69].

A conclusion, then, is that formally, the AdS_4–Schwarzschild braneworld black hole can be interpreted as a quantum black hole. The cutoff CFT, however, is special in that it does not explicitly backreact on the brane geometry, and it only serves to renormalize the induced cosmological constant. Geometrically, this is a manifestation of the bulk spacetime (289) being foliated by the AdS_4–Schwarzschild black hole. Consequently, the classical Kaluza–Klein graviton modes are not excited in the background solution. Observe,

moreover, the correction to the cosmological constant is independent of the black hole mass and hence its temperature. The brane black hole thus does not radiate, which is consistent with no excited Kaluza–Klein modes. This is at first puzzling from the perspective of AdS/CFT, as one would have expected a component of the holographic stress tensor to correspond to a thermal plasma of CFT degrees of freedom outside the black hole. As noted in [200], this is a consequence of the large-N super Yang–Mills theory confining to $\mathcal{O}(1)$ degrees of freedom.

It is worth emphasizing the implications of the static solution found from the AdS_5 black string [202]. There is no Hawking emission, and up to the term generating the Weyl anomaly, the quantum stress tensor is everywhere vanishing. Despite the lack of thermal radiation near infinity, the static state of the CFT is in thermal equilibrium with the black hole since they nonetheless obey the Kubo–Martin–Schwinger (KMS) condition. This suggests, from the bulk perspective, such braneworld black holes remain stuck to the brane, while from the brane perspective, the black hole evaporation is disallowed due to the large-N and large 't Hooft coupling of the holographic CFT.

6.4. Evaporating Braneworld Black Holes

Putting the status of the higher-dimensional static quantum black holes aside, braneworld holography has proven useful in studying black hole evaporation. Indeed, while some bulk black holes can get stuck on the brane and never shrink ('black droplets') [71] and hence are dynamically stable, there are other bulk black solutions that evaporate due to a Gregory–Laflamme instability [72], as originally suggested in [22,34]. The essential physical insight is that evaporation takes place when the brane black hole is coupled to an appropriate thermal bath modeled by thermalized $\mathcal{O}(N^2)$ degrees of freedom of the CFT. From the bulk perspective, this means the horizon of the black hole on the brane is to be connected to another horizon in the bulk. The bulk system will have a Gregory–Laflamme-like instability such that the black hole attached to the brane slides off the brane into the bulk, forming a (typically) larger black hole horizon. Thus, while the horizon on the brane reduces its size (evaporation), the horizon in the bulk does not shrink, which is consistent with the classical evolution of black hole horizons.

There are in fact several examples of evaporating braneworld black holes (see [72] for details). In all cases, the bulk system considers D-dimensional black holes in the large-D limit [212–214] that localize on either one or a pair of Karch–Randall branes[55]. In particular, these holes include the following: (i) A small AdS black string is stretched between two branes with black holes localizing on both branes. The string instability triggers either the evaporation of both black holes into a single bulk black hole or the evaporation of one brane black hole into the other brane black hole. (ii) A small AdS black hole on the brane is connected to a larger bulk black hole (bath) such that the brane black hole evaporates entirely into the bulk. (iii) A large unstable AdS black droplet is connected to a non-gravitating boundary (bath) via a thin black funnel, such that the droplet evaporates into the boundary.

In short, the exhaustive large-D analysis reveals holographic CFTs coupled to black holes have distinctive traits over their weakly interacting counterparts. According to [72,215], their semi-classical dynamics are always dual to classical Gregory–Laflamme-like dynamics of bulk black holes.

7. Outlook and Applications

We have seen how holographic braneworlds provide a means to exactly study the problem of semi-classical backreaction. In particular, there is a precise construction of quantum-corrected black holes and an exploration of their horizon thermodynamics. But this is only a small cross-section of the utility of braneworld holography. Phenomenological considerations aside—a historical motivation to study braneworld physics—holographic braneworlds have a number of applications, particularly in the interdisciplinary field of

holographic information theory. Below, we very briefly give a non-exhaustive and biased list of applications of quantum black holes and, more broadly, holographic braneworlds.

7.1. Applications

7.1.1. Holographic Entanglement and Gravitational Entropy

For a quantum mechanical system in state ρ, the von Neumann entropy is defined as

$$S_{\rm vN} \equiv -{\rm tr}\,[\rho \log \rho]. \tag{293}$$

If the system is in a pure quantum state, the entropy (293) is identically zero. When the system comprises smaller subsystems, $S_{\rm vN}$ quantifies how entangled the subsystems are. In quantum field theory, subsystems are often chosen to be spatial regions Σ of the entire quantum system. Intriguingly, for ground states of local Hamiltonians, the entanglement entropy, while divergent in the ultraviolet, generally adheres to an area law (in $d+1$-spacetime dimensions)

$$S_{\rm vN} = c_0 \frac{{\rm Area}[\partial\Sigma]}{\epsilon^{d-1}} + ..., \tag{294}$$

where c_0 refers to the constant, ϵ refers to the UV regulator, and the ellipsis refers to subleading UV divergences whose precise terms are state-dependent. Thus, $S_{\rm vN}$ scales with the boundary area of the subsystem rather than its volume, which is in contrast to the volume law typically observed in thermal states. The entropy–area relation (294) is clearly reminiscent of the Bekenstein–Hawking entropy formula for black holes, suggesting black hole entropy arises from vacuum entanglement due to quantum fields across the horizon, tracing out the interior degrees of freedom [131,216–220]. In particular, in scenarios of gravity induced due to matter loops [221,222], the Bekenstein–Hawking entropy is solely due to entanglement due to vacuum fluctuations [223–225], where the UV-cutoff dependence can be absorbed in a renormalization of Newton's constant [130].

Gravitational entropy, therefore, is imbued with an information–theoretic character. This is crystallized in AdS/CFT, where the entanglement entropy of a holographic CFT can be computed using the Ryu–Takayanagi (RT) formula [226,227]

$$S_A^{\rm vN} = \frac{{\rm Area}(\gamma)}{4G}. \tag{295}$$

Here, γ denotes a codimension-2 minimal surface in the bulk asymptotically AdS space, anchored to region A on the AdS boundary, such that $\partial\gamma = \partial A$ and γ is homologous to A. The RT prescription generalizes the Bekenstein–Hawking entropy formula for black holes: a black hole horizon is an example of a minimal surface, and the bulk AdS spacetime need not contain a black hole[56]. As such, it has led to numerous insights into gravitational physics, notably in understanding the emergence of gravity from quantum entanglement [233–238][57] following analogous insights from coarse-grained thermodynamics [240–245].

When the bulk theory includes higher curvature and semi-classical quantum corrections, the RT Formula (295) generalizes to the following extremization prescription [246]

$$S_A^{\rm vN} = \min_\gamma \left\{ \operatorname*{ext}_\gamma \left[\frac{{\rm Area}(\gamma)}{4G} + \mathcal{S}_{\rm DC}(\gamma) + S_A^{\rm bulk}(\Sigma_\gamma) \right] \right\}. \tag{296}$$

Here, $\mathcal{S}_{\rm DC}$ denotes the Dong–Camps anomaly terms [247,248] analogous to the Wald corrections to the Bekenstein–Hawking entropy, and $S_A^{\rm bulk}$ is the entanglement entropy of bulk fields across the entanglement wedge of A, Σ_γ, such that the quantity in brackets is recognized to be the generalized entropy $S_{\rm gen}(\gamma)$. Further, in the event there are multiple extremal surfaces, the prescription says the von Neumann entropy $S_A^{\rm vN}$ is given by choosing the extremal surface which minimizes the generalized entropy $S_{\rm gen}(\gamma)$. Notably, the

von Neumann entropy can undergo phase transitions as extremal surface configurations exchange dominance.

Holographic braneworlds provide additional evidence that gravitational entropy can be interpreted as entanglement entropy. Indeed, the gravity on the brane is induced from the cutoff CFT[58]. In combination with the RT prescription, it readily follows that the area entropy of black holes localized on an ETW brane is exactly equal to entanglement entropy [55]—the minimal surface coincides with the bulk black hole horizon intersecting the brane. Additionally, the braneworld set-up naturally resolves various subtleties in identifying Bekenstein–Hawking and entanglement entropies [251]. In particular, the UV cutoff ϵ for the CFT—equal to the bulk AdS length scale L_{d+1}— fixes the number of species of the dual CFT such that Newton's constant is correctly reproduced (cf. Equation (203)), thus resolving the 'species problem'. Heuristically, consider bulk AdS_4 with a black hole. The contribution of a single field to the CFT_3 entanglement entropy is of the order $S_A^{\rm vN} \sim \frac{c_0}{L_4}$. Then, for a large number of fields $c_3 = L_4^2/G_4 \sim L_4/G_3$, the total entanglement entropy is $S_A^{\rm vN} = c_3 c_0/L_4 \sim c_0/G_3$.

7.1.2. The Entropy of Hawking Radiation

Hawking's discovery that black holes emit thermal radiation leads to the information puzzle [252]: do black holes evolve unitarily or not? According to Hawking's original calculation, the fine-grained von Neumann entropy of radiation $S_{\rm vN}^{\rm rad}$ grows in time indefinitely, paradoxically surpassing the coarse-grained entropy of the black hole. Alternatively, if the black hole plus radiation obeys standard quantum principles, the radiation entropy instead follows a unitary Page curve [253], never exceeding the black hole entropy. Previously thought to be a problem only quantum gravity would solve, the paradox can be addressed in semi-classical gravity for which the extremization prescription (296) plays a prominent role [254–256]. In particular, a variant of (296) known as the 'island formula',

$$S_{\rm vN}(\Sigma_X) = \min_X \left\{ \operatorname*{ext}_X \left[\frac{\text{Area}(X)}{4G} + \mathcal{S}_{\rm DC}(X) + S_{\rm vN}^{\rm sc}(\Sigma_X) \right] \right\}, \tag{297}$$

can be used to explicitly compute unitary Page curves in evaporating or eternal black hole backgrounds. Here, $S_{\rm vN}(\Sigma_X)$ is the fine-grained entropy in the full quantum theory, $S_{\rm vN}^{\rm sc}$ is the von Neumann entropy of bulk quantum fields in the semi-classical approximation, and Σ_X is a codimension-1 slice bounded by a codimension-2 quantum extremal surface (QES) X and a cutoff surface. Generally, Σ_X is disconnected, $\Sigma_X = \Sigma_R \cup I$, where Σ_R is the region outside the black hole collecting radiation and I is an 'island' (with $X = \partial I$) lying primarily inside the black hole.

Originally achieved for models of two-dimensional dilaton gravity[59], holographic braneworlds confirm unitary Page curves arise in higher-dimensional gravity [65,260]. This is accomplished using 'double holography' (recall the description before Section 3.4). For simplicity, consider the boundary perspective, i.e., the vacuum state of the d-dimensional boundary CFT on $\mathbb{R} \times S^{d-1}$ coupled to a $(d-1)$-dimensional conformal defect along the equator of the sphere S^{d-1}. The entanglement entropy of the holographic boundary CFT can be computed using the RT prescription. Taking the bulk to be AdS_{d+1} with an AdS_d Dvali–Gabadadze–Porrati (DGP) brane [261] (where the brane action includes, e.g., its own Einstein–Hilbert term), the entropy of the boundary CFT vacuum reduced to a boundary region A is given by [54]

$$S_{\rm vN}(A) = \min_\gamma \left\{ \operatorname*{ext}_\gamma \left[\frac{\text{Area}(\gamma)}{4G_{d+1}} + \frac{\text{Area}(\gamma \cap \text{brane})}{4G_d} \right] \right\}, \tag{298}$$

for bulk extremal surface γ homologous to A and $\partial A = \partial \gamma$. The first term on the right-hand side is the familiar RT formula, while the second term is the gravitational contribution that arises when the bulk RT surface intersects the DGP brane. There are topologically distinct configurations for the bulk extremal surface γ: surfaces γ which do not intersect the brane

and (ii) surfaces that intersect the brane; only with (ii) does the second term in the brackets contribute. As both are candidate extremal surfaces, the entropy $S_{\mathrm{vN}}(A)$ is computed using the surface which gives the smallest value on the right-hand side (298). Transitions between 'disconnected' and 'connected' phases will occur depending on the size of γ and the brane tension and gravitational coupling.

The holographic entropy Formula (298) can be understood as a relation between the boundary and bulk perspectives. It is through the brane perspective that the right-hand side can be reinterpreted as the QES or island formula[60]. Qualitatively, the disconnected phase corresponds to the situation where, according to beings confined to the brane, no quantum extremal islands are formed, while in the connected phase, extremal islands appear[61]. By applying this doubly holographic reasoning to higher-dimensional topological black holes [65], black strings [264,265], and de Sitter space [82,266], the prescription (298) yields unitary Page curves except in cases where the horizon is extremal with a vanishing temperature.

Notably, thus far, all $3+1$-dimensional braneworld models that have been explored and exhibit island formation are described by *massive* gravity theories; islands disappear in the limit at which the graviton on the brane becomes massless [267] (see, e.g., [268] for a review). Further, long-range gravity theories have that the energy of an excitation localized to the island can be detected outside the island, which is inconsistent with the principle that operators in an entanglement wedge commute with operators in its complement [269]. Combined, this suggests the phenomenon of island formation is a feature of massive gravity, and it is even inconsistent in massless theories.

7.1.3. Holographic Complexity

Quantum complexity is another useful diagnostic in information theory. Loosely speaking, complexity measures the difficulty of constructing an arbitrary quantum state from a reference state using a specific set of resources. This concept has proven highly valuable in computer science and quantum computation, where the resources are given by some elementary operations ('gates') and the mapping between reference and target states defines a quantum circuit. Complexity has also been fruitful in gravitational physics, particularly as a tool to quantify the information processing of black holes. This application touches upon the foundational aspects of gravity and its interplay with quantum mechanics with some evidence suggesting that gravity itself may emerge from the minimization of complexity —that is, from efficient quantum computation [270–276].

Historically, computational complexity was proposed as a new entry in the holographic dictionary to address the puzzle of why black hole interiors continue to grow after scrambling [277]. Various conjectures for its precise duality have been proposed with the initial contenders being 'complexity=volume' (CV) [278,279] and 'complexity=action' (CA) [280,281]. CV posits that the complexity of a CFT state $|\Psi\rangle$ defined on a Cauchy slice σ is given by the maximal volume of a codimension-one bulk surface Σ anchored on the boundary slice σ,

$$\mathcal{C}_V(|\Psi\rangle) = \frac{\mathrm{Vol}(\Sigma)}{GL}. \tag{299}$$

On the other hand, CA asserts that complexity is defined by the on-shell gravitational action I evaluated within a codimension-zero bulk region known as the Wheeler–deWitt (WdW) patch $\mathcal{W}$, anchored at the given boundary slice σ,

$$\mathcal{C}_A(|\Psi\rangle) = \frac{I(\mathcal{W})}{\pi}. \tag{300}$$

Conceptually, CV is arguably more intuitive than CA, resembling the computational complexity of a tensor network circuit that captures the entanglement structure of the CFT

state [282–285]. For high-temperature thermofield double states, however, CV and CA complexities have the same late time behavior

$$\left.\frac{d\,\mathcal{C}_{V,A}}{dt}\right|_{t\gg\beta} \sim TS, \tag{301}$$

which is consistent with the expectation of complexity in such states.

More generally, an infinite number of gravitational duals to holographic complexity are technically possible [286,287]. Dubbed 'complexity=anything' (CAny), these generalizations are designed to encapsulate key aspects of complexity, including the anticipated linear growth following scrambling and the observed 'switchback effect' —a delay in the onset of linear growth caused by perturbations. While rigorous proof connecting any of these proposals to a concrete field theory definition of complexity is currently lacking, the notion is that they may be associated with ambiguities inherent in its definition. These ambiguities include the arbitrary choice of elementary gates, cost factors, and the reference state, among others.

Aspects of holographic complexity proposals have been explored using braneworlds [82,91,288–290], including the influence of backreaction effects using the static quantum BTZ black hole as a guide [91]. In summary,

- In the braneworld effective theory, CV admits a semi-classical expansion of the form

$$\mathcal{C}_V(|\Psi\rangle) = \frac{\mathrm{Vol}(\Sigma)}{GL} + \frac{\delta\mathrm{Vol}(\Sigma)}{GL} + \mathcal{V}(\Sigma) + \mathcal{C}_V^{\mathrm{bulk}}(|\phi\rangle) + \ldots, \tag{302}$$

  with the leading term being the complexity of the classical black hole, $\delta\mathrm{Vol}(\Sigma)$ is the change in the volume due to the quantum backreaction, $\mathcal{V}(\Sigma)$ represents higher curvature terms akin to the Wald corrections to the Bekentein–Hawking entropy, and $\mathcal{C}_V^{\mathrm{bulk}}(|\phi\rangle)$ is the complexity of the bulk state $|\phi\rangle$ defined on Σ. Note that the structure of (302) resembles an expansion of the QES prescription (296). Furthermore, (302) does satisfy the late time growth (301), upon replacing S with the generalized entropy S_{gen}.
- Conversely, CA does *not* simplify to the classical three-dimensional CA proposal plus corrections. The action involves cancellations among the bulk, boundary, and joint terms, making the late-time growth highly sensitive to quantum effects. As a result, the late time behavior (301) is not reproduced. This discrepancy arises because the WdW patch extends to the singularity, whose structure is significantly altered by quantum backreaction, leading to substantial quantum contributions to CA.

Analogous features have been observed for the rotating quantum BTZ [289]. Based on these preliminary studies, quantum black holes advocate the need for a semi-classical generalization of holographic complexity[62].

7.1.4. Singularity Probes and Quantum Cosmic Censorship

Black hole singularities reflect the fact that classical gravity is incomplete. Further, the Hawking–Penrose singularity theorems imply their inevitability. Due to their unphysical consequences, Penrose conjectured there must exist a type of cosmic censorship [158], known as weak cosmic censorship, where a horizon must shroud the singularity from null infinity. Singularities, moreover, mark a lack of predictive power in an otherwise classically deterministic theory. The strong cosmic censorship conjecture [292,293], which is independent of weak cosmic censorship, asserts classical general relativity should remain deterministic. In technical terms, for generic smooth initial data, the Cauchy evolution of a Cauchy hypersurface is inextendible beyond the Cauchy horizon. For example, for charged and rotating black holes, whose inner horizons are Cauchy horizons, the past timelike singularity heralds a lack of predictivity beyond the inner horizon. Conceivably, however, the infinitely blue-shifted energy of a particle entering from the exterior of the black hole should result in a large backreaction so as to turn the smooth (regular) inner Cauchy horizon into a non-smooth barrier [294,295].

It is natural to wonder whether either form of cosmic censorship holds when semi-classical backreaction effects are accounted for. Thus far, there is agreement that the expectation value of the quantum stress tensor of a free scalar field diverges at the inner horizon of a RN or Kerr black hole (in $D = d + 1 = 4$) on approach from the exterior [296–299], suggesting a type of strong cosmic censorship. A notable exception, however, is the classical rotating BTZ black hole, where the backreaction is mild enough such that the inner horizon does not become singular, indicating a violation in strong cosmic censorship [298,299][63]. A limitation of these works is that the analysis was only accomplished at leading order in backreaction. The rotating quantum BTZ black hole, on the other hand, which exactly accounts for all orders of backreaction, has essentially the structure of an AdS_4–Kerr black hole. Consequently, as argued in [300], and verified in [301] using the techniques of [299], rotating quantum BTZ has a singular inner horizon. Thus, for the BTZ black hole, strong cosmic censorship still holds once backreaction effects beyond leading order are accounted for.

There is an intuitive sense that quantum effects induce a weak form of cosmic censorship. Indeed, backreaction of the Casimir stress tensor modifies the conical (A)dS_3 and $Mink_3$ defect geometries such that the naked singularities become hidden behind a horizon. A standard test of (classical) weak cosmic censorship is to try to overspin or overcharge near-extremal black holes such that they shed their horizons. So far, Kerr–Newman black holes do not [302,303]. Likewise, the rotating quantum BTZ black hole cannot be overspun [176].

Another test of weak cosmic censorship is the conjectured classical Penrose inequality [304]. Loosely speaking, assuming there are no naked singularities and collapsing matter settles to a Kerr black hole, then the total mass M for a $D \geq 4$-dimensional asymptotically flat [305–308] or AdS spacetime [309,310] with a marginally trapped surface σ is bounded below by the area $A[\sigma]$

$$\frac{16\pi G_D M}{(D-2)\Omega_{D-2}} \geq \left(\frac{A[\sigma]}{\Omega_{D-2}}\right)^{\frac{D-3}{D-2}} + \ell_D^{-2}\left(\frac{A[\sigma]}{\Omega_{D-2}}\right)^{\frac{D-1}{D-2}}. \tag{303}$$

Here, G_D and ℓ_D denote the D-dimensional Newton's constant and curvature scale, respectively, and $\Omega_n \equiv 2\pi^{(n+1)/2}/\Gamma[(n+1)/2]$ is the volume of a unit n-sphere. In the limit $\ell_D \to \infty$, the Penrose inequality for asymptotically flat space is recovered. While the Penrose inequality has not been proven in general, any spacetime violating (303) is believed to be a counterexample to weak cosmic censorship. Notably, the classical Penrose inequality can be violated at leading order in perturbative backreaction [311,312]. This motivates the need for a semi-classical generalization of (303), i.e., a quantum Penrose inequality [311,312]

$$\frac{16\pi \mathcal{G}_D M}{(D-2)\Omega_{D-2}} \geq \left(\frac{4\mathcal{G}_D S_{\rm gen}}{\Omega_{D-2}}\right)^{\frac{D-3}{D-2}} + \ell_D^{-2}\left(\frac{4\mathcal{G}_D S_{\rm gen}}{\Omega_{D-2}}\right)^{\frac{D-1}{D-2}} \tag{304}$$

where the area $A[\sigma]$ has been replaced for the generalized entropy $S_{\rm gen}$ associated with a (quantum) marginally trapped surface. To test whether the quantum inequality (304) holds even for large backreaction effects, a three-dimensional inequality was proposed in [135]

$$8\pi \mathcal{G}_3 (M - M_{\rm cas}) \geq \ell_3^{-2}\left(\frac{4\mathcal{G}_3 S_{\rm gen}}{2\pi}\right)^2, \tag{305}$$

where $M_{\rm cas} = -1/8\mathcal{G}_3$ is the Casimir energy of backreacting quantum fields. All static and rotating quantum BTZ black holes were found to satisfy (305) at all orders of backreaction. This implies the existence of weak quantum cosmic censorship[64] in non-perturbative semi-classical gravity for which the quantum Penrose inequality would be a logical input.

7.1.5. Imprints of Quantum Backreaction Beyond Thermal Equilibrium

Realistic, astrophysical black holes are generally thought to be dynamical. Such non-stationary black holes lack an equilibrium thermodynamic description, and their horizons change shape and oscillate. One way to explore black hole dynamics is to consider (small) time-dependent perturbations to static or stationary black holes. Such perturbations display characteristic patterns of damped oscillations, dubbed quasi-normal modes (QNMs), that capture deviations away from equilibrium [314,315]. Furthermore, certain quasi-normal resonances serve as black hole signatures in gravitational wave astronomy.

Technically, QNMs are derived by examining the fluctuation equations of gauge-invariant perturbations. The simplest example involves the study of probe fields. For example, for a probe scalar field ϕ, the fluctuation equation is given by the Klein–Gordon equation,

$$(\Box + m^2)\phi = 0, \tag{306}$$

where ϕ is subsequently decomposed intro Fourier and harmonic modes, $\phi = e^{i\omega t} Y_l^m(\Omega)\Phi(r)$. The characteristic quasi-normal mode frequencies ω that solve the fluctuation equation are generally complex, $\omega = \omega_R - i\omega_I$, with a negative imaginary part indicating the decay of perturbations. For holographic AdS black holes, quasi-normal modes appear as poles in relevant retarded two-point correlators of the dual CFT, providing a field-theoretic characterization of black holes out of thermal equilibrium [316].

It is natural to wonder how a backreaction modifies characteristic traits of black hole dynamics. A detailed study of QNMs of the quantum BTZ black hole provides some preliminary insights [317]. Considering probe fields of brane localized matter, dual to CFT operators with conformal dimension $\Delta \in [1, 2]$ (accessible via the standard quantization) and spin $s = 0, \pm 1/2$, it was found that the QNMs and their overtones exhibit qualitatively different behavior depending on the branch of the qBTZ solution selected. This distinction can be used to differentiate between the types of singularities cloaked by a horizon: dressed conical singularities versus genuine quantum-corrected black holes. Furthermore, the magnitude ω_I of the imaginary part of the leading mode generally *decreases* with the strength of backreaction for the quantum-corrected black hole branch. This implies the thermalization time, $t_{\text{th}} \sim 1/\omega_I$, defined by the late-time decay of two-point correlators $\langle \mathcal{O}(0)\mathcal{O}(t)\rangle \sim e^{t/t_{\text{th}}}$, accelerates due to semi-classical effects. This phenomenon can be explained from the perspective of the dual CFT: quantum matter in the bulk with a large central charge corresponds to coupling a large number of light operators in the boundary CFT, increasing the number of degrees of freedom a small perturbation needs to excite before thermalization is reached.

The pole structure of retarded two-point CFT correlators dual to quantum BTZ QNMs, moreover, exhibits a markedly different behavior than its classical counterpart [317]. This includes, for example, 'pole-skipping', i.e., points in momentum space where the retarded Green's function is not unique. Specifically, for the quantum BTZ black hole, the momentum of the pole-skipping points exhibits a non-trivial dependence on the parameter controlling the strength of backreaction. This implies, given the connection between hydrodynamics and chaos in holographic CFTs [318,319], the chaotic dynamics of black holes are dramatically altered when backreaction is accounted for[65]. Further, by studying pole collisions in complex momentum space, quantum corrections have a significant impact on the analytic structure of the poles of retarded Green's functions. In particular, the quantum corrections intertwine the tower of modes in a series of level-crossing events noticeably distinct from the level-touching events observed in the classical BTZ geometry [322].

Author Contributions: All authors contributed equally to this review. All authors have read and agreed to the published version of the manuscript.

Funding: E.P. is funded by the Cosmoparticle Initiative at UCL. J.F.P. is funded by the 'Atracción de Talento' program grant 2020-T1/TIC-20495 and by the Spanish Research Agency through the grants

CEX2020-001007-S and PID2021-123017NB-I00, funded by MCIN/AEI/10.13039/501100011033 and by ERDF A way of making Europe. A.S. is funded by STFC consolidated grant ST/X000753/1.

Acknowledgments: This review is the culmination of numerous conversations with a plethora of colleagues and collaborators, particularly: José Barbón, Elena Cáceres, Rafael Carrasco, Casey Cartwright, Ana Climent, Roberto Emparan, Antonia Micol Frassino, Jaume Garriga, Ruth Gregory, Umut Gürsoy, Robie Hennigar, Seyed Hosseini Mansoori, Clifford Johnson, Eleni Kontou, David Kubizňák, Quim Llorens, José Navarro-Salas, Dominik Neuenfeld, Ayan Kumar Patra, Guim Planella Planas, Morteza Rafiee, Watse Sybesma, Marija Tomašević and Manus Visser. We especially thank Roberto Emparan for encouraging us to write this review.

Conflicts of Interest: The authors declare no conflicts of interest. The funders had no role in the design of the study; in the collection, analyses, or interpretation of data; in the writing of the manuscript; or in the decision to publish the results.

Appendix A. Conventions

Here, we summarize our conventions for bulk and hypersurface geometry. We also describe the variational principle with Neumann boundary conditions, leading to the brane equations of motion.

Appendix A.1. Background Geometry

Let $\mathcal{M}$ be a $d+1$ dimensional spacetime endowed with metric $\hat{g}_{ab}$ with coordinates x^a on $\mathcal{M}$. We take a 'mostly plus' convention for Lorentzian signature. The Riemann curvature tensor with respect to $\hat{g}_{ab}$ is

$$R^c{}_{dab} = \partial_a \Gamma^c{}_{bd} - \partial_b \Gamma^c{}_{ad} + \Gamma^c{}_{af}\Gamma^f{}_{bd} - \Gamma^c{}_{bf}\Gamma^f{}_{ad}. \tag{A1}$$

Appendix A.2. Hypersurface Geometry

Let Σ denote a timelike or spacelike d-dimensional hypersurface embedded in $\mathcal{M}$. The hypersurface is defined by a restriction on coordinates x^a, i.e., it introduces a scalar function $\Phi(x^a)$ which obeys the constraint $\Phi(x^a) = 0$. The unit normal n_a to this hypersurface is $n_a = \epsilon \mathcal{N} \partial_a \Phi$, with $\epsilon \equiv n^2 = n_a n^a = \pm 1$, where $\epsilon = +1$ indicates the hypersurface is timelike, $\epsilon = -1$ has Σ spacelike, and $\mathcal{N}$ is a normalization, $\mathcal{N} = |\hat{g}^{ab}\partial_a\Phi\partial_b\Phi|^{-1/2}$. Denote the induced metric h_{ij} on Σ and its inverse as h^{ij}, which are defined by

$$h_{ij} \equiv \hat{g}_{ab} e^a_i e^b_j, \quad e^i_a \equiv h^{ij} G_{ab} e^b_j, \tag{A2}$$

for vectors $e^a_i \equiv \frac{dx^a}{dy^i}$ tangent to curves contained in Σ and coordinates y^i intrinsic to Σ. By definition, $n_a e^a_i = 0$. In terms of the background metric $\hat{g}_{ab}$,

$$\hat{g}_{ab} = \epsilon n_a n_b + h_{ij} e^i_a e^j_b = \epsilon n_a n_b + h_{ab}, \quad h_{ab} \equiv h_{ij} e^i_a e^j_b, \tag{A3}$$

where h_{ab} is the projector onto hypersurfaces orthogonal to n_a. Similarly, $h^{ab} = \hat{g}^{ab} - \epsilon n^a n^b$. Note $h^{ab} n_a = h^{ab} n_b = 0$.

Define the extrinsic curvature K_{ij} as

$$K_{ij} \equiv (\nabla_b n_a) e^a_i e^b_j. \tag{A4}$$

The trace of the extrinsic curvature is

$$K = h^{ij} K_{ij} = \nabla_a n^a. \tag{A5}$$

Equivalently, the extrinsic curvature with respect to bulk coordinates is

$$K_{ab} = e^i_a e^j_b K_{ij} = -h^c_a h^d_b \nabla_c n_d. \tag{A6}$$

Using the decomposition (A3), it follows

$$K_{ab} = \nabla_a n_b - \epsilon n_a a_b, \tag{A7}$$

where a_b is the acceleration for the integral curves of the unit normal n_b, $a_b = n^a \nabla_a n_b$. Since $n^b a_b = 0$, then $K_{ab} n^b = n^b \nabla_a n_b = 0$. Further, $a_b \nabla_a n^b = -n^b \nabla_a a_b$, from which it follows $K = h^{ab} K_{ab} = \hat{g}^{ab} K_{ab}$.

Appendix A.3. Neumann Boundary Conditions and the Brane Equations of Motion

With these conventions, the Einstein–Hilbert action supplemented with a Gibbons–Hawking–York (GHY) boundary term is

$$I = \frac{1}{16\pi G_N} \int_{\mathcal{M}} d^{d+1}x \sqrt{-\hat{g}}(R - 2\Lambda) + \frac{1}{8\pi G_N} \int_{\partial\mathcal{M}} d^d\xi \sqrt{|h|}\epsilon K, \tag{A8}$$

where here, G_N is Newton's constant in $d+1$-dimensions. The GHY term makes the variational problem well posed, assuming the metric obeys Dirichlet or Neumann (see below) boundary conditions at boundary $\partial\mathcal{M}$. Indeed, a standard computation shows the metric variation of the Einstein–Hilbert term is (upon imposing the Einstein equations of motion)

$$16\pi G_N \delta I_{\rm EH} = \oint_{\partial\mathcal{M}} d^d y \sqrt{|h|}\epsilon(K_{ab} - K h_{ab})\delta h^{ab} - 2\delta\left(\oint_{\partial\mathcal{M}} d^d y \sqrt{|h|}\epsilon K\right), \tag{A9}$$

where we have assumed the manifold $\mathcal{M}$ is void of codimension-2 corners. Thus,

$$\delta I = \frac{1}{16\pi G_N} \oint_{\partial\mathcal{M}} d^d y \sqrt{|h|}\epsilon(K_{ab} - K h_{ab})\delta h^{ab}. \tag{A10}$$

The action is stationary when either Dirichlet boundary conditions are imposed, $\delta h^{ab}|_{\partial\mathcal{M}} = 0$, or Neumann boundary conditions are imposed

$$(K_{ab} - K h_{ab})|_{\partial\mathcal{M}} = 0. \tag{A11}$$

Next, consider introducing a brane of tension T at $\partial\mathcal{M}$, which is characterized by a brane action,

$$I_{\rm brane} = -\frac{T}{8\pi G_N} \int_{\partial\mathcal{M}} d^d y \sqrt{|h|}. \tag{A12}$$

The total action $I + I_{\rm brane}$ will be stationary provided the bulk Einstein equations hold and the Neumann boundary condition (A11) is modified to

$$\epsilon K_{ab}|_{\partial\mathcal{M}} = (\epsilon K - T) h_{ab}|_{\partial\mathcal{M}}, \tag{A13}$$

as is referred to as the brane equations of motion. Taking the trace, the tension is

$$T = \frac{\epsilon(d-1)}{d} K, \tag{A14}$$

such that the brane equation of motion (A13) becomes

$$\epsilon K_{ab}|_{\partial\mathcal{M}} = \frac{T}{(d-1)} h_{ab}|_{\partial\mathcal{M}}. \tag{A15}$$

Appendix B. Holographic Regularization: A Detailed Summary

Here, we review holographic renormalization á la [19] and derive the induced gravity action on the brane. For a less brute-force and algorithmic approach of deriving the effective action, see, e.g. [17,21,51,52].

Appendix B.1. Fefferman-Graham Expansion and Einstein's Equations

Following [19], express the asymptotically AdS_{d+1} bulk metric $\hat{g}_{ab}$ in a Fefferman–Graham (FG) expansion [48,49] near the asymptotic boundary

$$ds^2_{d+1} = \frac{L^2}{4\rho^2}d\rho^2 + \frac{L^2}{\rho}g_{ij}(\rho,x)dx^i dx^j, \tag{A16}$$

where L is the AdS_{d+1} curvature scale of the $d+1$-dimensional bulk, and the asymptotic boundary is located at $\rho = 0$[66]. Here, we use the hat notation to denote the bulk quantities, e.g., the bulk metric is represented by $\hat{g}_{ab}$. The d-dimensional boundary submanifold has metric $\hat{g}_{ij}(\rho,x) \equiv h_{ij}(\rho,x) = (L^2/\rho)g_{ij}(\rho,x)$.

The non-vanishing Christoffel symbols with respect to metric (A16) are

$$\begin{aligned} &\hat{\Gamma}^{\rho}_{\rho\rho} = -\frac{1}{\rho}, \quad \hat{\Gamma}^{\rho}_{ij} = 2\big(g_{ij} - \rho\partial_\rho g_{ij}\big), \\ &\hat{\Gamma}^{k}_{\rho i} = \frac{1}{2\rho}[-\delta^k_i + g^{jk}\rho\partial_\rho g_{ij}], \quad \hat{\Gamma}^{k}_{ij} = \Gamma^k_{ij}[g]. \end{aligned} \tag{A17}$$

Consequently, the non-zero components of the Riemann curvature tensor are[67]

$$\begin{aligned} &\hat{R}^{\rho}_{j\rho k} = -2\rho\partial^2_\rho g_{jk} - \frac{1}{\rho}g_{jk} + \rho g^{il}(\partial_\rho g_{jl})(\partial_\rho g_{ik}), \\ &\hat{R}^{\rho}_{jkl} = 2\rho(\nabla_l\partial_\rho g_{jk} - \nabla_k\partial_\rho g_{jl}), \\ &\hat{R}^{i}_{jkl} = R^i_{jkl}[g] + \frac{1}{\rho}[-\delta^i_k g_{jl} + \rho\delta^i_k\partial_\rho g_{jl} + \rho g^{im}g_{jl}\partial_\rho g_{km} - \rho^2 g^{im}(\partial_\rho g_{jl})(\partial_\rho g_{km})] \\ &-\frac{1}{\rho}[-\delta^i_l g_{jk} + \rho\delta^i_l\partial_\rho g_{jk} + \rho g^{im}g_{jk}\partial_\rho g_{lm} - \rho^2 g^{im}(\partial_\rho g_{jk})(\partial_\rho g_{lm})], \end{aligned} \tag{A18}$$

where ∇_i refers to the covariant derivative compatible with g_{ij}. It is also useful to know

$$\begin{aligned} \hat{R}_{ijkl} = &\frac{L^2}{\rho}R_{ijkl}[g] - \frac{L^2}{\rho^2}(g_{ik}g_{jl} - g_{il}g_{jk}) + \frac{L^2}{\rho}[g_{ik}\partial_\rho g_{jl} + g_{jl}\partial_\rho g_{ik} - g_{il}\partial_\rho g_{jk} - g_{jk}\partial_\rho g_{il}] \\ &+ L^2[(\partial_\rho g_{jk})(\partial_\rho g_{il}) - (\partial_\rho g_{jl})(\partial_\rho g_{ik})]. \end{aligned} \tag{A19}$$

Let us now work out the form of Einstein's equations near the conformal boundary. One route is to explicitly compute the Ricci tensor and scalar. Alternatively, we can use the fact that the bulk spacetime, asymptotically, has a vanishing Weyl tensor such that

$$\hat{R}_{abcd} = -\frac{1}{L^2}[\hat{g}_{ac}\hat{g}_{bd} - \hat{g}_{ad}\hat{g}_{bc}] \tag{A20}$$

near the boundary. In summary, we find

$$\begin{aligned} &R_{ijkl}[g] = g_{il}g'_{jk} + g_{jk}g'_{il} - g_{ik}g'_{jl} - g_{jl}g'_{ik} + \rho(g'_{jl}g'_{ik} - g'_{jk}g'_{il}), \\ &g''_{jk} - \frac{1}{2}g^{il}g'_{jl}g'_{ik} = 0, \\ &\nabla_l g'_{jk} - \nabla_k g'_{jl} = 0, \end{aligned} \tag{A21}$$

where we introduced the notation $\partial_\rho g_{ij} \equiv g'_{ij}$. Our expressions match Equations (7)–(9) of [50][68]. Equivalently, by contracting (A21) with g^{ij}, one often expresses Einstein's equations as

$$\begin{aligned} &\left(Ric[g] + (d-2)g' + \mathrm{Tr}(g^{-1}g')g + \rho(2g'g^{-1}g' - 2g'' - \mathrm{Tr}(g^{-1}g')g') \right)_{jl} = 0, \\ &\mathrm{Tr}(g^{-1}g'') - \frac{1}{2}\mathrm{Tr}(g^{-1}g'g^{-1}g') = 0, \\ &\nabla_l \mathrm{Tr}(g^{-1}g') - \nabla^j g'_{jl} = 0, \end{aligned} \tag{A22}$$

matching Equation (2.5) of [19][69]. Deriving the Einstein equations in this relied on using (A20), i.e., that the Weyl tensor vanishes near the boundary. Note that for $d = 2$, (A20) holds everywhere.

Appendix B.2. Perturbatively Solving Einstein's Equations

With Einstein's equations in hand, we now want to solve them perturbatively near the boundary $\rho = 0$. To this end, we expand the metric $g_{ij}(x, \rho)$ as

$$\begin{aligned} g(x,\rho) &= g_{(0)}(x) + \rho g_{(2)}(x) + \rho^2 g_{(4)}(x) + \ldots \quad (d \text{ odd}), \\ g(x,\rho) &= g_{(0)}(x) + \rho g_{(2)}(x) + \ldots + \rho^{d/2} g_{(d)}(x) + \rho^{d/2}(\log\rho) h_{(d)}(x) + \mathcal{O}(\rho^{d/2+1}) \quad (d \text{ even}). \end{aligned} \tag{A23}$$

As we will see, the tensors $g_{(k)}$ are given by some covariant expression with respect to the boundary metric $g_{(0)}$, its Riemann tensor, and their derivatives. Additionally, the subscript or superscript in $g_{(k)}$ indicates the number of derivatives with respect to coordinates x^i, e.g., $g_{(2)}$ contains two derivatives, $g_{(4)}$ contains four derivatives, and so forth. The basic algorithm for solving Einstein's equations order by order in ρ is to differentiate Einstein's Equation (A21) with respect to ρ and then take the limit when $\rho = 0$, recasting the coefficients $g_{(k\neq 0)}$ in terms of $g_{(0)}$. Notably, for even d, this procedure would have broken down at order $d/2$ had the logarithm proportional to $h_{(d)}$ not been introduced (A23). Further, the computation differs for $d = 2$ and $d > 2$ in that the expansion truncates in $d = 2$. Below, we will focus on the procedure for $d > 2$ (see [19,50,73] for the $d = 2$ case).

Coefficients $g_{(k)}$ for $k \neq d$: We can use the first of Einstein's equations in (A21) to cast coefficients $g_{(k)}$ for $k \neq d$ solely in terms of covariant expressions of $g_{(0)}$. Begin with $g_{(2)jk}$. Substitute $g(\rho, x) = g_{(0)} + \rho g_{(2)} + \rho^2 g_{(4)} + \ldots$ into the first expression in (A21), giving

$$R_{ijkl} = g^{(0)}_{il} g^{(2)}_{jk} + g^{(0)}_{jk} g^{(2)}_{il} - g^{(0)}_{ik} g^{(2)}_{jl} - g^{(0)}_{jl} g^{(2)}_{ik} + \rho(g^{(2)}_{il} g^{(2)}_{jk} - g^{(2)}_{jl} g^{(2)}_{ik}) + \mathcal{O}(\rho^2) + \ldots. \tag{A24}$$

Now, recall that in the limit $\rho \to 0$, the Weyl tensor W_{ijkl} on the boundary vanishes. Using the following useful expression for the Weyl tensor in d-dimensions,

$$W_{ijkl} = R_{ijkl} + (P_{jk} g_{il} + P_{il} g_{jk} - P_{ik} g_{jl} - P_{jl} g_{ik}), \tag{A25}$$

where P_{jk} is the Schouten tensor,

$$P_{jk}[g] = \frac{1}{(d-2)} \left(R_{jk}[g] - \frac{1}{2(d-1)} R[g] g_{jk} \right), \tag{A26}$$

it follows $W_{ijkl} = 0$ implies

$$R_{ijkl} = -(P_{jk} g_{il} + P_{il} g_{jk} - P_{ik} g_{jl} - P_{jl} g_{ik}). \tag{A27}$$

Thus, in the limit $\rho \to 0$,

$$\lim_{\rho\to 0} R_{ijkl} = -(P_{jk}[g_{(0)}]g^{(0)}_{il} + P_{il}[g_{(0)}]g^{(0)}_{jk} - P_{ik}[g_{(0)}]g^{(0)}_{jl} - P_{jl}[g_{(0)}]g^{(0)}_{ik}), \tag{A28}$$

with

$$P_{jk}[g_{(0)}] = \frac{1}{(d-2)}\left(R_{jk}[g_{(0)}] - \frac{1}{2(d-1)}R[g_{(0)}]g^{(0)}_{jk}\right). \tag{A29}$$

Here, we used that $\lim_{\rho\to 0} R_{ij}[g] = R_{ij}[g_{(0)}]$, which is easy to show since R_{ij}, using the expansion in terms of $g(\rho, x)$ will vanish for any term proportional to $g_{(k)}$ for $k \neq 0$.

Substituting $\lim_{\rho\to 0} R_{ijkl}$ (A28) into (A24) gives

$$g^{(0)}_{il}g^{(2)}_{jk} + g^{(0)}_{jk}g^{(2)}_{il} - g^{(0)}_{ik}g^{(2)}_{jl} - g^{(0)}_{jl}g^{(2)}_{ik} = -(P_{jk}[g_{(0)}]g^{(0)}_{il} + P_{il}[g_{(0)}]g^{(0)}_{jk} - P_{ik}[g_{(0)}]g^{(0)}_{jl} - P_{jl}[g_{(0)}]g^{(0)}_{ik}). \tag{A30}$$

Matching like terms, we find

$$g^{(2)}_{jk} = -P_{jk}[g_{(0)}] = -\frac{1}{(d-2)}\left(R_{jk}[g_{(0)}] - \frac{1}{2(d-1)}R[g_{(0)}]g^{(0)}_{jk}\right), \tag{A31}$$

recovering Equation (A.1) of [19] (up to an overall sign due to our convention). Note that this same argument also reveals $h_{(2)jk} = 0$. To go to higher order, e.g., $g^{(4)}_{ij}$ one takes ρ derivatives of R_{ijkl} and then takes the limit $\rho \to 0$.

Trace of $g_{(n)}$: The third Einstein equation in (A21) yields the trace of $g_{(n)}$ for any n. For example, substituting in the expansion (A23) up to $g_{(4)}$ and taking the limit $\rho \to 0$ gives

$$2g^{(4)}_{jk} - \frac{1}{2}g^{(2)}_{jl}g^{ml}g^{(2)}_{km} = 0 \Rightarrow g^{(4)}_{jk} = \frac{1}{4}g^{(2)}_{jl}g^{ml}g^{(2)}_{km}. \tag{A32}$$

Taking the trace with by contracting with g^{jk}, we are led to

$$\mathrm{Tr}g_{(4)} = \frac{1}{4}\mathrm{Tr}(g^2_{(2)}), \tag{A33}$$

where here, $\mathrm{Tr}g_{(4)} = g^{ij}_{(0)}g_{(4)ij}$ and matches Equation (A.2) in [19].

To reach the next order, write $g(\rho, x) = g_{(0)} + \rho g_{(2)} + \rho^2 g_{(4)} + \rho^3 g_{(6)}$, and take the derivative of the second Einstein Equation (A21) with respect to ρ and then set $\rho \to 0$, giving

$$6g^{(6)}_{jk} - \frac{1}{2}\left[4g^{(4)}_{ij}g^{il}g^{(2)}_{lk} - g^{(2)}_{ij}g^{(2)}_{lk}g^{(2)}_{mn}g^{im}g^{nl}\right] = 0. \tag{A34}$$

Taking the trace and simplifying gives

$$\mathrm{Tr}g_{(6)} = \frac{2}{3}\mathrm{Tr}(g_{(4)}g_{(2)}) - \frac{1}{6}\mathrm{Tr}(g^3_{(2)}). \tag{A35}$$

Following this procedure, it is also straightforward to show that $h_{(d)}$ is traceless, i.e., $g^{ij}_{(0)}h_{(0)ij} = 0$. Likewise, $g^{ij}_{(0)}g_{(3)ij} = g^{ij}_{(0)}g_{(5)ij} = 0$.

Covariant divergence of $g_{(k)}$: The second of Einstein's Equation (A21) fixes the covariant divergence of $g_{(k)}$ for any k. For example, substituting expansion (A23) up to order $\mathcal{O}(\rho)$ and taking the $\rho \to 0$ limit of both sides gives

$$\lim_{\rho\to 0} \nabla^j g'_{jl} = \nabla^i g^{(2)}_{ij} = \lim_{\rho\to 0} \nabla_j(g^{lk}g'_{lk}) = \nabla_j(g^{kl}_{(0)}g^{(2)}_{kl}) = \nabla^i(g^{(0)}_{ij}g^{kl}_{(0)}g^{(2)}_{kl}). \tag{A36}$$

Once the limit has been taken, it is understood that the covariant derivative is compatible with $g_{(0)}$. More compactly,

$$\nabla^i g^{(2)}_{ij} = \nabla^i (g_{(0)ij} \mathrm{Tr} g_{(2)}), \tag{A37}$$

matching the first expression in Equation (A.4) of [19]. To get to the next order, we take a ρ derivative of the equation of motion, keeping in mind that the covariant derivative itself has ρ dependence inside and then take the limit $\rho \to 0$ [19].

Appendix B.3. Regulated Bulk Action

Thus far, we have shown, given a conformal structure at infinity, and the metric can be determined asymptotically up to order $\rho^{d/2}$, i.e., the coefficient $g_{(d)}$. The aim now is to study the IR divergent structure of the bulk theory gravity, which is characterized by the action

$$I_{\text{bulk}} = \frac{1}{16\pi G}\left[\int_{\mathcal{M}} d^{d+1}x\sqrt{-\hat{g}}\left(\hat{R} + \frac{d(d-1)}{L^2}\right) + 2\int_{\partial\mathcal{M}} d^d x\sqrt{h}K\right], \tag{A38}$$

where K is the trace of the extrinsic curvature of the boundary submanifold $\partial\mathcal{M}$. Here, it is understood that G and L refer to the bulk Newton's constant and AdS curvature scale, respectively. As stated in the main text, the on-shell bulk gravity action will have IR divergences near the boundary $\rho = 0$. To regulate IR divergences of the theory, introduce an IR cutoff surface at $\rho = \epsilon$ near the asymptotic boundary, where the preceding analysis has taken place. Thus, in the bulk contribution, we consider the integration region $\epsilon \leq \rho \leq \rho_c$, where ρ_c is some value such that $\rho_c \gg \epsilon$[70]. The GHY boundary term is simply evaluated at $\rho = \epsilon$. Thence, the IR regulated bulk action is

$$I^{\text{reg}}_{\text{bulk}} = \frac{1}{16\pi G}\left[\int_{\rho\geq\epsilon} d^{d+1}x\sqrt{-\hat{g}}\left(\hat{R} + \frac{d(d-1)}{L^2}\right) + 2\int_{\partial\mathcal{M}} d^d x\sqrt{h}K|_{\rho=\epsilon}\right], \tag{A39}$$

To evaluate the bulk contribution, we use that on-shell $\hat{R} = -d(d+1)/L^2$ near the boundary. Consequently, the bulk contribution becomes

$$\int d^d x\int_{\rho\geq\epsilon} d\rho\frac{L^{d+1}}{2\rho^{d/2+1}}\left(-\frac{2d}{L^2}\right)\sqrt{g(\rho,x)} = \int d^d x\int_{\rho\geq\epsilon} d\rho\frac{dL^{d-1}}{\rho^{d/2+1}}\sqrt{g(\rho,x)}. \tag{A40}$$

The form of the boundary action requires a little more work. We have a hypersurface equation defined by $\Phi \equiv \rho - \epsilon = 0$ with unit normal $n_a = [\hat{g}^{ab}(\partial_a\Phi)(\partial_b\Phi)]^{-1/2}\partial_a\Phi$, whose only non-zero component is $n_\rho = \frac{2\rho}{L}$. The components of the extrinsic curvature $K_{ab} = \hat{\nabla}_a n_b$ are easily worked out to be

$$K_{\rho\rho} = K_{i\rho} = K_{\rho i} = 0, \quad K_{ij} = -\frac{L}{\rho}(g_{ij} - \rho\partial_\rho g_{ij}), \tag{A41}$$

where we used the Christoffel symbols (A17). The trace K is

$$K = \hat{g}_{ij}K_{ij} = -\frac{1}{L}\left(d - \rho g^{ij}\partial_\rho g_{ij}\right). \tag{A42}$$

Also, note $\sqrt{h} = \frac{L^d}{\rho^{d/2}}\sqrt{g(\rho,x)}$. Therefore, the GHY term becomes

$$\begin{aligned} 2\int_{\partial\mathcal{M}} d^d x\sqrt{h}K &= \int_{\partial\mathcal{M}} d^d x\left[-\frac{2L^{d-1}}{\rho^{d/2}}\sqrt{g(x,\rho)}\left(d - \rho g^{ij}\partial_\rho g_{ij}\right)\right]_{\rho=\epsilon} \\ &= \int_{\partial\mathcal{M}} d^d x\frac{L^{d-1}}{\rho^{d/2}}\left(-2d\sqrt{g(x,\rho)} + 2\rho\sqrt{g(x,\rho)}g^{ij}\partial_\rho g_{ij}\right)_{\rho=\epsilon} \\ &= \int_{\partial\mathcal{M}} d^d x\frac{L^{d-1}}{\rho^{d/2}}\left(-2d\sqrt{g(x,\rho)} + 4\rho\partial_\rho\sqrt{g(x,\rho)}\right)_{\rho=\epsilon}, \end{aligned} \tag{A43}$$

where to arrive to the final line, we used that $\delta\sqrt{g} = \frac{1}{2}\sqrt{g}g^{ij}\delta g_{ij}$.

Combining (A40) and (A43), the (on-shell) regulated bulk action to evaluate is

$$I_{\text{bulk}}^{\text{reg}} = \frac{L^{d-1}}{16\pi G}\int d^d x\left[\int_{\rho\geq\epsilon} d\rho \frac{d}{\rho^{d/2+1}}\sqrt{g(\rho,x)} + \frac{1}{\rho^{d/2}}\left(-2d\sqrt{g(x,\rho)} + 4\rho\partial_\rho\sqrt{g(x,\rho)}\right)_{\rho=\epsilon}\right]. \tag{A44}$$

All that remains is an evaluation of the metric determinant $\sqrt{g(\rho,x)}$ and performing the bulk integral. To evaluate the determinant, we apply perturbation theory, which says for $g_{ij} = g_{ij}^{(0)} + q_{ij}$, where q_{ij} is small compared to $g_{ij}^{(0)}$, then

$$\sqrt{g} = \sqrt{g_{(0)}}\left(1 + \frac{1}{2}q^i{}_i + \frac{1}{8}q^i{}_i q^j{}_j - \frac{1}{4}q^i{}_j q^j{}_i\right). \tag{A45}$$

For $d > 2$, $q_{ij} = \rho g_{ij}^{(2)} + \rho^2 g_{ij}^{(4)} + ...$, treating ρ small. Explicitly,

$$q^i{}_i = g_{(0)}^{ij}q_{ij} = g_{(0)}^{ij}\left(\rho g_{ij}^{(2)} + \rho^2 g_{ij}^{(4)} + ...\right) = \rho\text{Tr}(g_{(2)}) + \rho^2\text{Tr}(g_{(4)}) + ..., \tag{A46}$$

such that

$$q^i{}_i q^j{}_j = \rho^2(\text{Tr}g_{(2)})^2 + \rho^3(\text{Tr}g_{(2)})(\text{Tr}g_{(4)}) + ..., \tag{A47}$$

and

$$q^i{}_j q^j{}_i = g_{(0)}^{ik}g_{(0)}^{jl}\left[\rho^2 g_{kj}^{(2)}g_{li}^{(2)} + \rho^3(g_{kj}^{(4)}g_{li}^{(2)} + g_{kj}^{(2)}g_{li}^{(4)}) + ...\right]. \tag{A48}$$

Collecting terms,

$$\sqrt{g} \approx \sqrt{g_{(0)}}\left(1 + \frac{1}{2}\rho\text{Tr}g_{(2)} + \rho^2\left[\frac{1}{2}\text{Tr}g_{(4)} + \frac{1}{8}(\text{Tr}g_{(2)})^2 - \frac{1}{4}\text{Tr}(g_{(2)}^2)\right] + O(\rho^3)\right). \tag{A49}$$

Consequently, the term to evaluate on the boundary is, to order $O(\rho^2)$,

$$\frac{1}{\rho^{d/2}}\left(-2d\sqrt{g} + 4\rho\partial_\rho\sqrt{g}\right)_{\rho=\epsilon} = -\sqrt{g_{(0)}}\left[2d\epsilon^{-d/2} + (d-2)(\text{Tr}g_{(2)})\epsilon^{-d/2+1} + O(\epsilon^{-d/2+2})\right]. \tag{A50}$$

Meanwhile, the bulk term is

$$\begin{aligned}\int_\epsilon^{\rho_c} d\rho\sqrt{g}\frac{d}{\rho^{d/2+1}} = \sqrt{g_{(0)}}\Bigg\{&-2\rho_c^{-d/2} - \frac{d\text{Tr}g_{(2)}}{(d-2)}\rho_c^{-d/2+1} + O(\rho_c^{-d/2+2}) + 2\epsilon^{-d/2} \\ &+ \frac{d\text{Tr}(g_{(2)})}{(d-2)}\epsilon^{-d/2+1} + O(\epsilon^{-d/2+2})\Bigg\}.\end{aligned} \tag{A51}$$

Together, the regulated bulk action may be cast as

$$I_{\text{bulk}}^{\text{reg}} = I_{\text{div}} + I_{\text{fin}}, \tag{A52}$$

the sum of an IR divergent term

$$I_{\text{div}} = \frac{L}{16\pi G}\int d^d x\sqrt{g_{(0)}}\left[\epsilon^{-d/2}a_{(0)} + \epsilon^{-d/2+1}a_{(2)} + \epsilon^{-d/2+2}a_{(4)} + ...\right], \tag{A53}$$

with coefficients[71]

$$\begin{aligned}a_{(0)} &= 2(1-d)L^{d-2}, \quad a_{(2)} = -\frac{(d-1)(d-4)}{(d-2)}L^{d-2}\text{Tr}g_{(2)}, \\ a_{(4)} &= \left(\frac{-d^2+9d-16}{4(d-4)}\right)L^{d-2}[(\text{Tr}g_{(2)})^2 - \text{Tr}(g_{(2)}^2)],\end{aligned} \tag{A54}$$

and a finite contribution I_{fin}, whose explicit form we will not need.

This is not the full story, as the terms $\rho^{d/2} g_{(d)} + \rho^{d/2} \log \rho h_{(d)}$ in the expansion (A23) must be accounted for. These will enter the metric determinant at a higher order in ρ; however, generally, they lead to a logarithmic divergence as well as adding to the finite contributions. For example, reconsider the term

$$q^i{}_i = \rho \mathrm{Tr}(g_{(2)}) + \rho^2 \mathrm{Tr}(g_{(4)}) + ... + \rho^{d/2} \mathrm{Tr}(g_{(d)}) + \rho^{d/2} \log \rho \mathrm{Tr}(h_{(d)}). \tag{A55}$$

But $\mathrm{Tr}(h_{(d)}) = 0$ [19]. So, including the $\rho^{d/2} \mathrm{Tr}(g_{(d)})$ contribution to the metric determinant, adding to I_{fin} and a logarithmic divergence to I_{div}, i.e.,

$$\int_\epsilon^{\rho_c} \frac{d}{\rho^{d/2+1}} \left(\frac{1}{2} \rho^{d/2} \mathrm{Tr} g_{(d)} \right) = \frac{d}{2} \mathrm{Tr} g_{(d)} (\log \rho_c - \log \epsilon). \tag{A56}$$

Thus, taking into account this term, the divergent contribution to $I^{\mathrm{reg}}_{\mathrm{bulk}}$ is

$$I_{\mathrm{div}} = \frac{L}{16\pi G} \int d^d x \sqrt{g_{(0)}} \Big[\epsilon^{-d/2} a_{(0)} + \epsilon^{-d/2+1} a_{(2)} + \epsilon^{-d/2+2} a_{(4)} + ... + \epsilon^{-1} a_{(d-2)} - \log(\epsilon) a_{(d)} \Big], \tag{A57}$$

with $a_{(0)}$, $a_{(2)}$, and $a_{(4)}$ as in (A54) and, at this order,

$$a_{(d)} = L^{d-2} \frac{d}{2} \mathrm{Tr} g_{(d)}. \tag{A58}$$

Note that $a_{(d)}$ here is only including the first term and in general is more complicated (see Equation (B.1) of [19]).

Regulated Action on Boundary

Thus far, the regulated action is expressed in terms of the metric $g_{(0)}$. It is preferable to express the action in terms of the induced metric $h_{ij}(\epsilon, x) = \frac{L^2}{\epsilon} g_{ij}(\epsilon, x)$. Then,

$$\frac{\epsilon^{d/2}}{L^d} \sqrt{h(\epsilon, x)} = \sqrt{g(\epsilon, x)} = \sqrt{g_{(0)}(x)} \left(1 + \frac{1}{2} \epsilon \mathrm{Tr} g_{(2)} + \frac{1}{8} \epsilon^2 \Big[(\mathrm{Tr} g_{(2)})^2 - \mathrm{Tr}(g^2_{(2)}) \Big] + O(\rho^3) \right), \tag{A59}$$

where we used $\mathrm{Tr}(g_{(4)}) = \frac{1}{4} \mathrm{Tr}(g^2_{(2)})$. Rearranging and performing a power series expansion in ϵ yields

$$\sqrt{g_{(0)}} = \frac{\epsilon^{d/2}}{L^d} \sqrt{h(\epsilon, x)} \left(1 - \frac{1}{2} \epsilon \mathrm{Tr} g_{(2)} + \frac{1}{8} \epsilon^2 \Big[(\mathrm{Tr} g_{(2)})^2 + \mathrm{Tr}(g^2_{(2)}) \Big] + O(\epsilon^3) \right), \tag{A60}$$

matching the first expression in Equation (B.3) of [19].

The aim now is to evaluate quantities $\mathrm{Tr} g_{(2)}$ and $\mathrm{Tr}(g^2_{(2)})$. To this end, we first recall some relations from metric perturbation. It is sufficient for our purposes to consider $g_{ij} = g_{(0)ij} + \epsilon g_{(2)ij}$, with $g^{ij} = g^{ij}_{(0)} - \epsilon g^{ij}_{(2)}$. Then, the linear variation of the Christoffel symbol is

$$\delta \Gamma^k_{ij} \equiv \Gamma^k_{ij}[g] - \Gamma^k_{ij}[g_{(0)}] = \frac{\epsilon}{2} \Big[\nabla_i g^{\ k}_{(2)j} + \nabla_j g^{\ k}_{(2)i} - \nabla^k g_{(2)ij} \Big], \tag{A61}$$

where here, ∇_i refers to the Levi–Civita connection compatible with $g^{(0)}_{ij}$. Consequently,

$$\begin{aligned} \delta R^a_{bcd} &= \nabla_c \delta \Gamma^a_{bd} - \nabla_d \delta \Gamma^a_{bc} \\ &= \frac{\epsilon}{2} \Big[\nabla_c \nabla_b g^{\ a}_{(2)d} + \nabla_c \nabla_d g^{\ a}_{(2)b} - \nabla_c \nabla^a g_{(2)bd} - \nabla_d \nabla_c g^{\ a}_{(2)b} - \nabla_d \nabla_b g^{\ a}_{(2)c} + \nabla_d \nabla^a g_{(2)cb} \Big], \end{aligned} \tag{A62}$$

The leading order change to the Ricci tensor is then

$$\begin{aligned}\delta R_{ij} &= \frac{\epsilon}{2}\left[\nabla_a\nabla_i g^{\ a}_{(2)j} + \nabla_a\nabla_j g^{\ a}_{(2)i} - \Box g_{(2)ij} - \nabla_j\nabla_i g^{\ a}_{(2)a}\right] \\ &= -\frac{\epsilon}{2}\left[\nabla_a\Big(\nabla_i R^a_j[g_{(0)}] + \nabla_j R^a_i[g_{(0)}]\Big) - \frac{d}{2(d-1)}\nabla_i\nabla_j R[g_{(0)}]\right. \\ &\left. - \Box R_{ij}[g_{(0)}] + \frac{g_{(0)ij}}{2(d-1)}\Box R[g_{(0)}]\right].\end{aligned} \tag{A63}$$

where the second equality follows from substituting the expression for $g^{(2)}_{ij}$, (A31). Using[72]

$$\nabla_a\nabla_i R^a_{\ j} = \nabla_a\nabla_j R^a_{\ i} = \frac{1}{2}\nabla_i\nabla_j R + (R_{ik}R^k_{\ j} - R^k_{\ jai}R^a_{\ k}), \tag{A64}$$

we find

$$\begin{aligned}\delta R_{ij} = &-\frac{\epsilon}{2(d-2)}\left[\frac{d-2}{2(d-1)}\nabla_i\nabla_j R[g_{(0)}] - \Box R_{ij}[g_{(0)}] + \frac{g_{(0)ij}}{2(d-1)}\Box R[g_{(0)}]\right. \\ &\left. +2R_{ki}[g_{(0)}]R^k_{\ j}[g_{(0)}] - 2R_{ljki}[g_{(0)}]R^{lk}[g_{(0)}]\right].\end{aligned} \tag{A65}$$

Lastly, the Ricci scalar $R[g] = g^{ij}R_{ij}[g] = g^{ij}(R_{ij}[g_{(0)}] + \delta R_{ij})$, to leading order in an ϵ-expansion is

$$R[g] = R[g_{(0)}] + \frac{\epsilon}{d-2}\left(R^2_{ij}[g_{(0)}] - \frac{1}{2(d-1)}R^2[g_{(0)}]\right), \tag{A66}$$

where we used (A31) and that $g^{ij}_{(0)}\delta R_{ij} = 0$.

With these expressions, we have

$$\begin{aligned}g^{ij}_{(0)}g_{(2)ij} &= -\frac{1}{2(d-1)}R[g_{(0)}] \\ &\approx -\frac{1}{2(d-1)}\left[R[g] - \frac{\epsilon}{d-2}\left(R^{ij}[g]R_{ij}[g] - \frac{1}{2(d-1)}R^2[g]\right)\right] \\ &\approx -\frac{L^2}{\epsilon}\frac{1}{2(d-1)}\left[R[h] - \frac{L^2}{d-2}\left(R^{ij}[h]R_{ij}[h] - \frac{1}{2(d-1)}R^2[h]\right)\right],\end{aligned} \tag{A67}$$

where in the second line, we inverted (A66), and in the last line, we used $h_{ij} = \frac{L^2}{\epsilon}g_{ij}$, such that $R_{ij}[g] = R_{ij}[h]$. Meanwhile,

$$\begin{aligned}g^{ij}_{(2)}g_{(2)ij} &= \frac{1}{(d-2)^2}\left(R^{ij}[g_{(0)}]R_{ij}[g_{(0)}] - \frac{(3d-4)}{4(d-1)^2}R^2[g_{(0)}]\right) \\ &\approx \frac{L^4}{\epsilon^2}\frac{1}{(d-2)^2}\left(R^{ij}[h]R_{ij}[h] - \frac{(3d-4)}{4(d-1)^2}R^2[h]\right).\end{aligned} \tag{A68}$$

Consequently,

$$\begin{aligned}
\mathrm{Tr}g_{(2)} &\approx -\frac{L^2}{\epsilon}\frac{1}{2(d-1)}\left[R[h]-\frac{L^2}{d-2}\left(R_{ij}^2[h]-\frac{1}{2(d-1)}R^2[h]\right)\right],\\
\mathrm{Tr}(g_{(2)}^2) &\approx \frac{L^4}{\epsilon^2}\frac{1}{(d-2)^2}\left[R_{ij}^2[h]-\frac{(3d-4)}{4(d-1)^2}R^2[h]\right],\\
(\mathrm{Tr}g_{(2)})^2+\mathrm{Tr}g_{(2)}^2 &\approx \frac{L^4}{\epsilon^2}\left[\frac{1}{(d-2)^2}R_{ij}^2[h]+\frac{R^2[h]}{4(d-1)^2}\left(\frac{d^2-7d+8}{(d-2)^2}\right)+O(\mathcal{R}^3)+...\right],\\
(\mathrm{Tr}g_{(2)})^2-\mathrm{Tr}g_{(2)}^2 &\approx -\frac{L^4}{\epsilon^2}\left[\frac{1}{(d-2)^2}R_{ij}^2[h]-\frac{dR^2}{4(d-2)^2(d-1)}+O(\mathcal{R}^3)+...\right],
\end{aligned} \tag{A69}$$

where $O(\mathcal{R}^3)$ schematically refers to terms in cubic powers of curvature and the $+...$ corresponds to higher powers in curvature. The first two expressions match Equation (B.3) of [19]. Substituting these expressions into our perturbative expression for $\sqrt{g_{(0)}}$ (A60), we find

$$\sqrt{g_{(0)}}=\sqrt{h}\frac{\epsilon^{d/2}}{L^d}\left\{1+\frac{L^2}{4(d-1)}\left(R-\frac{L^2(d-3)}{2(d-2)^2}\left[R_{ij}^2-\frac{d}{4(d-1)}R^2\right]\right)+...\right\}. \tag{A70}$$

Substituting this into the divergent action (A57) along with coefficients (A54) gives

$$\begin{aligned}
I_{\mathrm{div}}=-\frac{L}{16\pi G(d-2)}\int d^dx\sqrt{h}\Bigg[&\frac{2(d-1)(d-2)}{L^2}+R\\
&+\frac{L^2}{(d-2)(d-4)}\left(R_{ij}^2-\frac{d}{4(d-1)}R^2\right)+...\Bigg].
\end{aligned} \tag{A71}$$

With the divergent action in hand, holographic renormalization is completed via minimal subtraction by adding to the regulated action (A52) a local counterterm action of the form $I_{\mathrm{ct}}=-I_{\mathrm{div}}$, rendering the action finite in the limit $\epsilon\to 0$. Alternatively, as described in the main text, in braneworld holography, where $\epsilon\neq 0$, a local counterterm need not be introduced.

Appendix C. Braneworld Basics

String theory is a candidate model of quantum gravity which requires the existence of extra dimensions. The observable universe, however, is well described by a four-dimensional spacetime, whose local gravitational dynamics is governed by Einstein's general relativity on macroscopic scales and the background on which the Standard Model of particle physics lives. Thus, it is of interest to come up with a mechanism which reduces the number of extra dimensions predicted by string theory such that our observable world emerges as an effective theory in some limit. Historically, the simplest way to reduce the number of extra dimensions is via Kaluza–Klein (KK) dimensional reduction, where the extra dimensions are compactified into a small but finite-dimensional internal manifold. Alternatively, braneworlds provide a mechanism in which a lower-dimensional 'brane' (or domain wall) lives in a higher-dimensional 'bulk' spacetime, where the brane effectively describes the observable world.

Broadly, braneworlds are in part motivated by the membrane-like solutions in string theory and higher-dimensional supergravity; indeed, some braneworld models have string theoretic realizations (though in this review, we will be agnostic to the stringy origins of any particular model). More specifically, braneworlds come in three types: (i) the Arkani–Hamed–Dimopoulos–Dvali (ADD) model [12], (ii) Randall–Sundrum (RS) [13,14] and Karch–Randall (KR) models [15], and the Dvali–Gabadadze–Porrati (DGP) model [261]. As we will briefly review below, the braneworld models distinguish themselves by the type of bulk spacetime the brane is embedded and the way in which gravity is localized on

the brane. In particular, the RS and KR models embed a brane inside a bulk anti-de Sitter spacetime—such that the AdS/CFT correspondence applies—and gravity localizes either in a way similar to KK reduction or via warped compactification.

Appendix C.1. Braneworld Bestiary

ADD model. Motivated by resolving the hierarchy problem in particle physics, the original braneworld construction, the ADD model consists of a tensionless brane inside a large bulk spacetime where the extra dimensions are compactified in a manner similar to KK reduction. The bulk spacetime is assumed to be governed by Einstein gravity with zero cosmological constant. Massive KK modes in the extra dimensions are largely ignored such that, upon integrating out the extra dimensions, the effective action is four-dimensional Einstein gravity with scales induced by the higher-dimensional parent theory. Notably, the case in which the bulk spacetime is five-dimensional is ruled out because the one-dimensional volume of the compactified directions is on astrophysical distance scales; ADD models with at least three extra dimensions are in principle observationally viable.

RS models. There are two distinct Randall–Sundrum models, which are known as RS-I [13] and RS-II [14]. In both models, the bulk is taken to be asymptotically AdS spacetime[73]. The brane geometry is either asymptotically Minkowski or de Sitter. In the RS-I model, the bulk is bounded two codimension-1 branes, one with positive tension τ_+ and the other with negative tension τ_-. In the RS-II model, the negative tension brane is sent to asymptotic infinity.

More explicitly, the bulk physics of the RS-I model is characterized by five-dimensional Einstein gravity with a negative cosmological constant $\Lambda_5 = -6/L_5^2$, plus an action characterizing the two branes:

$$\begin{aligned} I_{\text{RS-I}} = &\frac{1}{16\pi G_5}\int d^5x\sqrt{-\hat{g}}(\hat{R}-2\Lambda_5) \\ &-\int dy d^4x\sqrt{-h}[(\tau_+ + \mathcal{L}^{(+)}_{\text{mat}})\delta(y) + (\tau_- + \mathcal{L}^{(-)}_{\text{mat}})\delta(y-y_-)]. \end{aligned} \tag{A72}$$

Here, y denotes a bulk spatial coordinate to be integrated over, h_{ij} is the four-dimensional induced metric of the constant-y hypersurfaces, and $\mathcal{L}^{(\pm)}_{\text{mat}}$ refers to matter Lagrangians localized on their respective branes. A negative tension brane is positioned at $y = y_- > 0$ while a positive tension brane is at $y = 0$, and only the region $0 < y < y_-$ is retained. To complete the space, a $\mathbb{Z}_2$ reflection symmetry is assumed across each boundary plane, leading to a jump discontinuity in the extrinsic curvature of each brane. Thus, aside from the bulk Einstein equations, the bulk must obey brane boundary conditions, e.g., the Israel junction conditions which relate the discontinuity in the extrinsic curvature across the branes to the brane tension and the stress tensor $S^{(\pm)}_{ij}$,

$$\Delta K^{\pm}_{ij} - h_{ij}\Delta K^{\pm} = 8\pi G_5(\tau_\pm h_{ij} + S^{(\pm)}_{ij}), \tag{A73}$$

where $\Delta K_{ij} = K^+_{ij} - K^-_{ij}$ denotes the difference between the extrinsic curvature across the branes. Imposing the junction conditions sets the branes to have equal and opposite tensions. The simplest such solution to the bulk Einstein equations plus Israel junction conditions is the warped geometry (in horospherical coordinates)

$$ds_5^2 = dy^2 + e^{-2|y|/L_5}\eta_{ij}dx^i dx^j, \tag{A74}$$

where η_{ij} is the four-dimensional Minkowski spacetime, though it may be replaced by any four-dimensional metric which solves the four-dimensional brane theory. The AdS_5 horizon is located at $y = \infty$ (which includes a point at infinity) where the coordinate system (A74) breaks down (see Figure A1 for an illustration). Mass scales on the negative tension brane will be exponentially suppressed with respect to the positive tension brane. Consequently,

beings confined to the negative tension brane would experience weak gravity, while beings on the positive tension ('Planck') brane would experience strong gravity. The RS-I model thus provides a possible solution to the hierarchy problem of the standard model.

The starting point for the RS-II model is the same except that the negative tension brane of the RS-I model is sent off to infinity ($y_- \to \infty$), such that the five-dimensional warped geometry (A74) takes the form

$$\begin{aligned} ds_5^2 &\to dy^2 + e^{-2|y|/L_5}\eta_{ij}dx^i dx^j \\ &= \frac{L_5^2}{(L_5+|z|)^2}(dz^2 + \eta_{ij}dx^i dx^j), \end{aligned} \tag{A75}$$

where in the second line, the conformal coordinate $z \equiv \text{sign}(y)L_5(e^{|y|/L_5}-1)$ was introduced. Unlike the RS-I model, the RS-II model is not used to solve the hierarchy problem. Further, although the extra bulk spatial dimension becomes infinite in extent, the higher-dimensional gravity becomes localized on the brane nonetheless[74]. One way to see this is through a perturbative analysis of the weak gravitational created by isolated matter sources on the brane [323–325][75]. Define a bulk metric perturbation by $\gamma_{ab} \equiv \hat{g}_{ab} - \hat{g}^{(0)}_{ab}$ (with $\hat{g}^{(0)}_{ab}$ being the unperturbed five-dimensional background). Working in the Randall–Sundrum gauge,

$$h_{zz} = h_{iz} = 0, \quad \partial_i h^i{}_j = 0, \quad h^i{}_i = 0, \tag{A76}$$

the linearized equations of motion for the metric perturbation are

$$[-\partial_z^2 + V(z)]\psi_{ij} = \eta^{kl}\partial_k\partial_l\psi_{ij}, \tag{A77}$$

for $\psi_{ij} \equiv \sqrt{|z|+L_5}h_{ij}$ and 'Volcano' potential

$$V(z) = \frac{15}{4(|z|+L_5)^2} - 3L_5^2\delta(z). \tag{A78}$$

Separating variables as $\psi_{ij} \sim u_m(z)e^{ik_j x^j}$, one obtains an eigenvalue equation for eigenfunctions $u_m(z)$ characterizing an effective four-dimensional massive mode with mass $m^2 = -k_i k^i$. The general solution for $u_m(z)$ is given in terms of Bessel functions. Alongside the massive modes is a discrete set of massless 'zero modes'. From the mode functions, Green's function for $-\partial_z^2 + V(z)$ from which the induced brane metric for a spherical source of mass M will have components (in the RS gauge)

$$h_{tt} = \frac{2G_4M}{r}\left(1 + \frac{2L_5^2}{3r^2}\right), \quad h_{ij} = \frac{2G_4M}{r}\left(1 + \frac{L_5^2}{3r^2}\right)\delta_{ij}. \tag{A79}$$

The h_{tt} metic component is simply a modified Newtonian potential for a source M where the $1/r^3$ correction can be shown to be precisely of the form of the corrections to the Newtonian due to 1-loop quantum effects induced by the four-dimensional graviton propagator [62,63].

KR model. An important extension of the RS-II model is the Karch–Randall braneworld model [15]. In this set-up, the positive tension brane is detuned such that the four-dimensional brane geometry is asymptotically AdS_4[76]. To this, consider the RS-II model with a two-sided brane with a decreased tension

$$\tau = \frac{3(1+\delta)}{4\pi L_5 G_5}, \tag{A80}$$

for $\delta < 0$. The (unperturbed) five-dimensional warped geometry takes the form

$$ds^2 = \frac{L_5^2}{L_4^2\sin^2[(|z|+z_0)/L_4]}(h_{ij}dx^i dx^j + dz^2), \tag{A81}$$

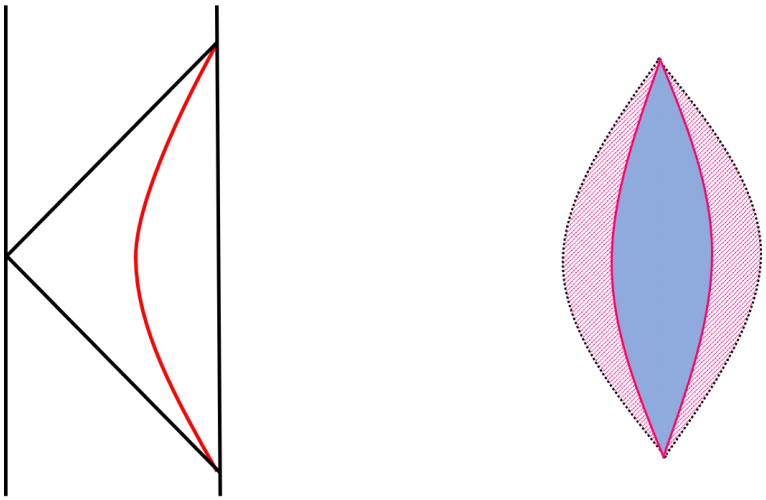

Figure A1. RS-I warped solution. Left: Bulk AdS with a 'horosphere' (red curve), and horizon at $y = \infty$ (diagonal lines). Vertical lines represent timelike infinity. **Right**: A positive and negative tension brane in bulk AdS_5 with the shaded (blue) region being retained. The dotted (magenta) regions are excluded and are identified.

with

$$h_{ij}dx^i dx^j = -\left(1 + \frac{r^2}{L_4^2}\right)dt^2 + \left(1 + \frac{r^2}{L_4^2}\right)^{-1} dr^2 + r^2 d\Omega_2^2, \tag{A82}$$

and $z_0 = L_4 \text{arcsin}(L_5/L_4)$. The brane is located at $z = 0$ and has an effective negative cosmological constant $\Lambda_4 = -3/L_4^2 \equiv 3(2\delta + \delta^2)/L_5^2$. A perturbative analysis similar to the RS-II case yields a linearized Equation (A77) though with a different potential $V(z)$. While we will not go into the details, the shape of the potential in the KR model leads to a totally discrete mass m^2 spectrum. Further, the $m^2 = 0$ zero mode is not normalizable. Imposing a normalizability condition shifts the zero mode to an 'almost zero mode' with mass $m \sim \mathcal{O}(L_5/L_4^2)$. Hence, localized four-dimensional gravity has a massive graviton. Massive gravity theories have the behavior that gravitational attraction becomes short-ranged as opposed to long ranged, and where gravity waves propagate at subluminal speeds. Note, however, for regions where $L_5/L_4^2 \ll 1$, the graviton becomes essentially massless.

DGP model. In the DGP model, an Einstein–Hilbert term is added to the brane action. The original incarnation of the model consisted of higher-dimensional Einstein gravity with a vanishing cosmological constant with the bulk being described by the action

$$I_{\text{DGP}} = \frac{1}{16\pi G_5}\int d^5x\sqrt{-\hat{g}}\hat{R} - \int d^4x\sqrt{-h}\left(\frac{1}{16\pi G_4}R_{4\text{D}} + \mathcal{L}_{\text{mat}}\right). \tag{A83}$$

A distinguishing feature of this model is that the graviton propagator is such that the effective four-dimensional theory is left unmodified at short distances.

Appendix C.2. Stringy Connections

The codimension-1 branes described above are not the same types of branes which appear in string theory; however, there is a stringy connection via AdS/CFT duality. Recall that in string theory, Dp-branes are extended p (spatial)-dimensional objects: open strings with endpoints obeying Dirichlet boundary conditions end on. D-branes are to be viewed as physical, dynamical objects with their own mass and (Ramond–Ramond) charges carried by the string endpoints [329]. In the case of N parallel Dp-branes, each open string endpoint can lie on one of N different branes, yielding a total of N^2 choices. When these N parallel

Dp-branes are coincident at the same location, the resulting string theory has a particle spectrum which in part describes a $U(N)$ gauge theory.

Since string theories have a low-energy effective description in terms of an appropriate theory of supergravity, a D-brane or a stack of coincident Dp-branes have a realization as a supergravity solution with a corresponding mass and charge. A relevant example is a stack of N coincident D3-branes in ten-dimensional spacetime. Such a set D-brane configuration exists in type IIB string theory with string coupling g_s and string length scale $\ell_s = \sqrt{\alpha'}$. In the decoupling limit, where $\alpha' \to 0$ and the ratio of the distance between the non-coincident configuration of parallel branes and coupling, $u \equiv r/\alpha'$, is kept fixed, the gauge theory on the brane is that of four-dimensional $\mathcal{N} = 4$ SU(N) super Yang–Mills theory (a superconformal field theory). The corresponding supergravity solution has line element [330]

$$ds_{10}^2 = f^{-1/2} dx_{\parallel} + f^{1/2} dx_{\perp}^2, \quad f = 1 + \frac{4\pi g_s \alpha'^2}{r^4}. \tag{A84}$$

Here, $dx_{\parallel}^2$ denotes the set of coordinates along the four-dimensional worldvolume of the D3-brane configuration, while $dx_{\perp}^2 = (dr^2 + r^2 d\Omega_5^2)$ is the collection of coordinates of the six-dimensional space perpendicular to the stack of branes where the radial coordinate r characterizes the distance between the branes (before taking the coincident limit) and $d\Omega_5^2$ denotes the metric of the unit 5-sphere.

Introduce coordinate $u \equiv r/\alpha'$ such that $f = 1 + \frac{4\pi g_s N}{\alpha'^2 u^4}$. The supergravity geometry (A84) of the aforementioned decoupling limit ($\alpha' \to 0$, u fixed) is valid when $g_s N \gg 1$, i.e., at large 't Hooft coupling $\lambda \equiv g_s N$. In this 'near horizon' limit, the 10-dimensional geometry is approximately

$$ds_{10}^2 \approx \ell_s^2 \left[\frac{u^2}{\sqrt{4\pi g_s N}} dx_{\parallel}^2 + \sqrt{4\pi g_s N} \frac{du^2}{u^2} + \sqrt{4\pi g_s N} d\Omega_5^2 \right]. \tag{A85}$$

This line element is simply $AdS_5 \times S^5$, with AdS_5 length $L_5 = \sqrt{4\pi g_s N} \ell_s^2$ and a 5-sphere of the same radius[77]. In other words, the supergravity solution has a dual description in terms of the four-dimensional superconformal field theory, which is a sharp realization of the AdS/CFT correspondence [6].

Now return to the RS-II model describing a single codimension-1 brane sitting inside of an asymptotically AdS_5 bulk spacetime. There are two comments worth mentioning here. First, Gubser observed when the bulk is the AdS_5–Schwarzschild black hole, the induced geometry on the brane is that of radiation-dominated FRW cosmology [331]. Via AdS/CFT, the thermal nature of the bulk black hole has a dual description in terms of a thermal CFT at strong coupling with temperature given by the Hawking temperature of the bulk black hole. This CFT can be viewed as living on the brane, giving rise to the ('dark') radiation cosmology. Second, in taking the near-horizon limit of the stack of D3-branes, the RS model may be viewed as effectively cutting off the spacetime outside of the stack of D-branes, such that the RS-brane serves as an end-of-the-world brane.

The precise connection to AdS/CFT is different for the Karch–Randall construction [15]. This is because in such a set-up, one is no longer in a near-horizon limit of a stack of D3-branes. Rather, one realization is that of a D5-probe brane intersecting a stack of D3 branes [16,327], leading to a doubly holographic interpretation.

Appendix D. Geometric Elements of the C-Metric

The C-metric, as noted in the main text, can be interpreted as an accelerating black hole or a pair of accelerating black holes[78]. In this Appendix, we briefly review the origins of the C-metric and then describe some of its geometric features relevant for the main text.

Appendix D.1. C-Metric from Plebanski–Demianski

In order to better understand the origins of the C-metric, it is useful to analyze its parent metric first, the Plebanski–Demianski (PD) geometry [89][79]. The PD metric describes the most general algebraic type-D spacetime solving Einstein–Maxwell theory in vacuum with an aligned, non-zero electromagnetic field and a cosmological constant Λ. The line element is

$$\begin{aligned} ds^2 = \frac{1}{(p+q)^2}\Bigg\{ &-\frac{Q(q)}{1+(pq)^2}(d\tau + p^2 d\sigma)^2 + \frac{1+(pq)^2}{Q(q)}dq^2 + \frac{1+(pq)^2}{P(p)}dp^2 \\ &+ \frac{P(p)}{1+(pq)^2}(d\sigma - q^2 d\tau)^2\Bigg\}, \end{aligned} \tag{A86}$$

with metric functions

$$\begin{aligned} Q &= -\frac{\Lambda}{6} + g^2 - \gamma - 2nq + \epsilon q^2 - 2mq^3 + \left(-\frac{\Lambda}{6} + e^2 + \gamma\right)q^4, \\ P &= -\frac{\Lambda}{6} - g^2 + \gamma - 2np - \epsilon p^2 - 2mp^3 + \left(-\frac{\Lambda}{6} - e^2 + \gamma\right)p^4. \end{aligned} \tag{A87}$$

The solution is completely characterized by seven parameters: namely, the cosmological constant Λ, and the real parameters $g, e, n, m, \epsilon, \gamma$. Of these, only e and g have a clear physical interpretation, corresponding to electric and magnetic charge, respectively. Parameters m, n, ϵ and γ have a less clear interpretation in general; however, often, m and n play the role of the mass and NUT parameters, respectively, while in certain instances, γ and ϵ are interpreted as angular momentum and acceleration. For convenience, one typically shifts $\gamma \to \gamma + g^2 + \frac{\Lambda}{6}$, such that the metric functions (A87) become

$$\begin{aligned} Q &= -\frac{\Lambda}{3} - \gamma - 2nq + \epsilon q^2 - 2mq^3 + (\gamma + e^2 + g^2)q^4, \\ P &= \gamma - 2np - \epsilon p^2 - 2mp^3 - \left(\gamma + e^2 + g^2 + \frac{\Lambda}{3}\right)p^4. \end{aligned} \tag{A88}$$

Further, while Λ here is generic, we will be primarily interested in the AdS_4 C-metric, where $\Lambda = -3/L_4^2$, with L_4 being the AdS_4 curvature scale.

By appropriate coordinate and parameter rescalings, the C-metric emerges from the PD metric. To see this, first introduce two real parameters a and A and perform the following coordinate rescalings

$$p \to \sqrt{aA}p, \quad q \to \sqrt{aA}q, \quad \tau \to \sqrt{\frac{a}{A^3}}\tau, \quad \sigma \to \sqrt{\frac{a}{A^3}}\sigma. \tag{A89}$$

Additionally, rescale the parameters as

$$\begin{aligned} &m \to \left(\frac{A}{a}\right)^{3/2} m, \quad n \to \left(\frac{A}{a}\right)^{1/2} n, \quad e \to \frac{A}{a}e, \quad g \to \frac{A}{a}g, \\ &\epsilon \to \frac{A}{a}\epsilon, \quad \gamma \to A^2\gamma, \quad P \to A^2 P, \quad Q \to A^2 Q. \end{aligned} \tag{A90}$$

The resulting metric is the AdS_4 (spinning) C-metric

$$\begin{aligned} ds^2 = \frac{1}{A^2(p+q)^2}\Bigg\{ &-\frac{Q(q)}{1+(aApq)^2}(d\tau + aAp^2 d\sigma)^2 + \frac{1+(aApq)^2}{Q(q)}dq^2 \\ &+ \frac{1+(aApq)^2}{P(p)}dp^2 + \frac{P(p)}{1+(aApq)^2}(d\sigma - aAq^2 d\tau)^2\Bigg\}, \end{aligned} \tag{A91}$$

together with

$$\begin{aligned} Q &= \frac{1}{A^2L_4^2} - \gamma - \frac{2nq}{A} + \epsilon q^2 - 2mAq^3 + A^2(\gamma a^2 + e^2 + g^2)q^4, \\ P &= \gamma - \frac{2np}{A} - \epsilon p^2 - 2mAp^3 + \left(\frac{a^2}{L_4^2} - A^2(\gamma a^2 + e^2 + g^2)\right)p^4. \end{aligned} \tag{A92}$$

Notably, the parameters ϵ and γ do not affect the geometry of the solution, as they do not appear in any curvature invariants [89], and they are sometimes dubbed 'kinematical parameters'. Consequently, these parameters are gauge choices and can be chosen to take specific values without affecting the local geometry. Alternatively, m, n, e, and g are said to be 'dynamical parameters' in that they generate curvature; setting $m = n = e = g = 0$ results in a maximally symmetric background with cosmological constant Λ.

Appendix D.2. C-Metric Used for Braneworld Black Hole

As written, the C-metric line element in (A90) is cosmetically quite different from the one used for studying braneworld black holes in [23,24]. To clarify the relation, first rename coordinates and metric functions as $q \to -y$, $p \to x$, $Q \to -H$, $P \to G$, $\tau \to t$, $\sigma \to \phi$, and $\epsilon \to -k$. Then, the metric functions (A92) become

$$\begin{aligned} H &= -\frac{1}{A^2L_4^2} + \gamma - \frac{2n}{A}y + ky^2 - 2mAy^3 - A^2(\gamma a^2 + e^2 + g^2)y^4, \\ G &= \gamma - \frac{2n}{A}x + kx^2 - 2mAx^3 + \left[\frac{a^2}{L_4^2} - A^2(\gamma a^2 + e^2 + g^2)\right]x^4. \end{aligned} \tag{A93}$$

Now, making use of the aforementioned gauge freedom, we set $\gamma = 1$ and further rescale $A^2a^2 \equiv a^2$ and $A^2(e^2 + g^2) = q^2$. Then,

$$\begin{aligned} H &= -\frac{1}{A^2L_4^2} + 1 - \frac{2n}{A}y + ky^2 - 2mAy^3 - (a^2 + q^2)y^4, \\ G &= 1 - \frac{2n}{A}x + kx^2 - 2mAx^3 + \left[\left(\frac{1}{A^2L_4^2} - 1\right)a^2 - q^2\right]x^4. \end{aligned} \tag{A94}$$

Further, introduce $\lambda \equiv \frac{1}{A^2L_4^2} - 1$, yielding

$$\begin{aligned} H &= -\lambda - \frac{2n}{A}y + ky^2 - 2mAy^3 - (a^2 + q^2)y^4, \\ G &= 1 - \frac{2n}{A}x + kx^2 - 2mAx^3 + (\lambda a^2 - q^2)x^4. \end{aligned} \tag{A95}$$

The line element, meanwhile, is

$$\begin{aligned} ds^2 = \frac{1}{A^2(x-y)^2}\Bigg[&\frac{H(y)}{\Sigma(x,y)}(dt + ax^2d\phi)^2 - \frac{\Sigma(x,y)}{H(y)}dy^2 \\ &+ \frac{\Sigma(x,y)}{G(x)}dx^2 + \frac{G(x)}{\Sigma(x,y)}(d\phi - ay^2dt)^2\Bigg], \end{aligned} \tag{A96}$$

with

$$\Sigma(x,y) = 1 + a^2x^2y^2. \tag{A97}$$

In this context, q represents both electric and magnetic charge, A is the 'acceleration' parameter, a is the angular rotation, and n is the NUT parameter. Setting $n = q = 0$ in the metric functions (A95) recovers the form of the C-metric used in [23,24] (cf. Equation (5.1) of [24]). We will explore further details of this metric momentarily.

Rindler form. It is easiest to see the accelerating nature of the C-metric by setting $a = n = q = m = 0$, $k = -1$ and $L_4 \to \infty$ such that $\lambda = -1$. Further rescale $t \to At$. Then, the line element (A96) with metric functions (A95) becomes

$$ds^2 = \frac{1}{A^2(x-y)^2}\left[-(y^2-1)A^2dt^2 + \frac{dy^2}{(y^2-1)} + \frac{dx^2}{(1-x^2)} + (1-x^2)d\phi^2\right]. \tag{A98}$$

Next, introduce the coordinate transformations

$$\xi = \frac{\sqrt{y^2-1}}{(x-y)}, \quad \rho = \frac{1}{A}\frac{\sqrt{1-x^2}}{(x-y)}, \tag{A99}$$

resulting in

$$ds^2 = -\xi^2 dt^2 + A^{-2}d\xi^2 + d\rho^2 + \rho^2 d\phi^2, \tag{A100}$$

which we recognize as the four-dimensional Rindler metric in cylindrical coordinates. An acceleration horizon with acceleration A occurs at $\xi = 0$, or, equivalently, $y = 1$.

Boyer–Lindquist form. It is also useful to express the metric in a Boyer–Lindquist-like form. Specifically, to describe an AdS_3 Karch–Randall brane, make the identifications

$$\lambda = \frac{\ell^2}{\ell_3^2}, \quad A = \frac{1}{\ell}, \quad k = -\kappa, \quad 2mA = \mu, \quad a \to \frac{a}{\sqrt{\lambda}\ell_3}, \tag{A101}$$

together with the coordinate rescaling and change

$$t \to \frac{t}{\ell}, \quad y = -\frac{\ell}{r}. \tag{A102}$$

Then, the metric (A96) becomes

$$\begin{aligned} ds^2 = \frac{\ell^2}{(\ell + xr)^2}\Bigg\{ &-\frac{H(r)}{\Sigma(x,r)}(dt + ax^2 d\phi)^2 + \frac{\Sigma(x,r)}{H(r)}dr^2 \\ &+ r^2\left[\frac{\Sigma(x,r)}{G(x)}dx^2 + \frac{G(x)}{\Sigma(x,r)}\left(d\phi - \frac{a}{r^2}dt\right)^2\right]\Bigg\} \end{aligned} \tag{A103}$$

with metric functions

$$\begin{aligned} H(r) &\equiv -\frac{r^2}{\ell^2}H(-\ell/r) = \frac{r^2}{\ell_3^2} + \kappa - 2nr - \frac{\mu\ell}{r} + \frac{(a^2 + q^2\ell^2)}{r^2}, \\ G(x) &= 1 - 2n\ell x - \kappa x^2 - \mu x^3 + \left(\frac{a^2}{\ell_3^2} - q^2\right)x^4, \\ \Sigma(x,r) &= 1 + \frac{a^2x^2}{r^2}. \end{aligned} \tag{A104}$$

Note that the n parameter may always be rescaled by ℓ or ℓ^{-1}. Setting $n = 0$ and taking the zero acceleration limit $\ell \to \infty$ (upon setting $\kappa = +1$, and rescaling $\mu\ell \to 2M$ and similarly for charge q^2), we recover the Kerr–Newman–AdS black hole in Boyer–Lindquist coordinates, with $x = \cos\theta$.

Alternatively, the parameter space giving positive curvature on the brane is easily reached from the above AdS solution. Indeed, simply replace $\ell_3 \to iR_3$ and set $a \to -a$ and $\kappa = +1$.

Appendix D.3. Factorized C-Metric

Thus far, the metric factors P, Q or H, G are quadratic functions of a single coordinate and are not readily factorizable. This makes finding the roots of the metric functions complicated. Further, for the rotating C-metric, even when $n = 0$, the solution still has a

non-zero NUT charge. In 2003 and 2004, Hong and Teo [339,340] found a way to express the C-metric in a factorized form, which not only simplified some calculations but also showed the factorized version of the rotating C-metric is physically distinct from its original non-factorized form.

To arrive at a factorized form of the rotating C-metric, recall AdS_4 spinning C-metric (A91) with metric functions Q and P (A92). Then, following Hong and Teo [340], use gauge freedom to set the kinematical parameters γ and ϵ to

$$\gamma = 1, \quad \epsilon = 1 + \frac{a^2}{L_4^2} - A^2(a^2 + e^2 + g^2). \tag{A105}$$

Then, in order to place the metric functions (A92) in a factorized form, further set $n = -mA^2$, leading to the C-metric (A91), now with factorized metric functions,

$$\begin{aligned} Q &= (q^2 - 1)\left(1 - 2mAq + A^2(a^2 + e^2 + g^2)q^2\right) + \frac{1}{A^2 L_4^2}(1 + a^2 A^2 q^2), \\ P &= (1 - p^2)\left(1 + 2mAp + p^2\left[A^2(a^2 + e^2 + g^2) - \frac{a^2}{L_4^2}\right]\right). \end{aligned} \tag{A106}$$

Incidentally, the choice $n = -mA^2$ which ultimately factorizes the metric functions leads to a solution with vanishing NUT charge. Consequently, the factorized and non-factorized forms of the C-metric are physically distinct, and they are not related by a coordinate transformation. Note, however, in the non-rotating case ($a = 0$) with $\Lambda = 0$, the factorized and non-factorized C-metrics are related by a coordinate transformation and are thus physically equivalent [339] (in the limit $a = 0$, n acts as a kinematical parameter). The difference between factorized and non-factorized rotating C-metrics arises because the latter has 'torsion singularities', conical singularities which have a non-zero angular velocity, while the former does not have torsion singularities. The effect is that the non-factorized rotating C-metric will possess closed timelike curves in a neighborhood of the torsion singularities [341][80].

Further, the factorized C-metric, line element (A91) with functions (A106), can be brought to a more standard Boyer–Lindquist form (cf. Equation (2.31) of [121]). The (extended) thermodynamics of this form of the factorized C-metric was analyzed in [118–120].

We can similarly bring the C-metric used to study braneworld black holes, line element (A95) with metric functions (A96), into a factorized form. All that is required is to use gauge freedom to set

$$k = -1 - \frac{a^2}{A^2 L_4^2} + (a^2 + q^2), \tag{A107}$$

and remove the NUT charge via $n = -mA^2$. The result is the rotating C-metric (A95), now with metric functions

$$\begin{aligned} H &= -(\lambda + 1)(1 + a^2 y^2) + (1 - y^2)\left(1 + 2mAy + (a^2 + q^2)y^2\right), \\ G &= (1 - x^2)\left(1 + 2Amx - (\lambda a^2 - q^2)x^2\right), \end{aligned} \tag{A108}$$

with $\lambda + 1 = (A^2 L_4^2)^{-1}$. We see the metric function H is completely factorized when $\Lambda = 0$. Making identifications $\lambda = \ell^2/\ell_3^2$, $A = \ell^{-1}$, $a \to a/\ell$, $2mA = \mu$, and using the coordinate

change (A102), puts the factorized C-metric in a more Boyer–Lindquist form (A103), with metric functions

$$\begin{aligned} H(r) &= (r^2+a^2)\left(\frac{1}{\ell_3^2}+\frac{1}{\ell^2}\right)+\left(1-\frac{r^2}{\ell^2}\right)\left(1-\frac{\mu\ell}{r}+\frac{(a^2+q^2\ell^2)}{r^2}\right), \\ G(x) &= (1-x^2)\left(1+\mu x-\left(\frac{a^2}{\ell_3^2}-q^2\right)x^2\right), \quad \Sigma(x,r)=1+\frac{a^2x^2}{r^2}. \end{aligned} \tag{A109}$$

Appendix D.4. Some Properties of the C-Metric

Let us now detail some of the properties of the C-metric used in the main text. Following the conventions of [24], begin with the uncharged, non-rotating AdS_4 C-metric

$$ds^2=\frac{1}{A^2(x-y)^2}\left[H(y)dt^2-\frac{dy^2}{H(y)}+\frac{dx^2}{G(x)}+G(x)d\phi^2\right], \tag{A110}$$

with

$$H(y)=-\lambda+ky^2-2mAy^3, \quad G(x)=1+kx^2-2mAx^3, \tag{A111}$$

obeying $H(\chi)=G(\chi)-(1+\lambda)$. Here, $k=+1,0,-1$, which will determine the black hole horizon topology. The bulk Ricci tensor satisfies $\hat{R}_{AB}=-(3/L_4^2)\hat{g}_{AB}$ where $L_4\equiv(A\sqrt{\lambda+1})^{-1}$ sets the scale for the bulk cosmological constant. Maintaining a negative cosmological constant in the bulk thus requires $\lambda>-1$, while $G(x)\geq 0$ to maintain a Lorentzian signature. The overall factor $(x-y)^{-2}$ in (A110) implies the point $y=x$ is infinitely far away from points $y\neq x$ (the point $y=x$ corresponds to the asymptotic AdS_4 boundary). The curvature invariants

$$\begin{aligned} \hat{R}^{ABCD}\hat{R}_{ABCD} &= 24A^4[2A^2m^2(x-y)^6+(1+\lambda)^2], \\ \hat{C}^{ABCD}\hat{C}_{ABCD} &= 48A^6m^2(x-y)^2, \end{aligned} \tag{A112}$$

reveal curvature singularities at $y\pm\infty$ and $x=\pm\infty$, while the Weyl tensor vanishes asymptotically at $y=x$. To avoid naked singularities, one must restrict coordinate ranges for a given set of parameters. To maintain a 'mostly plus' Lorentzian signature requires $G(x)\geq 0$, restricting the range of x.

To gain further intuition for the C-metric, it is instructive to consider the simplifying case when $mA=0$. Then, consider performing the coordinate transformation

$$\tilde{r}=\frac{\sqrt{y^2+\lambda x^2}}{A(x-y)}, \quad \rho=\sqrt{\frac{1+kx^2}{y^2+\lambda x^2}}, \tag{A113}$$

such that the metric (A110) becomes

$$ds^2=\frac{d\tilde{r}^2}{\frac{\tilde{r}^2}{\ell_4^2}-\lambda}+\tilde{r}^2\left[-(\lambda\rho^2-k)dt^2+\frac{d\rho^2}{\lambda\rho^2-k}+\rho^2d\phi^2\right]. \tag{A114}$$

Locally, the geometry is AdS_4, where surfaces of constant $\tilde{r}$ have constant Riemann curvature with a three-dimensional cosmological constant $\Lambda_3=-\lambda$. Thus, the sign of λ denotes different constant curvature slicings of AdS_4. There are three distinct cases: **(1)** $\lambda=0$, a flat slicing. In this case, one must choose $k=\pm1$, where for $k=-1$, the coordinate t is timelike everywhere; **(2)** $-1<\lambda<0$ leads to a three-dimensional de Sitter slicing. One must select $k=-1$ to have dS_3 in static patch coordinates and cosmological horizons, and **(3)** $\lambda>0$, an AdS_3 slicing where the three different values of k distinguish three slicings of AdS_3: global coordinates ($k=-1$), the massive BTZ black hole ($k=+1$), and the massless BTZ black hole ($k=0$).

Conical singularities. Each zero of $H(y)$ corresponds to a Killing horizon associated with the time translation Killing vector ∂_t. Meanwhile, the zeros of $G(x)$ correspond to an axis for the rotation symmetry ∂_ϕ, i.e., for $\xi^a = \partial^a_\phi$, then $\xi^2 \sim G(x)$, vanishing at a zero of $G(x)$. For a range of values of mA and k, there will be three distinct real zeros[81] to $G(x)$, $\{x_0, x_1, x_2\}$, with each zero leading to a distinct conical singularity. One singularity can be removed via[82]

$$\phi \sim \phi + \Delta\phi(x_i), \quad \Delta\phi(x_i) = \frac{4\pi}{|G'(x_i)|}, \tag{A115}$$

where x_i is one of the zeros. Once the period of ϕ has been fixed in this way (say at $x = x_1$), the coordinate ϕ cannot be readjusted to eliminate the remaining conical singularities at $x = x_0, x_2$. Thus, in general, there will be a conical singularity along the axis $x = x_i \neq x_1$ with angular deficit $\delta = \Delta\phi(x_1) - \frac{4\pi}{G'(x_i)}$[83]. This may be interpreted as a cosmic string with tension $\tau_{cs} = \delta/8\pi$. It is this feature which leads one to interpret the C-metric as a a single or pair of accelerating black holes. In the case of a single black hole, a cosmic string attaches at one pole in the background and the black hole, suspending it away from the center of the spacetime, thus inducing its acceleration. When the cosmic string hits the boundary, it produces a conical defect in the boundary geometry, which may or may not be hidden by a horizon on the boundary.

It is possible that the metric function $G(x)$ has degenerate roots. For example, when $k = -1$ and $mA = 1/3\sqrt{3}$, $G(x)$ has a double root x_d. Near $x = x_d$, the (x, ϕ)-sector of the line element takes the form of a Euclidean hyperboloid

$$ds^2_{x_d} = \frac{dx^2}{(x - x_d)^2} + (x - x_d)^2 d\phi^2, \tag{A116}$$

with a spatial divergence at $x = x_d$.

Boundary geometry. The asymptotic AdS_4 boundary is located at $y = x$. Stripping off the conformal factor via an appropriate conformal transformation, the boundary metric is

$$ds^2_{\text{bdry}} = H(x)dt^2 - \frac{dx^2}{H(x)G(x)} + G(x)d\phi^2. \tag{A117}$$

This line element describes a black hole with a Killing horizon located at values of x which coincide with the zeros y_i of $H(y)$, i.e., $x = y_i$. Proper distances between points on the boundary are given using this boundary metric, e.g., $x_{\text{proper}} = \int dx(-H(x)G(x))^{1/2}$. While beyond the scope of this review, it is worth highlighting that in the context of the AdS/CFT correspondence, specific limits of the AdS_4 C-metric are dual to holographic CFTs living on fixed three-dimensional black hole backgrounds [9,342]. Namely, two classes of asymptotically AdS_4 solutions include (i) *black funnels*, i.e., solutions that have a single connected but non-compact horizon, and (ii) *black droplets*, i.e., solutions with two disconnected horizons. In either case, the AdS_4 solution is attached to the boundary black hole horizon, where in (ii), the (compact) horizon connected to the boundary horizon is the 'droplet' and is suspended above a (deformed) planar black hole. Note that the $A \to \infty$ limit of the C-metric with a de Sitter slicing on the $x = 0$ hypersurface is a double-Wick rotation of the hyperbolic AdS_4 metric (see Appendix C of [26] for details).

Umbilic surfaces. The C-metric has the nice property that its $x = 0$ and $y = 0$ hypersurfaces are umbilic, i.e., when the extrinsic curvature of the hypersurface is proportional to the induced metric. To see this, the outward pointing unit normal to the $x = 0$ hypersurface is $n^i_x = -A\epsilon(x - y)\sqrt{G(x)}\partial^i_x$, where $\epsilon = \pm 1$ (we will take $\epsilon = +1$ since $x = 0$ is a timelike hypersurface). The non-vanishing components of the extrinsic curvature $K_{ij} = \nabla_i n_j$ obey

$$K^{(x)}_{ij} = A\epsilon h^{(x)}_{ij}, \tag{A118}$$

with $h^{(x)}_{ij}$ being the induced metric along the $x = 0$ surface. Similarly, the $y = 0$ hypersurface is umbilic: with outward pointing unit normal $n^i_y = -A\epsilon(x-y)\sqrt{H(y)}\partial^i_y$, then

$$K^{(y)}_{ij} = A\epsilon\sqrt{-\lambda}h^{(y)}_{ij}. \tag{A119}$$

where now $h^{(y)}_{ij}$ is the induced metric along $y = 0$.

With Rotation

Now, consider the neutral rotating AdS_4 C-metric, following the conventions of [24],

$$ds^2 = \frac{1}{A^2(x-y)^2}\left[\frac{H(y)}{\Sigma(x,y)}(dt + ax^2 d\phi)^2 - \frac{\Sigma(x,y)}{H(y)}dy^2 + \frac{\Sigma(x,y)}{G(x)}dx^2 + \frac{G(x)}{\Sigma(x,y)}(d\phi - ay^2 dt)^2\right], \tag{A120}$$

with metric functions

$$\begin{aligned} H(y) &= -\lambda + ky^2 - 2mAy^3 - a^2y^4, \quad \Sigma(x,y) = 1 + a^2x^2y^2 \\ G(x) &= 1 + kx^2 - 2mAx^3 + a^2\lambda x^4. \end{aligned} \tag{A121}$$

When $m \neq 0$, there is a curvature singularity when $1/y^2\Sigma(x,y) = 0$, i.e., when both $y \to -\infty$ and $x = 0$, which may be understood as a ring singularity familiar to Kerr black holes.

The zeros x_i of $G(x)$ now correspond to fixed orbits of the rotational Killing vector

$$\xi = \partial_\phi - ax_i^2\partial_t, \tag{A122}$$

instead of the Killing vector ∂^μ_ϕ (which no longer has a vanishing norm at $x = x_i$). Avoiding a conical defect at $x = x_1$ requires one identify points along the integral curves of ξ with an appropriate period, amounting to a coordinate transformation $\tilde{t} = t + ax_1^2\phi$, where ϕ has the same period (A115). To see this, expand the metric (A120) near a zero of $G(x)$. Without loss of generality, the $y = 0$ slice is, up to the conformal factor,

$$ds^2_{y=0} \approx -\lambda(dt + ax_i^2 d\phi)^2 + \frac{dx^2}{G'(x_i)(x - x_i)} + G'(x_i)(x - x_i)d\phi^2. \tag{A123}$$

Aside from the first term, the (x, ϕ) sector has the same form as in the non-rotating case, from which the periodicity of ϕ is (A115). Including rotation, however, this would not be the correct periodicity for ϕ. The situation is remedied via the coordinate transformation $\tilde{t} = t + ax_i^2\phi$, such that, at $x = x_i$, $d\tilde{t} = (dt + ax_i^2 d\phi)$. Similarly, at the roots y_i of $H(y)$, the Killing vector $\zeta = \partial_t + ay_i^2\partial_\phi$ becomes null, defining horizons with angular velocity $\Omega = ay_i^2$.

The asymptotic AdS_4 boundary is again at $x = y$ and again gives rise to boundary black holes. Notably, the $A \to \infty$ limit of the rotating C-metric (see below), with $k = +1$, is a double-Wick rotation of the Kerr–AdS_4 metric considered in [9] (see Appendix B of [25]).

Lastly, as in the static case, the $x = 0$ and $y = 0$ hypersurfaces are umbilic. Indeed, for spacelike unit normal $n^i_x = A(x-y)\sqrt{G(x)/\Sigma(x,y)}\partial^i_x$, the extrinsic curvature satisfies $K_{ij} = -Ah^{(x)}_{ij}$ at $x = 0$. Similarly, the $y = 0$ hypersurface, with unit normal $n^i_y = A\epsilon(x - y)\sqrt{H(y)/\Sigma(x,y)}\partial^i_y$, obeys $K_{ij} = (-A\epsilon\sqrt{-\lambda})h^{(y)}_{ij}$.

Appendix D.5. AdS C-Metric on the Poincaré Disk

Here, we review how to project the C-metric on the two-dimensional Poincaré disk of the unit radius to produce the plots shown in Figures 5, 9 and 10.

Appendix D.5.1. Hyperbolic Disk

First, recall that the two-dimensional hyperbolic space $\mathbb{H}^2$ can be embedded in three-dimensional Minkowski space coordinatized by $x^\mu = \{x^0, x^1, x^2\}$ and obeying $\eta_{\mu\nu}x^\mu x^\nu = -1$. Different choices of coordinates y^i on $\mathbb{H}_2$ correspond to different ways of embedding $\mathbb{H}^2$. Particularly relevant for our purposes include (see, e.g., [343]) the following:

- **Hyperbolic:** Let $\rho \in [0, \infty)$ be a radial coordinate and $\omega \in (-\infty, \infty)$ a hyperbolic angle. Then, the coordinate parametrization

$$\begin{cases} x^0 = \cosh\rho\cosh\omega \\ x^1 = \sinh\rho \\ x^2 = \cosh\rho\sinh\omega \end{cases} \tag{A124}$$

  leads to the induced two-dimensional geometry for $\mathbb{H}^2$

$$ds^2 = \eta_{\mu\nu}dx^\mu dx^\nu = d\rho^2 + \cosh^2(\rho)d\omega^2. \tag{A125}$$

- **Polar:** Let $\chi \in (-\infty, \infty)$ be a radial coordinate and $\varphi \in [0, 2\pi)$ a polar angle. Then

$$\begin{cases} x^0 = \cosh\chi \\ x^1 = \sinh\chi\cos\varphi \\ x^2 = \sinh\chi\sin\varphi \end{cases} \tag{A126}$$

  yields the two-dimensional induced geometry

$$ds^2 = d\chi^2 + \sinh^2(\chi)d\varphi^2. \tag{A127}$$

- **Exponential:** Let $\zeta \in (-\infty, \infty)$ be a radial coordinate and $\Psi \in (-\infty, \infty)$ a hyperbolic angle. With coordinates

$$\begin{cases} x^0 = \cosh(\zeta) + e^{-\zeta}\Psi^2/2 \\ x^1 = e^{-\zeta}\Psi \\ x^2 = \sinh(\zeta) + e^{-\zeta}\Psi^2/2 \end{cases} \tag{A128}$$

  the induced two-dimensional metric is

$$ds^2 = d\zeta^2 + e^{-2\zeta}d\Psi^2\,. \tag{A129}$$

Moreover, note it is possible to project the infinite $\mathbb{H}_d$ hyperbolic space onto the d-dimensional unit disk using the Poincaré projection

$$x^i_{\rm P} \equiv \frac{x^i}{1+x^0}\,. \tag{A130}$$

Appendix D.5.2. AdS_3 Foliations

As discussed in Section 4.1, it is possible to bring the static AdS_4 C-metric with vanishing mass parameter $\mu = 0$ into the form of empty AdS_4 (43), which is foliated by slices of AdS_3 using the coordinate transformation (42).

$$\cosh(\sigma) = \frac{\ell_3}{L_4}\frac{1}{|1+\frac{rx}{\ell}|}\sqrt{1+\frac{r^2x^2}{\ell_3^2}}, \qquad \hat{r} = r\sqrt{\frac{1-\kappa x^2}{1+\frac{r^2x^2}{\ell_3^2}}}. \tag{A131}$$

Constant t and ϕ slices of empty AdS_4 (43) have the induced geometry

$$ds^2 = L_4^2 d\sigma^2 + \frac{L_4^2}{\ell_3^2}\cosh^2(\sigma)\left(\kappa + \frac{\hat{r}^2}{\ell_3^2}\right)^{-1} d\hat{r}^2. \tag{A132}$$

This line element is reminiscent of two-dimensional $\mathbb{H}^2$ geometry (A125), where σ plays the role of ρ and $\hat{r}$ is the hyperbolic angle. Indeed, the coordinate transformation

$$\psi = \ell_3 \operatorname{arcsinh}\frac{\hat{r}}{\ell_3}, \tag{A133}$$

brings the metric on the constant t and ϕ slice to

$$ds^2 = L_4^2\left(d\sigma^2 + \cosh^2(\sigma)d\psi^2\right), \tag{A134}$$

which is conformally equivalent to (A125). One can subsequently use coordinates (A124) and the Poincaré projection (A130) to represent lines of constant x and r on the two-dimensional disk, as depicted in Figure 5.

A word of caution on coordinate ranges. To cover the whole disk, σ should range over all $\mathbb{R}$. In fact, for constant t and ϕ, the C-metric only covers half of the disk (here, we have chosen the $\sigma > 0$ range). Nonetheless, the rest of the disk is recovered by rotation of the ϕ coordinate. Moreover, the coordinate transformation (A131) is not one-to-one across the whole range of (x, r) coordinates. To make it so, we restrict the range of x for a given r to

$$\begin{cases} -\ell/r < x \leq 1 & r > 0 \\ x > 1 & r < 0. \end{cases} \tag{A135}$$

for inverse acceleration ℓ.

Appendix D.5.3. dS_3 Foliations

The coordinate transformation (141)

$$\sinh(\sigma) = \frac{R_3}{L_4}\frac{1}{|1+\frac{rx}{\ell}|}\sqrt{1-\frac{x^2r^2}{R_3^2}}, \quad \hat{r} = r\sqrt{\frac{1-x^2}{1-\frac{x^2r^2}{R_3^2}}}, \tag{A136}$$

brings the C-metric (with $\mu = 0$) into empty AdS_4 form (142) foliated by dS_3 slices (after the $\ell_3 \to iR_3$ Wick rotation). At constant t and ϕ slices, the two-dimensional metric is

$$ds^2 = L_4^2 d\sigma^2 + \frac{L_4^2}{R_3^2}\sinh^2(\sigma)\left(1 - \frac{\hat{r}^2}{R_3^2}\right)^{-1} d\hat{r}^2, \tag{A137}$$

having the form of (A125) where σ plays the role of χ and $\hat{r}$ is related to the angle φ, with $\hat{r} \in [0, R_3)$. The coordinate transformation

$$\psi = 2R_3 \arctan\left(\frac{\hat{r}}{-R_3 + \sqrt{R_3^2 - \hat{r}^2}}\right), \tag{A138}$$

brings the spatial metric to

$$ds^2 = L_4^2\left(d\sigma^2 + \sinh^2(\sigma)d\psi^2\right), \tag{A139}$$

which is conformally equivalent to (A126).

Note that σ is always positive in the coordinate transformation (A136). Consequently, the parametrization only covers the $\sigma \geq 0$ region of the disk, and it cannot be recovered by a simple rotation by the ϕ coordinate (as in the AdS case). The other half of the disk is covered by analytic continuation of the coordinate system, yielding Figure 9.

Appendix D.5.4. Flat Foliations

Empty AdS_4 can also be foliated by $Mink_3$ and can be understood as a limiting case of either the AdS_3 and dS_3 foliations as, respectively, ℓ_3 and R_3 tend to infinity. In particular, the coordinate transformation

$$e^{\sigma} = \ell + xr, \quad \hat{r} = r\sqrt{1-x^2}, \tag{A140}$$

produces the constant t-ϕ geometry

$$ds^2 = \ell^2\left(d\sigma^2 + e^{-2\sigma}d\hat{r}^2\right), \tag{A141}$$

coinciding with line element (A129). Contrary to the previous examples, here, $\hat{r}$ plays the role of the hyperbolic angle. For the coordinate transformation to be meaningful, we restrict the values of x such that

$$-\ell/r \leq x < 1\,, \tag{A142}$$

where, recall, $r \geq 0$. In principle, these coordinates cover only half of the disk, while the other half is recovered by a rotation of the angle ϕ, leading to Figure 10.

Appendix E. On-Shell Euclidean Action of AdS C-Metric

Here, we review the derivation of the thermodynamics of the bulk system of a regular (non-rotating) AdS_4 C-metric with a Karch–Randall or Randall–Sundrum brane using the on-shell Euclidean gravitational action [124].

Appendix E.1. Geometry

In Lorentzian signature, we work with the AdS_4 C-metric in the form

$$ds^2 = \frac{\ell^2}{(x-y)^2}\left(-H(y)dt^2 + \frac{dy^2}{H(y)} + \frac{dx^2}{G(x)} + G(x)d\phi^2\right), \tag{A143}$$

where

$$H(y) = \lambda - ky^2 + \mu y^3, \quad G(x) = 1 + kx^2 - \mu x^3, \tag{A144}$$

with $\lambda \equiv \ell^2/\ell_3^2$ and $\mu = 2mA$. To avoid a conical singularity at the zero $x = x_1$ of $G(x)$, the period of angular variable ϕ is fixed to be $\Delta\phi = \frac{4\pi}{|G(x_1)|}$, and for a black hole localized on the brane at $x = 0$, the x, y coordinate ranges are restricted to be $0 \leq x \leq x_1$ and $-\infty \leq y \leq x$, where $y = -\infty$ corresponds to a curvature singularity hidden behind the bulk horizon, located at $y = y_+$, which is the smallest root of $H(y)$. The region $x, y \to 0$ corresponds to an asymptotic region far from the black hole (this is apparent in Boyer–Lindquist form).

Recall that the surfaces $x = 0$ and $y = 0$ are umbilic, satisfying $K_{ij}^{(x)} = -A\epsilon h_{ij}^{(x)}$ (A118) and $K_{ij}^{(y)} = A\epsilon\sqrt{\lambda}h_{ij}^{(y)}$ (A119), respectively[84]. Boundary conditions on the $x = 0$ and $y = 0$ hypersurfaces are governed by Israel's junction conditions [53]. For purely tensional branes, the junction conditions fix the tensions τ_x and τ_y by relating the discontinuity in the extrinsic curvature across the $x = 0$ and $y = 0$ surfaces to their respective brane stress tensors $S_{ij}^{(x)}$ and $S_{ij}^{(y)}$. Specifically, for a $\mathbb{Z}_2$-symmetric brane configuration as utilized in the main text, the junction conditions give

$$2[K_{ij}^{(x,y)} - h_{ij}^{(x,y)}K^{(x,y)}] = 8\pi G_4 S_{ij}^{(x,y)} = -8\pi G_4 \tau_{x,y} h_{ij}^{(x,y)}, \tag{A145}$$

giving tensions

$$\tau_x = -\frac{\epsilon A}{2\pi G_4}, \qquad \tau_y = -\frac{\epsilon A\sqrt{\lambda}}{2\pi G_4}. \tag{A146}$$

The Euclidean AdS_4 C-metric is found by Wick rotating $t_E = it$, for Euclidean time t_E,

$$ds^2 = \frac{\ell^2}{(x-y)^2}\left(H(y)dt_E^2 + \frac{dy^2}{H(y)} + \frac{dx^2}{G(x)} + G(x)d\phi^2\right), \tag{A147}$$

using $A = \ell^{-1}$. In Euclidean signature, there will be a conical singularity at the location of the black hole horizon, $y = y_+$. To have a regular Euclidean section, the Euclidean time $t_E \sim t_E + \Delta t_E$ is periodicially identified with period

$$\Delta t_E = \frac{4\pi}{|H'(y_+)|}. \tag{A148}$$

In Euclidean signature, the brane and boundary satisfy the same umbilic conditions as before, however, $\epsilon = -1$ in the tensions (A146).

Appendix E.2. On-Shell Euclidean Action

We now follow Gibbons and Hawking [123] to evaluate the quantum gravitational canonical partition function $Z(\beta)$ in the semi-classical limit via the on-shell Euclidean action. Before we evaluate the on-shell action, two comments are in order. First, as an accelerating black hole, the AdS_4 C-metric has at least two horizons, a black hole horizon and an acceleration horizon. Due to the system having two horizons, generally with different surface gravities, the two-horizon system is not generically in thermodynamic equilibrium. One way to circumvent this problem is to work in a regime in which the black hole is slowly accelerating, where $A < L_4^{-1}$ [90]. This translates to $A < A\sqrt{1+\lambda}$, i.e., $\lambda > 0$, or an AdS_3 slicing on the brane. Below, we work in this regime such that we effectively have a single black hole with a single unique temperature given by β^{-1}. Meanwhile, a dS_3 slicing, where $-1 < \lambda < 0$, obeys $A > L_4^{-1}$, such that the bulk solution is interpreted as two black holes separated by an acceleration horizon [344], and the system is not in thermal equilibrium. This is consistent with the fact this scenario describes a de Sitter black hole localized on the brane, for which the black hole and cosmological horizons are not generally in equilibrium.

Second, in the evaluation of the on-shell action, it is common to encounter infrared divergences as a boundary is approached, requiring some regularization scheme. Traditionally, this is accomplished either by the method of background subtraction or in the case of asymptotically AdS spacetimes including a local counterterm action [18,345]. The key insight of [124] is that to recover the thermodynamics of the bulk black hole and, hence, the black hole localized on the brane, no background subtraction or local counterterms are needed. Rather, the potential IR divergences in the total on-shell action are exactly cancelled when branes at $x = 0$ and $y = 0$ are included.

To this end, the total action I characterizing the bulk Riemannian spacetime $\mathcal{M}$ endowed with Euclidean metric g, and branes $\mathcal{B}_x$ and $\mathcal{B}_x$ embedded at $x, y = 0$ is

$$I = I_{\rm EH} + I^{(x)}_{\rm GHY} + I^{(y)}_{\rm GHY} + I_{\mathcal{B}_x} + I_{\mathcal{B}_y}, \tag{A149}$$

where the bulk Einstein–Hilbert action

$$I_{\rm EH} = -\frac{1}{16\pi G_4}\int_{\mathcal{M}} d^4x\sqrt{g}(R - 2\Lambda), \tag{A150}$$

with $\Lambda = -3/L_4^2$. To have a well-posed variational problem, Gibbons–Hawking–York boundary (GHY) terms are needed for each brane,

$$I^{(x)}_{\rm GHY} = \frac{1}{8\pi G_4}\int_{\mathcal{B}_x} d^3x\sqrt{h_{(x)}}K^{(x)}, \qquad I^{(y)}_{\rm GHY} = -\frac{1}{8\pi G_4}\int_{\mathcal{B}_y} d^3x\sqrt{h_{(y)}}K^{(y)}. \tag{A151}$$

The brane actions are purely tensional and take the form

$$I_{\mathcal{B}_x} = -\tau_x\int_{\mathcal{B}_x} d^3x\sqrt{h_{(x)}}, \qquad I_{\mathcal{B}_y} = \tau_y\int_{\mathcal{B}_y} d^3x\sqrt{h_{(y)}}. \tag{A152}$$

Each action has IR divergences at $x, y = 0$. To remedy this, introduce cutoffs at $x = \epsilon_x$ and $y = \epsilon_y$, and at the end of the computation take the limit $\epsilon_{x,y} \to 0$.

Let us now evaluate actions (A150)–(A152) in the Euclidean background (A147). The Einstein–Hilbert term evaluates to

$$\begin{aligned} I_{\rm EH} &= \frac{6\ell^4}{16\pi G_4 L_4^2}\int_0^{\Delta t_E} dt_E\int_0^{\Delta\phi} d\phi\int_{\epsilon_x}^{x_1} dx\int_{y_+}^{\epsilon_y} dy\,\frac{1}{(x-y)^4} \\ &= \frac{6\ell^4}{16\pi G_4 L_4^2}\frac{\Delta t_E\Delta\phi}{3}\int_{\epsilon_x}^{x_1} dx\left(\frac{1}{(x-\epsilon_y)^3} - \frac{1}{(x-y_+)^3}\right) \\ &= \frac{\ell^4}{16\pi G_4 L_4^2}\Delta t_E\Delta\phi\left[\frac{1}{(x_1-\epsilon_y)^2} - \frac{1}{(x_1-y_+)^2} + \frac{1}{(y_+-\epsilon_x)^2} - \frac{1}{(\epsilon_x-\epsilon_y)^2}\right]. \end{aligned} \tag{A153}$$

where we used $R = -12/L_4^2$, and $\Lambda = -3/L_4^2$. The GHY term (A151) at $x = \epsilon_x$ is

$$\begin{aligned} I^{(x)}_{\rm GHY} &= \frac{1}{8\pi G_4}\int_{\mathcal{B}_x} d^3x\sqrt{h_{(x)}}K^{(x)} = -\frac{3\ell^2}{8\pi G_4}\int_{\mathcal{B}_x} dt_E d\phi dy\,\frac{1}{(\epsilon_x-y)^3} \\ &= -\frac{3\ell^2}{16\pi G_4}\Delta t_E\Delta\phi\left[\frac{1}{(\epsilon_x-y_+)^2} - \frac{1}{(\epsilon_x-\epsilon_y)^2}\right], \end{aligned} \tag{A154}$$

where we used $K^{(x)} = -\frac{3}{\ell}$ and $\sqrt{G(\epsilon_x)} \approx 1$ for $\epsilon_x \ll 1$. Similarly, at $y = \epsilon_y \ll 1$,

$$\begin{aligned} I^{(y)}_{\rm GHY} &= -\frac{1}{8\pi G_4}\int_{\mathcal{B}_y} d^3x\sqrt{h_{(y)}}K^{(y)} = -\frac{3\lambda\ell^2}{8\pi G_4}\int_{\mathcal{B}_y} dt_E d\phi dx\,\frac{1}{(x-\epsilon_y)^3} \\ &= -\frac{3\lambda\ell^2}{16\pi G_4}\Delta t_E\Delta\phi\left[\frac{1}{(\epsilon_x-\epsilon_y)^2} - \frac{1}{(x_1-\epsilon_y)^2}\right], \end{aligned} \tag{A155}$$

where we used $K^{(y)} = \frac{3\sqrt{\lambda}}{\ell}$ and $\sqrt{H(\epsilon_y)} \approx \sqrt{\lambda}$. Lastly, the brane actions (A152) give

$$I_{\mathcal{B}_x} = -\tau_x\int_{\mathcal{B}_x} d^3x\sqrt{h_{(x)}} = \frac{\ell^2\Delta t_E\Delta\phi}{4\pi G_4}\left[\frac{1}{(\epsilon_x-\epsilon_y)^2} - \frac{1}{(y_+-\epsilon_x)^2}\right], \tag{A156}$$

$$I_{\mathcal{B}_y} = \tau_y\int_{\mathcal{B}_y} d^3x\sqrt{h_{(y)}} = \frac{\lambda\ell^2\Delta t_E\Delta\phi}{4\pi G_4}\left[\frac{1}{(\epsilon_x-\epsilon_y)^2} - \frac{1}{(x_1-\epsilon_y)^2}\right], \tag{A157}$$

with tensions $\tau_x = \frac{1}{2\pi G_4\ell}$ and $\tau_y = \frac{\sqrt{\lambda}}{2\pi G_4\ell}$. Observe that $I_{\rm GHY} = -\frac{3}{4}I_{\mathcal{B}}$ for either brane. Adding together the Einstein–Hilbert, GHY, and brane actions, and accounting for the $\mathbb{Z}_2$ symmetry, the total on-shell Euclidean action is [124]

$$I_{\text{on-shell}} = \frac{\ell^2}{8\pi G_4}\Delta t_E\Delta\phi\left[\frac{(1+\lambda)}{(x_1-y_+)^2} - \frac{1}{x_1^2} - \frac{\lambda}{y_+^2}\right], \tag{A158}$$

where we implemented $L_4^{-2} = \ell^{-2}(1+\lambda)$, and since all IR divergences cancel, we safely take the limit $\epsilon_x, \epsilon_y \to 0$.

It proves useful to introduce parameter $z = -y_+/x_1$, from which we find

$$\begin{aligned} x_1^2 &= \frac{1}{z^2}\frac{\nu^2 - z^3}{k(1+z)}, \\ y_+^2 &= \frac{(\nu^2 - z^3)}{k(1+z)}, \\ \mu &= z(z^2+\nu^2)\sqrt{1+z}\left|\frac{k}{(\nu^2 - z^3)}\right|^{3/2}, \end{aligned} \tag{A159}$$

where we used $G(x_1) = H(y_+) = 0$ to solve x_1^2 and y_+^2 and $\mu = (1 + kx_1^2)/x_1^3$. Further, we set $\lambda = \nu^2$. Given the range of coordinates x, y, the parameter z ranges between 0 and ∞, depending on the value of k[85]. With the parameters (A159), note

$$\Delta t_E \Delta\phi = \frac{16\pi^2 x_1^2 z^3 (1+z)^2}{[z^3 + 2\nu^2 + 3z\nu^2][2z^3 + \nu^2 + 3z^2]}, \tag{A160}$$

where we used $H'(y_+) = -2ky_+ + 3\mu y_+^2 = 2kx_1 z + 3\mu x_1^2 z^2$, and $\mu x_1 = \frac{1+kx_1^2}{x_1^2}$. Then,

$$\begin{aligned} I_{\text{on-shell}} &= -\frac{\ell^2}{8\pi G_4}\frac{\Delta t_E \Delta\phi}{x_1^2}\left[\frac{\nu^2(1+2z) + z^3(2+z)}{z^2(1+z)^2}\right] \\ &= -\frac{16\pi^2\ell^2}{8\pi G_4}\frac{z(\nu^2 + 2z\nu^2 + 2z^3 + z^4)}{[z^3 + 2\nu^2 + 3z\nu^2][2z^3 + \nu^2 + 3z^2]} \\ &= -\frac{8\pi^2\ell^2 z}{8\pi G_4}\left(\frac{1}{(2z^3 + \nu^2 + 3z^2)} + \frac{z}{(z^3 + 2\nu^2 + 3\nu^2 z)}\right). \end{aligned} \tag{A161}$$

where in the first equality, we replaced $y_+ = -zx_1$, and in the second, we substituted in (A160). Notice the parameter k has dropped out of the final expression.

Appendix E.3. Thermodynamics in the Canonical Ensemble

Following Gibbons and Hawking [123], the gravitational canonical partition function is given by a Euclidean path integral, which to leading order in a stationary phase approximation is

$$Z(\beta) = \text{tr}(e^{-\beta\mathcal{H}}) \approx e^{-I_{\text{on-shell}}}, \tag{A162}$$

where β is the (inverse) temperature T of the system. Unlike, say, the Schwarzschild black hole, the period of Euclidean time Δt_E is not equal to β. This is because the coordinates (t_E, ϕ, y) are not canonically normalized in that $\phi \sim \phi + \Delta\phi$ instead of $\phi \sim \phi + 2\pi$. Thus, one should instead consider rescaled coordinates $\bar{\phi} = \eta^{-1}\phi$, $\bar{t}_E = \eta^{-1}\ell t_E$, and $\bar{y} = \eta^{-1} y$ with $\eta \equiv \Delta/2\pi$. In these canonically normalized coordinates, the periodicity of $\bar{t}_E$ is such that

$$\bar{t}_E \sim \bar{t}_E + \beta, \quad \beta = 2\pi\ell\frac{\Delta t_E}{\Delta\phi}. \tag{A163}$$

Using the parameters (A159), the inverse temperature may be cast as[86]

$$\beta = \frac{2\pi\ell}{z}\left(\frac{\nu^2 + 3z^2 + 2z^3}{2\nu^2 + 3z\nu^2 + z^3}\right). \tag{A164}$$

Since $\log Z(\beta) = -\beta F$, for free energy F, then

$$F = \beta^{-1} I_{\text{on-shell}} = -\frac{\ell z^2}{G_4}\frac{(z^3(2+z) + \nu^2(1+2z))}{(\nu^2 + 3z^2 + 2z^3)^2}. \tag{A165}$$

Further, the canonical energy E and entropy S are defined via

$$E \equiv -\partial_\beta \log Z, \qquad S = \beta E + \log Z, \tag{A166}$$

yielding (where we keep ν, ℓ and G_4 fixed)

$$E = \frac{\ell z^2}{G_4} \frac{(1+z)(\nu^2 - z^3)}{(\nu^2 + 3z^2 + 2z^3)^2}, \tag{A167}$$

$$S = \frac{2\pi \ell^2 z}{G_4(\nu^2 + 3z^2 + 2z^3)}. \tag{A168}$$

From here, it is easy to verify $F = E - \beta^{-1} S$.

To recover the thermodynamic relations of the static qBTZ black hole stated in the main text, simply rescale $z \to \nu z$ in the above quantities:

$$\begin{aligned}
I_{\text{on-shell}} &= -\frac{2\pi \ell^2 z}{G_4 \nu} \frac{[1 + 2\nu z + \nu z^3(2+\nu z)]}{(2 + 3\nu z + \nu z^3)(1 + 3z^2 + 2\nu z^3)}, \\
\beta &= \frac{2\pi \ell}{\nu z} \frac{(1 + 3z^2 + 2\nu z^3)}{(2 + 3\nu z + 2\nu z^3)}, \\
F &= -\frac{\ell z^2}{G_4} \frac{[1 + 2\nu z + \nu z^3(2+\nu z)]}{(1 + 3z^2 + 2\nu z^3)^2}, \\
E &= \frac{\ell z^2}{G_4} \frac{(1+\nu z)(1 - \nu z^3)}{(1 + 3z^2 + 2\nu z^3)^2}, \\
S &= \frac{2\pi \ell_3^2}{G_4} \frac{\nu z}{(1 + 3z^2 + 2\nu z^3)},
\end{aligned} \tag{A169}$$

and subsequently use $\mathcal{G}_3 = G_4/2\ell$ with $G_3 = \mathcal{G}_3 \sqrt{1+\nu^2}$.

Notes

1 In two-dimensional dilaton gravity, the analog of the semi-classical Einstein equations can be solved exactly. This is because the quantum effective Polyakov action [4] capturing the two-dimensional conformal anomaly encodes nearly all backreaction effects [5].

2 There exist a set of AdS boundary conditions for which the boundary metric becomes dynamical [10].

3 Going beyond the planar limit corresponds to including bulk quantum effects.

4 We will always work in units where the speed of light $c = 1$.

5 Since we have set $c = 1$, mass has dimensions of inverse length while G_3 has dimensions of length.

6 Unlike the higher-dimensional black holes, the BTZ black hole does not possess a curvature singularity at $r = 0$; indeed, the curvature is constant everywhere. Rather, $r = 0$ describes a timelike/causal singularity.

7 Here, we are considering vacuum general relativity. Black holes in dS_3 can arise in pure modified theories of gravity, e.g., 'new massive gravity' [36] or topological massive gravity [37,38].

8 The coordinate transformation (13) is now $\tilde{t} = \gamma t - \alpha L_3 \phi$, $\tilde{\phi} = \gamma \phi + \alpha t / L_3$ and $\tilde{r}/L_3 = \sqrt{\frac{(r/L_3)^2 + \alpha^2}{\gamma^2 - \alpha^2}}$.

9 See, e.g., [27,40,45] for rotating backgrounds.

10 For conical (A)dS_3, the attractive gravitational effect is a by-product of a negative Casimir energy density from (18), $\rho_{\text{Cas}} = -\langle T^t_t \rangle = -\hbar F(M)/8\pi r^3$. This follows because a region of localized negative energy has a repulsive effect on its exterior; however, the further one enters the region, the repulsive effect is lessened. Thus, at finite r, there is an effective attraction from the Casimir energy [26].

11 A concrete realization of AdS/CFT duality is that of $\mathcal{N} = 4$ super Yang–Mills theory, a superconformal field theory, which is dual to type IIB string theory on $AdS_5 \times S^5$, where the 't Hooft coupling λ controls the curvature scale of AdS_5 whilst the string coupling is $g_s \sim N^{-1}$. In the large-N limit, stringy interactions are thus suppressed and $\lambda \gg 1$ forces curvatures to be small, such that the string theory may be replaced by an effectively classical gravity.

12 In this section, we have set $\hbar = 1$.

[13] For bulk AdS_{d+1} $\mathcal{M}$ with conformal boundary $\partial\mathcal{M}$, the d-dimensional field theory lives on a d-dimensional manifold that belongs to the conformal class of $\partial\mathcal{M}$. By choosing an appropriate conformal, the field theory may be placed on $\partial\mathcal{M}$. The choice of boundary metric fixes the boundary condition the bulk saddle-point geometry must obey and amounts to fixing the non-normalizable mode of the bulk graviton.

[14] In principle, one would like to integrate $\epsilon < \rho < \infty$, where $\rho = \infty$ is the other side of the asymptotic boundary. However, for $d > 2$, the entire analysis takes place near the $\rho = 0$ region and breaks down far into the bulk to the $\rho = \infty$ region. Indeed, the expansion (24) is valid near the $\rho = 0$ boundary. When $d = 2$, however, the three-dimensional Weyl tensor is identically zero everywhere, such that the perturbative expansion truncates and the ρ-integration can be carried out explicitly, e.g., [19,50].

[15] A notion of double holography was proposed in a Randall–Sundrum set-up [26], where the analog of defect CFT_{d-1} is given by two Euclidean CFTs, which is disconnected from the boundary viewpoint.

[16] Concerns that double holography leads to superluminal signaling [60] are ameliorated when the brane description is treated as an effective theory, such that ETW brane models are consistent with causality [61].

[17] Equally, $L_{d+1}^2/L_d^2 \sim \epsilon$, and thus the gravitational brane action is recognized as an expansion in small ϵ. Moreover, from the brane perspective, the short-distance UV cutoff of the CFT_d goes like L_{d+1} such that the higher-derivative terms also correspond to an expansion in the UV cutoff.

[18] Historically, regarding the exact three-dimensional braneworld black holes [23,24], while interpreted as holographic quantum black holes in [22], the higher-derivative corrections in the induced gravity action on the brane were not explicitly accounted for until [22,25–27].

[19] Alternatively, one can study topological black holes on the brane, e.g., [54,65]. In this context, the bulk is $d+1$-dimensional AdS-Rindler, for which the Rindler horizon induces a Rindler horizon on the brane. Since the bulk geometry is simply vacuum AdS, it evades the no-go theorem of [66].

[20] There are other mechanisms to induce two-dimensional dilaton gravity on the brane without explicitly introducing a DGP term. These include, for example, using 'wedge holography' to uncover AdS- or dS-JT gravity [79–82], or via the holography of a deformed braneworld [83], which yields a host of dilaton-gravity models on a two-dimensional brane.

[21] Indeed, a black hole will grow if $T_{ij}k^ik^j > 0$ in the background for a null generator of the horizon k^i. A black hole thus remains static when $T_{ij}k^ik^j = 0$. Since the brane stress tensor is proportional to the induced metric, the static condition translates to $k^ik_i = 0$, i.e., the k^i lies entirely on the brane, which occurs when the radial direction orthogonal to the black hole is tangent to the brane.

[22] To see this, rearrange the bulk length scale (41) to find $\ell_3^{-2} = \frac{1}{L_4^2} - \frac{1}{\ell^2}$ and $H(r) = \kappa + \frac{r^2}{L_4^2} - \frac{r^2}{\ell^2} - \frac{\mu\ell}{r}$. It follows that the only positive real root to the cubic $H(r) = 0$ occurs when $\ell > L_4$. Moreover, cast in this way, it is clear the acceleration and negative curvature of AdS_4 counteract one another such that the restriction $\ell > L_4$ effectively removes the acceleration horizon.

[23] Our conventions for the sign of the normal vector and junction conditions match with [23]. These differ from [25], where the unit normal is $n^i = \left(\frac{x}{\ell} + \frac{1}{r}\right)\sqrt{G(x)}\partial_x^i$ such that $K_{ij} = -\ell^{-1}h_{ij}$, and where the junction conditions are $2(K_{ij} - h_{ij}K) = -8\pi G_4 S_{ij} = 8\pi G_4 \tau h_{ij}$, resulting in the same tension (50).

[24] Note taking c_3 large is consistent with keeping ν small. Indeed, the large central charge limit has $c_3 \sim \frac{\ell}{\hbar G_3} \gg 1$ (equivalently, the semi-classical bulk limit $L_P^{(4)}/L_4 \ll 1$ for four-dimensional Planck length $L_P^{(4)}$), which is consistent for solutions with $\nu \ll 1$ and when four-dimensional bulk quantum effects are neglected.

[25] Evidence of the $\mathcal{G}_3$ identification in (65) is that the relation can be derived exactly by integrating the bulk volume in the action with a bulk IR cutoff as $r \to \infty$ [23].

[26] Perturbative corrections to black hole solutions in semi-classical new massive gravity give rise to logarithmic terms in the blackening factor [93]. This suggests a resummation of the infinite tower of higher-derivative terms in the induced action (the $\mathcal{O}(\ell^2)$ term being that of new massive gravity) eliminates the logarithmic dependence.

[27] This can be easily seen by performing the coordinate transformation $t \to \tilde{t} - ax_1^2\tilde{\phi}$ and $\phi \to \tilde{\phi}$ in the brane geometry (80). For large r, the $h_{\tilde{t}\tilde{\phi}}$ component of the geometry diverges as r^2.

[28] In addition to the local counterterms in pure gravity, p-form fields F_p (where $p = 2$ corresponds to Maxwell) may require a local counterterm subtraction. As reported in [97], for a $d+1$-dimensional bulk, when $d < 2p$, there are no divergences, while a logarithmic divergence appears for $d = 2p$, and there will be divergences for $d > 2p$. Further, for $d = 2p + 2n$ with $n \in \mathbb{Z}^+$, derivatives of F_p and its coupling to curvature appear in the conformal anomaly such that counterterms are needed for $d > 2p + 2n$. Thus, the four-dimensional Maxwell action has no divergences as the IR cutoff $\epsilon \to 0$. Such terms, however, contribute to the brane because the brane effective action keeps the cutoff finite and non-zero.

[29] The rotating qBTZ metric (91) follows from the double replacement $\ell_3 \to iR_3$ and $a_{AdS_3} \to -a_{dS_3}$ such that $\tilde{a}_{AdS_3} \to i\tilde{a}_{dS_3}$.

[30] By AdS 'horizon', we mean the null hypersurface infinitely far from the brane in spacelike directions, but it can nonetheless be reached by an observer in finite proper time.

[31] In [22,23], only the naive brane metric is analyzed. While our analysis is qualitatively similar, some of the precise expressions differ.

[32] A first law for the charged C-metric with vanishing cosmological constant was derived in [122] using covariant phase space methods, where, moreover, 'boost time' was treated as canonical time.

[33] More carefully, the projection of the bulk Killing vector $\zeta^\mu = \partial_t^\mu$ is $k^a = h^a_\mu \zeta^\mu$ for projector h^a_μ. Consequently, the surface gravity κ on the brane coincides with the bulk surface gravity: $k^a D_a k^b = \kappa k^b$, for projected covariant derivative D_a, implies $h^a_\nu(\zeta^\mu \nabla_\mu \zeta^\nu) = h^a_\nu(\kappa \zeta^\nu)$.

[34] It is not obvious that Equation (205) is geometrically equal to the BTZ black hole entropy. Indeed, substituting $z = \ell_3/x_1 r_+$ into (205) does not yield the usual $S_{\rm BTZ} = 2\pi r_+/4G_3$. This is because the qBTZ represents a family of black hole solutions and a specific x_1 must be chosen to match the classical black hole. Nonetheless, for any z, the relation (205) holds.

[35] Strictly speaking, the entropy (207) follows from an application of the field redefinition method for computing entropy of higher-curvature theories [129]; see their Equation (20) with $a_1 = -1$, $a_2 = \frac{3}{8}$ and $16\pi G_3 \lambda = \ell^2$.

[36] Note $q^{ij} = h^{ij} + n^i n^j - u^i u^j$ for spacelike and timelike unit normals n^i and u^i, respectively. The binormal $\epsilon_{ij} = (n_i u_j - n_j u_i)$ satisfies $\epsilon^2 = -2$, and $\epsilon^k_{\ j} \epsilon_{kl} = (u_j u_l - n_l n_j) \equiv g^\perp_{jl} = g_{jl} - q_{jl}$ for bulk metric g_{ij}.

[37] If we replace $S^{(3)}_{\rm BH}$ by $S_{\rm BTZ}$ in the Iyer–Wald entropy (211), the leading contribution in $S^{(3)}_{\rm CFT}$ is precisely the second term in (204).

[38] The parametrization depends on $\kappa = \text{sign}(\nu z^3 - 1)$, such that the range of the three branches is covered by imposing $0 \leq \nu, z \leq \infty$.

[39] Start with $H(r_+) = 0$, replace $r_+ = \ell_3/z x_1$, $q x_1^2 = \gamma$, and $\mu = (1 - \kappa x_1^2 - \gamma^2)/x_1^3$, and then rearrange.

[40] The thermodynamics of the rotating qBTZ solution follows from the reassignments $\ell_3^2 \to -R_3^2$ and $a \to -a$, such that $z^2 \to -z^2$, $\nu^2 \to -\nu^2$ and $\nu z \to \nu z$.

[41] Note the mass (259) and temperature (261) differ from those reported in [22,23], which is a consequence of us working in canonically normalized coordinates. Moreover, the mass in [23] is identified as the result of explicitly integrating $T dS^{(4)}_{\rm BH} = T \partial_{\hat{x}} S^{(4)}_{\rm BH} d\hat{x}$.

[42] For $\mu \ll 1$, the real positive root x_1 to $G(x) = 0$ is $x_1 \approx 1 - \mu$, such that $\hat{x} = \mu x_1 \approx \mu$. Meanwhile, the real positive root x_1 for $\mu \gg 1$ is $x_1 \approx \mu^{-1/3}$.

[43] The interpretation of the thermodynamic volume remains fairly mysterious. In simple cases, e.g., static black holes in $d+1 \geq 4$, v coincides with the geometric volume occupied by the black hole, i.e., the amount of spacetime volume excluded by the black hole horizon. Generally, however, the thermodynamic volume (270) differs from the geometric volume [142–144].

[44] This is not to say the thermodynamic volume does not have a geometric character. Indeed, in classical gravity, the thermodynamic volume has a geometric definition in terms of Komar integrals. In this sense, moreover, the definition of the thermodynamic volume is independent of treating the cosmological constant as a thermodynamic variable.

[45] In $D \geq 4$, 'ultraspinning' black holes [160–162] were initially thought to obey $\mathcal{R} < 1$, thus violating (276); however, this has been called into question [163]. In $D = 3$, only the electrically charged BTZ black hole violates the reverse isoperimetric inequality [164].

[46] Other ensembles are equally intriguing. For a discussion on the constant c and V ensemble, characterized by the Gibbs free energy $G = M + PV - TS$, see for example [170,171].

[47] Notably, the three branches described here do not coincide with branches $1a$, $1b$, and 2 characterizing the mass of the qBTZ [25]. A more detailed study of these phases, including a stability analysis and their critical behavior, was given in [124,170,171]. Interestingly, in a fixed c and V ensemble, phase transitions between cold and hot black holes occur, demonstrating continuous critical phenomena along the coexistence curve, with critical exponents that deviate from those observed in mean-field Van der Waals fluids [171].

[48] Even in a fixed background, explicit computations of $\langle T_{ij} \rangle$ are complicated and limited, cf. [1,177].

[49] In [185], it was argued that one can construct exact analytic static, spherically symmetric solutions (see [186] for a stationary generalization) if one imposes an equation of state on the quantum stress tensor such that the type-B trace anomaly vanishes.

[50] There are, however, accelerating black holes in AdS_3, cf. [187–191].

[51] To arrive at the second equality, use that in d-spacetime dimensions $\hbar G_d = (L_{\rm P}^{(d)})^{d-2}$ and the relation between the brane and bulk Newton's constants (35). Then, for $d = 4$, $(L_{\rm P}^{(5)})^3 = L_5 (L_{\rm P}^{(4)})^2$.

[52] Roughly, the argument of [69] is as follows. Consider $\mathcal{N} = 4$ $SU(N)$ super Yang–Mills theory on a sphere of radius R. There are weakly interacting states ('glueballs') with energies $ER \ll N^2$ and strongly coupled states with energies $ER \gg N^2$. At large 't Hooft coupling λ, AdS/CFT says the field theory is dual to closed string theory, where the glueball states correspond to perturbative string excitations in the ambient spacetime. Further, in this limit, the energy separation for weakly interacting states goes like $\Delta E \sim \lambda^{1/4}/R$. Hence, the glueball spectrum is lifted to infinite energy apart from the $\mathcal{O}(1)$ massless states dual to the supergravity modes of the string and gravitational perturbations dual to $\mathcal{O}(1)$ of the $\mathcal{O}(N^2)$ states. A caveat to this reasoning, however, is that in the flat space limit $R \to \infty$, the mass gap might disappear.

[53] Fitzpatrick, Randall, and Wiseman also argue that the dynamical instability dual to semi-classical evaporation is unlikely to occur [69]. Even if it did, the timescales of the bulk Gregory–Laflamme instability and thermodynamic instability of the Schwarzschild black hole via Hawking radiation are different [209].

54 A detailed comparison of holographic versus non-holographic stress tensors was made in [202] using an approach developed by Page [211] to compute the renormalized stress tensor of a (non-holographiic) conformally coupled scalar field in AdS_4-Schwarzschild.

55 The appeal of the large-D limit is that the effective dynamics of the (bulk) black hole horizon is encoded in a set of two partial differential equations which can be solved numerically and quickly. A large-D expansion of the Israel junction conditions is then used to determine the location of the brane intersecting the bulk black hole, and it amounts to imposing a simple pair of Neumann boundary conditions. Note, however, a limitation of the large-D effective theory is that the induced brane theory is not well characterized by a $(D-1)$-dimensional gravity. This is because with these limits, the induced theory has large corrections on the brane from the higher-derivative terms such that the brane gravity behaves more like a D-dimensional theory. A possible interpretation is that the induced theory describes a semi-classical theory where backreaction effects are large.

56 The RT formula can be directly derived from the gravitational Rényi entropy [228] (see also [229–232]).

57 See also [239] for a similar treatment in the context of braneworlds.

58 Explicit realizations of the equivalence between gravitational and entanglement entropies in two-dimensional braneworld models pre-date the Ryu-Takayanagi prescription [249,250].

59 The island rule has been derived in two-dimensional Jackiw–Teitelboim gravity using the Euclidean gravitational path integral to compute the Rényi entropy [256–258] or the microcanonical action [134,259].

60 The homology constraint for the RT surfaces depends on which perspective in double holography is being employed [262].

61 The argument of [54,260] requires DGP couplings be turned on, which can affect the growth rate of entanglement entropy of subregions of the dual CFT [263]. Alternatively, the intersection term naturally arises using deformed braneworlds [83].

62 Semi-classical extensions of CV complexity have been proposed and explored with [288,291] and without [276] holographic braneworlds.

63 Alternatively, leading-order perturbative backreaction was found to yield singular inner horizons in [44,45].

64 A notion of weak quantum cosmic censorship may directly follow from 'cryptographic censorship' [313]: a theorem that states when the time evolution operator of a holographic CFT is approximately pseudorandom on a code subspace, there must be an event horizon in the corresponding bulk dual. Incidentally, certain types of singularities are compatible with approximately pseudorandom time evolution, and thus, by cryptographic censorship, are hidden behind event horizons.

65 The connection between hydrodynamics and chaos in 2+1 dimensional Einstein gravity is subtle, because metric fluctuations are pure gauge. This issue is alleviated in braneworld models as they typically contain a massive graviton. Furthermore, a general hydrodynamic framework for chaotic dynamics in 1+1 CFTs has been established [320], linking it to the field theory of soft modes associated with holomorphic and antiholomorphic parameterizations. For further discussion in the context of classical BTZ black holes, see [321].

66 The asymptotic boundary also lives at $\rho \to \infty$; however, we restrict ourselves to the region near $\rho = 0$.

67 We work in the convention where the Riemann curvature tensor is $R^{\rho}{}_{\sigma\mu\nu} = \partial_\mu \Gamma^{\rho}_{\nu\sigma} + \Gamma^{\rho}_{\mu\lambda}\Gamma^{\lambda}_{\nu\sigma} - (\mu \leftrightarrow \nu)$. Equivalently, $R^{\rho}{}_{\sigma\mu\nu} = -[\nabla_\mu, \nabla_\nu]V_\nu$ and $R^{\rho}{}_{\sigma\mu\nu}V^\sigma = [\nabla_\mu, \nabla_\nu]V^\rho$ for vectors V. This convention differs from the one used in [19] by an overall minus sign. In our convention, AdS curvature is negative, while in [19], AdS curvature is positive.

68 Note that Equation (7) of [50] differs by an overall sign and a factor of L^2 from our expression (A19). The difference in sign comes from a different convention for the Riemann tensor, one where the cosmological constant for AdS is 'positive', and the L^2 comes from the form of the metric where $h^{there}_{ij} = L^{-2}h^{here}_{ij}$.

69 To aid the reader, here, for example, $g^{jk}g'_{jk} = \mathrm{Tr}(g^{-1}g')$. Further, to find the first expression in (A22), contract the first expression in (A21) by g^{jk}. Then, add zero to the term proportional to ρ as $(g^{ik}g'_{jk}g'_{il} - g^{ik}g'_{jk}g'_{il})$ and use the second expression in (A21) to recast $g^{ik}g'_{jk}g'_{il} = 2g''_{jl}$.

70 Recall that for general dimension d, the analysis only applies near $\rho = 0$, where the Weyl tensor of the bulk spacetime vanishes. Consequently, ρ-integration is performed around $\rho = \epsilon$. Alternatively, when $d = 2$, since the three-dimensional Weyl tensor is identically zero everywhere, the perturbative expansion $g_{ij}(\rho, x)$ truncates and the ρ-integration can be carried out explicitly (see, e.g., [19,50]).

71 Note that naively, $a_{(2)}$ is not valid when $d = 2$. The correct term can be found by performing the analysis explicitly when $d = 2$, yielding $a^{d=2}_{(2)} = \mathrm{Tr}g_{(2)}$. Similarly, $a_{(4)}$ (which we did not explicitly compute; see [19]) has the coefficient in front replaced with $1/2$ when $d = 4$.

72 To see this, write $\nabla_a\nabla_i R^a_j = \nabla_i\nabla_a R^a_j + g^{ab}[\nabla_a, \nabla_i]R_{bj}$, and then use the contracted Bianchi identity $\nabla_a R^a_{\ j} = \frac{1}{2}\nabla_j R$ and $[\nabla_a, \nabla_i]R_{bj} = -R^k_{\ bai}R_{kj} - R^k_{\ jai}R_{bk}$.

73 Historically, the RS models assumed a five-dimensional bulk and four-dimensional brane. More generally, the bulk need not be restricted to five dimensions, e.g., in this review, we consider a four-dimensional bulk AdS spacetime and three-dimensional branes.

[74] Simply, KK excitations are light, have non-vanishing momentum along the extra dimension, and become suppressed near the brane, essentially decoupling from matter fields on the brane. Gravitational interactions between the matter fields are mediated by the 'zero mode'.

[75] Garriga and Tanaka [324] applied a similar perturbative analysis to the RS-I scenario and found the effective linearized gravity on either brane to be Brans–Dicke theory (with different Brans–Dicke parameters), where the Brans–Dicke scalar, i.e,. the 'radion' captures the displacement between the branes.

[76] Stringy realizations of the KR construction were uncovered in [16,326–328] (and more recently, [59]).

[77] A coordinate rescaling brings us to the $L_5 = L_{\rm P}^{(10)}(g_s N)^{1/4}$ in Section 6.

[78] Historically, the original C-metric belonged to a classification of types of black hole solutions to Einstein–Maxwell theory owed to Levi–Civita in 1918 [332]. These solutions we rediscovered in the 1960s and further classified, particularly by Ehlers and Kundt [333], giving the naming scheme of black holes of A,B and C-type metrics. It was not until 1970 that Kinnersley and Walker understood the C-metric as an accelerated black hole [334]. In 1976, Plebanski and Demianski [89] showed how the C-metric is embedded in a larger family of algebraic type-D solutions. For more on the history and aspects of the C-metric, see [121].

[79] Refer to Equation (2.1) [89] with metric functions in Equation (3.25). Here, however, we take p, q and σ to have opposite signs. For further details of the PD spacetimes and its various limits, see, e.g., [335–338].

[80] Hong and Teo note that the only way to remove the closed timelike curves is when the angular velocity of the conical singularities have the same constant value along the entire axis of symmetry [340].

[81] The cubic $G(x) = -2mAx^3 + kx^2 + 1 = 0$ can be solved by introducing $x = z - \frac{k}{3}$ and expressed in depressed form, $z^3 + pz + q = 0$, with $p = -\frac{k^2}{12(mA)^2}$, $q = -\frac{[2k^3+27(4mA)^2]}{27(2mA)^3}$, and discriminant $\Delta \equiv -(4p^3 + 27q^2) = -\frac{k^3+27(mA)^2}{4(mA)^4}$. For $\Delta > 0$, $G(x)$ has three distinct real roots. For example, for $k = -1$, three real roots $x_0 < x_2 < 0 < x_1$ exist when $0 < mA < \frac{1}{3\sqrt{3}}$ [23]. For $\Delta < 0$, $G(x)$ will have one real and two complex roots.

[82] To see this, introduce $\tilde{x}^2 = 4(x - x_i)/G'(x_i)$. Expand the (x, ϕ) sector of (A110) about a zero of $G(x)$,

$$G^{-1}(x)dx^2 + G(x)d\phi^2 \approx [G'(x_i)(x - x_i)]^{-1}dx^2 + G'(x_i)(x - x_i)d\phi^2 = \tilde{x}^2(G'(x_i)/2)^2 d\phi^2 + d\tilde{x}^2.$$

Periodicity (A115) then follows from imposing regularity at $\tilde{x} = 0$.

[83] This relation follows from having set the periodicity (A115), such that the coordinate range for ϕ is to $0 \le \phi \le \Delta\phi(x_1) - \delta$, where δ is the angular deficit associated with the other conical singularities at $x_i \neq x_1$.

[84] Since here we work with metric (A143), which differs from metric (A110) by $H(y) \to -H(y)$, the $\sqrt{-\lambda}$ coefficient in (A119) is replaced with $-\sqrt{\lambda}$.

[85] In particular, for $k = +1$, then $0 \le z < \nu^{2/3}$, while for $k = -1$, then $\nu^{2/3} < z \le \infty$. Meanwhile, for $k = 0$, one has $\mu = 1/x_1^{1/3}$, and $y_+ = (\nu^2/\mu)^{1/3}$, such that $z = \nu^{2/3}$.

[86] It is also useful to $\Delta\phi = 4\pi x_1/(3 + kx_1^2)$ and $\Delta t_E = 4\pi x_1/z(2kx_1^2 + 3z(1 + kx_1^2))$.

References

1. Birrell, N.D.; Davies, P.C.W. *Quantum Fields in Curved Space*; Cambridge Monographs on Mathematical Physics; Cambridge University Press: Cambridge, UK, 1984.
2. Wald, R.M. *Quantum Field Theory in Curved Space-Time and Black Hole Thermodynamics*; Chicago Lectures in Physics; University of Chicago Press: Chicago, IL, USA, 1995.
3. Page, D.N.; Geilker, C.D. Indirect Evidence for Quantum Gravity. *Phys. Rev. Lett.* **1981**, *47*, 979–982. [CrossRef]
4. Polyakov, A.M. Quantum Geometry of Bosonic Strings. *Phys. Lett. B* **1981**, *103*, 207–210. [CrossRef]
5. Christensen, S.M.; Fulling, S.A. Trace Anomalies and the Hawking Effect. *Phys. Rev. D* **1977**, *15*, 2088–2104. [CrossRef]
6. Maldacena, J.M. The Large N limit of superconformal field theories and supergravity. *Adv. Theor. Math. Phys.* **1998**, *2*, 231–252. [CrossRef]
7. 't Hooft, G. Dimensional reduction in quantum gravity. *Conf. Proc. C* **1993**, *930308*, 284–296.
8. Susskind, L. The World as a hologram. *J. Math. Phys.* **1995**, *36*, 6377–6396. [CrossRef]
9. Hubeny, V.E.; Marolf, D.; Rangamani, M. Hawking radiation in large N strongly-coupled field theories. *Class. Quant. Grav.* **2010**, *27*, 095015. [CrossRef]
10. Compere, G.; Marolf, D. Setting the boundary free in AdS/CFT. *Class. Quant. Grav.* **2008**, *25*, 195014. [CrossRef]
11. de Haro, S.; Skenderis, K.; Solodukhin, S.N. Gravity in warped compactifications and the holographic stress tensor. *Class. Quant. Grav.* **2001**, *18*, 3171–3180. [CrossRef]
12. Arkani-Hamed, N.; Dimopoulos, S.; Dvali, G.R. The Hierarchy problem and new dimensions at a millimeter. *Phys. Lett. B* **1998**, *429*, 263–272. [CrossRef]
13. Randall, L.; Sundrum, R. A Large mass hierarchy from a small extra dimension. *Phys. Rev. Lett.* **1999**, *83*, 3370–3373. [CrossRef]
14. Randall, L.; Sundrum, R. An Alternative to compactification. *Phys. Rev. Lett.* **1999**, *83*, 4690–4693. [CrossRef]
15. Karch, A.; Randall, L. Locally localized gravity. *J. High Energy Phys.* **2001**, *2001*, 8. [CrossRef]

16. Karch, A.; Randall, L. Open and closed string interpretation of SUSY CFT's on branes with boundaries. *J. High Energy Phys.* **2001**, *2001*, 63. [CrossRef]
17. Kraus, P.; Larsen, F.; Siebelink, R. The gravitational action in asymptotically AdS and flat space-times. *Nucl. Phys. B* **1999**, *563*, 259–278. [CrossRef]
18. Emparan, R.; Johnson, C.V.; Myers, R.C. Surface terms as counterterms in the AdS / CFT correspondence. *Phys. Rev. D* **1999**, *60*, 104001. [CrossRef]
19. de Haro, S.; Solodukhin, S.N.; Skenderis, K. Holographic reconstruction of space-time and renormalization in the AdS / CFT correspondence. *Commun. Math. Phys.* **2001**, *217*, 595–622. [CrossRef]
20. Skenderis, K. Lecture notes on holographic renormalization. *Class. Quant. Grav.* **2002**, *19*, 5849–5876. [CrossRef]
21. Papadimitriou, I.; Skenderis, K. AdS / CFT correspondence and geometry. *IRMA Lect. Math. Theor. Phys.* **2005**, *8*, 73–101. [CrossRef]
22. Emparan, R.; Fabbri, A.; Kaloper, N. Quantum black holes as holograms in AdS brane worlds. *J. High Energy Phys.* **2002**, *2002*, 43. [CrossRef]
23. Emparan, R.; Horowitz, G.T.; Myers, R.C. Exact description of black holes on branes. *J. High Energy Phys.* **2000**, *2000*, 7. [CrossRef]
24. Emparan, R.; Horowitz, G.T.; Myers, R.C. Exact description of black holes on branes. 2. Comparison with BTZ black holes and black strings. *J. High Energy Phys.* **2000**, *2000*, 21. [CrossRef]
25. Emparan, R.; Frassino, A.M.; Way, B. Quantum BTZ black hole. *J. High Energy Phys.* **2020**, *2020*, 137. [CrossRef]
26. Emparan, R.; Pedraza, J.F.; Svesko, A.; Tomašević, M.; Visser, M.R. Black holes in dS_3. *J. High Energy Phys.* **2022**, *2022*, 73. [CrossRef]
27. Panella, E.; Svesko, A. Quantum Kerr-de Sitter black holes in three dimensions. *J. High Energy Phys.* **2023**, *2023*, 127. [CrossRef]
28. Deser, S.; Jackiw, R.; 't Hooft, G. Three-Dimensional Einstein Gravity: Dynamics of Flat Space. *Ann. Phys.* **1984**, *152*, 220. [CrossRef]
29. Deser, S.; Jackiw, R. Three-Dimensional Cosmological Gravity: Dynamics of Constant Curvature. *Ann. Phys.* **1984**, *153*, 405–416. [CrossRef]
30. Banados, M.; Teitelboim, C.; Zanelli, J. The Black hole in three-dimensional space-time. *Phys. Rev. Lett.* **1992**, *69*, 1849–1851. [CrossRef]
31. Banados, M.; Henneaux, M.; Teitelboim, C.; Zanelli, J. Geometry of the (2+1) black hole. *Phys. Rev. D* **1993**, *48*, 1506–1525, Erratum in *Phys. Rev. D* **2013**, *88*, 069902. [CrossRef]
32. Souradeep, T.; Sahni, V. Quantum effects near a point mass in (2+1)-Dimensional gravity. *Phys. Rev. D* **1992**, *46*, 1616–1633. [CrossRef]
33. Soleng, H.H. Inverse square law of gravitation in (2+1) dimensional space-time as a consequence of Casimir energy. *Phys. Scr.* **1993**, *48*, 649–652. [CrossRef]
34. Tanaka, T. Classical black hole evaporation in Randall–Sundrum infinite brane world. *Prog. Theor. Phys. Suppl.* **2003**, *148*, 307–316. [CrossRef]
35. Ross, S.F.; Mann, R.B. Gravitationally collapsing dust in (2+1)-dimensions. *Phys. Rev. D* **1993**, *47*, 3319–3322. [CrossRef]
36. de Buyl, S.; Detournay, S.; Giribet, G.; Ng, G.S. Baby de Sitter black holes and dS_3/CFT_2. *J. High Energy Phys.* **2014**, *2014*, 20. [CrossRef]
37. Nutku, Y. Exact solutions of topologically massive gravity with a cosmological constant. *Class. Quant. Grav.* **1993**, *10*, 2657–2661. [CrossRef]
38. Anninos, D. Sailing from Warped AdS(3) to Warped dS(3) in Topologically Massive Gravity. *J. High Energy Phys.* **2010**, *2010*, 46. [CrossRef]
39. Bousso, R.; Maloney, A.; Strominger, A. Conformal vacua and entropy in de Sitter space. *Phys. Rev. D* **2002**, *65*, 104039. [CrossRef]
40. Steif, A.R. The Quantum stress tensor in the three-dimensional black hole. *Phys. Rev. D* **1994**, *49*, 585–589. [CrossRef]
41. Shiraishi, K.; Maki, T. Quantum fluctuation of stress tensor and black holes in three dimensions. *Phys. Rev. D* **1994**, *49*, 5286–5294. [CrossRef]
42. Lifschytz, G.; Ortiz, M. Scalar field quantization on the (2+1)-dimensional black hole background. *Phys. Rev. D* **1994**, *49*, 1929–1943. [CrossRef]
43. Martinez, C.; Zanelli, J. Back reaction of a conformal field on a three-dimensional black hole. *Phys. Rev. D* **1997**, *55*, 3642–3646. [CrossRef]
44. Casals, M.; Fabbri, A.; Martínez, C.; Zanelli, J. Quantum dress for a naked singularity. *Phys. Lett. B* **2016**, *760*, 244–248. [CrossRef]
45. Casals, M.; Fabbri, A.; Martínez, C.; Zanelli, J. Quantum-corrected rotating black holes and naked singularities in (2+1) dimensions. *Phys. Rev. D* **2019**, *99*, 104023. [CrossRef]
46. Gubser, S.S.; Klebanov, I.R.; Polyakov, A.M. Gauge theory correlators from noncritical string theory. *Phys. Lett. B* **1998**, *428*, 105–114. [CrossRef]
47. Witten, E. Anti-de Sitter space and holography. *Adv. Theor. Math. Phys.* **1998**, *2*, 253–291. [CrossRef]
48. Fefferman, C.; Graham, C.R. Conformal invariants. In *Élie Cartan et les Mathématiques D'aujourd'hui—Lyon, 25–29 Juin 1984*; Number S131 in Astérisque; Société Mathématique de France: Paris, France, 1985.
49. Fefferman, C.; Graham, C.R. The ambient metric. *Ann. Math. Stud.* **2011**, *178*, 1–128.

50. Skenderis, K.; Solodukhin, S.N. Quantum effective action from the AdS / CFT correspondence. *Phys. Lett. B* **2000**, *472*, 316–322. [CrossRef]
51. Elvang, H.; Hadjiantonis, M. A Practical Approach to the Hamilton-Jacobi Formulation of Holographic Renormalization. *J. High Energy Phys.* **2016**, *2016*, 46. [CrossRef]
52. Bueno, P.; Emparan, R.; Llorens, Q. Higher-curvature Gravities from Braneworlds and the Holographic c-theorem. *Phys. Rev. D* **2022**, *106*, 044012. [CrossRef]
53. Israel, W. Singular hypersurfaces and thin shells in general relativity. *Nuovo Cim. B* **1966**, *44*, 1–14; Erratum in *Nuovo Cim. B* **1967**, *48*, 463. [CrossRef]
54. Chen, H.Z.; Myers, R.C.; Neuenfeld, D.; Reyes, I.A.; Sandor, J. Quantum Extremal Islands Made Easy, Part I: Entanglement on the Brane. *J. High Energy Phys.* **2020**, *2020*, 166. [CrossRef]
55. Emparan, R. Black hole entropy as entanglement entropy: A Holographic derivation. *J. High Energy Phys.* **2006**, *2006*, 12. [CrossRef]
56. Myers, R.C.; Pourhasan, R.; Smolkin, M. On Spacetime Entanglement. *J. High Energy Phys.* **2013**, *2013*, 13. [CrossRef]
57. Takayanagi, T. Holographic Dual of BCFT. *Phys. Rev. Lett.* **2011**, *107*, 101602. [CrossRef]
58. Fujita, M.; Takayanagi, T.; Tonni, E. Aspects of AdS/BCFT. *J. High Energy Phys.* **2011**, *2011*, 43. [CrossRef]
59. Karch, A.; Sun, H.; Uhlemann, C.F. Double holography in string theory. *J. High Energy Phys.* **2022**, *2022*, 12. [CrossRef]
60. Omiya, H.; Wei, Z. Causal structures and nonlocality in double holography. *J. High Energy Phys.* **2022**, *2022*, 128. [CrossRef]
61. Neuenfeld, D.; Srivastava, M. On the causality paradox and the Karch-Randall braneworld as an EFT. *J. High Energy Phys.* **2023**, *2023*, 164. [CrossRef]
62. Duff, M.J.; Liu, J.T. Complementarity of the Maldacena and Randall-Sundrum pictures. *Phys. Rev. Lett.* **2000**, *85*, 2052–2055. [CrossRef]
63. Duff, M.J. Quantum corrections to the schwarzschild solution. *Phys. Rev. D* **1974**, *9*, 1837–1839. [CrossRef]
64. Tanahashi, N.; Tanaka, T. Black holes in braneworld models. *Prog. Theor. Phys. Suppl.* **2011**, *189*, 227–268. [CrossRef]
65. Chen, H.Z.; Myers, R.C.; Neuenfeld, D.; Reyes, I.A.; Sandor, J. Quantum Extremal Islands Made Easy, Part II: Black Holes on the Brane. *J. High Energy Phys.* **2020**, *2020*, 25. [CrossRef]
66. Bruni, M.; Germani, C.; Maartens, R. Gravitational collapse on the brane. *Phys. Rev. Lett.* **2001**, *87*, 231302. [CrossRef] [PubMed]
67. Kudoh, H.; Tanaka, T.; Nakamura, T. Small localized black holes in brane world: Formulation and numerical method. *Phys. Rev. D* **2003**, *68*, 024035. [CrossRef]
68. Kudoh, H. Six-dimensional localized black holes: Numerical solutions. *Phys. Rev. D* **2004**, *69*, 104019; Erratum in *Phys. Rev. D* **2004**, *70*, 029901. [CrossRef]
69. Fitzpatrick, A.L.; Randall, L.; Wiseman, T. On the existence and dynamics of braneworld black holes. *J. High Energy Phys.* **2006**, *2006*, 33. [CrossRef]
70. Yoshino, H. On the existence of a static black hole on a brane. *J. High Energy Phys.* **2009**, *2009*, 68. [CrossRef]
71. Figueras, P.; Wiseman, T. Gravity and large black holes in Randall-Sundrum II braneworlds. *Phys. Rev. Lett.* **2011**, *107*, 081101. [CrossRef]
72. Emparan, R.; Luna, R.; Suzuki, R.; Tomašević, M.; Way, B. Holographic duals of evaporating black holes. *J. High Energy Phys.* **2023**, *2023*, 182. [CrossRef]
73. Henningson, M.; Skenderis, K. The Holographic Weyl anomaly. *J. High Energy Phys.* **1998**, *1998*, 23. [CrossRef]
74. Carlip, S. Dynamics of asymptotic diffeomorphisms in (2+1)-dimensional gravity. *Class. Quant. Grav.* **2005**, *22*, 3055–3060. [CrossRef]
75. Nguyen, K. Holographic boundary actions in AdS_3/CFT_2 revisited. *J. High Energy Phys.* **2021**, *2021*, 218. [CrossRef]
76. Dvali, G. Black Holes and Large N Species Solution to the Hierarchy Problem. *Fortsch. Phys.* **2010**, *58*, 528–536. [CrossRef]
77. Jackiw, R. Lower Dimensional Gravity. *Nucl. Phys. B* **1985**, *252*, 343–356. [CrossRef]
78. Teitelboim, C. Gravitation and Hamiltonian Structure in Two Space-Time Dimensions. *Phys. Lett. B* **1983**, *126*, 41–45. [CrossRef]
79. Geng, H. Aspects of AdS_2 quantum gravity and the Karch-Randall braneworld. *J. High Energy Phys.* **2022**, *2022*, 24. [CrossRef]
80. Geng, H.; Karch, A.; Perez-Pardavila, C.; Raju, S.; Randall, L.; Riojas, M.; Shashi, S. Jackiw-Teitelboim Gravity from the Karch-Randall Braneworld. *Phys. Rev. Lett.* **2022**, *129*, 231601. [CrossRef]
81. Bhattacharjee, A.; Saha, M. JT gravity from holographic reduction of 3D asymptotically flat spacetime. *J. High Energy Phys.* **2023**, *2023*, 138. [CrossRef]
82. Aguilar-Gutierrez, S.E.; Patra, A.K.; Pedraza, J.F. Entangled universes in dS wedge holography. *J. High Energy Phys.* **2023**, *2023*, 156. [CrossRef]
83. Neuenfeld, D.; Svesko, A.; Sybesma, W. Liouville gravity at the end of the world: Deformed defects in AdS/BCFT. *J. High Energy Phys.* **2024**, *2024*, 215. [CrossRef]
84. Callan, C.G., Jr.; Giddings, S.B.; Harvey, J.A.; Strominger, A. Evanescent black holes. *Phys. Rev. D* **1992**, *45*, R1005. [CrossRef] [PubMed]
85. Russo, J.G.; Susskind, L.; Thorlacius, L. The Endpoint of Hawking radiation. *Phys. Rev. D* **1992**, *46*, 3444–3449. [CrossRef]
86. Susskind, L.; Thorlacius, L.; Uglum, J. The Stretched horizon and black hole complementarity. *Phys. Rev. D* **1993**, *48*, 3743–3761. [CrossRef]

87. Fiola, T.M.; Preskill, J.; Strominger, A.; Trivedi, S.P. Black hole thermodynamics and information loss in two-dimensions. *Phys. Rev. D* **1994**, *50*, 3987–4014. [CrossRef]
88. Emparan, R.; Horowitz, G.T.; Myers, R.C. Black holes radiate mainly on the brane. *Phys. Rev. Lett.* **2000**, *85*, 499–502. [CrossRef] [PubMed]
89. Plebanski, J.F.; Demianski, M. Rotating, charged, and uniformly accelerating mass in general relativity. *Ann. Phys.* **1976**, *98*, 98–127. [CrossRef]
90. Podolsky, J. Accelerating black holes in anti-de Sitter universe. *Czech. J. Phys.* **2002**, *52*, 1–10. [CrossRef]
91. Emparan, R.; Frassino, A.M.; Sasieta, M.; Tomašević, M. Holographic complexity of quantum black holes. *J. High Energy Phys.* **2022**, *2022*, 204. [CrossRef]
92. Cremonini, S.; Liu, J.T.; Szepietowski, P. Higher Derivative Corrections to R-charged Black Holes: Boundary Counterterms and the Mass-Charge Relation. *J. High Energy Phys.* **2010**, *2010*, 42. [CrossRef]
93. Chernicoff, M.; Giribet, G.; Moreno, J.; Oliva, J.; Rojas, R.; Torres, C.R.d.A. Quantum backreactions in (A)dS3 massive gravity and logarithmic asymptotic behavior. *Phys. Rev. D* **2024**, *110*, 044021. [CrossRef]
94. Caldarelli, M.M.; Cognola, G.; Klemm, D. Thermodynamics of Kerr-Newman-AdS black holes and conformal field theories. *Class. Quant. Grav.* **2000**, *17*, 399–420. [CrossRef]
95. Gibbons, G.W.; Perry, M.J.; Pope, C.N. The First law of thermodynamics for Kerr-anti-de Sitter black holes. *Class. Quant. Grav.* **2005**, *22*, 1503–1526. [CrossRef]
96. Lemos, J.P.S.; Luz, P. All fundamental electrically charged thin shells in general relativity: From star shells to tension shell black holes, regular black holes, and beyond. *Phys. Rev. D* **2021**, *103*, 104046. [CrossRef]
97. Taylor, M. More on counterterms in the gravitational action and anomalies. *arXiv* **2000**, arXiv:0002125.
98. Climent, A.; Emparan, R.; Hennigar, R.A. Chemical Potential and Charge in Quantum Black Holes. *J. High Energy Phys.* **2024**, *2024*, 150.
99. Feng, Y.; Ma, H.; Mann, R.B.; Xue, Y.; Zhang, M. Quantum Charged Black Holes. *arXiv* **2024**, arXiv:2404.07192. [CrossRef]
100. Martinez, C.; Teitelboim, C.; Zanelli, J. Charged rotating black hole in three space-time dimensions. *Phys. Rev. D* **2000**, *61*, 104013. [CrossRef]
101. Emparan, R.; Gregory, R.; Santos, C. Black holes on thick branes. *Phys. Rev. D* **2001**, *63*, 104022. [CrossRef]
102. Maldacena, J. Vacuum decay into Anti de Sitter space. *arXiv* **2010**, arXiv:1012.0274.
103. Barbon, J.L.F.; Rabinovici, E. Holography of AdS vacuum bubbles. *J. High Energy Phys.* **2010**, *2010*, 123. [CrossRef]
104. Barbon, J.L.F.; Rabinovici, E. AdS Crunches, CFT Falls And Cosmological Complementarity. *J. High Energy Phys.* **2011**, *2011*, 44. [CrossRef]
105. Coleman, S.R.; De Luccia, F. Gravitational Effects on and of Vacuum Decay. *Phys. Rev. D* **1980**, *21*, 3305. [CrossRef]
106. Nariai, H. On a New Cosmological Solution of Einstein's Field Equations of Gravitation. *Gen. Relativ. Gravit.* **1999**, *31*, 963–971. [CrossRef]
107. Booth, I.S.; Mann, R.B. Cosmological pair production of charged and rotating black holes. *Nucl. Phys. B* **1999**, *539*, 267–306. [CrossRef]
108. Bhattacharya, S. Kerr-de Sitter spacetime, Penrose process and the generalized area theorem. *Phys. Rev. D* **2018**, *97*, 084049. [CrossRef]
109. Anninos, D.; de Buyl, S.; Detournay, S. Holography For a De Sitter-Esque Geometry. *J. High Energy Phys.* **2011**, *2011*, 3. [CrossRef]
110. Climent, A.; Hennigar, R.; Panella, E.; Svesko, A. *Unpublished work.*
111. Bekenstein, J.D. Black holes and the second law. *Lett. Nuovo Cim.* **1972**, *4*, 737–740. [CrossRef]
112. Bekenstein, J.D. Black holes and entropy. *Phys. Rev. D* **1973**, *7*, 2333–2346. [CrossRef]
113. Hawking, S.W. Particle Creation by Black Holes. *Commun. Math. Phys.* **1975**, *43*, 199–220, Erratum in *Commun. Math. Phys.* **1976**, *46*, 206. [CrossRef]
114. Hawking, S.W. Black Holes and Thermodynamics. *Phys. Rev. D* **1976**, *13*, 191–197. [CrossRef]
115. Bardeen, J.M.; Carter, B.; Hawking, S.W. The Four laws of black hole mechanics. *Commun. Math. Phys.* **1973**, *31*, 161–170. [CrossRef]
116. Hawking, S.W.; Page, D.N. Thermodynamics of Black Holes in anti-De Sitter Space. *Commun. Math. Phys.* **1983**, *87*, 577. [CrossRef]
117. Podolsky, J.; Ortaggio, M.; Krtous, P. Radiation from accelerated black holes in an anti-de Sitter universe. *Phys. Rev. D* **2003**, *68*, 124004. [CrossRef]
118. Appels, M.; Gregory, R.; Kubiznak, D. Thermodynamics of Accelerating Black Holes. *Phys. Rev. Lett.* **2016**, *117*, 131303. [CrossRef]
119. Appels, M.; Gregory, R.; Kubiznak, D. Black Hole Thermodynamics with Conical Defects. *J. High Energy Phys.* **2017**, *2017*, 116. [CrossRef]
120. Anabalón, A.; Appels, M.; Gregory, R.; Kubizňák, D.; Mann, R.B.; Ovgün, A. Holographic Thermodynamics of Accelerating Black Holes. *Phys. Rev. D* **2018**, *98*, 104038. [CrossRef]
121. Appels, M. Thermodynamics of Accelerating Black Holes. PhD Thesis, Department of Mathematical, Durham University, Durham, UK, 2018.
122. Ball, A.; Miller, N. Accelerating black hole thermodynamics with boost time. *Class. Quant. Grav.* **2021**, *38*, 145031. [CrossRef]

123. Gibbons, G.W.; Hawking, S.W. Action Integrals and Partition Functions in Quantum Gravity. *Phys. Rev. D* **1977**, *15*, 2752–2756. [CrossRef]
124. Kudoh, H.; Kurita, Y. Thermodynamics of four-dimensional black objects in the warped compactification. *Phys. Rev. D* **2004**, *70*, 084029. [CrossRef]
125. Myers, R.C.; Ruan, S.M.; Ugajin, T. Double Holography of Entangled Universes. *J. High Energy Phys.* **2024**, *2024*, 35. [CrossRef]
126. Bekenstein, J.D. Generalized second law of thermodynamics in black hole physics. *Phys. Rev. D* **1974**, *9*, 3292–3300. [CrossRef]
127. Wald, R.M. Black hole entropy is the Noether charge. *Phys. Rev. D* **1993**, *48*, R3427–R3431. [CrossRef]
128. Iyer, V.; Wald, R.M. Some properties of Noether charge and a proposal for dynamical black hole entropy. *Phys. Rev. D* **1994**, *50*, 846–864. [CrossRef]
129. Jacobson, T.; Kang, G.; Myers, R.C. On black hole entropy. *Phys. Rev. D* **1994**, *49*, 6587–6598. [CrossRef] [PubMed]
130. Susskind, L.; Uglum, J. Black hole entropy in canonical quantum gravity and superstring theory. *Phys. Rev. D* **1994**, *50*, 2700–2711. [CrossRef] [PubMed]
131. Solodukhin, S.N. Entanglement entropy of black holes. *Living Rev. Rel.* **2011**, *14*, 8. [CrossRef]
132. Cooperman, J.H.; Luty, M.A. Renormalization of Entanglement Entropy and the Gravitational Effective Action. *J. High Energy Phys.* **2014**, *2014*, 45. [CrossRef]
133. Pedraza, J.F.; Svesko, A.; Sybesma, W.; Visser, M.R. Semi-classical thermodynamics of quantum extremal surfaces in Jackiw-Teitelboim gravity. *J. High Energy Phys.* **2021**, *2021*, 134. [CrossRef]
134. Svesko, A.; Verheijden, E.; Verlinde, E.P.; Visser, M.R. Quasi-local energy and microcanonical entropy in two-dimensional nearly de Sitter gravity. *J. High Energy Phys.* **2022**, *2022*, 75. [CrossRef]
135. Frassino, A.M.; Hennigar, R.A.; Pedraza, J.F.; Svesko, A. Quantum inequalities for quantum black holes. *arXiv* **2024**, arXiv:2406.17860.
136. Spradlin, M.; Strominger, A.; Volovich, A. Les Houches lectures on de Sitter space. In Proceedings of the Les Houches Summer School: Session 76: Euro Summer School on Unity of Fundamental Physics: Gravity, Gauge Theory and Strings, Les Houches, France, 30 July–31 August 2001; Volume 10, pp. 423–453.
137. Morvan, E.K.; van der Schaar, J.P.; Visser, M.R. On the Euclidean Action of de Sitter Black Holes and Constrained Instantons. *SciPost Phys.* **2022**, *14*, 22. [CrossRef]
138. Morvan, E.K.; van der Schaar, J.P.; Visser, M.R. Action, entropy and pair creation rate of charged black holes in de Sitter space. *arXiv* **2022**, arXiv:2212.12713. [CrossRef]
139. Draper, P.; Farkas, S. de Sitter black holes as constrained states in the Euclidean path integral. *Phys. Rev. D* **2022**, *105*, 126022. [CrossRef]
140. Bousso, R.; Hawking, S.W. Pair creation of black holes during inflation. *Phys. Rev. D* **1996**, *54*, 6312–6322. [CrossRef]
141. Kastor, D.; Ray, S.; Traschen, J. Enthalpy and the Mechanics of AdS Black Holes. *Class. Quant. Grav.* **2009**, *26*, 195011. [CrossRef]
142. Dolan, B.P. The cosmological constant and the black hole equation of state. *Class. Quant. Grav.* **2011**, *28*, 125020. [CrossRef]
143. Cvetic, M.; Gibbons, G.W.; Kubiznak, D.; Pope, C.N. Black Hole Enthalpy and an Entropy Inequality for the Thermodynamic Volume. *Phys. Rev. D* **2011**, *84*, 024037. [CrossRef]
144. Johnson, C.V. Thermodynamic Volumes for AdS-Taub-NUT and AdS-Taub-Bolt. *Class. Quant. Grav.* **2014**, *31*, 235003. [CrossRef]
145. Chamblin, A.; Emparan, R.; Johnson, C.V.; Myers, R.C. Charged AdS black holes and catastrophic holography. *Phys. Rev. D* **1999**, *60*, 064018. [CrossRef]
146. Kubiznak, D.; Mann, R.B. P-V criticality of charged AdS black holes. *J. High Energy Phys.* **2012**, *2012*, 33. [CrossRef]
147. Kubiznak, D.; Mann, R.B. Black hole chemistry. *Can. J. Phys.* **2015**, *93*, 999–1002. [CrossRef]
148. Johnson, C.V. Holographic Heat Engines. *Class. Quant. Grav.* **2014**, *31*, 205002. [CrossRef]
149. Kubiznak, D.; Mann, R.B.; Teo, M. Black hole chemistry: Thermodynamics with Lambda. *Class. Quant. Grav.* **2017**, *34*, 063001. [CrossRef]
150. Dolan, B.P. Bose condensation and branes. *J. High Energy Phys.* **2014**, *2014*, 179. [CrossRef]
151. Kastor, D.; Ray, S.; Traschen, J. Chemical Potential in the First Law for Holographic Entanglement Entropy. *J. High Energy Phys.* **2014**, *2014*, 120. [CrossRef]
152. Caceres, E.; Nguyen, P.H.; Pedraza, J.F. Holographic entanglement entropy and the extended phase structure of STU black holes. *J. High Energy Phys.* **2015**, *2015*, 184. [CrossRef]
153. Karch, A.; Robinson, B. Holographic Black Hole Chemistry. *J. High Energy Phys.* **2015**, *2015*, 73. [CrossRef]
154. Caceres, E.; Nguyen, P.H.; Pedraza, J.F. Holographic entanglement chemistry. *Phys. Rev. D* **2017**, *95*, 106015. [CrossRef]
155. Rosso, F.; Svesko, A. Novel aspects of the extended first law of entanglement. *J. High Energy Phys.* **2020**, *2020*, 8. [CrossRef]
156. Frassino, A.M.; Pedraza, J.F.; Svesko, A.; Visser, M.R. Higher-Dimensional Origin of Extended Black Hole Thermodynamics. *Phys. Rev. Lett.* **2023**, *130*, 161501. [CrossRef]
157. Penrose, R. Structure of space-time. In Proceedings of the Battelle Rencontres, Seattle, WA, USA, 16–31 July 1967; pp. 121–235.
158. Penrose, R. Gravitational collapse: The role of general relativity. *Riv. Nuovo Cim.* **1969**, *1*, 252–276. [CrossRef]
159. Amo, M.; Frassino, A.M.; Hennigar, R.A. Entropy Bounds for Rotating AdS Black Holes. *Phys. Rev. Lett.* **2023**, *131*, 241401. [CrossRef] [PubMed]
160. Klemm, D. Four-dimensional black holes with unusual horizons. *Phys. Rev. D* **2014**, *89*, 084007. [CrossRef]

161. Hennigar, R.A.; Kubizňák, D.; Mann, R.B. Entropy Inequality Violations from Ultraspinning Black Holes. *Phys. Rev. Lett.* **2015**, *115*, 031101. [CrossRef]
162. Hennigar, R.A.; Kubizňák, D.; Mann, R.B.; Musoke, N. Ultraspinning limits and super-entropic black holes. *J. High Energy Phys.* **2015**, *2015*, 96. [CrossRef]
163. Appels, M.; Cuspinera, L.; Gregory, R.; Krtouš, P.; Kubizňák, D. Are "Superentropic" black holes superentropic? *J. High Energy Phys.* **2020**, *2020*, 195. [CrossRef]
164. Frassino, A.M.; Mann, R.B.; Mureika, J.R. Lower-Dimensional Black Hole Chemistry. *Phys. Rev. D* **2015**, *92*, 124069. [CrossRef]
165. Johnson, C.V. Instability of super-entropic black holes in extended thermodynamics. *Mod. Phys. Lett. A* **2020**, *35*, 2050098. [CrossRef]
166. Johnson, C.V.; Martin, V.L.; Svesko, A. Microscopic description of thermodynamic volume in extended black hole thermodynamics. *Phys. Rev. D* **2020**, *101*, 086006. [CrossRef]
167. Maldacena, J.M.; Strominger, A. AdS(3) black holes and a stringy exclusion principle. *J. High Energy Phys.* **1998**, *1998*, 5. [CrossRef]
168. Birmingham, D.; Sachs, I.; Solodukhin, S.N. Relaxation in conformal field theory, Hawking-Page transition, and quasinormal normal modes. *Phys. Rev. D* **2003**, *67*, 104026. [CrossRef]
169. Frassino, A.M.; Pedraza, J.F.; Svesko, A.; Visser, M.R. Reentrant phase transitions of quantum black holes. *Phys. Rev. D* **2024**, *109*, 124040. [CrossRef]
170. Johnson, C.V.; Nazario, R. Specific Heats for Quantum BTZ Black Holes in Extended Thermodynamics. *arXiv* **2023**, arXiv:2310.12212.
171. Hosseini Mansoori, S.A.; Pedraza, J.F.; Rafiee, M. Criticality and thermodynamic geometry of quantum BTZ black holes. *arXiv* **2024**, arXiv:2403.13063.
172. Gunasekaran, S.; Mann, R.B.; Kubiznak, D. Extended phase space thermodynamics for charged and rotating black holes and Born-Infeld vacuum polarization. *J. High Energy Phys.* **2012**, *2012*, 110. [CrossRef]
173. Altamirano, N.; Kubiznak, D.; Mann, R.B. Reentrant phase transitions in rotating anti–de Sitter black holes. *Phys. Rev. D* **2013**, *88*, 101502. [CrossRef]
174. Frassino, A.M.; Kubiznak, D.; Mann, R.B.; Simovic, F. Multiple Reentrant Phase Transitions and Triple Points in Lovelock Thermodynamics. *J. High Energy Phys.* **2014**, *2014*, 80. [CrossRef]
175. Ahmed, M.B.; Cong, W.; Kubiznak, D.; Mann, R.B.; Visser, M.R. Holographic CFT phase transitions and criticality for rotating AdS black holes. *J. High Energy Phys.* **2023**, *2023*, 142. [CrossRef]
176. Frassino, A.M.; Rocha, J.V.; Sanna, A.P. Weak cosmic censorship and the rotating quantum BTZ black hole. *J. High Energy Phys.* **2024**, *2024*, 226. [CrossRef]
177. Anderson, P.R.; Hiscock, W.A.; Samuel, D.A. Stress-energy tensor of quantized scalar fields in static spherically symmetric space-times. *Phys. Rev. D* **1995**, *51*, 4337–4358. [CrossRef]
178. Hawking, S.W.; Hertog, T.; Reall, H.S. Trace anomaly driven inflation. *Phys. Rev. D* **2001**, *63*, 083504. [CrossRef]
179. Herzog, C.P.; Huang, K.W. Stress Tensors from Trace Anomalies in Conformal Field Theories. *Phys. Rev. D* **2013**, *87*, 081901. [CrossRef]
180. Fabbri, A.; Farese, S.; Navarro-Salas, J.; Olmo, G.J.; Sanchis-Alepuz, H. Semiclassical zero-temperature corrections to Schwarzschild spacetime and holography. *Phys. Rev. D* **2006**, *73*, 104023. [CrossRef]
181. Fabbri, A.; Farese, S.; Navarro-Salas, J.; Olmo, G.J.; Sanchis-Alepuz, H. Static quantum corrections to the Schwarzschild spacetime. *J. Phys. Conf. Ser.* **2006**, *33*, 457–462. [CrossRef]
182. Ho, P.M.; Matsuo, Y. Static Black Holes With Back Reaction From Vacuum Energy. *Class. Quant. Grav.* **2018**, *35*, 065012. [CrossRef]
183. Arrechea, J.; Barceló, C.; Carballo-Rubio, R.; Garay, L.J. Schwarzschild geometry counterpart in semiclassical gravity. *Phys. Rev. D* **2020**, *101*, 064059. [CrossRef]
184. Beltrán-Palau, P.; del Río, A.; Navarro-Salas, J. Quantum corrections to the Schwarzschild metric from vacuum polarization. *Phys. Rev. D* **2023**, *107*, 085023. [CrossRef]
185. Cai, R.G.; Cao, L.M.; Ohta, N. Black Holes in Gravity with Conformal Anomaly and Logarithmic Term in Black Hole Entropy. *J. High Energy Phys.* **2010**, *2010*, 82. [CrossRef]
186. Fernandes, P.G.S. Rotating black holes in semiclassical gravity. *Phys. Rev. D* **2023**, *108*, L061502. [CrossRef]
187. Astorino, M. Accelerating black hole in 2+1 dimensions and 3+1 black (st)ring. *J. High Energy Phys.* **2011**, *2011*, 114. [CrossRef]
188. Xu, W.; Meng, K.; Zhao, L. Accelerating BTZ spacetime. *Class. Quant. Grav.* **2012**, *29*, 155005. [CrossRef]
189. Arenas-Henriquez, G.; Gregory, R.; Scoins, A. On acceleration in three dimensions. *J. High Energy Phys.* **2022**, *2022*, 63, [CrossRef]
190. Arenas-Henriquez, G.; Cisterna, A.; Diaz, F.; Gregory, R. Accelerating Black Holes in 2+1 dimensions: Holography revisited. *J. High Energy Phys.* **2023**, *2023*, 122. [CrossRef]
191. Tian, J.; Lai, T. Aspects of three-dimensional C-metric. *J. High Energy Phys.* **2024**, *2024*, 79. [CrossRef]
192. Camps, J.; Emparan, R. A New Class of Accelerating Black Hole Solutions. *Phys. Rev. D* **2010**, *82*, 024009. [CrossRef]
193. Kodama, H. Accelerating a Black Hole in Higher Dimensions. *Prog. Theor. Phys.* **2008**, *120*, 371–411. [CrossRef]
194. Chamblin, A.; Hawking, S.W.; Reall, H.S. Brane world black holes. *Phys. Rev. D* **2000**, *61*, 065007. [CrossRef]
195. Gregory, R. Black string instabilities in Anti-de Sitter space. *Class. Quant. Grav.* **2000**, *17*, L125–L132. [CrossRef]
196. Gregory, R.; Laflamme, R. Black strings and p-branes are unstable. *Phys. Rev. Lett.* **1993**, *70*, 2837–2840. [CrossRef]
197. Gregory, R.; Laflamme, R. The Instability of charged black strings and p-branes. *Nucl. Phys. B* **1994**, *428*, 399–434. [CrossRef]

198. Emparan, R.; Garcia-Bellido, J.; Kaloper, N. Black hole astrophysics in AdS brane worlds. *J. High Energy Phys.* **2003**, *2003*, 79. [CrossRef]
199. Chamblin, A.; Karch, A. Hawking and Page on the brane. *Phys. Rev. D* **2005**, *72*, 066011. [CrossRef]
200. Hubeny, V.E.; Marolf, D.; Rangamani, M. Hawking radiation from AdS black holes. *Class. Quant. Grav.* **2010**, *27*, 095018. [CrossRef]
201. Tanahashi, N.; Tanaka, T. Time-symmetric initial data of large brane-localized black hole in RS-II model. *J. High Energy Phys.* **2008**, *2008*, 41. [CrossRef]
202. Gregory, R.; Ross, S.F.; Zegers, R. Classical and quantum gravity of brane black holes. *J. High Energy Phys.* **2008**, *2008*, 29. [CrossRef]
203. Figueras, P.; Lucietti, J.; Wiseman, T. Ricci solitons, Ricci flow, and strongly coupled CFT in the Schwarzschild Unruh or Boulware vacua. *Class. Quant. Grav.* **2011**, *28*, 215018. [CrossRef]
204. Abdolrahimi, S.; Cattoen, C.; Page, D.N.; Yaghoobpour-Tari, S. Large Randall-Sundrum II Black Holes. *Phys. Lett. B* **2013**, *720*, 405–409. [CrossRef]
205. Abdolrahimi, S.; Cattoën, C.; Page, D.N.; Yaghoobpour-Tari, S. Spectral methods in general relativity and large Randall-Sundrum II black holes. *J. Cosmol. Astropart. Phys.* **2013**, *2013*, 39. [CrossRef]
206. Figueras, P.; Tunyasuvunakool, S. CFTs in rotating black hole backgrounds. *Class. Quant. Grav.* **2013**, *30*, 125015. [CrossRef]
207. Banerjee, S.; Danielsson, U.; Giri, S. Dark bubbles and black holes. *J. High Energy Phys.* **2021**, *2021*, 158. [CrossRef]
208. Biggs, W.D.; Santos, J.E. Rotating Black Holes in Randall-Sundrum II Braneworlds. *Phys. Rev. Lett.* **2022**, *128*, 021601. [CrossRef]
209. Fabbri, A.; Procopio, G.P. Quantum effects in black holes from the Schwarzschild black string? *Class. Quant. Grav.* **2007**, *24*, 5371–5382. [CrossRef]
210. Hirayama, T.; Kang, G. Stable black strings in anti-de Sitter space. *Phys. Rev. D* **2001**, *64*, 064010. [CrossRef]
211. Page, D.N. Thermal Stress Tensors in Static Einstein Spaces. *Phys. Rev. D* **1982**, *25*, 1499. [CrossRef]
212. Emparan, R.; Suzuki, R.; Tanabe, K. The large D limit of General Relativity. *J. High Energy Phys.* **2013**, *2013*, 9. [CrossRef]
213. Bhattacharyya, S.; De, A.; Minwalla, S.; Mohan, R.; Saha, A. A membrane paradigm at large D. *J. High Energy Phys.* **2016**, *2016*, 76. [CrossRef]
214. Emparan, R.; Herzog, C.P. Large D limit of Einstein's equations. *Rev. Mod. Phys.* **2020**, *92*, 045005. [CrossRef]
215. Emparan, R.; Licht, D.; Suzuki, R.; Tomašević, M.; Way, B. Black tsunamis and naked singularities in AdS. *J. High Energy Phys.* **2022**, *2022*, 90. [CrossRef]
216. Sorkin, R.D. On the Entropy of the Vacuum outside a Horizon. In Proceedings of the 10th International Conference on General Relativity and Gravitation, Padova, Italy, 4–9 July 1983; Volume 2, pp. 734–736.
217. Bombelli, L.; Koul, R.K.; Lee, J.; Sorkin, R.D. A Quantum Source of Entropy for Black Holes. *Phys. Rev. D* **1986**, *34*, 373–383. [CrossRef]
218. Srednicki, M. Entropy and area. *Phys. Rev. Lett.* **1993**, *71*, 666–669. [CrossRef]
219. Frolov, V.P.; Novikov, I. Dynamical origin of the entropy of a black hole. *Phys. Rev. D* **1993**, *48*, 4545–4551. [CrossRef]
220. Callan, C.G., Jr.; Wilczek, F. On geometric entropy. *Phys. Lett. B* **1994**, *333*, 55–61. [CrossRef]
221. Sakharov, A.D. Vacuum quantum fluctuations in curved space and the theory of gravitation. *Dokl. Akad. Nauk Ser. Fiz.* **1967**, *177*, 70–71. [CrossRef]
222. Visser, M. Sakharov's induced gravity: A Modern perspective. *Mod. Phys. Lett. A* **2002**, *17*, 977–992. [CrossRef]
223. Jacobson, T. Black hole entropy and induced gravity. *arXiv* **1994**, arXiv:9404039.
224. Frolov, V.P.; Fursaev, D.V.; Zelnikov, A.I. Statistical origin of black hole entropy in induced gravity. *Nucl. Phys. B* **1997**, *486*, 339–352. [CrossRef]
225. Frolov, V.P.; Fursaev, D.V. Mechanism of generation of black hole entropy in Sakharov's induced gravity. *Phys. Rev. D* **1997**, *56*, 2212–2225. [CrossRef]
226. Ryu, S.; Takayanagi, T. Holographic derivation of entanglement entropy from AdS/CFT. *Phys. Rev. Lett.* **2006**, *96*, 181602. [CrossRef]
227. Ryu, S.; Takayanagi, T. Aspects of Holographic Entanglement Entropy. *J. High Energy Phys.* **2006**, *2006*, 45. [CrossRef]
228. Lewkowycz, A.; Maldacena, J. Generalized gravitational entropy. *J. High Energy Phys.* **2013**, *2013*, 90. [CrossRef]
229. Takayanagi, T.; Tamaoka, K. Gravity Edges Modes and Hayward Term. *J. High Energy Phys.* **2020**, *2020*, 167. [CrossRef]
230. Botta-Cantcheff, M.; Martinez, P.J.; Zarate, J.F. Rényi entropies and area operator from gravity with Hayward term. *J. High Energy Phys.* **2020**, *2020*, 227. [CrossRef]
231. Kastikainen, J.; Svesko, A. Gravitational Rényi entropy from corner terms. *Phys. Rev. D* **2024**, *109*, 126017. [CrossRef]
232. Kastikainen, J.; Svesko, A. Cornering gravitational entropy. *J. High Energy Phys.* **2024**, *2024*, 160. [[CrossRef]
233. Lashkari, N.; McDermott, M.B.; Van Raamsdonk, M. Gravitational dynamics from entanglement 'thermodynamics'. *J. High Energy Phys.* **2014**, *2014*, 195. [CrossRef]
234. Faulkner, T.; Guica, M.; Hartman, T.; Myers, R.C.; Van Raamsdonk, M. Gravitation from Entanglement in Holographic CFTs. *J. High Energy Phys.* **2014**, *2014*, 51. [CrossRef]
235. Haehl, F.M.; Hijano, E.; Parrikar, O.; Rabideau, C. Higher Curvature Gravity from Entanglement in Conformal Field Theories. *Phys. Rev. Lett.* **2018**, *120*, 201602. [CrossRef]
236. Swingle, B.; Van Raamsdonk, M. Universality of Gravity from Entanglement. *arXiv* **2014**, arXiv:1405.2933.

237. Agón, C.A.; Cáceres, E.; Pedraza, J.F. Bit threads, Einstein's equations and bulk locality. *J. High Energy Phys.* **2021**, *2021*, 193. [CrossRef]
238. Agón, C.A.; Pedraza, J.F. Quantum bit threads and holographic entanglement. *J. High Energy Phys.* **2022**, *2022*, 180. [CrossRef]
239. Cooper, S.; Neuenfeld, D.; Rozali, M.; Wakeham, D. Brane dynamics from the first law of entanglement. *J. High Energy Phys.* **2020**, *2020*, 23. [CrossRef]
240. Jacobson, T. Thermodynamics of space-time: The Einstein equation of state. *Phys. Rev. Lett.* **1995**, *75*, 1260–1263. [CrossRef]
241. Parikh, M.K.; Sarkar, S. Beyond the Einstein Equation of State: Wald Entropy and Thermodynamical Gravity. *Entropy* **2016**, *18*, 119. [CrossRef]
242. Guedens, R.; Jacobson, T.; Sarkar, S. Horizon entropy and higher curvature equations of state. *Phys. Rev. D* **2012**, *85*, 064017. [CrossRef]
243. Parikh, M.; Svesko, A. Einstein's equations from the stretched future light cone. *Phys. Rev. D* **2018**, *98*, 026018. [CrossRef]
244. Parikh, M.; Sarkar, S.; Svesko, A. Local first law of gravity. *Phys. Rev. D* **2020**, *101*, 104043. [CrossRef]
245. Svesko, A. Equilibrium to Einstein: Entanglement, Thermodynamics, and Gravity. *Phys. Rev. D* **2019**, *99*, 086006. [CrossRef]
246. Engelhardt, N.; Wall, A.C. Quantum Extremal Surfaces: Holographic Entanglement Entropy beyond the Classical Regime. *J. High Energy Phys.* **2015**, *2015*, 73. [CrossRef]
247. Dong, X. Holographic Entanglement Entropy for General Higher Derivative Gravity. *J. High Energy Phys.* **2014**, *2014*, 44. [CrossRef]
248. Camps, J. Generalized entropy and higher derivative Gravity. *J. High Energy Phys.* **2014**, *2014*, 70. [CrossRef]
249. Hawking, S.; Maldacena, J.M.; Strominger, A. DeSitter entropy, quantum entanglement and AdS / CFT. *J. High Energy Phys.* **2001**, *2001*, 1. [CrossRef]
250. Fursaev, D.V. Black hole thermodynamics, induced gravity and gravity in brane worlds. In Proceedings of the International Conference on Quantization, Gauge Theory, and Strings: Conference Dedicated to the Memory of Professor Efim Fradkin, Moscow, Russia, 5–10 June 2000; Volume 6, pp. 462–470.
251. Jacobson, T. On the nature of black hole entropy. *AIP Conf. Proc.* **1999**, *493*, 85–97. [CrossRef]
252. Hawking, S.W. Breakdown of Predictability in Gravitational Collapse. *Phys. Rev. D* **1976**, *14*, 2460–2473. [CrossRef]
253. Page, D.N. Information in black hole radiation. *Phys. Rev. Lett.* **1993**, *71*, 3743–3746. [CrossRef]
254. Penington, G. Entanglement Wedge Reconstruction and the Information Paradox. *J. High Energy Phys.* **2020**, 2020, 2. [CrossRef]
255. Almheiri, A.; Engelhardt, N.; Marolf, D.; Maxfield, H. The entropy of bulk quantum fields and the entanglement wedge of an evaporating black hole. *J. High Energy Phys.* **2019**, 2019, 63. [CrossRef]
256. Almheiri, A.; Hartman, T.; Maldacena, J.; Shaghoulian, E.; Tajdini, A. Replica Wormholes and the Entropy of Hawking Radiation. *J. High Energy Phys.* **2020**, *2020*, 13. [CrossRef]
257. Penington, G.; Shenker, S.H.; Stanford, D.; Yang, Z. Replica wormholes and the black hole interior. *J. High Energy Phys.* **2022**, *2022*, 205. [CrossRef]
258. Goto, K.; Hartman, T.; Tajdini, A. Replica wormholes for an evaporating 2D black hole. *J. High Energy Phys.* **2021**, *04*, 289. [CrossRef]
259. Pedraza, J.F.; Svesko, A.; Sybesma, W.; Visser, M.R. Microcanonical action and the entropy of Hawking radiation. *Phys. Rev. D* **2022**, *105*, 126010. [CrossRef]
260. Almheiri, A.; Mahajan, R.; Maldacena, J.; Zhao, Y. The Page curve of Hawking radiation from semiclassical geometry. *J. High Energy Phys.* **2020**, *2020*, 149. [CrossRef]
261. Dvali, G.R.; Gabadadze, G.; Porrati, M. 4-D gravity on a brane in 5-D Minkowski space. *Phys. Lett. B* **2000**, *485*, 208–214. [CrossRef]
262. Neuenfeld, D. Homology conditions for RT surfaces in double holography. *Class. Quant. Grav.* **2022**, *39*, 075009. [CrossRef]
263. Lee, J.H.; Neuenfeld, D.; Shukla, A. Bounds on gravitational brane couplings and tomography in AdS_3 black hole microstates. *J. High Energy Phys.* **2022**, *2022*, 139. [CrossRef]
264. Geng, H.; Karch, A.; Perez-Pardavila, C.; Raju, S.; Randall, L.; Riojas, M.; Shashi, S. Entanglement phase structure of a holographic BCFT in a black hole background. *J. High Energy Phys.* **2022**, *2022*, 153. [CrossRef]
265. Karch, A.; Perez-Pardavila, C.; Riojas, M.; Youssef, M. Subregion entropy for the doubly-holographic global black string. *J. High Energy Phys.* **2023**, *2023*, 195. [CrossRef]
266. Geng, H.; Nomura, Y.; Sun, H.Y. Information paradox and its resolution in de Sitter holography. *Phys. Rev. D* **2021**, *103*, 126004. [CrossRef]
267. Geng, H.; Karch, A. Massive islands. *J. High Energy Phys.* **2020**, *2020*, 121. [CrossRef]
268. Geng, H. Revisiting Recent Progress in the Karch-Randall Braneworld. *arXiv* **2023**, arXiv:2306.15671.
269. Geng, H.; Karch, A.; Perez-Pardavila, C.; Raju, S.; Randall, L.; Riojas, M.; Shashi, S. Inconsistency of islands in theories with long-range gravity. *J. High Energy Phys.* **2022**, *2022*, 182. [CrossRef]
270. Czech, B. Einstein Equations from Varying Complexity. *Phys. Rev. Lett.* **2018**, *120*, 031601. [CrossRef] [PubMed]
271. Caputa, P.; Magan, J.M. Quantum Computation as Gravity. *Phys. Rev. Lett.* **2019**, *122*, 231302. [CrossRef]
272. Susskind, L. Complexity and Newton's Laws. *Front. Phys.* **2020**, *8*, 262. [CrossRef]
273. Pedraza, J.F.; Russo, A.; Svesko, A.; Weller-Davies, Z. Lorentzian Threads as Gatelines and Holographic Complexity. *Phys. Rev. Lett.* **2021**, *127*, 271602. [CrossRef] [PubMed]

274. Pedraza, J.F.; Russo, A.; Svesko, A.; Weller-Davies, Z. Sewing spacetime with Lorentzian threads: Complexity and the emergence of time in quantum gravity. *J. High Energy Phys.* **2022**, *2022*, 93. [CrossRef]
275. Pedraza, J.F.; Russo, A.; Svesko, A.; Weller-Davies, Z. Computing spacetime. *Int. J. Mod. Phys. D* **2022**, *31*, 2242010. [CrossRef]
276. Carrasco, R.; Pedraza, J.F.; Svesko, A.; Weller-Davies, Z. Gravitation from optimized computation: Einstein and beyond. *J. High Energy Phys.* **2023**, *2023*, 167. [CrossRef]
277. Susskind, L. Entanglement is not enough. *Fortsch. Phys.* **2016**, *64*, 49–71. [CrossRef]
278. Stanford, D.; Susskind, L. Complexity and Shock Wave Geometries. *Phys. Rev. D* **2014**, *90*, 126007. [CrossRef]
279. Susskind, L. Computational Complexity and Black Hole Horizons. *Fortsch. Phys.* **2016**, *64*, 24–43. Addendum in *Fortsch. Phys.* **2016**, *64*, 44–48. [CrossRef]
280. Brown, A.R.; Roberts, D.A.; Susskind, L.; Swingle, B.; Zhao, Y. Complexity, action, and black holes. *Phys. Rev. D* **2016**, *93*, 086006. [CrossRef]
281. Brown, A.R.; Roberts, D.A.; Susskind, L.; Swingle, B.; Zhao, Y. Holographic Complexity Equals Bulk Action? *Phys. Rev. Lett.* **2016**, *116*, 191301. [CrossRef] [PubMed]
282. Swingle, B. Entanglement Renormalization and Holography. *Phys. Rev. D* **2012**, *86*, 065007. [CrossRef]
283. Swingle, B. Constructing holographic spacetimes using entanglement renormalization. *arXiv* **2012**, arXiv:1209.3304.
284. Bao, N.; Penington, G.; Sorce, J.; Wall, A.C. Beyond Toy Models: Distilling Tensor Networks in Full AdS/CFT. *J. High Energy Phys.* **2019**, *2019*, 69. [CrossRef]
285. Jahn, A.; Eisert, J. Holographic tensor network models and quantum error correction: A topical review. *Quantum Sci. Technol.* **2021**, *6*, 033002. [CrossRef]
286. Belin, A.; Myers, R.C.; Ruan, S.M.; Sárosi, G.; Speranza, A.J. Does Complexity Equal Anything? *Phys. Rev. Lett.* **2022**, *128*, 081602. [CrossRef]
287. Belin, A.; Myers, R.C.; Ruan, S.M.; Sárosi, G.; Speranza, A.J. Complexity equals anything II. *J. High Energy Phys.* **2023**, *2023*, 154. [CrossRef]
288. Hernandez, J.; Myers, R.C.; Ruan, S.M. Quantum extremal islands made easy. Part III. Complexity on the brane. *J. High Energy Phys.* **2021**, *2021*, 173. [CrossRef]
289. Chen, B.; Liu, Y.; Yu, B. Holographic complexity of rotating quantum black holes. *J. High Energy Phys.* **2024**, *2024*, 55. [CrossRef]
290. Aguilar-Gutierrez, S.E.; Craps, B.; Hernandez, J.; Khramtsov, M.; Knysh, M.; Shukla, A. Holographic complexity: Braneworld gravity versus the Lloyd bound. *J. High Energy Phys.* **2024**, *2024*, 173. [CrossRef]
291. Carrasco, R.; Pedraza, J.F.; Svesko, A. *Work in progress*.
292. Penrose, R. Gravitational Collapse. In *Gravitational Radiation and Gravitational Collapse*; Dewitt-Morette, C., Ed.; Springer: Dordrecht, The Netherlands, 1974; Volume 64, p. 82.
293. Penrose, R. Singularities and time asymmetry. In *General Relativity: An Einstein Centenary Survey*; Cambridge University Press: Cambridge, UK, 1980; pp. 581–638.
294. Simpson, M.; Penrose, R. Internal instability in a Reissner-Nordstrom black hole. *Int. J. Theor. Phys.* **1973**, *7*, 183–197. [CrossRef]
295. Poisson, E.; Israel, W. Internal structure of black holes. *Phys. Rev. D* **1990**, *41*, 1796–1809. [CrossRef]
296. Lanir, A.; Ori, A.; Zilberman, N.; Sela, O.; Maline, A.; Levi, A. Analysis of quantum effects inside spherical charged black holes. *Phys. Rev. D* **2019**, *99*, 061502. [CrossRef]
297. Zilberman, N.; Levi, A.; Ori, A. Quantum fluxes at the inner horizon of a spherical charged black hole. *Phys. Rev. Lett.* **2020**, *124*, 171302. [CrossRef]
298. Dias, O.J.C.; Reall, H.S.; Santos, J.E. The BTZ black hole violates strong cosmic censorship. *J. High Energy Phys.* **2019**, *2019*, 97. [CrossRef]
299. Hollands, S.; Wald, R.M.; Zahn, J. Quantum instability of the Cauchy horizon in Reissner–Nordström–deSitter spacetime. *Class. Quant. Grav.* **2020**, *37*, 115009. [CrossRef]
300. Emparan, R.; Tomašević, M. Strong cosmic censorship in the BTZ black hole. *J. High Energy Phys.* **2020**, *2020*, 38. [CrossRef]
301. Kolanowski, M.; Tomašević, M. Singularities in 2D and 3D quantum black holes. *J. High Energy Phys.* **2023**, *2023*, 102. [CrossRef]
302. Wald, R. Gedanken experiments to destroy a black hole. *Ann. Phys.* **1974**, *82*, 548–556. [CrossRef]
303. Sorce, J.; Wald, R.M. Gedanken experiments to destroy a black hole. II. Kerr-Newman black holes cannot be overcharged or overspun. *Phys. Rev. D* **2017**, *96*, 104014. [CrossRef]
304. Penrose, R. Naked singularities. *Annals N. Y. Acad. Sci.* **1973**, *224*, 125–134. [CrossRef]
305. Huisken, G.; Ilmanen, T. The Inverse Mean Curvature Flow and the Riemannian Penrose Inequality. *J. Differ. Geom.* **2001**, *59*, 353–437. [CrossRef]
306. Bray, H.L. Proof of the Riemannian Penrose Inequality Using the Positive Mass Theorem. *J. Differ. Geom.* **2001**, *59*, 177–267. [CrossRef]
307. Bray, H.L.; Lee, D.A. On the Riemannian Penrose inequality in dimensions less than 8. *Duke Math. J.* **2009**, *148*, 81–106. [CrossRef]
308. Mars, M. Present status of the Penrose inequality. *Class. Quant. Grav.* **2009**, *26*, 193001. [CrossRef]
309. Itkin, I.; Oz, Y. Penrose Inequality for Asymptotically AdS Spaces. *Phys. Lett. B* **2012**, *708*, 307–308. [CrossRef]
310. Folkestad, r. Penrose Inequality as a Constraint on the Low Energy Limit of Quantum Gravity. *Phys. Rev. Lett.* **2023**, *130*, 121501. [CrossRef] [PubMed]

311. Bousso, R.; Shahbazi-Moghaddam, A.; Tomasevic, M. Quantum Penrose Inequality. *Phys. Rev. Lett.* **2019**, *123*, 241301. [CrossRef] [PubMed]
312. Bousso, R.; Shahbazi-Moghaddam, A.; Tomašević, M. Quantum Information Bound on the Energy. *Phys. Rev. D* **2019**, *100*, 126010. [CrossRef]
313. Engelhardt, N.; Folkestad, r.; Levine, A.; Verheijden, E.; Yang, L. Cryptographic Censorship. *arXiv* **2024**, arXiv:2402.03425.
314. Berti, E.; Cardoso, V.; Starinets, A.O. Quasinormal modes of black holes and black branes. *Class. Quant. Grav.* **2009**, *26*, 163001. [CrossRef]
315. Konoplya, R.A.; Zhidenko, A. Quasinormal modes of black holes: From astrophysics to string theory. *Rev. Mod. Phys.* **2011**, *83*, 793–836. [CrossRef]
316. Horowitz, G.T.; Hubeny, V.E. Quasinormal modes of AdS black holes and the approach to thermal equilibrium. *Phys. Rev. D* **2000**, *62*, 024027. [CrossRef]
317. Cartwright, C.; Gürsoy, U.; Pedraza, J.F.; Planella Planas, G. Perturbing a quantum black hole. *arXiv* **2024**, arXiv:2408.08010.
318. Grozdanov, S.; Schalm, K.; Scopelliti, V. Black hole scrambling from hydrodynamics. *Phys. Rev. Lett.* **2018**, *120*, 231601. [CrossRef]
319. Blake, M.; Davison, R.A.; Grozdanov, S.; Liu, H. Many-body chaos and energy dynamics in holography. *J. High Energy Phys.* **2018**, *2018*, 35. [CrossRef]
320. Haehl, F.M.; Rozali, M. Effective Field Theory for Chaotic CFTs. *J. High Energy Phys.* **2018**, *2018*, 118. [CrossRef]
321. Cartwright, C. An example of the convergence of hydrodynamics in strong external fields. *arXiv* **2024**, arXiv:2403.12638. [CrossRef]
322. Grozdanov, S.; Kovtun, P.K.; Starinets, A.O.; Tadić, P. The complex life of hydrodynamic modes. *J. High Energy Phys.* **2019**, *2019*, 97. [CrossRef]
323. Sasaki, M.; Shiromizu, T.; Maeda, K.i. Gravity, stability and energy conservation on the Randall-Sundrum brane world. *Phys. Rev. D* **2000**, *62*, 024008. [CrossRef]
324. Garriga, J.; Tanaka, T. Gravity in the brane world. *Phys. Rev. Lett.* **2000**, *84*, 2778–2781. [CrossRef] [PubMed]
325. Csaki, C.; Erlich, J.; Hollowood, T.J.; Shirman, Y. Universal aspects of gravity localized on thick branes. *Nucl. Phys. B* **2000**, *581*, 309–338. [CrossRef]
326. Karch, A.; Randall, L. Localized gravity in string theory. *Phys. Rev. Lett.* **2001**, *87*, 061601. [CrossRef] [PubMed]
327. DeWolfe, O.; Freedman, D.Z.; Ooguri, H. Holography and defect conformal field theories. *Phys. Rev. D* **2002**, *66*, 025009. [CrossRef]
328. Aharony, O.; DeWolfe, O.; Freedman, D.Z.; Karch, A. Defect conformal field theory and locally localized gravity. *J. High Energy Phys.* **2003**, *2003*, 30. [CrossRef]
329. Polchinski, J. Dirichlet Branes and Ramond-Ramond charges. *Phys. Rev. Lett.* **1995**, *75*, 4724–4727. [CrossRef]
330. Horowitz, G.T.; Strominger, A. Black strings and P-branes. *Nucl. Phys. B* **1991**, *360*, 197–209. [CrossRef]
331. Gubser, S.S. AdS / CFT and gravity. *Phys. Rev. D* **2001**, *63*, 084017. [CrossRef]
332. Levi-Civita, T. Ds2 einsteiniani in campi newtoniani. *Atti Accad. Nazl. Lincei* **1918**, *27*.
333. Ehlers, J.; Kundt, W. *Exact Solutions of the Gravitational Field Equations*; John Wiley & Sons: Hoboken, NJ, USA, 1962.
334. Kinnersley, W.; Walker, M. Uniformly accelerating charged mass in general relativity. *Phys. Rev. D* **1970**, *2*, 1359–1370. [CrossRef]
335. Griffiths, J.B.; Podolsky, J. A New look at the Plebanski-Demianski family of solutions. *Int. J. Mod. Phys. D* **2006**, *15*, 335–370. [CrossRef]
336. Podolsky, J.; Griffiths, J.B. Accelerating Kerr-Newman black holes in (anti-)de Sitter space-time. *Phys. Rev. D* **2006**, *73*, 044018. [CrossRef]
337. Griffiths, J.B.; Krtous, P.; Podolsky, J. Interpreting the C-metric. *Class. Quant. Grav.* **2006**, *23*, 6745–6766. [CrossRef]
338. Podolsky, J.; Vratny, A. New improved form of black holes of type D. *Phys. Rev. D* **2021**, *104*, 084078. [CrossRef]
339. Hong, K.; Teo, E. A New form of the C metric. *Class. Quant. Grav.* **2003**, *20*, 3269–3277. [CrossRef]
340. Hong, K.; Teo, E. A New form of the rotating C-metric. *Class. Quant. Grav.* **2005**, *22*, 109–118. [CrossRef]
341. Bonnor, W.B. Closed timelike curves in general relativity. *Int. J. Mod. Phys. D* **2003**, *12*, 1705–1708. [CrossRef]
342. Hubeny, V.E.; Marolf, D.; Rangamani, M. Black funnels and droplets from the AdS C-metrics. *Class. Quant. Grav.* **2010**, *27*, 025001. [CrossRef]
343. Costa, S.S. A Description of several coordinate systems for hyperbolic spaces. *arXiv* **2001**, arXiv:0112039.
344. Dias, O.J.C.; Lemos, J.P.S. Pair of accelerated black holes in anti-de Sitter background: AdS C metric. *Phys. Rev. D* **2003**, *67*, 064001. [CrossRef]
345. Balasubramanian, V.; Kraus, P. A Stress tensor for Anti-de Sitter gravity. *Commun. Math. Phys.* **1999**, *208*, 413–428. [CrossRef]